University of Sheffield

Title: Ex vivo drug screening using human tissue to personalise cancer therapy and replace murine avatars

Name: Hannah Jane Gagg

A thesis submitted in partial fulfilment of the requirements for the degree of
Doctor of Philosophy

The University of Sheffield
Faculty of Medicine, Dentistry and Health
Department of Oncology and Metabolism

Date of submission – November 2023

Abstract

Due to the diminishing returns and common failures seen in traditional preclinical and animal-based drug discovery methods, there is a growing focus on alternative drug discovery approaches, such as ex vivo methods. These alternative approaches represent a departure from both traditional preclinical animal models and conventional clinical strategies. Their goal is to address the variability among and within patients at an earlier stage of drug discovery. Moreover, these approaches could potentially enable precise treatment stratification for patients within a week of tumour removal, guiding a tailored treatment plan. One specific group of tumours that could greatly benefit from ex vivo techniques is high-grade gliomas. These tumours exhibit significant heterogeneity, cellular adaptability, and therapy-resistant glioma stem cell environments. Historical preclinical models have failed to produce new therapies for these tumours, resulting in a stagnant survival rate of approximately 15 months post-diagnosis for the past 50 years. This PhD study has focused on the successful development and optimization of a high-throughput ex vivo drug screening platform, which utilizes freshly dissociated surgical tissue to maintain glioma stem cell (GSC) populations. As a proof-of-concept, we have fine-tuned the responses to standard-of-care chemoradiotherapy treatments, allowing us to accurately predict the *MGMT* status based on temozolomide sensitivity. We have conducted screening experiments involving over 30+ small molecule therapeutics and preclinical compounds, using tissue samples from 18 different patients, including spatially heterogeneous regions from individual tumours. Our data within this thesis serves as a robust foundation for expanding ex vivo screening, to include combination-based oncology therapeutics in conjunction with standard-of-care treatments. This approach is vital as a preclinical model for assessing experimental therapeutics for potential clinical translation, enabling the rapid identification of effective treatment strategies tailored to individual glioblastoma cases.

THE UNIVERSITY OF SHEFFIELD: COVID-19 IMPACT FORM

This form is not compulsory but is intended to be a helpful note to examiners. You may submit this form alongside (not in) your thesis. The purpose of the form is to detail how your thesis has been impacted by the Covid-19 disruption.

STUDENT'S DETAILS	
Name: Hannah Jane Gagg	Registration Number:200184261
Department: Oncology and Metabolism	Faculty: Medicine, Dentistry and Health

Please provide a brief summary of the work you were planning to complete before covid-19 restrictions were implemented (max 300 words)

At the beginning of the project the number of patients which were recruited was significantly reduced due to COVID-19, I would have anticipated an additional 10 (minimum) samples that could have been screened using our ex vivo drug plates. Additionally due to the split shift system within the department within the first 9 months it was incredibly difficult to complete experiments (due to short 5-hour shifts) and obtain any relevant training due to staff being on different shift patterns. For instance my project required in-depth training for the high-content microscope and image analysis software, this was very difficult to fully grasp in the beginning due to the staff member who provided the training being on a different shift pattern. Without COVID-19 disruptions I do believe that I would have gotten much further collecting data for my final V02 plates. Additionally due to time constraints I was unable to analyse and incorporate whole exome sequencing data which would have formed an additional important chapter of my thesis.

Please provide a summary of plans for specific studies you were intending to conduct in the future (see note 1) (max 300 words)

See future work

Where relevant, please provide details of changes to your personal circumstances (see note 2) (max 150 words)

N/A

If your thesis includes Covid-related research, please include a brief statement of how it relates to your overall research aims (see note 3) (max 150 words)

N/A

Please provide details of any previous funded extension, tuition-free extension or non-medical Covid-related leave of absence approved since March 2020

N/A

Note 1. This information could form a basis for discussion at the viva examination and give Examiners additional means to assess the volume and standard of the work completed. Detailed information could be included in a future work section in the thesis itself.

Note 2. For example, ill health or additional caring responsibilities. Additional difficulty related to an underlying disability, returned to clinical service, or has worked in a voluntary capacity for Covid-related research. These data could contextualise the judgement made by Examiners as to the most appropriate outcome.

Note 3. If in doubt, consult with your supervisor and Departmental PGR Lead.

Declaration

I hereby declare that all work presented within this these has not been previously submitted for any academic award at this or any other institution. All work submitted is my own, unless otherwise stated and has not been plagiarised.

Hannah Jane Gagg

Acknowledgements

Dedication

I would like to dedicate this thesis to my late mother, Debra. Without you, the motivation to pursue this research would not exist. Your memory continues to inspire and drive me forward.

Publications & Manuscripts

Gagg H, Williams ST, Conroy S *et al. Ex-vivo drug screening of surgically resected glioma stem cells to replace murine avatars and provide personalise cancer therapy for glioblastoma patients. F1000Research* 2023, 12:954 (https://f1000research.com/articles/12-954/v2)

Williams ST, Wells G, Conroy S, **Gagg H**, Allen R, Rominiyi O, Helleday T, Hullock K, Pennington CEW, Rantala J, Collis SJ, Danson SJ. *Precision oncology using ex vivo technology: a step towards individualised cancer care?* Expert Rev Mol Med. 2022 Oct 3;24:e39. Doi: 10.1017/erm.2022.32. PMID: 36184897; PMCID: PMC9884776.

List of Presentations

Talk – British Neuro-Oncology Society (BNOS) Annual Meeting (Manchester, UK, March 2023) – Hannah Gagg, Sophie T. Williams, Samantha Conroy, Katie N. Myers, Connor McGarrity-Cottrell, Callum Jones, Thomas Helleday, Rantala J, Ola Rominiyi, Sarah J. Danson, Spencer J. Collis[1] and Greg Wells. ***Development of GliExP; a high-throughput ex vivo drug screening platform for glioblastoma***

Poster talk – World Federation of Neuro-Oncology Societies (Seoul, South Korea, March 2022) – F1286 – Hannah Gagg, Sophie Williams, Richard Allen, Samantha Conroy, Ola Rominiyi, Greg Wells, Juha Rantala, Sarah Danson, Thomas Helleday, Spencer Collis**. *Ex vivo-led drug discovery in glioblastoma***

Talk – NC3R Summer School Research Event (June 2021) – Hannah Gagg, Sophie Williams, Richard Allen, Samantha Conroy, Ola Rominiyi, Greg Wells, Juha Rantala, Sarah Danson, Thomas Helleday, Spencer Collis**. *Ex-vivo drug screening using human tissue to personalise cancer therapy and replace murine avatars.***

Contents

List of Figures

List of Tables

List of equations

Abbreviations

2-HG – 2-hydroxyglutarate

5-ALA – 5-aminolevulinic acid

AIC – 4-amino-5-imidazole-carboxamide

AML - Acute myeloid leukaemia

APE1 – AP endonuclease 1

ATCC – American Type Culture Collection

ATM – Ataxia talengiectasia mutated

ATR – Ataxia talengiectasia and rad-3 related

ATRX – ATP-dependent helicase

AUC – Area under curve

BBB – Blood brain barrier

BER – Base excision repair

BME – Basement membrane extract

BSA – Bovine serum albumin

CD133 – Prominin-1

CD7 – Cell discoverer 7

Cdk – Cyclin dependent kinase

CDKN2A – Cyclin dependent kinase 2A

CDKN2B – Cyclin depdendent kinase 2B

CE – Conformité Européenne

CHK1 – Checkpoint kinase 1

CHK2 – Checkpoint kinase 2

CML – Chronic myloid leukemia

CNS – Central nervous system

COV – Coefficient of variation

CRISPR – Clustered Regularly Interspaced Short Palindromic Repeats

CSC – Cancer stem cell

CT – Computed tomography

CTG – CellTiter-Glo

DAXX – Death domain-associated protein

DDR – DNA damage response

DDR – DNA damage response

DDRi – DNA damage response inhibitor

DIPG – Diffuse intrinsic pontine glioma

D-loop – Displacement loop

DMEM – Dulbecco's modified eagle medium

DMSO – Dimethylsulfoxide

DNA-PK – DNA dependent protein kinase

DSB – Double strand breaks

ECM – Extracellular matrix

ECS – Embryonic stem cells

EDTA – Ethylenediaminetetraacetic acid

EGF – Epidermal growth factor

EGFR – Epidermal growth factor receptor

ERBB2/3 – Erythroblastic leukaemia viral oncogene homolog

ERK – Extracellular-signal-regulated kinases

FA – Fanconi Anemia

FACS – Fluorescence-activated cell sorting

FBS - Fetal bovine serum

FDA – Food and Drug Administration

FEN1 – Flap Endonuclease 1

FGF – Fibroblast growth factor

FGS – Fluorescence guided surgery

G4 – G-quadruplex

GABBR1 – gamma-aminobutyric acid type B receptor subunit 1

G-CIMP – Glioma CpG island methylator phenotype

GEMM – Genetically engineered mouse models

GEMMs – Genetically engineered mouse models

GFAP – Glial fibrillary acidic protein

GG-NER – Global genome nucleotide excision repair

GSC – Glioma Stem Cells

H3 – Histone Variant 3

HDAC – Histone deacetylase

HGFR – Hepatocyte growth factor receptor

HIF – Hypoxia inducible factor

hPSC – Human pluripotent stem cell

HR – Homologous recombination

HTS – High throughput screening

IC_{50} – Half-maximal inhibitory concentration

ICL – Interstrand crosslinks

IDH – Isocitrate dehydrogenase

IDL – Insertion deletion loops

IF – Immunofluorescence

IGFR-1 – Insulin-like growth factor receptor

IHC – Immunohistochemistry

IMS – industrial methylated spirit

iPSC – Induced pluripotenet stem cell

IQR – Interquartile Range

IR – Ionising radiation

KAP1 – Krab associated protein 1

LIG3 – DNA ligase 3

LOH – Loss of heterozygosity

LP – Long patch

MAD – Median absolute deviation

MAPK – Mitogen activated protein kinase

MDT – Multidisciplinary team

MEM – Minimum essential medium

MGMT – O-6-methylguanine-DNA methyltransferase

MMR – Mismatch repair

MPBTP – Minderoo Precision Brain Tumour Programme

MRI – magnetic resonance imaging

MTIC - 5-(3-methyltriazole-1-yl)imidazole-4-carbox-amide

MTT – 2,5-diphenyl-2h-tetrazolium bromide

NAD – Nicotinamide adenine dinucleotide

NBS1 – Nibrin / 24ijmegen breakage syndrome 1

NCAM – Neural adhesion molecule

NCCTG -North Central Cancer Treatment Group

NCI-MATCH – Molecular Analysis for Therapy Choice

NEFL – Neurofilament light polypeptide

NER – Nucleotide Excision Repair

NF1 – Neurofibromatosis 1

NGS – Next-Generation Sequencing

NHEJ – Non-homologous end joining

NHS – National Health Service

NICE – National Institute for Health and Care Excellence

NMN – Nicotinamaide mononucleotide

NOS – Not otherwise specified

NRH – Dihydronicotinamide riboside

NSC – Neural stem cell

NSCLC – Non-small cell lung cancer

NTRK – Neurotrophic tyrosine receptor kinase

O6-MG – O^6-Methylguanine

OLIG2 – Oligodendrocyte transcription factor – 2

OPC – Oligodendrocyte precursor cell

OS – Overall survival

PARP1 – Poly ADP-ribose polymerase 1

PBS – Phosphate-buffered saline

PCAM1 – Platelet endothelial cell adhesion molecule (CD31)

PCNA – Proliferating cell nuclear antigen

PD – Pharmacodynamic

PDGFRA – Platelet derived growth factor receptor a

PDX – Patient derived xenograft

PFA – Paraformaldehyde

PFS – Progression-free survival

PI3K – Phosphoinositide 3-kinases

PIP$_2$ – Phosphatidynositol-4,5-bisphosphate

PIP$_3$ – Phosphatidynositol-4,5-trisphosphate

PK – Pharmacokinetic

Polβ – DNA polymerase beta

PpIX – Protoporphyrin IX

PTEN – Phosphatase and tensin homolog

RAF – Rapidly accelerated fibrosarcoma

RAS – Rat Sarcoma

Rb – Retionoblastoma protein

RCF – Relative centrifugal force

RFC-1 – Replication factor X subunit 1

RNA-seq – Whole transcriptome sequencing

ROS – Reactive oxygen species

ROS1 – Proto-oncogene tyrosine kinase

RT – Radiotherapy

RTK – Receptor tyrosine kinase

SoC – Standard-of-care

SOX2 – Sex Determining Region Y – Box 2

SP – Short patch

SSB – Single Strand Break (DNA)

SVZ – Subventricular zone

TCGA – The Cancer Genome Atlas

TC-NER – Transcription coupled nucleotide excision repair

TERT – Telomerase reverse transcriptase

TET – Ten eleven translocation

TMZ – Temozolomide

TOP2A – DNA Topoisomerases II

TP53 – Tumour suppressor tumour protein p53

TTFields – Tumour Treating Fields

UV – Ultraviolet

VEGF – Vascular endothelial growth factor

VEGFR – Vascular endothelial growth factor receptor

WES – Whole exome sequencing

WGS – Whole genome sequencing

WHO – World Health Organisation

XRCC1 – X-Ray repair cross complementing 1

α-KG – α-ketoglutarate

α-KGDD – α-KG-dependent dioxygenases

Chapter 1 – Introduction

1.1 Introduction to Glioblastoma

1.1.1 What is glioblastoma?

Every year in the UK alone approximately 5,400 individuals lose their lives to brain tumours. Among all cancer types, brain cancer demonstrates the most significant reduction in life expectancy, averaging 20 years (*Deaths registered in England and Wales - Office for National Statistics*, 2019). Classified by the World Health Organization (WHO), adult diffuse gliomas are graded into grade II and III astrocytic tumours, grade II and III oligodendrogliomas and grade IV glioblastomas (Louis *et al.*, 2016). Glioblastoma is a grade IV astrocytoma, which occurs within the brain or spinal cord originating from glial cells, that provide support and protection to nerve cells. Glioblastoma is the most common and lethal primary brain tumour found in adults, and prognosis is poor, with less than 5% of patients survive more than 5 years following diagnosis (Verhaak *et al.*, 2010). Standard-of-care (SoC) therapy for glioblastoma includes surgical removal (de-bulking) of the tumour, followed by radiotherapy (RT) and chemotherapy with the oral alkylating agent temozolomide (TMZ). TMZ was approved as a SoC treatment in 2005 after it was found to improve the median survival of patients by 2.5 months (Stupp *et al.*, 2005). Despite decades of research and medical advances, the bleak prognosis for glioblastoma patients has seen little improvement over the past four decades. Consequently, there is a pressing need for innovative strategies to enhance treatment outcomes for these patients.

1.1.2 Diagnosis of glioblastoma

Common symptoms of a brain tumour include headaches, seizures, nausea, vomiting, drowsiness, vision and speech impairments, mental and behavioural changes and weakness or paralysis on one side of the body (Ozawa *et al.*, 2019). If a patient is experiencing a persistence or combinations of these symptoms a health care provider will refer the patient to a specialist such as a neurologist, who will confirm using several tests which may include neurological exam which involves testing your vision, hearing, alertness, muscle strength, reflexes and coordination. Some brain tumours can be detected via an eye test, due to swelling of the optic disk or nerve.

If a brain tumour is suspected, patients will be referred for a head scan. Head computed tomography (CT) scans are commonly used if an emergency scan is required to determine the cause of symptoms, or when patients are unable to have an magnetic resonance imaging (MRI) scan due to the presence of a pacemaker (Omuro and DeAngelis, 2013). CT scans are also useful for whole body imaging to check for cancer in other parts of the body, which can help determine whether the brain tumour has metastasised from a separate malignancy. The gold standard for imaging suspected brain tumours is an MRI scan, as they are more suitable at showing the complexity and heterogeneity of tumour, including whether the tumour is low or high grade (Hanif *et al.*, 2017). If the MRI or CT scan is suggestive of a brain tumour the patient will then be referred to a neuro-oncology multidisciplinary team (MDT) consisting of surgical, medical and radiation oncologists. This team is responsible for deciding on a suitable treatment plan based on the type, size and location of the tumour alongside overall health of the patient.

Often the first stage of treatment regimen would be surgical de-bulking of the tumour, however sometimes due to the location of the tumour and the health of the patient, this is not possible. In these cases, the patient will undergo a hollow needle biopsy under general aesthetic, to obtain a small sample of tumour cells. Testing of these tumours or biopsies permits phenotypic and genotypic analysis which can help to guide a suitable treatment plan. This is particularly important as there have been reports of higher-grade glioblastoma mimicking meningiomas on MRI scans, despite pathology revealing glioblastoma (Patel *et al.*, 2016).

1.1.3 Primary vs Secondary Gliomas

Glioblastoma classification often considers its clinical progression, primarily distinguishing between primary and secondary forms. Primary glioblastoma represents the more prevalent of the two and is classified as de novo due to its rapid onset, lack of evidence for a less malignant precursor lesion, and its tendency to affect predominantly older patients. Primary glioblastomas are genetically characterized by epidermal growth factor receptor (*EGFR*) amplification, tumour suppressor phosphatase tensin homolog (*PTEN*) gene mutations alongside absence of isocitrate dehydrogenase (*IDH*) mutations (Ohgaki *et al.*, 2004). A

population-based study completed in Switzerland determined the frequency of major genetic alterations in primary glioblastoma mainly affect the elderly and were genetically characterised by loss of heterozygosity 10q (LOH) (70%), *EGFR* amplification (36%), tumour suppressor tumour protein p53 (*TP53*) gene mutations (25%), p16^{INK4a} homozygous deletion (31%) and *PTEN* mutations (25%). In contrast, secondary glioblastomas are less common (~5%); they show evidence of progression from a lower grade pre-existing astrocytoma (grade II or III), They typically occur in younger patients and are associated with a more favourable prognosis (Nicolaidis, 2015). In the same population based study secondary glioblastomas were characterised by *TP53* mutations (65%), frequent LOH 10q (63%) and loss of *EGFR* amplification (8%) (Ohgaki *et al.*, 2004).

1.1.4 Proliferative, Mesenchymal & Proneural sub-Classification

Initially Phillips *et al* (2006) conducted an exploration and characterisation of glioblastoma, categorising into three distinct subtypes known as proliferative, mesenchymal and proneural. They achieved this by identifying specific gene expression patterns using microarray DNA analysis. Among these subtypes, the proneural subtype exhibited the closest resemblance to normal brain tissue, demonstrating the expression of neuron-associated markers such as neural cell adhesion molecule (*NCAM*) and gamma-aminobutyric acid type B (*GABBR1*). Prognosis was notably improved in cases where this subtype was more abundant, which was more common among younger patients. The mesenchymal subtype, on the other hand, was characterised by the overexpression of vascular endothelial growth factor (*VEGF*), vascular endothelial growth factor receptor 2 (*VEGFR2*) and endothelial marker platelet endothelial cell adhesion molecule (*PECAM1*), all of which play a role in the formation of new blood vessels. In contrast, the proliferative subtype exhibited gene expression patterns associated with cell proliferation, including markers such as DNA topoisomerase II alpha (*TOP2A*) and proliferating cell nuclear antigen (*PCNA*). Patients with glioblastomas falling into either the proliferative or mesenchymal subtypes experienced the least favourable survival outcomes (Phillips *et al.*, 2006).

1.1.5 Verhaak Classification

Previous studies initially grouped subtypes based on the most common genetic abnormalities. However, it became evident that additional heterogeneity existed within these groups, highlighting the necessity for more advanced profiling methods on a larger scale. Genomic profiling data published by The Cancer Genome Atlas Network (TCGA) identified recurring gene expression abnormalities involving *EGFR*, neurofibromin 1 (*NF1*), platelet derived growth factor receptor (*PDGFR)*, and *IDH1*. This led to the classification of glioblastoma into four distinct subtypes: Proneural, Classical, Mesenchymal, and what was initially referred to as the Neural subtype (Verhaak *et al.*, 2010), as detailed below:

- ***Proneural subtype:*** Predominately found in younger patients, characterized by *PDGFRA* abnormalities, *IDH1* and *TP53* mutations. Displays similarities between secondary glioblastoma and has the most favourable prognosis of all 4 subtypes.

- ***Classical subtype:*** Marked by increased *EGFR* amplification due to copy number increase, alongside loss of *PTEN* and cyclin-dependent kinase inhibitor 2A (*CDKN2A*). It often involves amplification of chromosome 7 and loss of chromosome 10, inactivation of retinoblastoma-associated protein (Rb), and notably lacks TP53 mutations, which are the most common in glioblastoma.

- ***Mesenchymal subtype:*** Demonstrates mutations and/or loss of tutor suppressor genes *TP53*, *NF1*, and *CDKN2A*. It exhibits increased necrosis and inflammation and is associated with the poorest prognosis among the four subtypes (Colman *et al.*, 2010).

- ***Neural subtype***: Initially considered to resemble normal brain tissue in terms of gene expression of nerve associated genes neurofilament light polypeptide (*NEFL*) and *GABRA1*. However, it was later discovered to be an artifact due to non-tumour cell contamination of cancer specimens, revealing that there are only three, rather than four, distinct forms of glioblastoma (Sidaway, 2017; Wang *et al.*, 2017).

While the classification of glioblastoma into these subtypes theoretically offers a path toward more personalized and effective treatments, there is still significant overlap among the subtypes. Additionally, it is widely accepted within the research community that a substantial degree of heterogeneity persists within these subgroups.

1.1.6 World Health Organisation Update 2016

Recent advancements in the classification of glioblastoma have emerged after the publication of 'The 2016 World Health Organization Classification of Tumours of the Central Nervous System'. This represents the fourth revision since its inception nearly a century ago in 1926, originally formulated by Bailey & Cushing. Before this revision, glioblastomas were primarily categorized based on their histological characteristics, relying on microscopic appearances after immunohistochemical staining. However, the current approach integrates multiple methods to extract the maximum amount of information about the tumour. It combines molecular testing for diagnostic biomarkers, such as IDH, immunohistochemistry (IHC) testing for ATP-dependent helicase (*ATRX*) loss, alongside histological tumour classification and WHO grading, as depicted in figure 1.1 (Louis *et al.*, 2016; Komori, 2017).
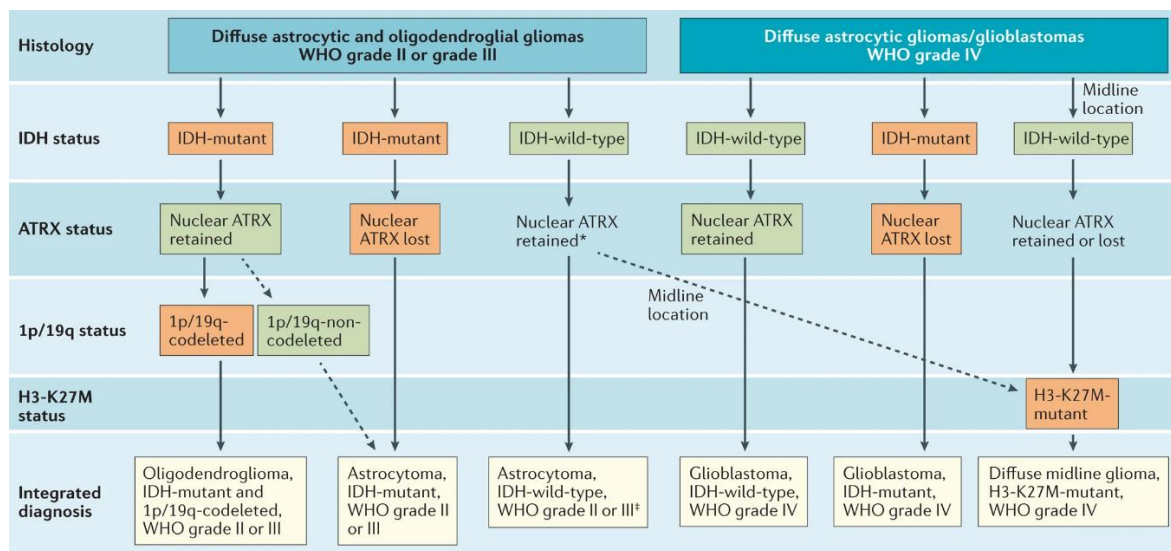
Figure 1.1 - Integrated histological and molecular classification of diffuse gliomas according to the 2016 WHO classification of tumours of the central nervous system - Initially tumours are histologically graded into grade II & III diffuse astrocytic, oligodendroglioma gliomas or grade IV astrocytic gliomas & glioblastoma. Tumours are next graded based on their *IDH1/2* mutation status. Immunohistochemistry is used to determine the *ATRX* expression, which is a nuclear transcriptional regulator, its mutation leads to loss of function. Following this, patients with both IDH-mutant status but retained *ATRX* are further classified by a test for 1p/19q codeletion. IDH wildtype gliomas found in the midline (thalamus, brainstem, or spinal cord) are further classified through H3-K27M mutations. This integrated layering

1.1.7 World Health Organisation Update 2021

Following the previous 2016 update, astrocytic glioblastomas were graded into grade 4 *IDH* mutant and *IDH* wild-type tumours. However, the most recent 2021 revision of the WHO classification of central nervous system (CNS) tumours has introduced significant changes in the nomenclature of tumours displaying *IDH* and *H3* mutations. The updated classification flow diagram for the 2021 update is depicted by figure 1.2. Tumours harbouring these mutations will no longer be classified as glioblastoma multiforme, instead classified as diffuse astrocytoma, IDH mutant grade 4. Additionally, updates no longer allow the use of not otherwise specified (NOS) when reporting glioblastoma. This reclassification of these *IDH* mutant tumours will lead to a drastic change in the average age and sex demographic of the disease, as the majority of mutant tumours are more common in young people under 50 and also within females (Bleeker, Molenaar and Leenstra, 2012).
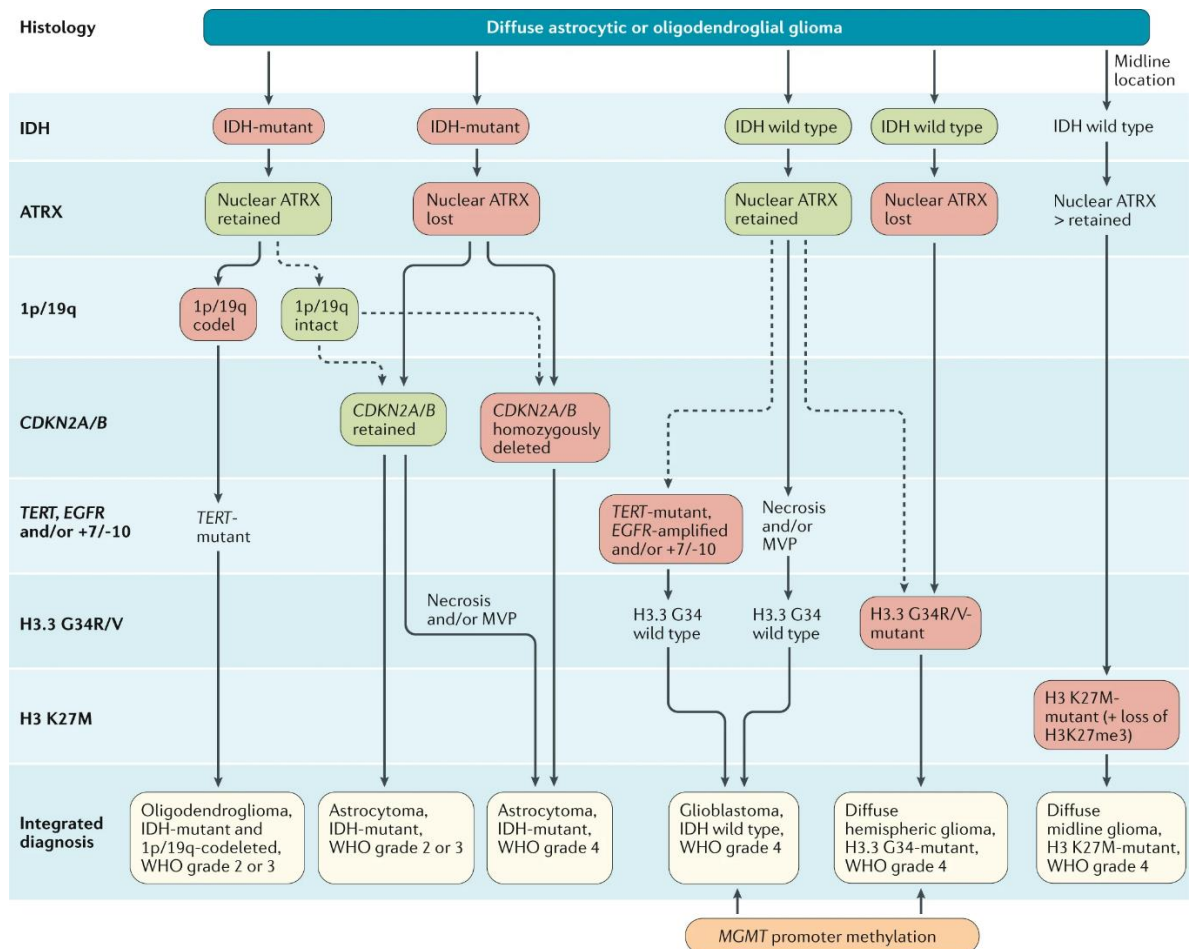
Figure 1.2 - Integrated histological and molecular classification of diffuse gliomas according to the 2021 WHO classification of tumours of the central nervous system – Routine immunohistochemical evaluation of biopsy samples from patients with diffuse gliomas involves the assessment of R132H-mutant IDH1 and the absence of nuclear ATRX. For patients over 55 years with histologically typical glioblastoma and specific clinical characteristics, the absence of IDH1 R132H immunopositivity is adequate to classify the tumour as IDH-wild-type glioblastoma. In all other cases of diffuse gliomas, the absence of IDH1 R132H immunopositivity should prompt IDH1 and IDH2 DNA sequencing to identify non-canonical mutations. IDH-wild-type diffuse astrocytic gliomas without microvascular proliferation or necrosis should be tested for EGFR amplification, TERT promoter mutation, and a +7/−10 cytogenetic signature, which are molecular characteristics of IDH-wild-type glioblastomas. Additionally, the presence of histone H3.3 G34R/V mutations should be determined through immunohistochemistry or DNA sequencing to identify H3.3 G34-mutant diffuse hemispheric gliomas, especially in young patients with IDH-wild-type gliomas, such as those under 50 years of age with nuclear ATRX loss in tumour cells. For diffuse gliomas located in the thalamus, brainstem, or spinal cord, assessment for histone H3 K27M mutations and loss of nuclear K27-trimethylated histone H3 (H3K27me3) is essential to identify H3 K27M-mutant diffuse midline gliomas. The figure highlights the presence and absence of the most diagnostically relevant molecular alterations for each tumour type with red and green boxes, including microvascular proliferation (MVP). Figure adapted from Weller *et al* (2020), copyright permissions obtained from publisher (Open Access).

1.1.8 Malignant transformation

A study which investigated the North Central Cancer Treatment Group (NCCTG) database investigated tissues taken at time of initial diagnosis and at recurrence. Tissues which

progressed from low (WHO grade II) to high (WHO grade III-IV) included 45% low grade oligodendrogliomas with median overall survival (OS) 8.8 years, 70% low grade oligoastrocytomas, median OS 4.4 years and 74% low grade astrocytomas, median OS 3.1 years. The mean time to recurrence was also estimated, showing patients with glioblastoma at initial and recurrence with smallest timepoint 1.1 ± 1.1 years, those with non- glioblastoma at initial and glioblastoma at recurrence 2.9 ± 1.8 years and finally those with non-glioblastoma at both time points 4.0 ± 2.9 years (Jaeckle *et al.*, 2011).

1.2 Diagnostic and therapeutic biomarkers of Glioblastoma

Diagnostic and therapeutic biomarkers play a vital role in glioblastoma management. They allow for precise tumour classification and the identification of subtypes with distinct biological features. Moreover, these biomarkers provide essential prognostic information, helping to predict disease progression and patient survival. By understanding the genetic and molecular characteristics of glioblastoma, healthcare providers can better inform patients about their individual prognosis and expected treatment responses.

1.2.1 *MGMT* Methylation

The *MGMT* gene encodes for the O-6 methylguanine-DNA transferase (MGMT) DNA repair enzyme, which plays a crucial role in effectively protecting cells against alkylating agents such as TMZ and lomustine. MGMT is 207 amino acids long and consists of a highly conserved proline-cysteine-histidine-arginine sequence, with active site located at the c-terminus (Bai *et al.*, 2023). It restores DNA alkylation damage (*O6*-MG or other *O6*-AlkylG adducts) via the 'Glu172-His146-water-Cys145' hydrogen bond network, transferring alkyl groups from DNA to the Cys145 residue (figure 1.3) (Hegi *et al.*, 2005; Tubbs, Pegg and Tainer, 2007). This reaction is irreversible and results in a conformational change of MGMT which causes its degradation through the ubiquitin-proteasome system (Srivenugopal *et al.*, 1996).
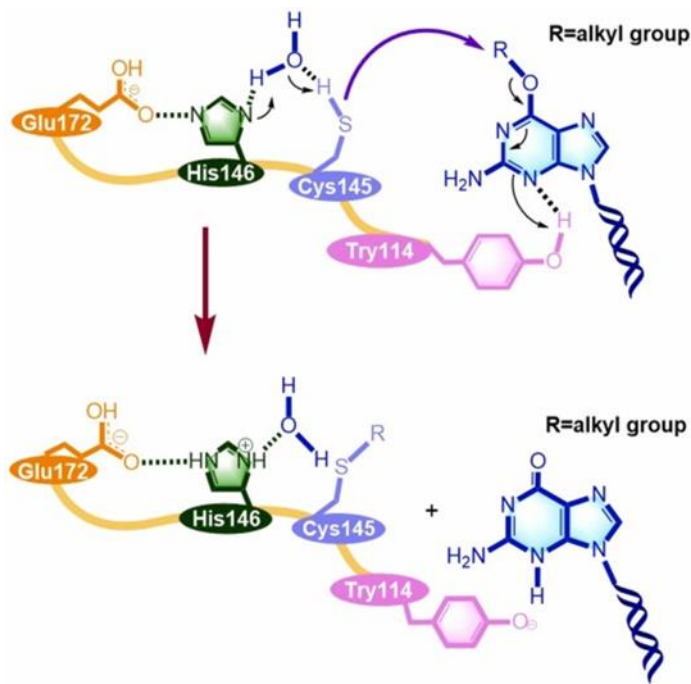
Figure 1.3 – MGMT repair mechanism.

In the presence of water His146 can deprotonate Cys145. This then results in nucleophilic attack of O6-alkyl by Cys145 residue, resulting in repair of guanine and protonation at N3 position mediated by Try114 residue. Figure adapted from Bai *et al* (2023), copyright permissions obtained from publisher (Open Access).

The *MGMT* gene is often rendered inactive through epigenetic silencing caused by promoter methylation, which, in turn, permits unaddressed chemotherapy-induced damage to instigate cytotoxicity and apoptosis (Liu and Gerson, 1996; Ochs and Kaina, 2000). At present, treatment protocols uniformly prescribe all glioblastoma patients with TMZ and/or IR irrespective of *MGMT* gene status. In a randomised trial evaluating 206 tumours over half of the patients (~55%) did not exhibit *MGMT* promoter methylation. Whilst it is established that patients with a unmethylated *MGMT* promoter do not statistically benefit from TMZ treatment, the treatment remains unchanged irrespective of survival benefit. In this study patients with methylated *MGMT* promoter saw a 6.4-month survival benefit from having TMZ alongside RT (Hegi *et al.*, 2005). Within clinical trials it has been deemed acceptable to remove TMZ from the treatment regimes in unmethylated *MGMT* patients, provided that alternative treatment options are offered to patients (Wick *et al.*, 2016; Fulton *et al.*, 2018). Ex vivo drug screening has emerged as a potential approach for guiding these "alternative treatment" strategies by identifying patient-specific tumour drug sensitivities.

The most recent 2021 WHO classification has led to *MGMT* gene promoter methylation being the only statistically significant prognostic factor for predicting patient response to TMZ therapy and survival (Weller *et al.*, 2020). A recent study investigated the survival of a cohort of 58 *MGMT* unmethylated and methylated patients', revealing a mean survival of *MGMT*

methylated tumours being 15.7 months versus 4.7 months in unmethylated *MGMT* tumours, which was statistically significant (Stoyanov *et al.*, 2022). These findings corroborate a prior study involving a population of 206 patients, which also found a significant difference in median OS, with *MGMT* methylated patients surviving for 18.2 months compared to 12.2 months for unmethylated patients (Hegi *et al.*, 2005). Despite this knowledge all patients still receive TMZ treatment, irrespective of their *MGMT* status and clinical benefit.

1.2.2 1p/19q co-deletion

The chromosome arms 1p and 19q contains genes associated with DNA repair, spindle checkpoint function, apoptosis, multiple microRNAs, WNT signalling pathway, tumour suppression and antioxidant activities (Payne *et al.*, 2011; Li *et al.*, 2015). Whilst primarily being associated with oligodendrogliomas, the co-deletion of short arm of chromosome 1 and long arm of chromosome 19 is essential for distinguishing between different glioblastoma subtypes (Jeuken, Von Deimling and Wesseling, 2004). Patients who harbour both this deletion and an IDH mutation have the most favourable clinical outcome, with TGCA analysis of clinical data showed this combination had a median OS of 8 years, versus 6.3 years in patients with only IDH mutations (DJ *et al.*, 2015), although the underlying molecular mechanisms of this relationship are currently not determined.

1.2.3 Isocitrate dehydrogenase

Humans possess three isocitrate dehydrogenase enzymes (IDH1/2/3) which catalyse the oxidative decarboxylation of isocitrate into α-ketoglutarate (α-KG) during the citric acid cycle, summarised by figure 1.4 (Jennings, Minard and Mcalister-Henn, 1997; Yan *et al.*, 2009). IDH2 and IDH3 enzymes are located in the mitochondria whilst IDH1 is located in the cytosol and peroxisome (Dang, Yen and Attar, 2016). During this decarboxylation process, NADP+ is reduced to NADPH, which serves as the main reducing power donor for the vast majority of reactive oxygen species (ROS) detoxifying enzymes, thus important in oxidative stress resistance (Fernandez-Marcos and Nóbrega-Pereira, 2016). Additionally α-KG acts as a cofactor, for the main removal pathway of methyl groups on DNA (oxidative demethylation), which is performed by enzymes known as Fe(II)/ α-KG-dependent dioxygenases (α-KGDD) (Kuznetsov, Kanazhevskaya and Fedorova, 2021). These include enzymes such as; ten-eleven

translocation (TET) family 5-methylcytosine hydroxylases and the Jumonji-C-domain-containing histone-lysine demethylases, important in epigenetic regulation (Figueroa *et al.*, 2010).

Mutations to these IDH enzymes occur mainly in lower grade II/III astrocytic or oligodendroglioma cases, in higher grade gliomas these mutations are mainly found in secondary gliomas which account for 73% of clinical cases, it is very rare to see *IDH* mutations in primary gliomas (3.7.%) (Nobusawa *et al.*, 2009; Louis *et al.*, 2016). The mutations are commonly heterozygous missense mutation at residue R132 of IDH1 replacing arginine with histidine, or less commonly at the R172 residue in IDH2 (Yan *et al.*, 2009). The majority of *IDH* mutations reported are heterozygous, with cancer cells retaining one wild-type copy of the relevant *IDH1/2* allele, however there is increasing evidence of rare homozygous mutation in a number of glioblastoma cases in the literature (Gupta *et al.*, 2013; Jin *et al.*, 2013; Stancheva *et al.*, 2014). Following the updated 2021 WHO classification of CNS tumours, IDH-mutant tumours are no longer classified at glioblastoma but instead as diffuse astrocytoma, IDH mutant grade IV.
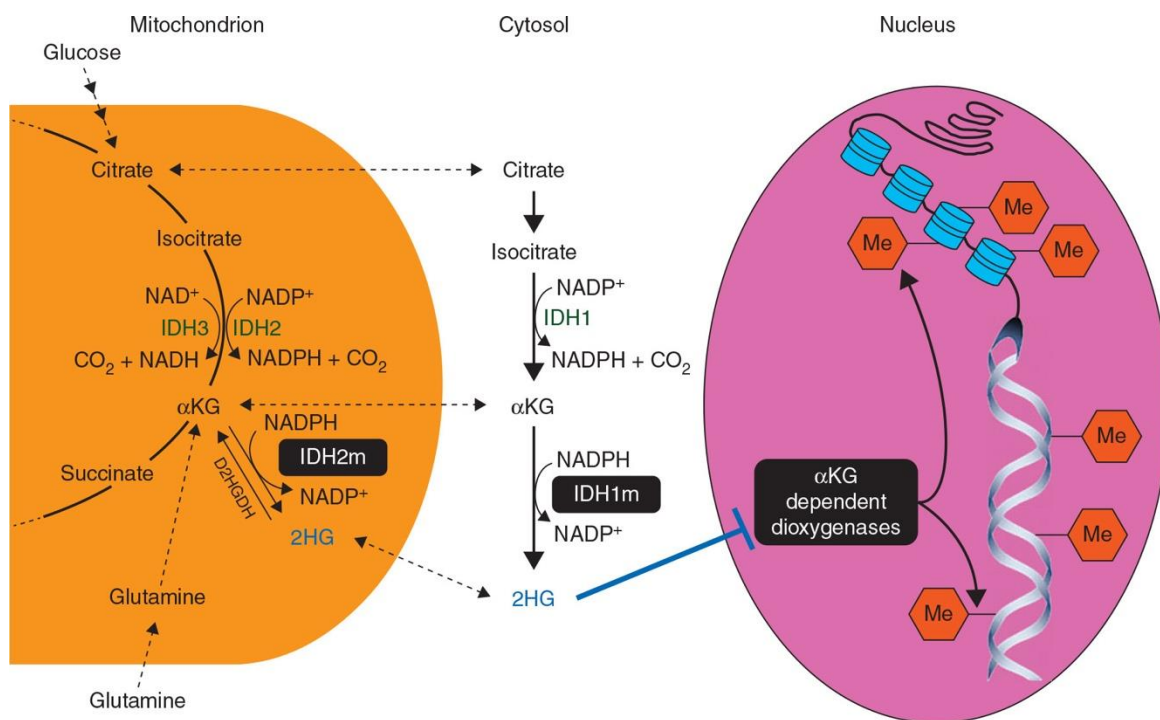
Figure 1.4 - Wild-type and mutant activity of IDH - During normal cellular function metabolic IDH enzymes are key players within the citric acid cycle, converting isocitrate into α-KG via oxidative decarboxylation. Within the mitochondria this is performed via IDH2/3 and within the cytosol via IDH1 enzymes. When IDH is mutated, this leads to overproduction of 2-HG via conversion of α-KG, these both

In IDH-mutant cells, the mutated enzyme converts a-KG into novel onco-metabolite 2-hydroxyglutarate (2-HG), levels of this metabolite can accumulate to extremely high levels of ~5-35μmol/g in glioblastoma (Dang *et al.*, 2009). The only difference between 2-HG and α-KG is the oxidation state at carbon-2 position, thus structural similarities result in competitive inhibition of α-KGDDs by 2-HG (Pirozzi and Yan, 2021). Cells harbouring *IDH* mutations undergo substantial metabolic reprogramming; other metabolites such as branched chain amino acids, glutamine and glutamate serve to compensate the loss in cellular metabolism. Mutant cells are more sensitive to inhibition of glutaminase, highlighting the dependency on other metabolic processes such as glutaminolysis to maintain metabolic homeostasis (Seltzer *et al.*, 2010). Specifically to glioblastoma, *IDH* mutations can lead to CpG island hypermethylation, a common phenotype often referred to as glioma CpG island methylator phenotype (G-CIMP) (Noushmehr *et al.*, 2010; Cohen, Holmen and Colman, 2013). These G-CIMP tumours often belong to the proneural subtype, which harbour the most favourable clinical outcome (Noushmehr *et al.*, 2010).

IHD1 mutations in particular are usually an indication of early tumorigenesis events and improved prognosis of the patient (Stieber, Abdul Rahim and Niclou, 2011). Williams et al (2008) completed a genome wide analysis on 22 human tumour samples to identify genetic alterations in glioblastoma, the mutation status of the *IDH1* gene was shown to correlate with the younger age of the patient and an improved prognosis; patients' median survival with mutated *IDH1* gene was 3.8 years compared to 1.1 years for patients with wild-type *IDH1* (Williams *et al.*, 2008). The enhanced survival shown in these IDH mutated gliomas may be a result of the 2-HG accumulation inhibiting homologous recombination (HR) DNA repair, inducing "BRCAness" phenotype. This phenotype corroborates increased dependency on alternative DNA damage response mechanisms such as PARP-guided base excision repair (BER) to maintain genomic integrity, provoking vulnerability to drugs targeting these other DNA repair pathways such as PARP and ATR inhibitors (Sulkowski *et al.*, 2017).

1.2.4 ATRX loss

ATRX is a transcriptional regulator belonging to the SWI/SNF family of chromatin remodelling proteins. ATRX is one of the most commonly mutated tumour suppressor genes in cancer and within glioblastoma it is the third most mutated gene (Aguilera and López-Contreras, 2023). Within glioblastoma, mutations within the ATRX chromatin modelling pathway are most common within adolescents and young adults aged between 10-30 (Schwartzentruber, Korshunov, X.-Y. Liu, *et al.*, 2012). In adults aged >30 the mutation of ATRX it is most commonly associated with lower grade (WHO II and III) and secondary glioblastomas, it is less prevalent in primary higher grade glioblastomas (Jiao *et al.*, 2012). The mutation results in the loss of expression for this chromatin remodelling factor. Within adult gliomas the mutation seems to be also associated with both *IDH1* and *TP53* mutations (Nandakumar, Mansouri and Das, 2017), whereas in paediatric cancers it is commonly associated with histone H3.3 and *TP53* mutations (Schwartzentruber, Korshunov, X. Y. Liu, *et al.*, 2012; Koschmann *et al.*, 2016). Research suggests ATRX plays a central role within the maintenance of chromatin state, gene expression and DNA damage, its multiple roles are summarised in Figure **1.5**.
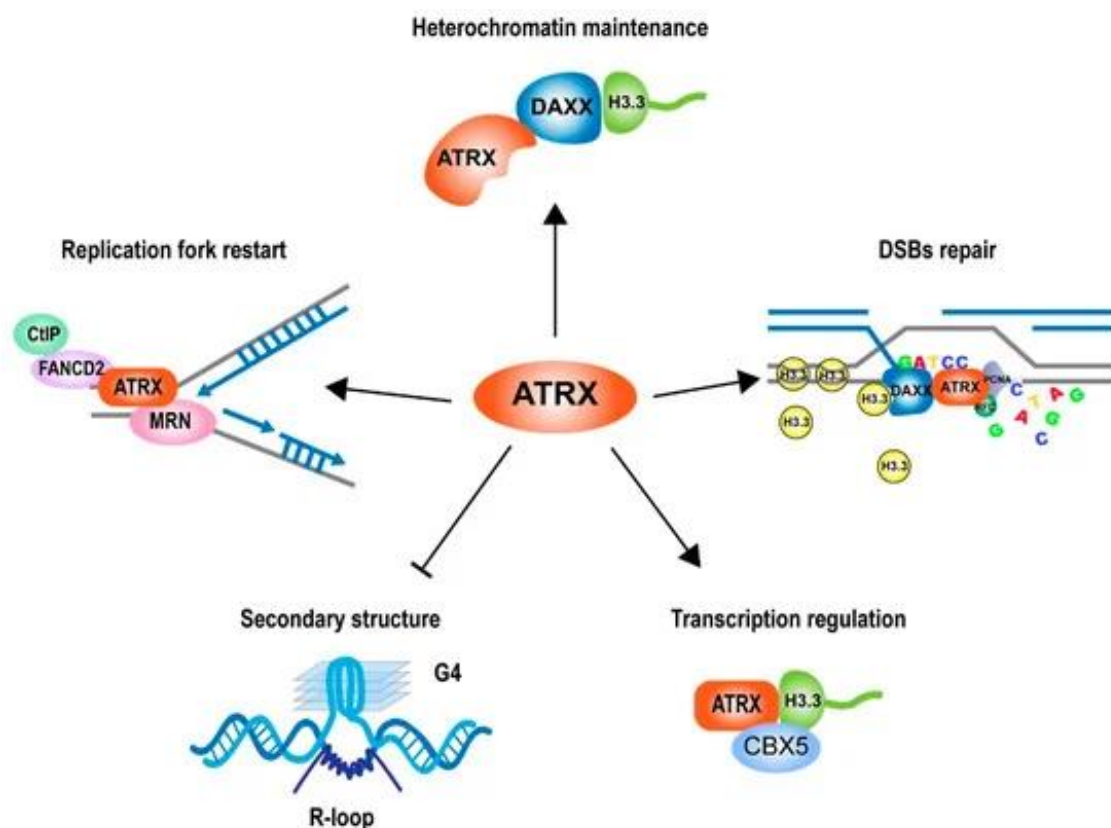
One crucial role of ATRX involves its depositing of H3.3 onto telomeres, pericentric heterochromatin and other repetitive DNA sites, it does this together with chaperone protein, death domain associated protein (DAXX), forming a histone chaperone complex (Goldberg *et al.*, 2010; Garbarino *et al.*, 2021). In eukaryotes, DNA is organised via wrapping around 'spool' like structures known as nucleosomes. These nucleosomes are histone octamers composed of two copies of four core histones H2A, H2B, H3 and H4, which are wrapped 1.7 times by 147 base pairs of DNA (Luger *et al.*, 1997). The role of these histone proteins is to package DNA and regulate accessibility of genes. H3.3 is the most common variant of histone H3, it differs in structure by only 4-5 amino acids, this subtle change allows for the recognition of H3.3 by variant specific chaperone DAXX (Liu *et al.*, 2012). Its difference in structure confers altered nucleosome stability resulting in alterations in the wrapping of DNA.

ATRX also plays an essential role DNA repair synthesis and exchange of sister chromatids (Chapman, Taylor and Boulton, 2012). During HR, following 5' strand resection, RAD51 is loaded onto the single stranded ends of damaged DNA, allowing for invasion of the sister chromatid to find the complimentary DNA strand. Research suggests ATRX-dependent H3.3 deposition occurs following successful RAD51 homology search, which is thought to overcome topological constraints at the moving displacement loop (D-loop), as unwinding of the DNA can lead to torsional stress (Juhá Sz *et al.*, 2018). ATRX then interacts with PCNA and replication factor X subunit 1 (RFC-1) which are essential for DNA repair synthesis during HR.

Initially ATRX function was found to protect against hydroxyurea induced stalled replication forks and the promotion of replication fork restart (Leung *et al.*, 2013; Clynes *et al.*, 2014; Huh *et al.*, 2016). The Fanconi anaemia (FA) pathway, is activated in response to interstrand crosslinks (ICL) inducing agents such as cisplatin, and mitomycin c. More recent evidence suggests ATRX also interacts with FANCD2 to promote HR dependent replication fork restart as depicted by figure 1.5. Studies show both ATRX and FANCD2 are required for the

recruitment of HR factors such as CtBP interacting protein and also promote MRE11 exonuclease dependent fork restart (Raghunandan *et al.*, 2020).

ATRX also prevents replication stress by resolving non-B form DNA structures called G-quadruplexes (G4) ahead of the replication forks (Teng *et al.*, 2021). G4s arise within high GC rich areas, initially four guanine residues form a G-quartet through cyclic hydrogen bonding these planar G-quartets can then stack upon one another forming large stable four stranded helical structures (Rhodes and Lipps, 2015). These structures prevent replication machinery to proceed along the leading and lagging strand during replication, this in turn leads to replication fork collapse and double stranded DNA breaks (Técher *et al.*, 2017). It is thought that ATRX aids in the replication of these highly stable structures, as ATRX deficient cells and tumours have increased G4 formation, replication stress and DNA damage, this confers increased sensitivity to effects of ionising radiation (IR) and hydroxyurea (Wang *et al.*, 2019), whilst exogenous expression of ATRX in deficient cells decreases the amount of G4 structures and has shown to protect against chemical treatment of G4 stabilisers such as CX-5461 (Xu *et al.*, 2017; Wang *et al.*, 2019).

Depletion of ATRX within cell lines has shown to induce cell cycle defects, inducing lobulated nuclei, intranuclear DNA bridges, poor proliferation, prolonged transition between pro-metaphase and metaphase indicating its role within normal mitotic progression (Ritchie *et al.*, 2008). ATRX-deficient glioblastoma cells show enhanced sensitivity to IR (Koschmann, Lowenstein and Castro, 2016; Koschmann *et al.*, 2017) and DNA damaging and/or repair inhibitors such as WEE1 and PARP. Further analysis has shown ATRX to bind to regulatory elements of checkpoint kinase 1 (CHK1) in glioma cells and loss of ATRX is consistent with loss of cell-cycle regulator CHK1, causing premature release from G2/M checkpoint following RT. The loss of CHK1 and ataxia telangiectasia and Rad3-related kinase (ATR) increases the cells reliance on ataxia telangiectasia mutated (ATM) and checkpoint kinase 2 (CHK2), therefore inhibition of ATM may sensitize ATRX deficient tumours to RT treatment (Qin *et al.*, 2022). The effect of ATRX on the G2/M and G1/S cell cycle checkpoints is depicted below (figure 1.6). Note; DNA damage response/repair pathways are discussed in more detail below (see section 1.6).
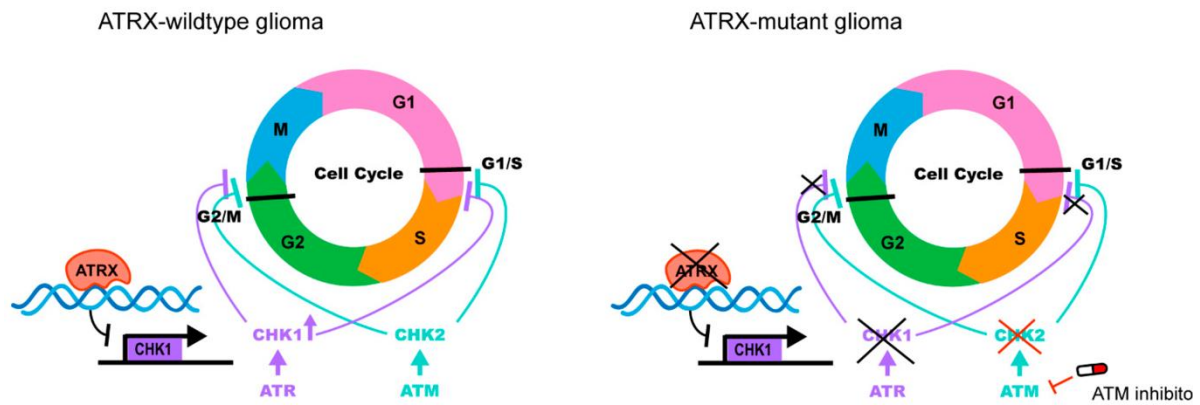
Figure 1.6 – How ATRX indirectly effects cell cycle checkpoints G2/M and G1/S. - ATRX binds to regulatory element on CHK1, this increases transcription of CHK1 resulting in inhibition of M and S phase transition. ATRX deficiency results in reduces levels of CHK1, thus reduced capacity to maintain G2/M checkpoint, which causes an increased reliance on ATM/CHK2, which can be therapeutically targeted (Pang *et al.*, 2023). Copyright permissions obtained from publisher (Open Access).

ATRX-deficiency was assessed within animal glioblastoma models utilizing the Sleeping Beauty transposase system. Mice harbouring both ATRX and p53 loss were compared with p53 loss alone, the former group of mice were found to be more sensitized to DNA damaging agents through an impairment of non-homologous end joining (NHEJ) DNA repair correlating with loss of activated DNA-dependent protein kinase (DNA-PKcs) staining (Koschmann *et al.*, 2016). When left untreated, loss of ATRX increases tumour proliferation and reduces median survival within animal models, this genetic instability however can be targeted therapeutically as it sensitizes glioblastoma tumour cells to DNA damaging agents such as IR. It is thought that ATRX loss causes restricted access to heterochromatin bound NHEJ proteins such as DNA-PKcs.

1.3 Genomic abnormalities of molecular pathways

A previous TGCA study highlighted dysregulation of three core biological pathways in both primary and secondary glioblastomas: RTK/RAS/PI3K signalling (88%), Rb (78%), and tumour protein p53 (87%) (McLendon *et al.*, 2008). The most common genetic aberrations which were observed in glioblastoma *IDH* wild-type tumours were *PTEN* mutation or homozygous deletion, *CDKN2A* and *CDKN2B* homozygous deletion, *TERT*-promoter mutations, chromosomal rearrangements (gain of chromosome 7 and monosomy of chromosome 10), receptor tyrosine kinase (RTK) gene amplifications (commonly *EGFR*) and less common

mutations which involve *TP53*, *NF1*, *PIK3CA* and *PIK3R1*. These will be discussed in more detail below.

1.3.1 p53 pathway

Often called "guardian of the genome", *TP53* is a tumour suppressor gene which encodes protein p53 which plays an important role in regulating genes involved in the cell cycle regulation, cell death and differentiation, DNA repair and neovascularisation. It maintains genome integrity and prevents the proliferation of cells with damaged DNA through inducing cell cycle arrest (checkpoint regulation) and apoptosis, therefore preventing tumorigenesis (Bessette *et al.*, 1992). *TP53* is one of the most commonly deregulated genes in cancer, in glioblastoma specifically 87% of cases studied by TCGA exhibit alterations in p53 signalling pathway and 28-35% contained a mutation or deletion (McLendon *et al.*, 2008; Brennan *et al.*, 2013). With respect to tumour grade, a population based study revealed that 65% of secondary glioblastoma cases had p53 mutations compared to 28% in primary cases (Ohgaki *et al.*, 2004). Mutations within p53 usually disrupt the ability of p53 to bind to DNA or modifying the folding of the DNA-binding domain, therefore altering transcription factor activity, often through gain-of-function mutations.

p53 is activated through a variety of stress signals such as DNA damage, hypoxia, heat/cold shock. The p53 protein transactivates p21 which in turn results in cell cycle arrest in G1 or G2 through p21 inhibitory binding to cyclin-dependent kinase Cdk2/CyclinD, Cdk2/Cyclin E complexes and p53 indirect repression of Cyclin B transcription (Krause *et al.*, 2000; He *et al.*, 2005). Specific mutations of p53 compromise its tumour suppressor functions, resulting in an increased risk of genomic instability (Negrini, Gorgoulis and Halazonetis, 2010). This instability can lead to the initiation and progression of cancer in multiple ways. For instance, some p53 mutations affect the ability to efficiently activate DNA repair mechanisms in response to DNA damage. Mutant p53 can also lose its ability to activate cell cycle arrest, thus allowing cells with damaged DNA to continue replicating. Additionally, other p53 mutations can lead to anti-apoptotic properties, as a result some cancer cell can evade programmed cell death, even when the damage is severe (Levine, Hu and Feng, 2006; Zhang *et al.*, 2020). Due to the very high prevalence of p53 mutations in glioblastomas, nanotechnology-based gene therapy approaches have been used to deliver wildtype-p53 to tumour cells, which successfully re-

sensitise temozolomide resistant tumours to treatment both *in-vitro* and *in-vivo* (Kim *et al.*, 2015)*,* however, further clinical implementation of this approach has not to date been realised.

1.3.2 Retinoblastoma pathway

The Rb protein is a tumour suppressor, which plays an important role in the negative control of the cell cycle and tumour progression via its interaction with transcription factor E2F, resulting in down regulation of cell cycle progression genes (Weinberg, 1995; Nevins, 2001). Within glioblastoma, Rb signalling is altered in approximately 78% of cases studied, with a homozygous deletion of Rb protein in 11% (McLendon *et al.*, 2008). Attempts have been made to re-establish the Rb pathway in glioblastoma by employing Palbocilib, an inhibitor of Cdk4/6. This compound functions to impede the downstream suppression of Rb and has demonstrated efficacy in restraining the growth of intracranial glioblastoma xenograft models (Michaud *et al.*, 2010).

1.3.3 RTK Signalling

Within glioblastoma mutations or amplification of RTKs is observed in approximately 80% of primary tumours, the most common are the PDGFR and EGFR (Ohgaki and Kleihues, 2009; Brennan *et al.*, 2013). Activation of EGFR plays a pivotal role, within two major pathways being the RAS/RAF/MAPK pathway, which drives cellular proliferation, differentiation, and migration, and the PI3K/AKT/mTOR pathway, primarily responsible for enhancing cell proliferation and ensuring cell survival by regulating the cell cycle and inhibiting apoptosis (Ohgaki and Kleihues, 2009).

The Ras-RAF-MAPK pathway, also known as the mitogen-activated protein kinase (MAPK) pathway consists of a series of proteins which transmit signals from the membrane bound cytoplasmic RAS family across the cytoplasm to within the nucleus. The RAF family constitutes the initial tier of this signalling cascade and comprises three isoforms: Raf-1/c-Raf, B-Raf, and A-Raf, each encoded by distinct genes. These isoforms all possess three conserved regions denoted as CR1-3. CR1, situated at the N-terminal, encompasses the RAS binding domain (Matallanas *et al.*, 2011). In contrast, CR3 is located at the C-terminal and serves as the site

for activation of the serine/threonine kinase mitogen-activated protein kinase 1/2 (MEK1/2). All RAF proteins exhibit a limited range of substrates, including MEK1/2, which constitutes the second tier of the MAPK cascade. MEK1/2 functions as dual-specificity tyrosine/threonine protein kinases, sharing the characteristic narrow substrate range with the RAF family. Their substrates encompass extracellular-signal-regulated kinases (ERK)1/2, the third tier of the MAPK pathway (Roskoski, 2012). In contrast to BRAF and MEK1/2, ERK1/2 possesses a broader spectrum of substrates and can migrate from the cytoplasm to the nucleus. The subsequent phosphorylation of the threonine and tyrosine residues of ERK1/2 ultimately culminates in the activation of pro-survival transcription factors, such as ELK-1 and CREB, and the deactivation of the apoptotic transcription factor FOXO3 (Mebratu and Tesfaigzi, 2009).

Upon activation of RTK through binding of respective ligand, phosphatidylinositol 3-kinase (PI3K) is recruited which phosphorylates phosphatidynositol-4,5-bisphosphate (PIP$_2$) to the respective 3-phosphate (PIP$_3$). This then activates downstream targets such as Akt and mTOR, which results in increased proliferation and survival of the cell through blocking of apoptosis (Mao *et al.*, 2012). The kinase activity of *PI3K* is directly regulated by tumour suppressor *PTEN*, which counteracts *PI3K* signalling by dephosphorylating PIP$_3$ to PIP$_2$ (Mellinghoff *et al.*, 2005; Zhao and Vogt, 2008). *PI3K* mutations occur in 21% of glioblastoma, and were shown to be mutually exclusive of *PTEN* mutations/deletions with 59.4% of samples showing only one (Brennan *et al.*, 2013). Loss of *PTEN* is observed in approximately 36% of glioblastomas (McLendon *et al.*, 2008), it is thought to be a contributing factor to EGFR therapy resistance, through the dissociation of EGFR signalling from downstream PI3K pathway inhibition (Mellinghoff *et al.*, 2005).

1.3.4 CDKN2A

CDKN2A gene is located on chromosome 9 and is responsible for the production of several tumour suppressor proteins. The most studied are the INK4 family member p16 (p16INK4a) and the p14(ARF) proteins which regulate both the p53 and Rb pathway respectively (Møller *et al.*, 1999). The p16(INK4A) protein is responsible for the inhibitory binding to Cdk 4 and 6, disrupting their binding to cyclin D, thereby preventing phosphorylation of Rb and therefore cell cycle progression (Jiao, Feng and Wang, 2018). The p14(ARF) protein protects degradation and nuclear export of tumour suppressor protein p53, through indirect sequestering of

MDM2 (Pomerantz *et al.*, 1998; Zhang, Xiong and Yarbrough, 1998). Mutations within this gene results in the inability to form stable complexes with enzymes, uncontrolled phosphorylation of Rb leads to abnormal cell cycle progression where cells gain uncontrolled proliferation (Romagosa *et al.*, 2011), while lack of p14(ARF) protein results in increased MDM2 resulting in the inability of p53 to exert it apoptosis and growth arrest functions (Pomerantz *et al.*, 1998).

1.4 Glioblastoma Treatment & Resistance

1.4.1 Surgical Removal of Tumour

The initial treatment route for glioblastoma is surgical resection of the tumour bulk, however it is not suitable for all patients. Surgery is dependent upon the patient's health and the anatomical location, for instance brainstem gliomas are usually inoperable due to risk associated with surgical resection. Where surgery is not possible, or metastatic disease is suspected, fine needle aspiration biopsy is performed (where accessible) (Schultz *et al.*, 2005). The primary challenge associated with the surgical resection of brain tumours is distinguishing between healthy and cancerous brain tissue. Whilst it is imperative to extract as much cancerous tissue as possible, there is the risk of also removing healthy essential brain tissue, essential for speech, motor function and senses. Therefore, a large amount of tumour often remains following surgery, especially at the tumour margin where it can be difficult to differentiate as the tumour cells invade healthy brain tissue. Recent advances have helped to improve surgical resection, for instance; Food and Drug Administration (FDA) approved optical imaging agent called 5-Aminolevulinic Acid (5-ALA), which acts as a fluorescent marker for brain tumour cells. Prior to surgery patients are orally administered a 'pink drink' containing 5-ALA, this produces a fluorescent metabolite protoporphyrin IX (PpIX) by intracellular synthesis in malignant glioma cells. This metabolite can be visualised after excitation by 400-410 nm blue light, thus helping neurosurgeons properly distinguish between healthy and cancerous tissue (W. Stummer *et al.*, 1998; Walter Stummer *et al.*, 1998). Additionally intraoperative MRI imaging is also used, providing the highest resolution for tumour resection, its only disadvantage is the high cost of equipment and maintenance (Kuhnt *et al.*, 2011).

Due to the heterogenous nature of gliomas, it is important that the surgical resection is reflective of the whole tumour; markers such as IDH and MGMT are usually homogenously present throughout. However, there are often biological differences between tumour core and residual cells which are often left behind following resection. Recent advances have allowed the separation of glioblastomas into bulk tumour cells and glioblastoma stem-like cells (GSC), it is hypothesised that it is in fact the GSC's left behind following surgery which give rise to tumour recurrence and subsequent drug resistance. As such, identification of effective drug targets in residual disease models is particularly appealing to study as their heterogeneity and response to treatment will be most reflective of what is left behind following surgery, thus a better disease model for the patient (Rominiyi, Al-Tamimi and Collis, 2019; Weller and Le Rhun, 2020).

1.4.2 Chemotherapeutics

Glioblastoma is not only heterogeneous at a cellular level but also genetically. This heterogeneity makes it extremely difficult to treat using singular targeted molecular therapies, therefore there is a requirement into the investigation of combination therapies which can target multiple genotypes/phenotypic traits. Therapeutic treatment is also restricted due to the inability of suitable chemotherapeutic drugs to pass through the blood brain barrier (BBB) from systemic or oral delivery. The BBB is a protective physical obstruction in the CNS between blood and neural tissue, its role is to block any toxins including drugs from reaching brain tissue and causing irreversible damage (Bicker *et al.*, 2014). The ability of novel drugs to pass through the BBB is only demonstrated once a drug discovery pipeline has reached testing within murine models. It is estimated that 98% of low-molecular weight drugs and almost all large molecules such as antibodies are unable to penetrate the BBB (Pardridge, 2005; Neuwelt *et al.*, 2008). As such, a lot of time and money is often wasted developing successful drugs *in-vitro* only to be unsuitable within *in-vivo* models and pre-clinical studies.

There have been developments to try and circumvent the BBB issue, including the development of trans-cranial drug delivery systems which comprise: intracerebral implantation, intracerebroventricular infusion and convection-enhanced diffusion, of the three approaches the latter is most superior as does not require drug diffusion from specific site, instead it is able to deliver the chemotherapeutics directly into the tumour through

catheters (Neuwelt *et al.*, 2008). However, this is a highly invasive drug delivery mechanism which may not be suitable for all patients. Given this, it is perhaps not surprising that there are only four FDA approved chemotherapeutics for treating glioblastoma; lomustine, carmustine, temozolomide and bevacizumab. Lomustine, carumustine and temozolomide are all alkylating agents which affix to guanine and adenine residues on DNA attaching methyl groups, thus inducing mutagenic DNA legions. The lipophilic nature of these three drugs allows them to pass through the BBB and permits oral administration (Lee, 2016). Out of the three, carmustine has limited BBB permeability and therefore is commonly administered at the resection site of tumour in the form of a biodegradable wafer (Perry *et al.*, 2007).

1.4.3 Temozolomide (TMZ) – Standard of Care

Alkylating agents form strong covalent bonds with oxygen rich atoms within biological molecules, they were first discovered for the treatment of cancer following the use of sulphur gases in World War I. There are two different types of alkylating agents, monofunctional and bifunctional; bifunctional alkylating agents work by forming an irreversible bond between two base pairs within DNA known as ICLs these include agents such as carmustine and lomustine, whilst monofunctional alkylating agents react with just one strand of a pair of bases which include TMZ and dacarbazine.

As mentioned previously, part of the current SoC treatment for glioblastoma is the alkylating agent TMZ. The mechanism of action is summarised by figure 1.7. At physiological pH TMZ undergoes a ring opening hydrolysis to generate compound 5-(3-methyltriazole-1-yl)imidazole-4-carbox-amide (MTIC), which is further metabolised into 4-amino-5-imidazole-carboxamide (AIC) and active methyl diazonium ion (Clark *et al.*, 1995). This highly electrophilic ion methylates nucleophilic sites on DNA including specific sites on guanine (N7 and O6) and adenine residues (O3). The most detrimental of these modifications is the alkylation of O6-guanine, which leads to the incorrect insertion of thymine, instead of cytosine, on the complementary strand during DNA replication. Under normal cellular conditions a de-alkylating repair enzyme known as MGMT is responsible for sequestering any mutagenic DNA legions of O^6-methylguanine (O6-MG) back to its original guanine state, thus repairing DNA damage. However epigenetic silencing of the *MGMT* gene through methylation of the upstream promoter region is able to prevent the synthesis of the repair enzyme,

resulting in additional mutagenic DNA legions, amplified cell cycle arrest and therefore increased levels of cell death as a result of alkylating agent TMZ (Hegi *et al.*, 2005). If the O6-MG lesion is not sucessfully resolved by the MGMT enzyme, it persists as a miscoding base, which results in mismatch with thymine on the opposite strand. MMR machinery can remove this incorrect thymine, however due to the O6-MG lesion persisting, thymine will continously be reincorperated leading to futile cycles of MMR. This futile cycling can ultimately lead to the formation of double stranded breaks, stalled replication forks and eventual cell death via apoptosis.
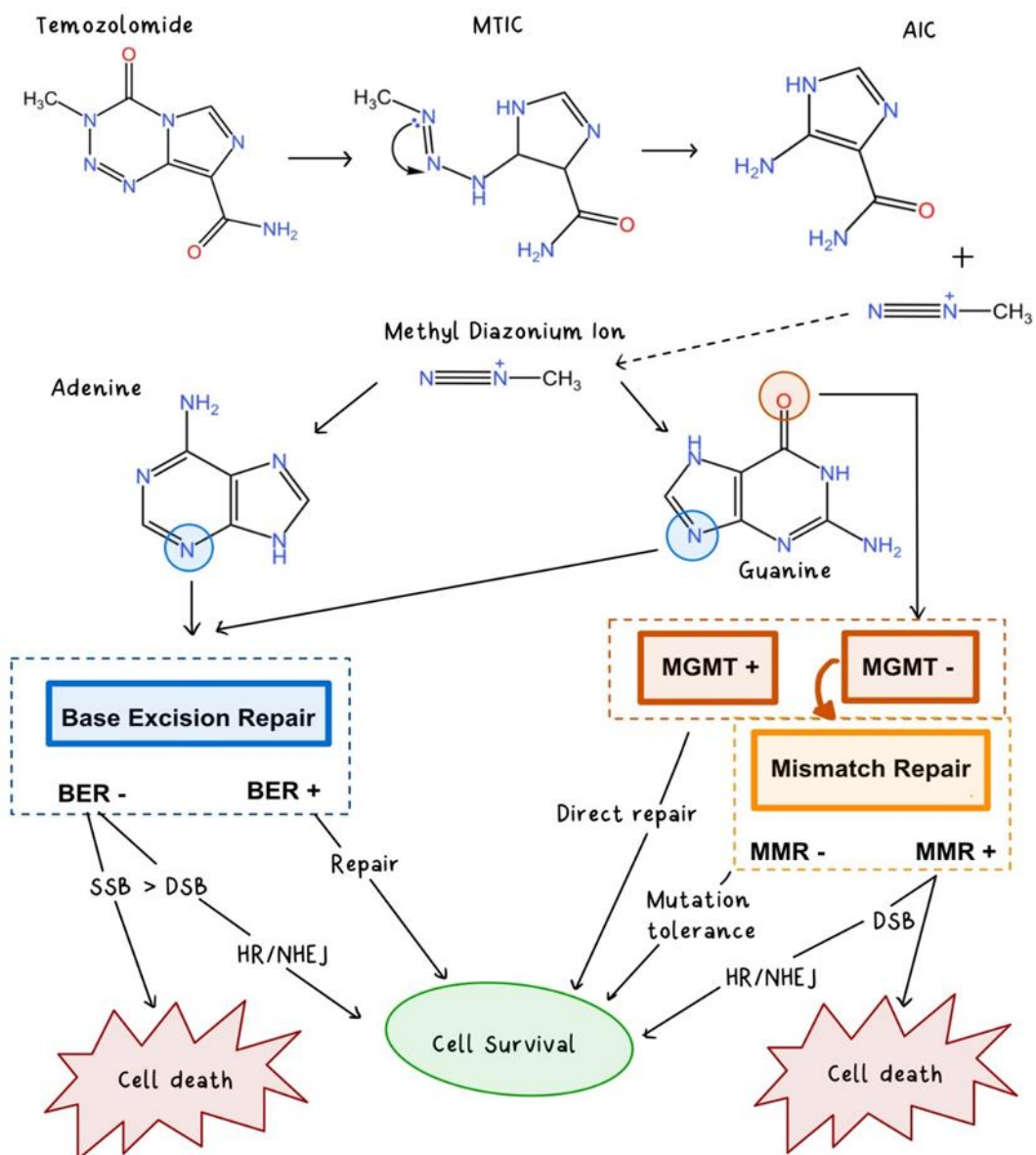
Figure 1.7 - Summary of TMZ mechanism of action and DNA repair mechanisms involved with TMZ-induced damage - Initially TMZ undergoes hydrolysis and metabolism into active methyl diazonium ion.

This ion methylates guanine and adenine residues on DNA to form N7-methylguanine (70%), N3-methyl adenine (9%) and the most lethal, O6-methyl guanine (O6-MG) (5.3%). The former lesions are repaired via BER, however the O6-MG lesions are repaired by direct repair via MGMT enzymes. When MGMT is defective the O6-MG lesion causes mismatch with thymine on the complementary stand, which is recognised by mismatch repair (MMR) machinery. When MMR is functional this thymine residue is excised, however due to the O6-MG lesion persisting, will later by rematched with thymine upon repair synthesis. This repetitive incorporation and removal of thymine on the opposite strand leads to futile cycles of repair by MMR machinery, leading to replication fork arrest, DNA double strand breaks and eventual cell death. Figure adapted from (Strobel *et al.*, 2019).

Promoter methylation of the *MGMT* gene reduces cellular levels of the enzyme and therefore impedes its ability to repair DNA and thus improves the efficacy of alkylating agent and standard treatment TMZ. Despite being a prognostic marker of TMZ sensitivity, *MGMT* gene methylation status testing is not currently standard practice within the NHS (Hegi *et al.*, 2005). There are still cases though where *MGMT* methylation is present but mRNA levels of MGMT are abundant therefore evidencing that anomalies do exist. As such, *MGMT* methylation status unfortunately does not always correlate with overall patient treatment response (Sasmita, Wong and Ling, 2018).

1.4.4 Radiotherapy -Standard of Care

Following surgical resection, patients will often wait up to four weeks for the wound to heal prior to starting any therapy. Before 2005 patients received only RT, however since the Stupp regimen showed an increase in median survival to 14.6 months versus 12.1 with RT alone, TMZ is given both concomitantly and after RT (Stupp *et al.*, 2005). RT treatment kills cancer cells through the formation of electrically charged particles which can pass through tissues transferring energy. This energy deposit to cells results in the damage to deoxyribonucleic acid (DNA) through single strand breaks (SSB) and double strand breaks (DSB), often via ionisation of water molecules (radiolysis) producing damaging oxygen free radicals. This can result in the damage of cells beyond repair causing growth arrest and/or activation of cell death mechanisms such as apoptosis, mitotic catastrophe, necrosis, senescence and autophagy. Being SoC for many cancers, the DNA damage caused by RT is not able to differentiate between healthy and normal cells, however advances in guided external beam therapy techniques has allowed for a more accurate pinpointed delivery methods thus sparing normal healthy tissue.

1.4.5 Monoclonal Antibody Bevacizumab

Bevacizumab is a anti angiogenic humanised monoclonal antibody which is a direct antagonist against VEGF. It directly blinds to VEGF cell surface receptors, preventing the production of microvascular tumour blood vessels thus limiting nutrient supply to tumour tissues. In 2009 bevacizumab was granted accelerated approval by the FDA for the treatment of patients with recurrent glioblastoma (Cohen *et al.*, 2009; Chamberlain, 2011). Its use has been extensively explored in clinical trials for both recurrent and newly diagnosed glioblastoma, despite showing minimal efficacy. For newly diagnosed glioblastoma, two stage III clinical trials have involved the use of bevacizumab alongside SoC TMZ and RT. In both trials an improved progression free survival (PFS) was observed with bevacizumab treatment 10.7 to 7.3 months (Gilbert *et al.*, 2013) the other 10.6 to 6.2 months (Chinot *et al.*, 2014), however the OS was not altered significantly between the treatment and placebo groups. Additionally, there was an abundance in adverse side effects, therefore bevacizumab was not selected as it did not meet the improvement target. A separate phase II clinical trial for the treatment of patients with progressive glioblastoma investigated the combination of bevaciumab and alkylating agent lomustine, the PFS was improved in the combination therapy by 2.7 months. Furthermore the OS was improved from 8.6 months in the monotherapy group to 9.1 in the combination group, however this improvement is only minimal, nevertheless it still led to full approval of its use in 2017 (Wick *et al.*, 2017).

1.4.6 Tumour Treating Fields (TTFields)

Tumour Treating Fields (TTFields) is an emerging non-invasive cancer therapy involving the introduction of low intensity (1-3V/cm), intermediate frequency (100-200kHz), alternating electrical fields that disrupt cancer cell division resulting in cell death. This most widely used, clinically approved delivery system, Optune (Novocure™), consists of four transducer arrays, a field generator, and a power source. The alternating electric fields are delivered to the patient through transducer arrays which are adhered to the patients scalp for at least 18 hours per day (Rominiyi *et al.*, 2020). TTFields induces anti-mitotic effects during the metaphase of the cell cycle through disrupting the tubulin dimers, also during anaphase preventing the localisation of septin proteins to the mitotic spindle which both cause unequal separation of the sister chromatids, therefore leading to abnormal cell segregation and ultimately mitotic cell death. There is also evidence that TTFields can down regulate DNA

repair proteins, cause replication stress, activate autophagy, stimulate anti-tumour immunity, stimulate anti-migratory pathways and also promote cell membrane permeability (Rominiyi *et al.*, 2020).

The EF-14 trial which assessed TTFields efficacy, is the only trial since addition of TMZ to SoC in 2005 which demonstrated significant increased OS for newly diagnosed glioblastoma patients. TTFields plus TMZ led to increased OS by an average of 2.8 months (Stupp *et al.*, 2015). This data resulted in the approval of TTFields by the FDA in 2015. Despite this encouraging clinical data, TTFields has not been approved yet in the UK due to National Institute for Health and Care Excellence (NICE) considering the treatment as cost ineffective therefore not justified for use within the NHS, although some UK-based patients can access TTFields therapy through private healthcare providers.

1.5 Clinical Trials – Future treatments

There are currently 167 active ongoing clinical trials (non-recruiting) for glioblastoma, of which 10 have study results available. These are summarised in table 1.1; the majority of the trials include SoC (surgical removal of tumour, TMZ and RT) in combination with new therapies currently under investigation. Data was obtained from the clinical trial database (https://clinicaltrials.gov/).

Table 1.1 - Summary table of active clinical trials, not recruiting with results publicly available.

Trial Number	Therapeutic	Target Details	Chemotherapy	Radiotherapy	Diagnosis Stage	Phase
NCT02586857	ACP-196	BTK inhibitor	N/A	N/A	Recurrent	1b/2
NCT03661723	Pembrolizumab	PD-1 immunotherapy	N/A	Yes	Recurrent	II
NCT04225039	INCMGA00012	PD-1 immunotherapy	N/A	Yes	Recurrent	II
NCT02152982	ABT-888 (veliparib)	PARP inhibitor	Temozolomide	N/A	Newly Diagnosed	II/III
NCT02455557	SurVaxM	Immunotherapy	Temozolomide	N/A	Newly Diagnosed	II
NCT02017717	Nivolumab	PD-1 immunotherapy	Bevaciszumab/ Ipilimumab	N/A	Recurrent	III
NCT02337686	Pembrolizumab	PD-1 immunotherapy	N/A	N/A	Recurrent	II
NCT02142803	MLN0128	TORC1/2 inhibitor	Bevacizumab	N/A	Recurrent	I
NCT01817751	Sorafenib, Valproic acid, sildenafil	Kinase inhibitor, HDAC inhibitor	N/A	N/A	Recurrent	II

1.6 DNA repair pathways

1.6.1 Overview of DNA damage response

It is estimated that our cells go through approximately 10^4-10^5 spontaneous DNA damaging lesions each day (Lindahl, 1993; Lindahl and Barnes, 2000; De Bont and van Larebeke, 2004). These lesions include DNA SSB and DSB, base damage, cytosine deamination, cyclopurine adducts, depyrimidination, DNA-protein crosslinks, mis-matched base pairing and DNA crosslinks (Hoeijmakers, 2001; Ciccia and Elledge, 2010). Such lesions can be caused by endogenous sources (cellular metabolic processes) such as oxidative damage, hydrolysis, alkylation and DNA replication errors or exogenous sources (environmental factors) including ultraviolet (UV) radiation, ionizing radiation and various chemical agents such as from carcinogens in cigarette smoke. All these lesions pose a threat, and therefore evolutionary mechanisms have evolved to detect, signal, and repair the lesions; collectively known as the DNA-damage response (DDR), which involves a complex network of signalling and DNA repair mechanisms (figure 1.8) working in concert with the cell cycle progression/checkpoint machinery to preserve and maintain genomic integrity (figure 1.9). Improper functioning of these DNA damage response checkpoints and repair pathways can cause the accumulation of unrepaired DNA which can pass onto daughter cells and lead to mutations that can drive cancer development and progression.
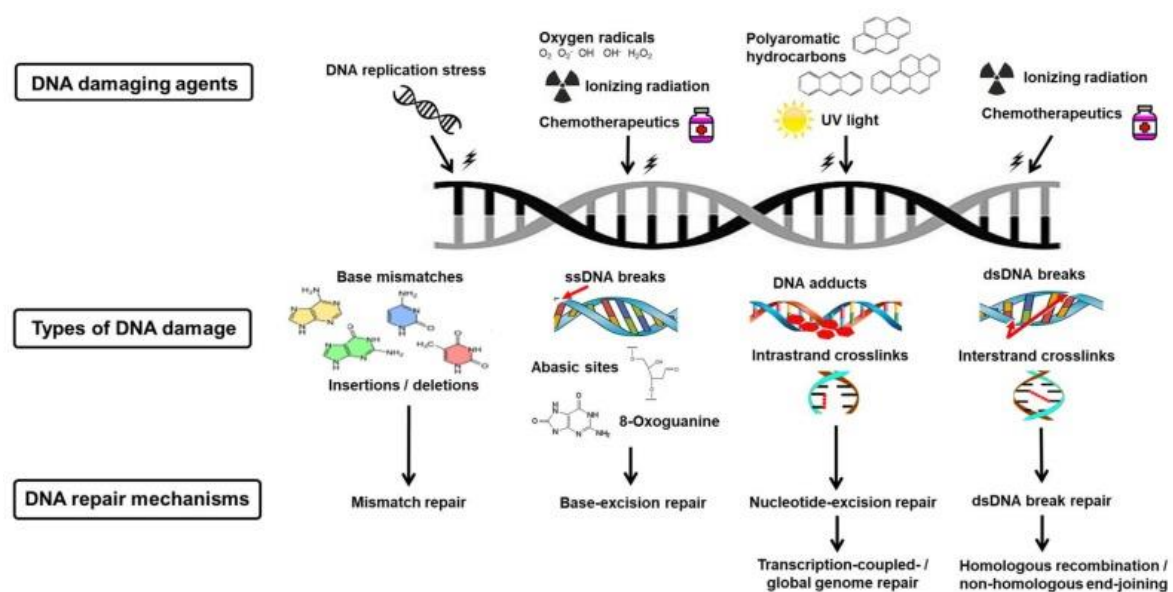
Figure 1.8 - Overview of DNA damage and types of response mechanisms involved - DNA damage can occur through endogenous and exogenous factors. These types of damage include base mismatch, single stand breaks, single base damage, bulky lesions, crosslinking (intra and interstrand) and double stranded

breaks. Each type of damage activates a particular repair mechanism, which include, base excision repair, nucleotide excision repair, base mismatch, non-homologous end-joining and homologous recombination. Figure from Helena *et al* (2018), Copyright permissions obtained from publisher (Open Access).

There are three regulatory checkpoints known as G1/S, intra-S phase and G2/M, owed to the phase of the cell cycle in which they exist. Maintenance of the genome not only relies on efficient DNA repair mechanisms but also the ability for the cell cycle checkpoints to be activated, therefore allowing time for DNA damage to be repaired. Early DDR processes involve the activation of several kinases, which in turn regulate cell cycle progression through checkpoint activation. These kinases include ATM, ATR and DNA-PK. These kinases, along with various Cdk's and the central cell cycle regulator p53 and its associated factors, regulate the intricate pathways involved (figure 1.9) (Hustedt and Durocher, 2016; Rominiyi and Collis, 2022).
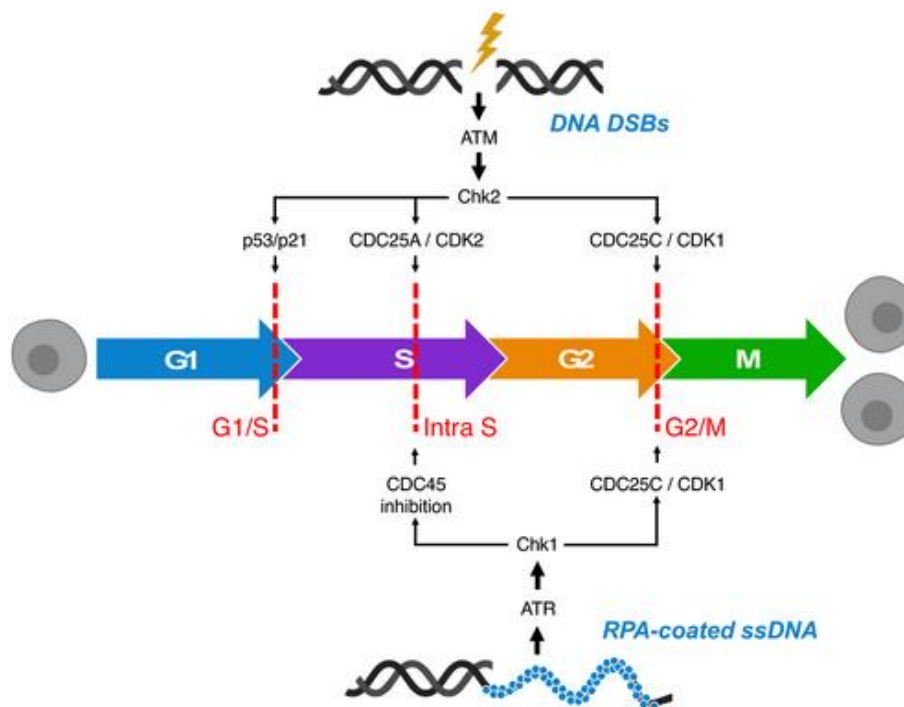
Figure 1.9 - The function of ATM and ATR in regulating the cell cycle after DNA damage is a crucial aspect of cellular control - *The cell cycle encompasses phases such as mitosis (M) and DNA synthesis (S), which are divided by gap phases called G1 and G2. The progression of mitotic cells through the cell cycle is under the governance of CDKs and cyclins, which periodically accumulate and are subsequently degraded. To ensure proper cell cycle progression, three principal checkpoints (G1/S, intra-S, and G2/M checkpoints) act as safeguards against inappropriate advancement, indicated by dashed red lines. In the event of DNA damage, activating these checkpoints becomes pivotal as it grants adequate time for recruiting the necessary molecular machinery to preserve genomic integrity. Figure from Rominiyi and Collis (2022), Copyright permissions obtained from publisher (Open Access).*

1.6.2 Mismatch Repair

MMR is responsible for the restoration of base mismatches and insertion deletion loops (IDLs) which have escaped proofreading by polymerases (Liu, Keijzers and Rasmussen, 2017). Mismatched bases are detected by MutS proteins, that form two heterodimers, MutSα (MSH2-MSH6) and MutSβ (MSH2-MSH3). Once detected they bind to the damaged DNA, following this MutL recruits the DNA helicase II to separate the two complimentary DNA strands. Consequently, the endonuclease activity of MLH1-PMS1 is activated, allowing excision of the nicked DNA strand by EXO1. Finally the new stand is synthesised by Pol δ and ligated by DNA ligase I (LIG1) (Chakraborty and Alani, 2016; Lodovichi *et al.*, 2020).

MMR status is also an important predictor of TMZ efficacy alongside *MGMT* gene expression (McFaline-Figueroa *et al.*, 2015). Typically, O6-MG residues caused by alkylating agent TMZ are directly repaired by MGMT enzyme, however when the *MGMT* gene is hypermethylated, this damage persists resulting in O6-MG:Thymine mismatch, following an initial round of replication. The MMR pathway will attempt to repair this damage, removing the patch of newly synthesized DNA containing the thymine residue. However, without the removal of the initial O6-MG on the template strand, incorrect incorporation of thymine will persist on the opposite strand, leading to futile cycling of the MMR system. This then results in fork collapse, double strand breaks, G2/M arrest and eventual cell death (Drabløs *et al.*, 2004). Often when MMR machinery is defective, the mismatched thymine residue will be left unrepaired, leading to increase in mutational tolerance, TMZ resistance and cell survival. Which may in turn lead to survival advantage, through heightened levels of mutations within oncogenes and tumour suppressor genes resulting in clonal expansion (Von Bueren *et al.*, 2012).

A recent multicentre study showed that partial and complete IHC loss of MMR protein expression was present in 43/355 high grade glioma samples, of which 15% showed a complete loss in one MMR protein (Caccese *et al.*, 2020). Also TCGA data demonstrated that MMR gene MutS homolog 6 (MSH6) was mutated within approximately 26% of recurrent tumours, which had received alkylating agent TMZ (McLendon *et al.*, 2008), suggesting MSH6 mutations are selected for during TMZ treatment and are casually associated with TMZ resistance (Yip *et al.*, 2009).

1.6.3 Base Excision Repair

BER resolves SSB base oxidation, deamination and alkylation which are typically non-distorting to the DNA helix (Krokan and Bjørås, 2013). Typically, BER is usually activated following spontaneous decay of DNA or though other factors such as ROS and IR. There are two distinct BER pathways; short patch (SP) repair for single base sites and long patch (LP) repair for oxidized and reduced sites. Both SP and LP repair involve initial detection of damaged lesion by one of at least 11 DNA glycosylases, these are enzymes that cleave the bond between the deoxyribose and modified lesion. This removal creates an abasic site, which is cleaved by the AP endonuclease (APE1) (Lee and Kang, 2019). For SP repair DNA polymerase β (Polβ) is recruited to fill the gap and ligation by DNA ligase 3 (Lig3) complexed with XRCC1 (Lodovichi *et al.*, 2020). LP repair requires assistance of flap endonuclease 1 (FEN1) to displace the larger 5'-flap structure it then utilises PCNA, DNA polymerase δ/ε (Polδ/ε) to fill the gap alongside ligation by DNA ligase 1 (Lig1) (Lee and Kang, 2019). This process is summarised below (figure 1.10).
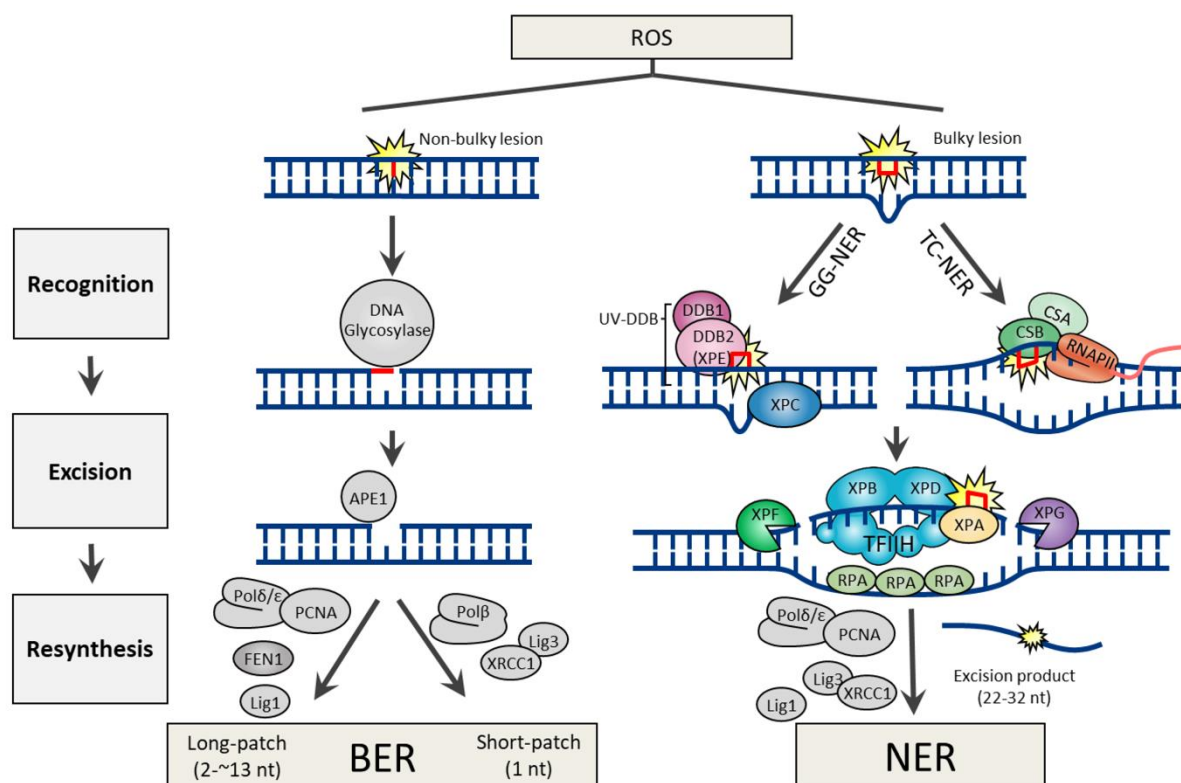
Figure 1.10 – Overview of DNA excision repair pathways for bulky distorting (nucleotide excision repair) and non-bulky lesions (base excision repair) caused by reactive oxygen species (ROS) - Figure obtained from Lee and Kang (2019), copyright permissions obtained from publisher (Open Access).

1.6.4 Nucleotide excision repair

Nucleotide excision repair (NER) is specific to bulky single stranded DNA helix distorting lesions, which can block DNA replication and transcription. NER is famed for its ability to remove a large range of structurally unrelated DNA lesions, including: cyclobutene-pyrimidine dimers and 6-4 pyrimidine-primidone photoproducts which are the common lesions produced by UV radiation, bulky chemical adducts and ICLs caused by cisplatin and cyclopurines generated by ROS (Marteijn *et al.*, 2014). There are two types of NER, both summarised above in figure 1.10. One type is known as global genome NER (GG-NER) which surveys the entire genome for damage by sensor XPC and UV-DDB (ultraviolet (UV) radiation-DNA damage-binding protein) complex. The other type is transcription-coupled NER (TC-NER), which only identifies damage in actively transcribed DNA, the damage is indirectly activated following RNA polymerase II (RNA pol II) stalling during transcript elongation at a lesion (Gillet and Schärer, 2006; Hanawalt and Spivak, 2008). The affinity of CSB and RNA Pol II then increases, causing the Cockayne syndrome WD repeat protein (CSA-CSB) to form, causing reverse translocation allowing access to DNA lesion (Marteijn *et al.*, 2014).

Following activation within both types of NER the transcription initiation factor IIH is recruited, which possesses helicase activity to open the double helix. The helicase subunit XPD verifies the existence of lesions with the help of the ATPase activity XPB subunit and XPA, which binds to single stranded chemically altered nucleotides. Consequently the single-stranded DNA binding protein RPA is recruited and coats the undamaged strand. Endonucleases XPF and XPG are then recruited to the damage strand where they create a 5' and 3' incision respectively, which excises the damaged lesion within 22-30 nucleotides. Following the initial 5' incision by XPF, the PCNA ring is loaded which recruits Pol δ, Pol κ or Pol ε for gap-filling and finally sealing the nick with DNA Lig1 or Lig3 (Marteijn *et al.*, 2014).

1.6.5 Homologous Recombination

Homologous recombination repairs DSBs during S/G2 phase of cell cycle (Branzei and Foiani, 2008). It is the least error prone of all repair mechanisms, as it uses the sister chromosome as a template. Overview of the HR mechanism of action is depicted by figure 1.11. Initially the DSB is detected by MRN complex (MRE11A-NBS1-RAD50) which binds to it and recruits ATM.

Next the MRN resects the DSB on the 5' ends of both hands to give 3' overhang requiring BRCA1 activity. Next PALB2 recruits BRCA2 to the DSB and sequesters RAD51 to the resected ssDNA regions. RAD51 is involved in the search for homologous DNA and aids invasion of homologous double stranded DNA, making a d-loop. DNA polymerases synthesise new DNA strands using the homologous ssDNA as the primer. DNA is ligated and cleaved before the break is completely restored either through non-cross over HR repair or cross over HR repair (most common).
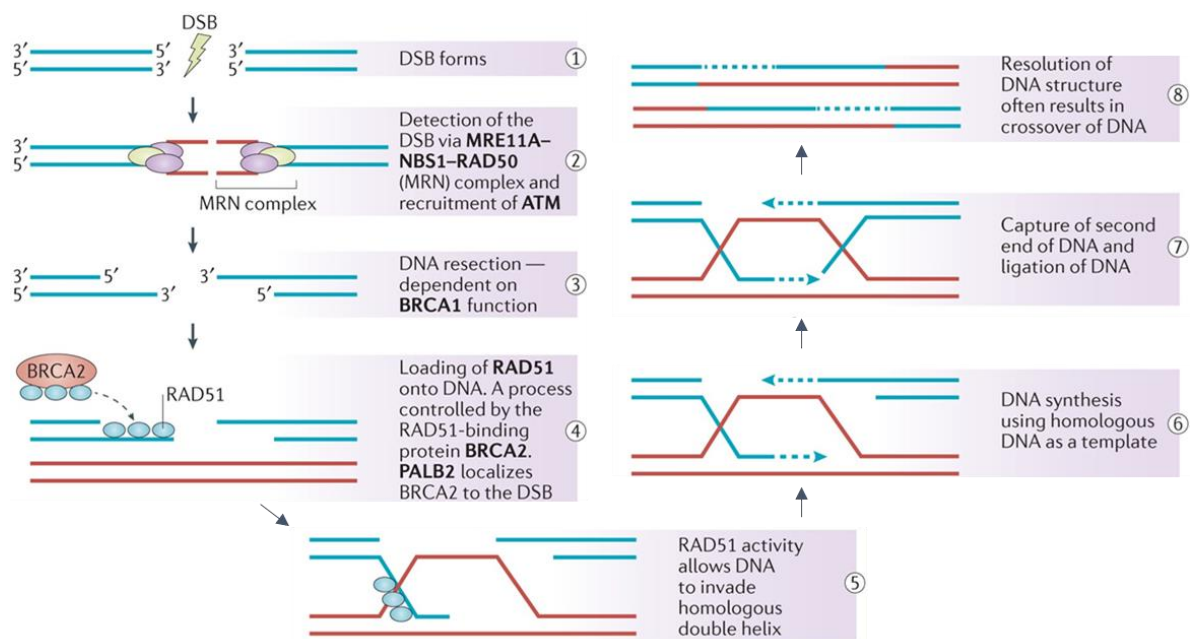
Figure 1.11 - Schematic overview of the HR mediated DNA repair - Initially the DSB is detected by the MRN complex comprised of MRE11A-NSB1-RAD50 which recruits ATM. The damaged DNA is processed to create 3' overhang. BRCA2 controls the loading of RAD51 onto the overhang, which permits the invasion of homologous template on the sister chromatid. The invasive strand displaces the complimentary strand on homologous DNA creating a d-loop structure. DNA polymerases synthesise a new DNA strand based on the sister template, repairing the DNA damage. Sometimes the resolution of DNA results in a crossover event where genetic material is exchanged between the homologous chromosomes. Adapted Lord and Ashworth (2016), copyright permissions obtained from publisher, licence number 5660150681331.

1.6.6 Non-homologous End joining (NHEJ)

NHEJ is another DNA DSB repair mechanism acting mostly in the G1-phase, this is more error prone as bases can be trimmed by nucleases which can lead to loss of genetic information. Summarised in figure 1.12, initially the Ku70 and Ku80 dimerise to form Ku complex which recognises DNA DSBs and recruits other NHEJ proteins. DNA-PKcs are recruited to the Ku heterodimer bound to the DNA to form the DNA-PK complex. This now active DNA-PKcs

complex recruits NHEJ proteins such as ARTEMIS (5'3' exonuclease activity, trims overhangs into blunt ends), DNA polymerase, XRCC4, XLF, DNA ligase and H2AX. H2AX is a well-established DNA DSB marker which also recruits further DSB proteins. Multiple rounds of nucleotide additions and deletions often occur before ligation DNA ends to produce repaired DNA (Chang *et al.*, 2017).
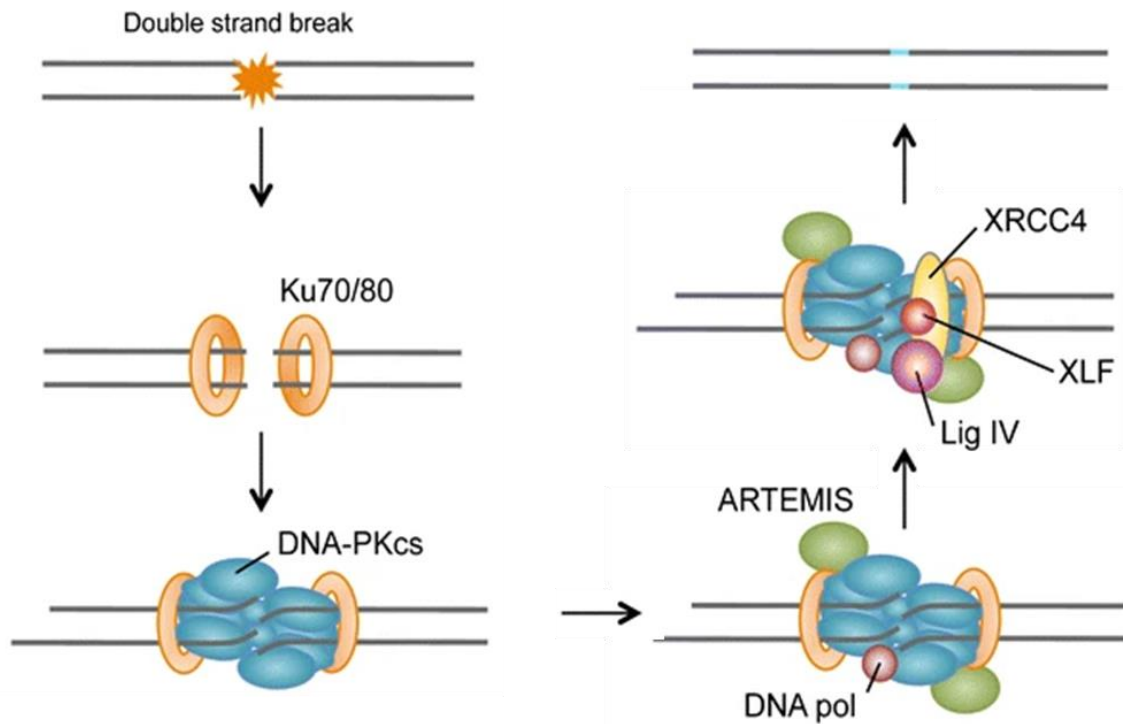
Figure 1.12 - Schematic overview of the non-homologous end joining mediated DNA repair - The Ku80-Ku70 heterodimer plays a pivotal role in detecting and responding to double-strand breaks (DSBs) in the DNA. This detection initiates a cascade of events, starting with the recruitment of the DNA-dependent protein kinase catalytic subunit, DNA-PKcs. Subsequently, the DNAPK complex forms and its kinase activity is activated. DNA-PK, in turn, enhances the recruitment of key repair proteins, including Artemis, XRCC4, DNA ligase IV, and XLF. These proteins work collaboratively to complete the final re-joining step. Figure adapted from (Brochier and Langley, 2013). Copyright permissions obtained from publisher, licence number 5660181197219.

1.7 Glioma Stem Cells

1.7.1 Cancer Stem Cell Theory

The cancer stem cell (CSC) theory stipulates that a rare subpopulation of cells harbour the ability to undergo unlimited regeneration and possess self-renewal properties (Reya *et al.*, 2001; Pardal, Clarke and Morrison, 2003). Following the proposal of this CSC theory, there followed an influx of studies describing brain CSCs, which for the purpose of this thesis we

will refer to as glioma stem cells (GSC's) (Ignatova *et al.*, 2002; Hemmati *et al.*, 2003; Galli *et al.*, 2004; Singh *et al.*, 2004). Glioblastomas consist of both bulk tumour cells and GSCs and it is thought to be the latter which give rise to tumour heterogeneity, secondary foci and drug resistance within patients (Bao *et al.*, 2006; Chen *et al.*, 2012). Following surgical removal of bulk tumour population, it is hypothesized that GSC's left behind can infiltrate the brain and migrate to form secondary tumour foci and therefore it is this subpopulation of residual cells which needs to be targeted and utilised to test novel drugs and treatment methods.

There is controversy regarding the origin of GSCs. There is evidence to suggest they develop from malignant mutations within neural stem cells (NSC) which arise from the subventricular zone (SVZ) of the lateral ventricles and the subgranular zone (SGZ) of the hippocampus in the dentate gyrus (Lee *et al.*, 2018). GSCs and NSCs possess similar gene expression profiles, additionally they both express neuronal and glial markers such as CD133 (Jackson and Alvarez-Buylla, 2008). Other evidence suggests that GSCs arise from other mature cells which possess the ability to self-renew and differentiate into various tumour types (Bachoo *et al.*, 2002; Gimple *et al.*, 2019). Advances in cell culture methods have now made it possible to maintain GSCs *in-vitro,* replacing the media containing serum used for established cell lines with conditions optimal for normal NSCs allowing them to maintain self-renewal capabilities; neurobasal serum free media supplemented with growth factors fibroblast growth factor (FGF) and epidermal growth factor (EGF) (Lee *et al.*, 2006).

Early studies conducted by Singh *et al* (2004), revealed a subset of brain tumour cells were positive for cell surface stem cell antigen CD133, also commonly known as prominin-1. Experimental work revealed that following magnetic sorting CD133-positive cells exhibited the ability to initiate new tumours in immunocompromised mice with as few as 100 cells, whereas CD133-negative human brain tumour cells were completely unable to form tumours *in-vivo*. These findings led to the assumption that CD133 serves as marker for GSC's, instigating further exploration of the relationship between glioblastoma and GSCs. Additionally, separate research conducted by Galli *et al* (2004) provided further support for the GSC theory by identifying a population of neural tumour cells with the capability to 'establish, sustain and expand tumours'. Experimental procedures involved the successful isolation and identification of NSCs from glioblastoma and performed a successful orthotopic

transplantation immunocompromised mouse despite challenging conditions set by serial transplantation experiments, thus also approving the human glioblastoma GSCs theory. Markers frequently used to identify and/or isolate GSCs include: CD133, CD33, CD15, CD70, S100A4, ALDH1A3, Nanog, OCT-4, SOX-2, and Nestin (Hassn Mesrati *et al.*, 2020).

1.7.2 Plasticity In glioblastoma

Typical neural differentiation involves the transformation of NSCs or progenitor cells into specialised neural cell types which include neurons, astrocytes and oligodendrocytes. These differentiated neural cells become terminally specialized and contribute to the structure and function of the nervous system. In contrast, the differentiation of glioblastoma tumour cells is a highly transient process, they have the ability to jump between a spectrum of phenotypic states from quiescent to proliferative and multipotent to differentiated. This is due to their permissive epigenetic and transcriptomic landscape, which contributes towards their treatment resistance (De Silva, Stringer and Bardy, 2023). Single cell RNA seq analysis of 28 tumours revealed 4 distinct cellular states which are responsible for driving glioblastoma heterogeneity (Neftel *et al.*, 2019). These cellular states are defined as neural-progenitor-like, oligodendrocyte-progenitor-like, astrocyte-like and mesenchymal-like. One potential treatment strategy is the induction of differentiation in these glioblastoma cultures into a specific lineage. For instance, the knockdown of OLIG2 has been shown to induce differentiation into cells resembling either glial fibrillary acidic protein (GFAP) + astrocyte-like or CD44+ mesenchymal-like state like. The direction of differentiation depends on the presence of EGFR and PDGFRA amplification (Kupp *et al.*, 2016). This approach aims to manipulate the transient cellular states within glioblastoma to potentially target specific tumour characteristics or vulnerabilities.

1.8 Frequently utilised GSC markers

1.8.1 CD133 (Prominin-1)

CD133 also known as prominin-1 is a transmembrane protein, It was initially identified as surface antigen expressed on hemopoietic stem cells (Miraglia *et al.*, 1997; Bauer *et al.*, 2011), later in NSCs (Corbeil *et al.*, 2010) and also GSC's (Singh *et al.*, 2004). Analysis of a series of newly diagnosed and recurrent glioblastoma neurospheres using fluorescence-activated cell

sorting (FACS) revealed that there is high variability of CD133 expression in glioblastoma. A study revealed 4/11 neurospheres displayed high abundance of CD133 positive cells (from 84.8% to 58.1%), whilst the remaining 7/11 contained much lower populations of CD133 positive cells (from 8.4-1.0%) (Brescia *et al.*, 2013). The percentage of CD133 positive cells was also analysed over several *in-vitro* passages and therefore may not be an artifact of cell cycle dependent expression of the CD133 protein. Despite some neurospheres showing low levels of CD133 during FACS analysis, considerable levels of transcript were observed, suggesting mRNA levels do not always corroborate with CD133 plasma membrane expression levels. It is hypothesized CD133 appears in an interconvertible state, changing expression and subcellular localisation between the cytoplasm and the plasma membrane depending on multiple stimuli such as cell cycle progression, supply of oxygen and nutrients (Barrantes-Freer *et al.*, 2015).

Contradictory to previous reports, both CD133-positive and CD133-negative cell fractions sorted from glioblastoma patient derived neurospheres and tumour specimens showed similar self-renewal capabilities *in-vitro* and have the ability to regenerate tumours in mice models (Joo *et al.*, 2008; Brescia *et al.*, 2013). The knockdown of CD133 using short hairpin RNA was able to impair GSC growth and self-renewal capabilities linking it to GSC tumorigenic capacity, suggesting it could be used as therapeutic target in glioblastoma (Brescia *et al.*, 2013). This is interesting as one would expect to see the same loss of tumorigenic potential in CD133-negative cells. It is possible that in previous experiments CD133-negative cells may have been labelled incorrectly, due to specific antibodies only targeting the AC133 specific epitope, which is located in one of the extracellular domains of membrane-bound CD133 (Barrantes-Freer *et al.*, 2015).

Previous work by (Bao *et al.*, 2006) showed that following IR treatment of human CD133-positive and CD133-negative glioma xenografts, the CD133-positive subpopulation increased 3-5 times relative to control xenografts. Additionally, freshly isolated glioblastoma cultures showed an increase of CD133-postive cells from 2-3% to 6-10% after IR treatment. Interestingly irradiation did not induce CD133 expression in CD133-negative cells. Through comparison of the DNA damage response proteins the CD133-positive cells had significantly higher activating phosphorylation of ATM, CHK1, CHK2 and Rad17, indicating CD133-positive

cells show greater checkpoint activation in response to IR induced DNA damage. Additionally, the baseline phosphorylation of crucial DNA damage checkpoint regulator Rad17 was significantly higher in the CD133-positive cells, suggesting these cells may be better primed to respond to DNA damage. Comet assay results revealed that following IR treatment comet tails decreased 2-9 times more rapidly in CD133-positive cells indicating that they were able to repair DNA damage more efficiently than CD133-negative cells, thus corroborating the DDR protein data. This data confirms that CD133-positive cells have greater radio resistance and tumour repopulation potential through heightened checkpoint response and DNA repair mechanisms.

1.8.2 SOX-2

SOX-2; sex determining region Y (SRY)-box2 is a transcription factor which controls gene expression throughput embryonic development and is involved in neurogenesis and gliogenesis. Its expression is downregulated when neural cells mature and exit the cell cycle (Uwanogho *et al.*, 1995; Kamachi, Uchikawa and Kondoh, 2000), however in glioma, SOX-2 expression is frequently high (90%) with expression corelating positively with tumour grade (Schmitz *et al.*, 2007), suggesting its involvement in maintaining the undifferentiated state of GSCs (Schmitz *et al.*, 2007). Silencing of SOX2 in glioblastoma cells resulted in loss of proliferative activity, most likely due to becoming more mature and exiting the cell cycle (Maria *et al.*, 2009). Additionally, when cells were placed into differentiating conditions, the expression of SOX2 dramatically decreased (Maria *et al.*, 2009).

1.8.3 Nestin

Intermediate filaments, microtubules and microfilaments are all structural components of the cytoskeleton, which provide mechanical and stress-coping mechanisms to cells (Snider and Omary, 2014). Nestin is an intermediate filament protein that is expressed in NSCs and is commonly used as a marker for GSCs. Nestin positive cells are highly proliferative and have the ability to differentiate into multiple lineages making them an attractive target for therapy (Bernal and Arranz, 2018). Similar to SOX-2, knockdown of nestin supressed the proliferation and invasion of glioblastoma cells (Wei *et al.*, 2008). As progenitor cells differentiate their

nestin filaments are replaced by other intermediate filament proteins such as GFAP (Lu *et al.*, 2011).

1.9 Glioblastoma Models

1.9.1 Established 'classic' cell lines

Established cell lines are frequently employed in research due to their practicality, cost-effectiveness, reproducibility and minimal ethical considerations (Wang *et al.*, 2009). Classic cell lines have been immortalised, ensuring they do not undergo senescence and proliferative rapidly. Despite their initial derivation from glioblastoma patient tumours, these cell lines rarely represent the clinical characteristics of primary cells from which they originated often diverging genetically and epigenetically. Lee *et al* (2006) demonstrated that xenograft tumours developed from serum-grown cell lines did not accurately represent true glioblastoma characteristics. This divergence can be attributed to genetic modifications that enable indefinite growth, the addition of growth factors, and the phenotypic and genotypic variations that can occur with consecutive passaging on plastic surfaces. As a result, their use is typically confined to initial clinical experiments, such as testing agents and conducting mechanistic studies. There is also the issue of cross contamination with mycoplasma and other cell lines, which can additionally affect the outcome of experiments leading to false results. For instance in 1970 Walter Nelson-Rees showed that the majority of cell lines were in fact cross-contaminated with highly proliferative HeLa cells (Nelson-Rees, Daniels and Flandermeyer, 1981).

1.9.2 Patient-derived 'primary' cell lines

Patient-derived primary cell lines are obtained directly from resected tumour samples or biopsies and cultivated in the laboratory. Despite altering the tumours original architecture and environment, it offers several advantages. Primary cell lines enable a higher degree of control over experimental conditions, making it possible to test multiple drug combinations that could be ethically problematic in *in-vivo* testing. Additionally, these models make it easier to study the effects of treatment on tissues during and after the process using imaging techniques that would be otherwise unfeasible in an *in-vivo* setting. Compared to established cell lines, utilising a primary cell approach gives a more accurate representation of

glioblastoma tumours and their response to drug treatment. One key reason for this is that dissociated tumour cells retain all the different cellular populations, including immune, fibroblasts and endothelial cells. Furthermore, patient derived primary cell lines have not undergone multiple passaging on plastic which can promote selection of specific cell types and thus cause genetic and phenotypic changes that may not accurately reflect the original patient tumour. As a result, primary cell models exist as a valuable tool in glioblastoma research, offering a more faithful representation of the disease and its response to therapeutic interventions.

The challenge of establishing consistent culture conditions for glioblastoma cells is evident, with a plethora over 20 possible culture conditions within the literature (i.e, NSC media, oligodendrocyte precursor cell (OPC media, and fetal bovine serum (FBS) containing media) (Ledur *et al.*, 2017). This extensive variation in culture conditions, presents a significant hurdle in making direct comparisons across studies. For instance, it has been shown culturing cell lines within DMEM media containing FBS, stimulates differentiation towards astrocytic cell state, whereas serum-free conditions containing growth factors EGF and FGF-2 are able to propagate cell lines with NSC properties which avoid differentiation (Conti *et al.*, 2005; Sun *et al.*, 2008). It is worth noting, culturing glioblastoma cells within EGF and FGF-2 has shown to increase expression and signalling of EGFR, this correlated with an increase in sensitivity to EGFR inhibitors Gefitinib and AG-1478. Hence, careful consideration of appropriate cell culture conditions is paramount before undertaking cell-based screening to avoid misleading results (Ledur *et al.*, 2017). It is known that glioblastoma cells grown under serum free conditions are more representative of their parent tumour (Lee *et al.*, 2006; De *et al.*, 2008), alarmingly the majority of early research involving cell line and/or Xenograft models have used these serum culture conditions. This raises the unsettling possibility that numerous potential therapeutic strategies may have been prematurely dismissed due to the genetic drift resulting from these early experiments employing serum-containing growth conditions.

Culturing of primary glioblastoma cell lines can be performed as either 2D monolayers or in 3D suspension. To initiate adherent monolayer formation, a basement membrane extract (BME) such as Matrigel or Cultrex is essential, as neurospheres form in suspension cultures in the absence of such support. Neurospheres, which replicate the 3D morphology of the

original tumour, come with some disadvantages. These include slower expansion rates, elevated levels of cell death, and an increased presence of differentiation markers compared to adherent cultures (Pollard *et al.*, 2009). Leveraging neurosphere cultures for drug screening poses several challenges. Firstly, conducting robust screenings necessitates a substantial quantity of neurospheres due to their relatively low expansion rates. Quantifying cell proliferation within these spheres is more complex than 2D methods requiring more sophisticated microscopy techniques and methods of analysis. Moreover, neurospheres exhibit variable levels of cell death and differentiation, and the fusion of multiple neurospheres can further complicate analysis when assessing either the number or size of these structures. To address these complexities, the utilization of adherent monolayers of glioma NSCs emerges as the more favourable approach, particularly in the context of drug screening.

1.9.3 Organoid Structure Models

Organoids are multicellular miniaturized three-dimensional cultures, constructed from stem cells *in-vitro.* Cerebral organoids with self-renewal and self-organising properties can be constructed from stem cells, either through the induction of embryonic stem (ESC) or pluripotent stem cells (iPSCs). Human cerebral organoids have been successfully developed to model human developmental disorders such as Timothy and Phelan-McDermid syndrome (Birey *et al.*, 2017; Miura *et al.*, 2020). Glioblastoma can be modelled using cerebral organoids through gene editing techniques such as clustered regularly interspaced short palindromic repeats (CRISPR) to initiate mutagenesis through targeting glioblastoma specific genetic aberrations (Bian *et al.*, 2018; Ogawa *et al.*, 2018). Nevertheless, this approach is limited to studying the initiation and progression of the disease. Alternatively, organoids can model glioblastoma through implantation of patient derived GSCs, to initiate growth of glioblastoma within a 3D model brain environment (Ogawa *et al.*, 2018).

Unlike cell cultures, organoids can be co-cultured with both tumour and healthy cells and therefore interactions between these two cells environments and individual drug response profiles can be monitored within the same system, thus highlighting any potential side effects on healthy cells or the interaction with other cell types such as the immune complement. Organoids are limited, they do lack essential cell types such as endothelial cells, microglial,

other issues include the ability for cerebral organoids cells to fully differentiate into the six layers of the cortex, only the deepest layers have been produced. Nevertheless, since (Pham *et al.*, 2018) showed it is feasible to vascularize brain organoids using the patient's own iPSC derived endothelial cells, many more improvements and strategies have been developed, including a more recent advanced approach which also incorporated a functional BBB like structure as well as microglial cells into brain organoids, which are brain specific immune cells (Sun *et al.*, 2022).

Despite showing promise there are limitations to the organoid model, as they are not a perfect replica of the human brain. Cerebral organoids most commonly used for glioblastoma research lack endothelial cells meaning there is no vasculature, the centres of organoids can turn necrotic due to lack of oxygen and nutrients, therefore extra experimental design is needed in order to achieve vascularization of brain organoids (Pham *et al.*, 2018). Furthermore, the human cerebral cortex consists of six layers, but only the deepest of these have been expressed in cerebral organoids showing that *in-vitro* the stem cells are not able to fully differentiate (Ogawa *et al.*, 2018). Culturing organoids is also an expensive process as they take months in order to grow and mature thus reducing their efficiency as a glioblastoma model and also their practicality for high-throughput screening methods (Hubert *et al.*, 2016; Qian, Song and Ming, 2019). Finally, there is large variability between organoid culture within research laboratories. This is due to protocols relying on human pluripotent stem cells (hPSC) self-organisation meaning no two organoids being identical, limiting the reproducibility and therefore the quality of research produced through organoid models (Qian, Song and Ming, 2019).

1.9.4 Murine models

Mouse models are commonly employed in glioblastoma research due to their accessibility and cost-effectiveness. Mice and humans share relatively similar genomic and physiological characteristics, it is predicted that mice share approximately 80% of humans orthologue genome (Waterston *et al.*, 2002). The preclinical glioblastoma mouse models are categorized into three categories; xenografts, genetically engineered mouse models (GEMMs) and syngeneic mouse models. Murine models provide researchers with a useful tool to investigate

basic mechanisms of cancer development, treatment response and insight into pharmacokinetic (PK) and pharmacodynamics (PD) of drugs.

There is a long-standing debate as to whether animal models such as mice can accurately predict human therapy response. Drug development is a high risk, costly and lengthy process, which suffers from high attrition rates, approximately 90% of clinical drug developments fail. In particular, oncology has the lowest possibility for success in drug development programmes (Jardim *et al.*, 2017; Wong, Siah and Lo, 2019). The main causes of failures are due to lack of efficacy and increased toxicity of drugs within humans, which only becomes apparent in the late stages of clinical trials. Equally lead compounds may be eliminated at early pre-clinical stages due to their toxicity in animals, which may have acceptable risk profiles in humans. Clearly suggesting that drug development success is highly dependent on the pre-clinical animal model used. Certainly, efficacy can be improved through the use of more clinically relevant models for instance replacing cell line xenograft models with patient-derived models. Toxicity can only be monitored through testing within humans, provided that safety has been shown within animal studies, however this can be avoided through the repurposing of pre-approved drugs.

1.9.5 Xenograft Models

Xenograft models can be classified as either traditional cell line or patient-derived xenografts (PDX). Both can be accomplished through either orthotopic or subcutaneous transplantation. For glioblastoma establishing orthotopic models involves the transplantation of spheres or biopsies directly into the brains of mice and are therefore more closely related to the clinical setting as they provide mouse brain microenvironment. In comparison to subcutaneous xenografts where spheres or biopsies are transplanted directly into flanks of mice, orthotopic intercranial models are more technically challenging to produce.

It is important to note that xenograft models have limitations, particularly in representing the host's antitumor immune response in human glioblastoma. The absence of a functional immune system in xenograft models make them redundant in the testing of immunotherapies which are becoming increasingly desirable to investigate due to increases in SoC for many cancers. Additionally, the loss of immune complement has considerable effects on increasing

the growth rates of the implanted tumours, clearly making them more susceptible to antiproliferative agents, often providing false drug efficacy information.

1.9.6 Cell line Xenograft

Traditional xenograft models involve the transplantation of human cancer cells into immunocompromised mice. Multiple established glioblastoma cell lines such as U87, U251 and LN18 have been successfully xenografted. These models have advantages of high engraftment, reliable disease growth and progression, high growth rates with good reproducibility for investigating glioblastoma. Immortalised cell lines can be easily expanded *in-vitro*, to yield large numbers of tumour cells for experimental use (Huszthy *et al.*, 2012). Despite this, cell line xenografts often do not resemble the complex clinical characteristics of the original tumour they are presumed to model (Kerbel, 2003; Martens *et al.*, 2008). For instance the U87MG cell line which was originally obtained in 1966 was recently re-sequenced in 2018, evidently the results indicated a large number of indels, copy number variations and translocation presumably due to years of cell culture (Eskin, 2010). This suggests that the U87MG cell line used today is drastically different to the original tumour, despite being one of the most widely used glioblastoma cell models with over 3,800 entries in PubMed over the last 10 years. Why are we continuing to use these dated glioblastoma cell line models when they don't mimic the true characteristics of original patient tumours?

1.9.7 Patient Derived Xenograft

The most clinically relevant *in-vivo* model is the PDX, where surgically removed tumour biopsies or spheroids are implanted into immunocompromised mice. There are two main methods for establishing PDX models, the first involves the direct injection of biopsy tumour tissue and the second is injection of cultured tumour cells or spheres. Both methods can maintain the genetic and phenotypical features of original patient tumour. Nevertheless, injecting biopsy tissue may be more clinically relevant as the architecture of original tissue is maintained, along with endothelium, extracellular matrix and resident macrophages (Kijima and Kanemura, 2017).

PDX models have the clear advantage of retaining both the genetic and histological features of the original patient tumour (Kijima and Kanemura, 2017). One main reason for this is

tumours are propagated through successive generations of mice, preventing the selection events and phenotypic drift that often occur in cell culture (Dangles-Marie *et al.*, 2007; Daniel *et al.*, 2009). One major caveat of PDX models is unsuccessful engraftment due to tumour size, aggressiveness, and low viability. PDX models are highly reliant on large tumour samples with good viability, to achieve successful engraftment, which is not always possible for every patient. This makes it increasingly difficult to model lower grade tumour such as oligodendrogliomas which proliferate much slower than higher grade tumours, more invasive tumours which are surgically difficult to remove and smaller sized tumours in general. Once engraftment is successful it can take between 2-11 months for sufficient tumour growth (Wang *et al.*, 2009).

1.9.8 Genetically Engineered

Better understanding of the genomic mutations involved in primary brain tumours and their classifications has led to the development of GEMMs, which represent an important tool to expose the genetic aberrations involved in tumour initiation and progression. GEMMs are genetically modified to give rise to mutations, deletions or overexpression in one or several genes thought to be involved in the progression of glioblastoma (Richmond and Su, 2008). Gene expression is manipulated using Tet-regulation or Cre-inducible gene alleles, allowing gene expression to be tightly controlled is a tissue specific and/or time specific manner. Again, these models also require up to a year to develop prior to drug screening (Richmond and Su, 2008), which for the purpose of producing rapid reliable models is one of its downfalls.

When comparing GEMMs to PDX models, each have their own strengths and weaknesses. Firstly, GEMMs are established in immunocompetent animals, therefore will allow the testing of immunotherapies. Nevertheless, the tumour and the immune response is of mouse origin and therefore cannot reliably mimic glioblastoma behaviour and immune response in humans. The cascade of mutational events which lead to specific glioblastoma classifications is extremely complex and not fully understood, it is therefore questionable whether GEMMs can truly mimic the tumour initiating events in human glioblastoma. Additionally, not only the tumour environment but the tumour itself is of mouse origin, for this reason PDX models are more suitable when the goal is to create a clinically relevant model to for the investigation of

novel treatments. However, if purpose is understanding the mutational events involved in the initiation of glioblastoma and tumour progression, then GEMMs are suitable models.

1.9.9 Syngeneic Mouse Models

Syngeneic mouse models come in two varieties: spontaneous or those induced by carcinogens or chemicals. The tumour cells in these models originate from mice themselves, either developing spontaneously or, more frequently, induced through mutagenic substances or transposons (Ausman, Shapiro and Rail, 1970; Genoud *et al.*, 2018). Syngeneic mouse models are immunocompetent, therefore can recapitulate host immunity and therefore are the most preferred model for the analysis of immunotherapeutic therapies (Genoud *et al.*, 2018). Syngeneic mouse models have contributed significantly to our understanding of cancer biology and the development of new cancer therapies. They provide a controlled and reproducible system for studying tumour growth, progression, and the effects of therapeutic interventions within the context of an intact immune system. The degree to which murine induced glioma models reflect human glioblastoma and human immunity is unknown therefore clinical relevance is questionable. For example, when examining the mutational load of syngeneic models and comparing it to human glioblastoma, these models frequently exhibit a substantially elevated mutational burden (often hundreds of times higher) (Johanns *et al.*, 2016; Genoud *et al.*, 2018).

1.10 Ex vivo drug screening

1.10.1 Introduction

In the realm of precision medicine, personalized therapy is often synonymous with genetic biomarkers/profiles, as indicated by Letai (2017). This approach has yielded remarkable success in tailoring treatments based on genetic biomarkers in specific cancer types, such as the use of EGFR inhibitors in non-small cell lung cancer (NSCLC) and BRAF inhibitors in melanoma (Bria *et al.*, 2011; Hauschild *et al.*, 2012). Nevertheless, several studies have demonstrated that a significant proportion of cancer patients undergoing genomic testing alone do not experience the advantages of a precision medicine strategy. For instance, data from a sequencing program conducted at the MD Anderson Cancer Centre in Houston showed that only11% (83/2000) participants enrolled were eligible for genotype-matched trials based

on the presence of actionable mutations (Meric-Bernstam *et al.*, 2015). Similarly, a Molecular Analysis for Therapy Choice (NCI-MATCH) trial conducted at the US National Cancer Institute could only match 2% of the 795 participants enrolled with targeted therapies (Flaherty *et al.*, 2020). In the context of glioblastoma, advancements in genomics have enabled clinicians to subdivide the disease into different subtypes but despite these developments, there has been no corresponding improvement in patient survival rates. A recently initiated pilot program within the NHS, known as the Minderoo Precision Brain Tumour Programme in Cambridge, aims to introduce personalized medicine to patients with glioblastoma, based on genomic sequencing data. Nevertheless, it is yet to be determined whether this trial will achieve success. The limitations of genomics in guiding treatment decisions have prompted the exploration of alternative approaches to personalized medicine. One such approach involves integrating genomic data with drug screening of patient's tumour samples or biopsies (Pauli *et al.*, 2017), or even as a standalone technique in blood-based malignancies and rare cancers (Snijder *et al.*, 2017; Arjonen *et al.*, 2020; Nykänen *et al.*, 2021). A summary of the important factors to be considered whilst implementing an ex vivo screening pipeline into clinical practice is shown below in figure 1.13.
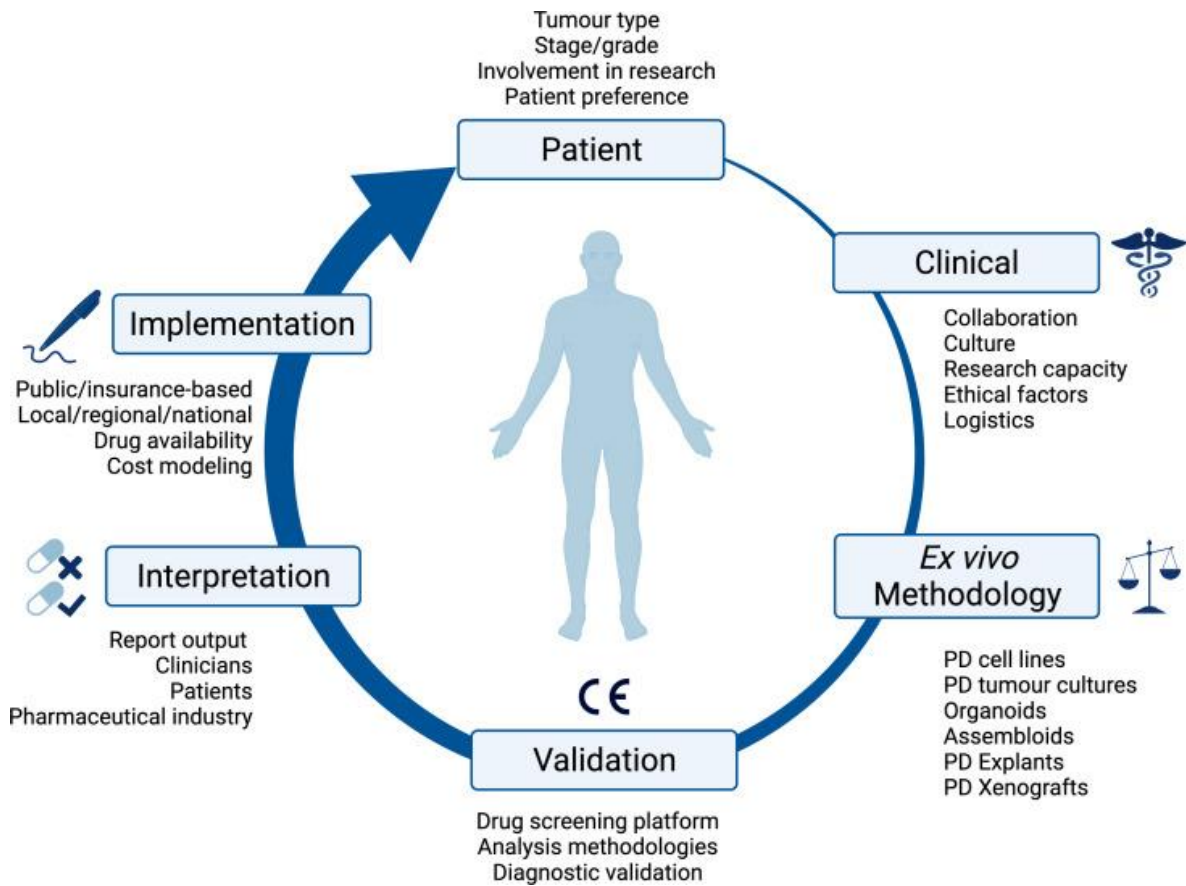
Figure 1.13 – Examination of the factors to be considered when incorporating ex vivo methods into clinical practice - Patient derived (PD), Conformité Européenne (CE). Figure adapted from Williams *et al* (2022). Copyright permissions obtained from publisher (Open Access).

1.10.2 Success of ex vivo screening

An ex vivo screening approach for personalised therapy in advanced haematological cancers has successfully reached clinical trials (NCT03389347) (https://clinicaltrials.gov/). A study by Snijder *et al* (2017) investigated the use of ex vivo screening of 17 leukaemia and multiple myeloma patient against a library consisting of 139 drug compounds. The study combined immunofluorescence (IF), high-throughput microscopy and single cell image analysis named "Pharmacoscopy" and integrated this into the clinic, allowing eligibility for any patient who had exhausted all standard treatments, or were not suitable for any ongoing clinical trial. Drug response was measured through comparison between marker-positive viable cells following treatment to marker-positive cells in dimethyl sulfoxide (DMSO) control wells. Significant results were then be assessed by a panel of experts consisting of haematologists, pathologists, pharmacists and molecular biologists to approve the pharmacoscopy guided treatment as safe and available for the candidate. In the study patients who received ex vivo

guided treatment experienced significantly longer PFS and positive overall response compared to their previous most recent treatment regimens, with 15/17 patients showing complete remission or partial response, compared to 4/17 respectively.

Diffuse intrinsic pontine glioma (DIPG) is a childhood brain tumour and is the main cause of child brain tumour related death. Similar to glioblastoma prognosis is poor, survival has remained unchanged over the past 20 years with median survival less than one year (Hargrave, Bartels and Bouffet, 2006). SoC is limited to conventional RT, despite numerous clinical trials investigating its use in combination with chemotherapy, no single chemotherapeutic alone or in combination has been able to improve disease free survival or OS in children (Hargrave, Bartels and Bouffet, 2006; Khatua *et al.*, 2011). Unlike glioblastoma, surgical resection is not a standard practise, as removal can cause severe neurological damage or be fatal, hence the use of biopsy and autopsy tissue mentioned below. A previous study by (Grasso *et al.*, 2015) screened a panel of 83 drug compounds in patient-derived DIPG cultures obtained from biopsy and autopsy samples. The research was able to identify histone deacetylase (HDAC) inhibitor panobinostat as a promising agent for DIPG both *in-vitro* and orthotopic xenograft models, the results have led to multiple clinical trials into the use of panobinostat in DIPG treatment (NCT03632317, NCT02717455, NCT03566199). Further work by the same group (Lin *et al.*, 2019) has advanced this high throughput screening (HTS) application through testing combinatorial drug therapies in DIPG. Several drug screens were performed combining 9195 drug-drug combinations in order to identify possible combination therapies for DIPG. This study identified HDAC inhibitor panobinostat and proteosome inhibitor marizomib as a potential drug combination, this has then guided another phase I clinical trial combining these two identified drugs (NCT04341311).

1.10.3 Ex vivo screening in glioblastoma

Regarding glioblastoma, previous research conducted by Quartararo (2015) involved screening a variety of compounds, including those in clinical development or FDA-approved, using eight patient-derived glioblastoma models. These models were cultured either in adherent two-dimensional monolayers on laminin or as neurospheres, which are 3D clusters enriched with CSCs. By comparing the sensitivity data obtained from these patient-derived glioblastoma models with publicly available data from traditional glioblastoma cell lines, the

study identified the Bcl-2 targeting drug ABT-263 and the mTOR inhibitor AZD-8055 as hits. Interestingly, these drugs had previously shown no sensitivity in established glioblastoma cell lines. This observation is significant as it suggests that many other potential drugs might have been overlooked in investigations using conventional cell line models. It underscores the value of this study in providing an opportunity to re-evaluate drugs that were previously dismissed, or repurpose already approved compounds, using a more suitable model that reflects real patient tumours.

A larger study by Hothi *et al* (2012) screened a 2,000 drug compound library against five GSC cultures, the library consisted of FDA approved drugs, those reaching late clinical trials, experimental drugs and also natural products. The study identified disulfiram (a clinically approved drug to treat chronic alcoholism) as a potential potent inhibitor of GSC proliferation. This is an example of how HTS approaches can identify possible new treatment methods, as disulfiram is an FDA approved drug for which human PK are already established; is able to penetrate the BBB and is fairly non-toxic (Johansson, 1992). Additionally, the timeline for which pre-clinical and early phase clinical testing can be carried out from the initial HTS hit discovery towards a potential glioblastoma treatment would be significantly less in comparison to novel experimental drugs, which require a full drug discovery process which usually take ~15 years to ensure the drug is suitable for human consumption and the adverse side effects are minimal.

A more recent study conducted by Skaga *et al* (2019) employed HTS for recurrent glioblastoma patients undergoing secondary surgery following SoC treatment. This study expanded primary cell cultures for approximately 6 weeks until an appropriate cellular yield was reached prior to completion of any assays, facilitating the ability to screen a much broader drug library and potentially combination therapies. Despite this, the prolonged cell culture may induce differentiation and mutagenesis, for instance work by (Vik-Mo *et al.*, 2010) has shown that brain tumour biopsies dissociated into cells and grown in serum free conditions have adapted to conditions, e.g increased growth rates. Consequently, it could be argued that the methodologies used in this project may yield cells that are less representative of tumour cells in their original state. Nevertheless, none of the resected cell models displayed any sensitivity to TMZ, confirming clinical response data.

1.10.4 Benefits and limitations to ex vivo screening

The overarching advantages and disadvantages of HTS ex vivo screening approaches are summarised in table 1.2 below. *In-vivo* glioblastoma models that are considered more clinically relevant often involves PDX. This entails the orthotopic or subcutaneous implantation of surgically removed tumour biopsies or spheroids into immunocompromised mice. PDX models can be established either by directly injecting tumour biopsy tissue or by injecting cultured tumour spheres or monolayer cells. When comparing ex vivo methodology with the generation of PDX models involving the direct injection of tumour biopsy tissue, the latter approach offers the advantage of preserving the tumour's architectural features, as well as maintaining elements like endothelial cells, the extracellular matrix, and resident macrophages (Kijima and Kanemura, 2017). While this method closely reflects clinical relevance, it is important to acknowledge a significant drawback: its reliance on larger tumour samples with high viability for successful engraftment. This dependence leads to the generation of fewer PDX models using tumour biopsy tissue and, consequently, limits the scope of drug compounds that can be tested. The culturing of these cells for drug screening and before PDX implantation may introduce some phenotypic changes and selection processes while they are on plasticware, potentially affecting the representation of the original tumours characteristics (Dangles-Marie *et al.*, 2007; Daniel *et al.*, 2009).

Within HTS there are multiple available microplates which contain either 96, 384, 1536, 3456 or 6144 individual wells, therefore depending on the dose range and number of replicates of each drug it is possible to test ~6000+ different compounds. Obtaining the necessary number of PDX avatars per patient required to recapitulate the capabilities of HTS would be highly challenging. Typically, testing a single treatment within PDX model requires approximately 5-10 mice. If we were to design a screen testing 30 different compounds within 30 patients, in order the replicate this in *in-vivo*, a minimum of 5,250 PDX models would be needed (175 models for each patient). This constitutes an exceptionally large sample size, and the process of serially transplanting into multiple cohorts of mice would be both financially astronomical and extremely time-consuming. Investigation of the literature highlighted that successful PDX engagement can take anywhere between four to eight months (Rubio-Viqueira *et al.*, 2006; Zhang *et al.*, 2018), without considering the additional 2-11 months it can take for sufficient

tumour growth (Wang *et al.*, 2009). When this timeline is considered alongside the average life expectancy of glioblastoma patients, which is typically 12-18 months, attempting to utilize PDX models to guide treatment therapy could be considered unethical and impractical.

It is important to note that HTS does not come without its limits; firstly it does not take into account the BBB and also endothelial cell drug efflux pumps (Daher and de Groot, 2018), also it is not a model that can be used to completely replace murine models indefinitely but instead reduce and replace their use. If drug sensitivities are investigated and shown to be significant through HTS, future work would entail investigating the PK and PD properties of the drugs in mice (if not already known).

Table 1.2 - Advantages & Disadvantages of ex vivo drug screening

Advantages	Disadvantages
Cheaper and more rapid than PDX models	New field of research therefore limited availability of expertise
Can give individual patient response to treatment in 7 days of surgery	Tumour integrity e.g vascularity broken down during dissociation
Possible to test large drug libraries on one individual sample	Does not give any information regarding drugs PK and PD properties
Sample is more reflective of original tumour compared to cell lines due to less time on plasticware	Not possible to perform direct biological repeats using freshly dissociated patient samples
More ethical as does not involve the use of animal models which would usually experience moderate/severe symptoms	Non approved drugs & drug combinations will often still require pre-clinical investigation within animals

1.11 Study Aims

1.11.1 Aims of the study

We anticipate that the development of this ex vivo screening approach will become a standard tool integrated into the post-surgery pipeline of glioblastoma. This platform could serve as a primary screening method, especially for patients with functioning *MGMT* genes who do not statistically benefit from the SoC TMZ treatment in terms of PFS. Ex vivo screening represents a highly personalized approach, with suitable drug choices determined on an individual patient basis, in contrast to traditional clinical studies that rely on overall improvements within patient populations.

1.11.2 Hypothesis

- Ex vivo drug screening methodologies can be developed using solid glioblastoma tissue.
- We can predict clinical response to TMZ based on their MGMT gene methylation status.
- Highlight drugs which can specifically target the glioma stem cell populations through optimisation of suitable IF markers.

Chapter 2 – Materials and Methods

2.1 Materials

Table 2.1 - General laboratory equipment

Item	Company
Cellometer Mini Automated Cell Counter	Nexcelom Bioscience
Cell Discoverer 7 Microscope	Carl Zeiss
Centrifuge	Eppendorf
Incubator (tissue culture)	Sanyo
Multichannel Pipette E1-ClipTip 5-125uL pipette	Thermo Scientific
Multidrop™ Combi Reagent Dispenser	Thermo Scientific
Repetman™ Electronic Pipette	Gilson
Waterbath	Cleaver Scientific
Mr Frosty™ freezing container,	Corning
NanoDrop 2000 Spectrophotometer	Thermo Scientific
Thermal Cycler T100	BioRad
Real-Time PCR (Applied Biosystems 7900HT)	Thermo Scientific
SpectraMax iD5 Plate Reader	Molecular Devices
Matrix Plate Mate Plus	Thermo Scientific
Echo 550	Labcyte Inc
ThermoMixer® C	Eppendorf (5382000031)
Caesium (137) Irradiator	Cis Bio International (IBL 437 C)

Table 2.2 - Table of consumables.

Item	Company (Product Code)
Tissue Culture Flasks (Nunclon™ Delta Surface EasYFlask™) – 25cm2, 75cm2	Fisher Scientific
CellBIND – 384-well plate	Corning (3770)
Perkin Elmer Cell Carrier Ultra 384-well	Perkin Elmer (6057302)
6 Well Tissue Culture Treated Plates	Costar
Disposable Serological Pipettes – 5ml, 10ml & 25ml	FisherBrand™
Centrifuge Tubes - 50mL	Scientific Laboratory Supplies
Centrifuge Tubes – 25 mL	Scientific Laboratory Supplies
Cryovials	Sarstedt
Eppendorfs – 0.2ml, 0.5ml, 1.5ml & 2ml	Scientific Laboratory Supplies
Disposable Reservoirs (50mL)	Fisher
Breathe-Easy sealing membrane	Scientific Laboratory Supplies

Nunc™ Cell Scrapers	Thermo Fisher Scientific (179707PK)
Filter Tips – 0.1-10µl, 2-20µl, 2-200µl, 100-1000µl	Starlab
Optical Adhesive Film (MicroAmp™)	Thermo Fisher Scientific (4311971)
Repetman™ Sterile Pipet Tips – 1.25ml, 5ml, 12.5ml	Gilson
PCR Tubes – 200µl	Starlab
QAIshredder Tubes (50)	Qiagen (79654)
Reagent Reservoir – 50ml	Corning
RNeasy Mini Kit	Qiagen (74104)
MicroAmp™ Optical Adhesive Film	Applied Biosystems (4311971)
BreatheEasy® Sealing Membrane	Sigma (Z380059-1PAK)

Table 2.3 - Table of reagents

Item	Company (product code)
1,4-dithiothreitol (DTT)	Sigma (DTT-RO)
4',6-Diamidino-2-Phenylindole, Dihydrochloride (DAPI)	Thermo Fisher Scientific (D1306)
Accutase™ StemPro™ Cell Dissociation Reagent	Invitrogen (A11105-01)
ACK lysing buffer	Gibco (A1049201)
Advanced DMEM/F-12 (Dulbecco's Modified Eagle Medium/Ham's F-12)	Invitrogen (12634028)
Amphotericin B (Fungizone)	Gibco (15290)
B-27 Supplement (50x) Serum Free	Invitrogen (17504-044)
B-Nicotinamide mononucleotide	Sigma (N3501)
Benzonase Nuclease	Novagen (70664-3)
Bovine Serum Albumin (BSA)	Sigma-Aldrich (A2153-100G)
Cultrex™ Stem Cell Qualified RGF basement membrane extract	R&D Systems (3434-005-02)
Dimethyl Sulfoxide (DMSO)	Fisher Scientific (BP231-100)
EGF Recombinant Human Protein	Invitrogen (PHG0313)
Ethylenediaminetetraacetic acid (EDTA)	Sigma (1233508)
FGF Recombinant Human Protein	Invitrogen (PHG0263)

Foetal Calf Serum	Lonza (BE12-60F4)
Heparin Sodium Salt	Sigma (H3393-10KU)
High-Capacity RNA-to-cDNA™ Kit	Thermo Fisher Scientific (4387406)
L-Glutamine-200mM (100x)	Invitrogen (25030081)
Minimum Essential Medium (MEM)	Invitrogen (10370-047)
N-2 Supplement (100x) Serum Free	Invitrogen (17502-048)
NuPAGE™ 4-12% Bis-Tris Protein Gels – 1.5mm, 10 well	Thermo Fisher Scientific (NP0335BOX)
NuPAGE™ 4-12% Bis-Tris Protein Gels – 1.5mm, 15 well	Thermo Fisher Scientific (NP0336BOX)
NuPAGE™ LDS Sample Buffer (4X)	Thermo Fisher Scientific (NP0007)
NuPAGE™ MOPS SDS Running Buffer (20X)	Thermo Fisher Scientific (NP0001)
NuPAGE™ Transfer Buffer (20X)	Thermo Fisher Scientific (NP0006)
NuPAGE™ Tris-Acetate SDS Running Buffer (20X)	Thermo Fisher Scientific (LA0041)
Paraformaldehyde (PFA) – 4% solution in PBS	Thermo Fisher Scientific (J60401)
Penicillin-Streptomycin (10,000U/ml)	Invitrogen (15140122)
Phosphatase Inhibitor Tablets (PhosSTOP™)	Sigma (4906845001)
PierceECL Western Blotting Substrate	Thermo Fisher Scientific (32106)
Prolong Gold Antifade Mountant	Thermo Fisher Scientific (P36930)
Protease Inhibitor Cocktail (cOmplete™ ULTRA Tablets Mini *EASYpack*)	Sigma (5892970001)
RNeasy Mini Kit	Qiagen (74104)
Sodium chloride	Sigma (S7653)
TaqMan™ Universal PCR Master Mix (No AmpErase™ UNG)	Applied Biosystems (4324018)
Tris Hydrochloride	Sigma (10812846001)
Triton™ X-100	Sigma-Aldrich
Trypan Blue	Sigma (T8154-20ML)

TWEEN® 20	Sigma (P1379)
Nitrocellulose Membrane (Protran®)	VWR (10600010)

Table 2.4 - Table of antibodies.

Antigen	Raised in	Conjugated	Application & Dilution	Company
a-PAR	Rabbit	Unconjugated	WB 1:1000	Millipore (MABE1016)
ATM	Mouse	Unconjugated	WB 1:1000	Santa Cruz (sc-23921)
ATR	Goat	Unconjugated	WB 1:1000	Santa Cruz (sc-1887)
Aurora A	Mouse	Unconjugated	WB 1:500	Abcam (ab13824)
Aurora B	Rabbut	Unconjugated	WB 1:1000	Abcam (ab2254)
B-Actin	Mouse	Unconjugated	WB 1:2000	Santa Cruz (sc-47778)
BRCA2	Mouse	Unconjugated	WB 1:1000	Calbiochem (OP95)
CD133	Rabbit	Unconjugated	IF 1:250	Abcam (ab216323)
CD133 (Prominin)	Rabbit	Alexa Fluor® 488	IF 1:500	Abcam (ab252126)
CDK1	Rabbit	Unconjugated	WB 1:500	AbClonal (WH224668)
CHK1	Mouse	Unconjugated	WB 1:1000	Sigma (C9358)
CHK2	Rabbit	Unconjugated	WB 1:1000	Cell Signalling (2662S)
DNA-PK (Thr2609)	Rabbit	Unconjugated	IF 1:250	Thermo Fisher(PA1-29541)
DNA-PKcs	Mouse	Unconjugated	WB 1:1000	Abcam (ab1832)
FANCD2	Mouse	Unconjugated	WB 1:1000	Abcam (ab12450)
GAPDH	Mouse	Unconjugated	WB 1:5000	Abcam (ab174646)
GFAP	Mouse	Alexa Fluor® 549	IF 1:500	Santa Cruz (SC-33673)
GFAP	Mouse	Unconjugated	WB 1:1000	Santa Cruz (sc-58766)
KAP1	Mouse	Unconjugated	WB 1:1000	Bethyl Laboratories (A300-274A)
Nestin	Mouse	Alexa Fluor® 647	IF 1:500	Abcam (ab196693)
Nestin	Mouse	Unconjugated	WB 1:250	Abcam (ab6142)
P53	Rabbit	Unconjuagated	WB 1:500	Abcam (ab131442)

PARG	Mouse	Unconjugated	WB 1:500	Santa Cruz (sc-398563)
PARP-1	Mouse	Unconjugated	WB 1:1000	Santa Cruz (sc-8007)
pATM (Ser1981)	Rabbit	Unconjugated	WB 1:1000	Abcam (ab81292)
p-CDC2	Rabbit	Unconjugated	WB 1:1000	Cell Signalling (9111)
pCHK1 (Ser345)	Rabbit	Unconjugated	WB 1:500	Cell Signalling (133D3)
pCHK2 (Thr68)	Rabbit	Unconjugated	WB 1:500	Cell Signalling (13C1)
pDNA-PKcs (s2056)	Rabbit	Unconjugated	WB 1:1000	Abcam (ab18192)
pKAP1 (s821)	Mouse	Unconjugated	WB 1:1000	Bethyl Laboratories (A300-767A-M)
Rad51	Mouse	Unconjugated	WB 1:1000	Abcam (ab213)
yH2AX (Ser139)	Mouse	Unconjugated	IF 1:500	Millipore (JBW301)

Table 2.5- Table of secondary antibodies

Secondary Antibody	Application & Dilution	Company (Product Code)
Alexa Fluor ® 555 Goat Anti-mouse	IF 1:500	Life Technologies (A21424)
Alexa Fluor ® 647 Goat Anti-rabbit	IF 1:500	Life Technologies (A21245)

Table 2.6 - Inhibitors and Cytotoxic agents.

Drug	Target	Solvent	Stock Conc	Company
Alisertib	AURKA	DMSO	10mM	apex bio
Aphidicolin	PKC	DMSO	10Mm	apex bio
AX15836	ERK5	DMSO	10mM	Med chem express
AZD0156	ATM	DMSO	10mM	Selleckchem
AZD1775 (Adavosertib MK-1775)	WEE1	DMSO	10mM	apex bio
AZD6244 (Selumetinib)	MEK1/2	DMSO	10mM	apex bio

AZD6738	ATR	DMSO	10mM	Selleckchem
AZD9291 (Osimertinib)	EGFR	DMSO	10mM	apex bio
AZD1390	ATM	DMSO	10mM	Selleckchem
AZD7648	DNA-PK	DMSO	10mM	Selleckchem
Bevacizumab	Anti-VEGF	PBS	1mg/mL	Selleckchem
Bleomycin	DNA strand breaks	DMSO	10mM	apex bio
BLU-554	FGFR4	DMSO	10mM	Selleckchem
Butamben	Calcium channels	DMSO	10mM	apex bio
Cisplatin	DNA synthesis	H_2O	10mM	Sigma Aldrich
Curcumin	FA Pathway; NK-kB	DMSO	10mM	apex bio
D-Penicillamine	Copper chelator	DMSO	10mM	apex bio
Debrafenib	CdK18-binding	DMSO	10mM	apex bio
Dexamethasone	Glucocorticoid receptor, IL receptor	DMSO	10mM	apex bio
Ipilimumab	Anti-CTLA-4	PBS	1mg/mL	Selleckchem
KU55933	ATM	DMSO	10mM	Selleckchem
LNT 1	FEN1	DMSO	10mM	Biotechne
M3814 (Nedisertib)	DNA-PK	DMSO	10mM	LKT labs inc
Metformin	AMPK	DMSO	10mM	apex bio
Olaparib (AZD2281)	PARP-1	DMSO	10mM	apex bio
Ouabain	Na/K-ATPase,FA Pathway	DMSO	10mM	Sigma Aldrich
Palmoic acid	Pol beta	DMSO	10mM	apex bio
PDD00017273	PARG inhibitor	DMSO	10mM	apex bio
Pembrolizumab	Anti-PD1	PBS	1mg/mL	Selleckchem
Pyrvinium Pamoate	Androgen receptor	DMSO	10mM	apex bio
RAD51 Inhibitor B02	RAD51	DMSO	10mM	apex bio
Staurosporine	DNA synthesis	DMSO	10mM	apex bio
Temozolomide	DNA synthesis	DMSO	100mM	Sigma Aldrich
TH9619	MTHFD2	DMSO	10mM	Helleday lab, KI.
Tinostamustine	Pan-HDACi & alkylating	DMSO	10mM	Selleckchem
VE-821	ATR	DMSO	10mM	Selleckchem

Volasertib	PLK-1	DMSO	10mM	apex bio
Paxalisib	PI3K, AKT, and mTOR	DMSO	10mM	Selleckchem

Table 2.7 - List of long-term primary cultured cells.

https://drive.google.com/file/d/1B2n3lcdkp1x0QsnKmzrNwp4dL7RSaM7A/view

Cell Line Name	Type	*MGMT* status	Age	Sex
LN18	Established	Unmethylated	65	M
Ox5 Edge	Long-term GSC	Unmethylated	76	F
Ox5 Core	Long-term GSC	Unmethylated	76	F
Cx18 Core 1	Long-term GSC	Methylated	59	F
Cx18 Core 2	Long-term GSC	Methylated	59	F
Cx18 Edge 1	Long-term GSC	Methylated	59	F
Cx18 Edge 2	Long-term GSC	Methylated	59	F
Cx18 BULK	Long-term Bulk culture	Methylated	59	F

Table 2.8 - List of patient samples screened using GBM V01 plate.

Sample Identifier	WHO grade	*MGMT* status	Age	Sex	IDH1 status	Primary/ Recurrent
GBM07	4	Unmethylated (2.3%)	47	F	wt	Primary
GBM08	4	Unmethylated	65	M	wt	Primary
GBM09	3	NR	34	M	Mut (R132H)	Primary
GBM10 (A,B,C)	4	Unmethylated	72	M	wt	Primary
GBM11	4	Methylated (40.5)	78	M	wt	Primary
GBM12	4	Unmethylated (2.2%)	67	M	wt	Primary
GBM13	4	Unmethylated	44	M	wt	Recurrent
GBM14	4	Methylated (41.7%)	77	F	wt	Primary
GBM16	4	Methylated	64	F	wt	Primary
GBM17	4	Unmethylated	67	M	wt	Recurrent
GBM18	4	Unmethylated	56	M	wt	Primary
GBM19	4	Methylated	71	F	wt	Primary
GBM20 (A & B)	4	Unmethylated	72	M	wt	Recurrent
GBM21	4	Methylated (21.5%)	50	M	mut	Primary
GBM23	4	Unmethylated	69	M	wt	Primary
GBM24	4	Unmethylated	55	M	wt	Primary
GBM25	4	Methylated (33.9%)	78	M	wt	Primary

Table 2.9 - List of patient samples screened using GBM V02 plate.

Sample Identifier	WHO Grade	*MGMT* status	Age	Sex	IDH1	Primary/ recurrent
GBM26 (A, B & C)	4	Unmethylated		M	wt	Primary
GBM27	4	Methylated		M	wt	Primary
GBM30	4	Methylated		M	wt	Primary

Table 2.10 - TaqMan ™ gene expression probes for quantitative PCR.

Gene	Assay ID	Fluorescent Reporter Dye	Company
GAPDH	Hs02758991_g1	FAM	ThermoFisher
CD133	Hs01009259_m1	FAM	ThermoFisher
NESTIN	Hs04187831_g1	FAM	ThermoFisher
SOX2	Hs01053049_s1	FAM	ThermoFisher

Methods

2.1 Established human cell line culture

2.1.1 Obtaining established glioblastoma cell lines

LN18 cells were obtained from laboratory stocks originally purchased from American Type Culture Collection (ATCC).

2.1.2 Cell Culture

The handling of live cells and any cell culture experiments were performed in a Class II sterile laminar flow hood using only sterile plasticware and solutions. The laminar flow hoods were cleaned thoroughly before and after their use using chemgene disinfectant spray followed by industrial methylated spirit (IMS) to avoid any contamination.

2.1.3 Growth Conditions

Cell lines were propagated as adherent monolayers in flat sided flasks of $75cm^2$ containing 10mL DMEM with 10% FBS in an incubator at 37°C, 5% CO_2 and 21% O_2. Cells were routinely passaged every 3-5 days once they had reached a confluency of approximately 80%.

2.1.4 Serial passaging of established cell lines

Cells were serially passaged upon microscopic investigation of flasks reaching between 70-80% confluence. Media was aspirated off gently before the cell monolayer was washed twice with PBS in order to remove residual media and any cell debris. Cell layers were then treated with pre warmed trypsin-Versene/EDTA (1mL) and returned to the incubator until cells began to detach from the flask surface (approximately 2-3 mins). Upon removal from the incubator flasks were gently agitated and returned to the hood, 8-9mL of warm media was then added in order to inactivate trypsin and dilute the cell suspension. Cells were agitated mixed thoroughly to provide a single cell suspension, which was then used to seed into new flasks at a ratio of 2:5-1:10 depending on their doubling times.

2.1.5 Counting cells

Cells were detached from monolayers using pre warmed trypsin-Versene/EDTA (1mL) as above. Cells were then resuspended up to 10mL with warm media and mixed thoroughly by pipetting up and down. Then 20uL of the single cell solution was added to a Nexcelom™ Cellometer Disposable Counting Chamber, this was then inserted into the Nexcelom™ Cellometer automated cell counter, the focus was manually adjusted before the count per mL of solution was calculated.

2.1.6 Cryopreservation

Cells were detached from monolayers using pre warmed trypsin-Versene/EDTA (1mL) and diluted with media as above. Cell solution was then collected and centrifuged at 1000rpm for 2 minutes before discarding media. The cells were then resuspended in 3mL cryopreserve DMEM media for each 75cm^2 flask containing 10% DMSO and 10% FBS. 1ml aliquots of cell solution were placed into labelled cryovials before storing at -80°C for at least 24 hours within a Mr Frosty™ freezing container to achieve a cooling rate close to -1°C/minute, after this time cryovials were moved to a separate labelled cryogenic box for short term storage.

2.1.7 Thawing Cells

Cryovials were removed from -80°C and immediately placed into a 37°C water bath. Once thawed the cells were added to a 25cm^2 flask containing 9mL warm media and left to adhere overnight, the following day media was changed. Cells were then transferred to a larger 75cm^2 flask once 70-80% confluence was reached using passaging methods above.

2.2 Patient-derived primary cell line culture

2.2.1 Obtaining primary glioblastoma cell lines

G7 stem cells were obtained from the Collis laboratory but had been previously gifted by Professor Colin Watts (University of Birmingham, Brain Cancer Programme Chair) and Professor Anthony Chalmers (University of Glasgow, Chair of Clinical Oncology), they have been previously characterised and used by multiple groups to facilitate glioblastoma research (Fael Al-Mayhani *et al.*, 2009; Ahmed *et al.*, 2015). Ox5 and Cx18 cells were derived from patient samples by previous members of the Collis lab: Ola Rominiyi, PhD thesis and Connor McGarrity, PhD thesis.

2.2.2 Patient-derived primary glioblastoma cell line growth conditions

Primary glioblastoma cell lines were maintained in advanced DMEM F12 medium containing 1% B27, 1% L-glutamine, 1% Penicillin-streptomycin, 0.1% amphotericin B, 4ug/ml heparin, 20ng/ml EGF and 20ng/ml FGF. To maintain stem cell populations, cell cultures were seeded onto BME, Matrigel^{TM} coated plasticware. Prior to use 1ml aliquots of Matrigel^{TM} were defrosted on ice and diluted with cold advanced DMEM F12 (without supplements) at a dilution of 1:40. This was then coated on plasticware at various volumes (75cm^2 flasks – 2.5mL and 25cm^2 flasks – 1.5mL), in order for the gel to polymerise flasks were incubated at 37°C for one hour. The flasks were then stored in the refrigerator at 4°C for up to two weeks.

2.2.3 Serial passaging of patient-derived primary cell lines

Cells were serially passaged until flasks had reached a confluency of approximately 70-80%. Media was gently aspirated before the cell monolayer was washed twice with PBS in order to remove residual media and any cell debris. Cell layers were then treated with pre warmed

accutase (0.5mL) and returned to the incubator until cells began to detach from the cell surface (2-3 mins). Upon removal from the incubator flasks were gently agitated and returned to the hood, 4.5mL of warm media was then added in order to inactivate accutase and dilute the cell suspension. Cells were agitated mixed thoroughly to provide a single cell suspension, which was then used to seed into new Matrigel^{TM} coated flasks at a ratio of 2:5-1:10 depending on their doubling times.

2.2.4 Counting Cells

Cells were detached from monolayers using pre warmed accutase (0.5mL) as above. Cells were then resuspended up to 5mL with warm media and mixed thoroughly by pipetting up and down. Then 20µL of the single cell solution was added to a Nexcelom™ Cellometer Disposable Counting Chamber, this was then inserted into the Nexcelom™ Cellometer automated cell counter, the focus was manually adjusted before the count per mL of solution was calculated.

2.2.5 Cryopreservation

Cells were detached from monolayers using pre warmed accutase (0.5mL) and diluted with media as above. Cell solution was then collected and centrifuged at 1000rpm for 2 minutes before discarding media. The cells were then resuspended in 3mL cryopreserve DMEM media for each 75cm^2 flask containing 10% DMSO. 1ml aliquots of cell solution were placed into labelled cryovials before storing at -80°C for at least 24 hours within Mr Frosty™ freezing container to achieve a cooling rate close to -1°C/minute, after this time cryovials were moved to a separate labelled cryogenic box for short term storage.

2.2.6 Thawing Cells

Cryovials were removed from -80°C and immediately placed into a 37°C water bath. Once thawed the cells were added to a Matrigel^{TM} coated 25cm^2 flask containing 9mL warm media and left to adhere overnight, the following day media was changed. Cells were then transferred to a larger 75cm^2 flask once 70-80% confluence was reached using passaging methods above.

2.3 Optimization Experiments

2.3.1 Seeding cells

Once cells had been counted, they were seeded at a volume of 45uL onto 384 well plates using automated multidrop equipment. Prior to use the equipment was primed using water, 70% ethanol and plain media, ensuring that all nozzles were dispensing properly with no blockages. Cell solution was then primed, and appropriate plate columns could be selected for automated seeding. Following use the equipment was then cleaned using water and 70% ethanol.

2.3.2 Fixing and Staining of 384-well drug plates

For IF imaging, cells were initially fixed and permeabilized with 4% PFA and 0.6% Triton-x for 30 min. Following this the cells were then washed twice in phosphate-buffered saline (PBS) ready for staining with antibody markers. All antibodies used were diluted in PBS containing 0.05% TWEEN20 and 3% bovine serum albumin (BSA), which were left to incubate at 4°C overnight in the dark. Following the incubation of conjugated antibodies, plates were washed with PBS and ready for imaging. For primary antibody incubation: secondary antibodies were then added for 1hr at room temperature, plates were then washed with PBS and ready for imaging.

2.3.3 Dimethylsufoxide titration

The growth of LN18 cells was investigated through increasing DMSO concentrations compared to media. DMSO was diluted using plain DMEM to give concentration ranges between 0.02%-1%, these dilutions were then seeded onto a 384 well plate 5uL per well. Before the LN18 cells could be seeded they were detached from flasks and counted using above methods and made up to a density of 1,000 cells per well. The cell solution was then seeded at a volume of 45μL using the automated multidrop to avoid human error. Once seeded the cells were then incubated at 37°C, 5% CO_2 for a 4-day period. On day 4 plates were then fixed and stained using DAPI, before microscope analysis on the Cell Discoverer 7.

2.4 Development of drug plates

The drug library chosen for this project was a mixture of therapeutic and preclinical compounds with a focus on DNA damage repair pathway inhibitors given that SoC TMZ and IR induced DNA damage in treated cells. The IC_{50} values for the initial V01 drug plates were chosen based on the literature. The drug concentrations for second batch of V02 plates were selected based off primary glioblastoma cell line Ox5 Core and Edge responses, these responses are shown within our supplementary chapter 8, figure 8.1.

2.4.1 Drug Preparation

All compounds were purchased directly from Selleckchem as either solids or pre diluted liquids and diluted in DMSO or water (for platinum-based compound cisplatin) to stock working concentrations of 5-10mM and stored in -80°C. Immune drugs (bevacizumab, pembrolizumab, and ipilimumab) were added diluted as required straight into media (25μg/ml). Compounds purchased as liquid were stored according to manufacturer's instructions, to avoid any extra freeze thaw cycles these were thawed and aliquoted as appropriate on day of drug plate printing. A master plate layout was created ensuring all drug repeats and dilutions were evenly spread across the innermost 308 wells of a 384 well plate (Perkin Elmer 384 Cell Carrier Ultra) to avoid any bias resulting from edge evaporation effects or well positioning. These outermost wells would be filled with 100μL of media following cell seeding. Two different liquid dispensers were tested in this project, the first batch of V01 drug plates we used a Thermo Scientific – Matrix Platemate, whilst the second V02 plates were used using an acoustic liquid handing device Echo 550 (Labcyte Inc.).

2.4.2 Drug Plate Printing - Batch V01

For the V01 drug plates, all drugs were diluted to 10X their top concentration and serially diluted into 4 concentrations using a 1:2 dilution, in four 96 well master plates, in duplicate. These compounds and their concentrations within each master plate are shown within table 2.11, the coordinates of each of the compounds within the 96 well master plate is depicted by figure 2.1. A Thermo Scientific – Matrix Platemate Plus dispensed 5μL from the four master plates onto the allocated 384-well plate well, in addition to any vehicle control wells. Once the 384-well plates were printed, they were briefly centrifuged and sealed with a non-

permeable cover and immediately frozen at -80°C. The final V01 drug plate layout is shown within figure 2.2, negative control DMSO was dispensed into 24 wells across the plate at a concentration of 0.3%. Positive controls staurosporine and aphidicolin were both dispensed into 4 wells at a concentration of 5µM and 2µM respectively.

Table 2.11 - Drugs and concentrations used on V01 384-well drug plates.

Drug	Concentration (µM)			
	P1	**P2**	**P3**	**P4**
Stausporine	5	5	5	5
Aphidicolin	2	2	2	2
Alisertib	5	2.5	1.25	0.625
AX15836	20	10	5	2.5
AZD0156	5	2.5	1.25	0.625
AZD1775(Adavosertib MK-1775)	5	2.5	1.25	0.625
AZD6244 (Selumetinib)	2	1	0.5	0.25
AZD6738	5	2.5	1.25	0.625
AZD9291 (Osimertinib)	5	2.5	1.25	0.625
Bevacizumab	25	12.5	6.25	3.125
Bleomycin	20	10	5	2.5
Fisogatinib (BLU-554)	10	5	2.5	1.25
Butamben	20	10	5	2.5
Cisplatin	20	10	5	2.5
Curcumin	10	5	2.5	1.25
D-Penicillamine	20	10	5	2.5
Dabrafenib	25	12.5	6.25	3.125
Dexamethasone	5	2.5	1.25	0.625
Ipilimumab	25	12.5	6.25	3.125
KU55933	10	5	2.5	1.25
LNT 1	5	2.5	1.25	0.625
M3814 (Nedisertib)	5	2.5	1.25	0.625
Metformin	50	25	12.5	6.25
Olaparib (AZD2281)	10	5	2.5	1.25
Ouabain	2	1	0.5	0.25
Palmoic acid	10	5	2.5	1.25
Paxalisib	5	2.5	1.25	0.625
PDD00017273	5	2.5	1.25	0.625
Pembrolizumab	25	12.5	6.25	3.125
Pyrvinium Pamoate	10	5	2.5	1.25
RAD51 Inhibitor B02	10	5	2.5	1.25
Temozolomide	500	250	125	62.5
Tinostamustine	5	2.5	1.25	0.625

VE-821	5	2.5	1.25	0.625
Volasertib	2	1	0.5	0.25

Master plate top conc

	1	2	3	4	5	6	7	8	9	10	11	12
A	H2O	H2O	H2O	H2O	H2O	H2O	H2O	H2O	H2O	H2O	H2O	H2O
B	H2O	DMSO	STAU	BLU5	PYRV	APHI	IPIL	9619	VOLA	OUAB	6244	DMSO
C	H2O	TMZO	METF	DMSO	AZD9	BLEO	E821	Z156	LNT1	DMSO	DEBR	APHI
D	H2O	ALIS	LNT1	1775	TINO	DMSO	BUTA	DMSO	7273	CISP	5836	3814
E	H2O	DEXA	CURC	5933	7273	6738	PENI	3814	STAU	PEMB	PALM	BEVA
F	H2O	6244	Z156	E821	PEMB	DEBR	RAD5	METF	TMZO	AZD9	BLEO	RAD5
G	H2O	OLAP	BEVA	CISP	5836	OUAB	DEXA	ALIS	5933	PYRV	1775	BUTA
H	H2O	PENI	IPIL	9619	PALM	VOLA	BLU5	OLAP	CURC	6738	TINO	H20

Master plate 1/2

	1	2	3	4	5	6	7	8	9	10	11	12
A	H2O	DMSO	PAX1	BLU5	PYRV	PAX2	IPIL	9619	VOLA	OUAB	6244	DMSO
B	H2O	TMZO	METF	DMSO	AZD9	BLEO	E821	Z156	LNT1	DMSO	DEBR	PAX4
C	H2O	ALIS	LNT1	1775	TINO	DMSO	BUTA	DMSO	7273	CISP	5836	3814
D	H2O	DEXA	CURC	5933	7273	6738	PENI	3814	PAX3	PEMB	PALM	BEVA
E	H2O	6244	Z156	E821	PEMB	DEBR	RAD5	METF	TMZO	AZD9	BLEO	RAD5
F	H2O	OLAP	BEVA	CISP	5836	OUAB	DEXA	ALIS	5933	PYRV	1775	BUTA
G	H2O	PENI	IPIL	9619	PALM	VOLA	BLU5	OLAP	CURC	6738	TINO	H20
H	H20	H2O	H20	H20	H20	H20	H20	H20	H20	H20	H20	H20

Master plate 1/4

	1	2	3	4	5	6	7	8	9	10	11	12
A	H2O	DMSO	PAX1	BLU5	PYRV	PAX2	IPIL	9619	VOLA	OUAB	6244	DMSO
B	H2O	TMZO	METF	DMSO	AZD9	BLEO	E821	Z156	LNT1	DMSO	DEBR	PAX4
C	H2O	ALIS	LNT1	1775	TINO	DMSO	BUTA	DMSO	7273	CISP	5836	3814
D	H2O	DEXA	CURC	5933	7273	6738	PENI	3814	PAX3	PEMB	PALM	BEVA
E	H2O	6244	Z156	E821	PEMB	DEBR	RAD5	METF	TMZO	AZD9	BLEO	RAD5
F	H2O	OLAP	BEVA	CISP	5836	OUAB	DEXA	ALIS	5933	PYRV	1775	BUTA
G	H2O	PENI	IPIL	9619	PALM	VOLA	BLU5	OLAP	CURC	6738	TINO	H20
H	H20	H2O	H20	H20	H20	H20	H20	H20	H20	H20	H20	H20

Master plate 1/8

	1	2	3	4	5	6	7	8	9	10	11	12
A	H2O	H2O	H2O	H2O	H2O	H2O	H2O	H2O	H2O	H2O	H2O	H2O
B	H2O	DMSO	STAU	BLU5	PYRV	APHI	IPIL	9619	VOLA	OUAB	6244	DMSO
C	H2O	TMZO	METF	DMSO	AZD9	BLEO	E821	Z156	LNT1	DMSO	DEBR	APHI
D	H2O	ALIS	LNT1	1775	TINO	DMSO	BUTA	DMSO	7273	CISP	5836	3814
E	H2O	DEXA	CURC	5933	7273	6738	PENI	3814	STAU	PEMB	PALM	BEVA
F	H2O	6244	Z156	E821	PEMB	DEBR	RAD5	METF	TMZO	AZD9	BLEO	RAD5
G	H2O	OLAP	BEVA	CISP	5836	OUAB	DEXA	ALIS	5933	PYRV	1775	BUTA
H	H2O	PENI	IPIL	9619	PALM	VOLA	BLU5	OLAP	CURC	6738	TINO	H20

Figure 2.1 - Master 96-well plate layouts - Initially compounds were diluted to x10 the top concentration to be used and added to their corresponding wells on the x10 master plate. Drugs from this plate were then serially diluted down 1:2 into x5, x2.5 and x1.25 master plates. Vehicle control (DMSO) and positive controls (Staurosporine and Aphidicoline) were added to the plate independently at single concentrations.

	1	2	3	4	5	6	7	8	9	10	11	12	13	14	15	16	17	18	19	20	21	22	23	24
A	H2O	P2 H20	H2O	P2 H20	H2O	P2 H20	H2O	P2 H20	H2O	P2 H20	H2O	P2 H20	H2O	P2 H20	H2O	P2 H20	H2O	P2 H20	H2O	P2 H20	H2O	P2 H20	H2O	P2 H20
B	P3 H2O	P4 H20	P3 DMSO	P4 TINO	P3 PAX1	P4 6738	P3 BLU5	P4 CURC	P3 PYRV	P4 OLAP	P3 PAX2	P4 BLU5	P3 IPIL	P4 VOLA	P3 9619	P4 PALM	P3 VOLA	P4 9619	P3 OUAB	P4 IPIL	P3 6244	P4 PENI	P3 DMSO	P4 H20
C	H2O	P2 H20	DMSO	P2 TINO	STAU	P2 6738	BLU5	P2 CURC	PYRV	P2 OLAP	APHI	P2 BLU5	IPIL	P2 VOLA	9619	P2 PALM	VOLA	P2 9619	OUAB	P2 IPIL	6244	P2 PENI	DMSO	P2 H20
D	P3 H2O	P4 BUTA	P3 TMZO	P4 1775	P3 METF	P4 PYRV	P3 DMSO	P4 5933	P3 AZD9	P4 ALIS	P3 BLEO	P4 DEXA	P3 E821	P4 OUAB	P3 Z156	P4 5836	P3 LNT1	P4 CISP	P3 DMSO	P4 BEVA	P3 DEBR	P4 OLAP	P3 PAX4	P4 H20
E	H2O	P2 BUTA	TMZO	P2 1775	METF	P2 PYRV	DMSO	P2 5933	AZD9	P2 ALIS	BLEO	P2 DEXA	E821	P2 OUAB	Z156	P2 5836	LNT1	P2 CISP	DMSO	P2 BEVA	DEBR	P2 OLAP	APHI	P2 H20
F	P3 H2O	P4 RAD5	P3 ALIS	P4 BLEO	P3 LNT1	P4 AZD9	P3 1775	P4 TMZO	P3 TINO	P4 METF	P3 DMSO	P4 RAD5	P3 BUTA	P4 DEBR	P3 DMSO	P4 PEMB	P3 7273	P4 E821	P3 CISP	P4 Z156	P3 5836	P4 6244	P3 3814	P4 H20
G	H2O	P2 RAD5	ALIS	P2 BLEO	LNT1	P2 AZD9	1775	P2 TMZO	TINO	P2 METF	DMSO	P2 RAD5	BUTA	P2 DEBR	DMSO	P2 PEMB	7273	P2 E821	CISP	P2 Z156	5836	P2 6244	3814	P2 H20
H	P3 H2O	P4 BEVA	P3 DEXA	P4 PALM	P3 CURC	P4 PEMB	P3 5933	P4 STAU	P3 7273	P4 3814	P3 6738	P4 PENI	P3 PENI	P4 6738	P3 3814	P4 7273	P3 PAX3	P4 5933	P3 PEMB	P4 CURC	P3 PALM	P4 DEXA	P3 BEVA	P4 H20
I	H2O	P2 BEVA	DEXA	P2 PALM	CURC	P2 PEMB	5933	P2 PAX3	7273	P2 3814	6738	P2 PENI	PENI	P2 6738	3814	P2 7273	STAU	P2 5933	PEMB	P2 CURC	PALM	P2 DEXA	BEVA	P2 H20
J	P3 H2O	P4 3814	P3 6244	P4 5836	P3 Z156	P4 CISP	P3 E821	P4 7273	P3 PEMB	P4 DMSO	P3 DEBR	P4 BUTA	P3 RAD5	P4 DMSO	P3 METF	P4 TINO	P3 TMZO	P4 1775	P3 AZD9	P4 LNT1	P3 BLEO	P4 ALIS	P3 RAD5	P4 H20
K	H2O	P2 3814	6244	P2 5836	Z156	P2 CISP	E821	P2 7273	PEMB	P2 DMSO	DEBR	P2 BUTA	RAD5	P2 DMSO	METF	P2 TINO	TMZO	P2 1775	AZD9	P2 LNT1	BLEO	P2 ALIS	RAD5	P2 H20
L	P3 H2O	P4 APHI	P3 OLAP	P4 DEBR	P3 BEVA	P4 DMSO	P3 CISP	P4 LNT1	P3 5836	P4 Z156	P3 OUAB	P4 E821	P3 DEXA	P4 BLEO	P3 ALIS	P4 AZD9	P3 5933	P4 DMSO	P3 PYRV	P4 METF	P3 1775	P4 TMZO	P3 BUTA	P4 H20
M	H2O	P2 PAX4	OLAP	P2 DEBR	BEVA	P2 DMSO	CISP	P2 LNT1	5836	P2 Z156	OUAB	P2 E821	DEXA	P2 BLEO	ALIS	P2 AZD9	5933	P2 DMSO	PYRV	P2 METF	1775	P2 TMZO	BUTA	P2 H20
N	P3 H2O	P4 DMSO	P3 PENI	P4 6244	P3 IPIL	P4 OUAB	P3 9619	P4 VOLA	P3 PALM	P4 9619	P3 VOLA	P4 IPIL	P3 BLU5	P4 APHI	P3 OLAP	P4 PYRV	P3 CURC	P4 BLU5	P3 6738	P4 STAU	P3 TINO	P4 DMSO	P3 H20	P4 H20
O	H2O	P2 DMSO	PENI	P2 6244	IPIL	P2 OUAB	9619	P2 VOLA	PALM	P2 9619	VOLA	P2 IPIL	BLU5	P2 PAX2	OLAP	P2 PYRV	CURC	P2 BLU5	6738	P2 PAX1	TINO	P2 DMSO	H20	P2 H20
P	P3 H2O	P4 H20	P3 H20	P4 H20	P3 H20	P4 H20	P3 H20	P4 H20	P3 H20	P4 H20	P3 H20	P4 H20	P3 H20	P4 H20	P3 H20	P4 H20	P3 H20	P4 H20	P3 H20	P4 H20	P3 H20	P4 H20	P3 H20	P4 H20

Figure 2.2 - Final V01 plate layout layouts - Controls are colour coordinated. Negative control DMSO is highlighted in yellow, positive control STAU (staurosporine) is highlighted orange and APHI (aphidicolin) is highlighted in grey. All compounds are labelled with P1-P4 prefix to determine the exact concentrations, which specified previously in table 2.11. All outer wells are filled with water and are not used for any drug plate analysis.

2.4.3 Drug Plate Printing - Batch V02

For the second batch of V02 drug plates we generated the plates using the acoustic Echo 550 (Labcyte Inc.) liquid plate dispenser. The equipment uses acoustic energy to transfer liquids from the microplate to the desired wells within the 384-well drug plate in 2.5nl increments to reach the desired final well concentration. Stock solutions of drugs (10mM) were loaded into the master microplate by hand, each drug well coordinate, and its stock concentration was logged, any drugs required at lower concentrations (lower than concentration corresponding to 2.5 nl) were further diluted in DMSO and loaded into a separate well location on the microplate. The plate layout was designed using the built in equipment software, which is depicted within figure 2.2. All compounds were dispended onto the final plate in duplicate, at 6 different concentrations using a 1:3 dilution, these compounds and their concentrations are specified within table 2.13. Negative control DMSO was dispensed into 24 wells across the plate at a concentration of 0.3%. Positive controls staurosporine and aphidicolin were both dispensed into 4 wells at a concentration of 5µM and 2µM respectively. We also normalised DMSO concentration within each well to highest concentration of the plate (0.3%).

The main benefit of this equipment is that it eliminates the rick of cross contamination caused using tips, has a high degree of accuracy and repeatability of results, it also preserves the integrity of the drug samples during transfer and storage on liquid nitrogen. Additionally, it enables the user to easily make small adjustments to any drug concentrations, the microplate is stored on liquid nitrogen and once the plate layout and microplate is set up it requires minimal interaction from the user, so new drug plates with adjusted concentrations can be made rapidly.

Table 2.12 -Drugs and concentrations used on V02 384-well drug plates.

Drug	Concentration (µM)					
	P1	**P2**	**P3**	**P4**	**P5**	**P6**
Stausporine	5	5	5	5	5	5
Aphidicolin	2	2	2	2	2	2
Alisertib	2	0.667	0.222	0.074	0.025	0.008
AZD1775(Adavosertib MK-1775)	2	0.667	0.222	0.074	0.025	0.008
AZD6244 (Selumetinib)	15	5	1.5	0.55	0.2	0.05
AZD6738	5	1.680	0.550	0.175	0.050	0.025
AZD9291 (Osimertinib)	15	5	1.5	0.55	0.2	0.05
AZD7648	15	5	1.5	0.55	0.2	0.05
AZD1390	15	5	1.5	0.55	0.2	0.05
Bleomycin	5	1.680	0.550	0.175	0.050	0.025
Fisogatinib (BLU-554)	15	5	1.5	0.55	0.2	0.05
Butamben	100	33.5	11	3.50	1.0	0.5
Cisplatin	20	6.66	2.22	0.72	0.25	0.08
Curcumin	100	33.5	11	3.50	1.0	0.5
Dabrafenib	15	5	1.5	0.55	0.2	0.05
Dexamethasone	100	33.5	11	3.50	1.0	0.5
LNT 1	15	5	1.5	0.55	0.2	0.05
Metformin	100	33.33	11.11	3.66	1.22	0.4
Olaparib (AZD2281)	15	5	1.5	0.55	0.2	0.05
Ouabain	0.3	0.1	0.333	0.111	0.003	0.001
Palmoic acid	100	33.5	11	3.50	1.0	0.5
Paxalisib	15	5	1.5	0.55	0.2	0.05
PDD00017273	5	1.680	0.550	0.175	0.050	0.025
Pyrvinium Pamoate	1	0.333	0.111	0.037	0.012	0.004
RAD51 Inhibitor B02	15	5	1.5	0.55	0.2	0.05
Temozolomide	800	266	88.5	29.5	9.57	3.31
Tinostamustine	5	1.680	0.550	0.175	0.050	0.025
Volasertib	0.3	0.1	0.333	0.111	0.003	0.001

	1	2	3	4	5	6	7	8	9	10	11	12	13	14	15	16	17	18	19	20	21	22	23	24
A	H2O	H2O	H2O	H2O	H2O	H2O	H2O	H2O	H2O	H2O	H2O	H2O	H2O	H2O	H2O	H2O	H2O	H2O	H2O	H2O	H2O	H2O	H2O	H2O
B	H2O	DMSO	P1 ALIS	P1 6738	P1 BLEO	P1 OUAB	P1 7273	P1 TINO	P1 VOLA	P1 7648	P1 6244	P1 LNT1	P1 1390	P1 1775	P1 AZD9	P1 BLU5	DMSO	P1 OLAP	P1 PYRV	P1 RAD5	P1 PAX	P1 DEBR	DMSO	H2O
C	H2O	P1 1775	P1 AZD9	P1 BLU5	P1 OLAP	P1 PYRV	P1 RAD5	P2 7648	P2 6244	P2 LNT1	P2 1390	P1 CURC	P1 PALM	P1 DEXA	P1 BUTA	P1 ALIS	P1 6738	P1 BLEO	P1 OUAB	P1 7273	P1 TINO	P1 VOLA	APHI	H2O
D	H2O	P2 ALIS	P2 6738	DMSO	P2 BLEO	P2 OUAB	P2 7273	P2 TINO	P2 VOLA	P1 PAX	P1 DEBR	P2 1775	P2 AZD9	P2 BLU5	P2 OLAP	P2 PYRV	P2 RAD5	P2 PAX	P2 DEBR	P1 CURC	P1 PALM	P1 DEXA	P1 BUTA	H2O
E	H2O	P2 1775	P2 AZD9	P2 BLU5	P2 OLAP	P2 PYRV	P2 RAD5	P2 PAX	P2 DEBR	DMSO	P2 ALIS	P2 6738	P2 BLEO	DMSO	P2 OUAB	P2 7273	P2 TINO	P2 VOLA	P1 7648	P1 6244	DMSO	P1 LNT1	P1 1390	H2O
F	H2O	APHI	P3 7648	P3 6244	P3 LNT2	DMSO	P3 1391	P2 CURC	P2 PALM	P2 DEXA	P2 BUTA	P3 1775	P3 AZD9	P3 BLU5	P3 OLAP	P3 PYRV	P3 RAD5	P3 PAX	P3 DEBR	P2 CURC	P2 PALM	P2 DEXA	P2 BUTA	H2O
G	H2O	P3 ALIS	P3 6738	P3 BLEO	P3 OUAB	P3 7273	APHI	P3 TINO	P3 VOLA	DMSO	P3 ALIS	P3 6738	P3 BLEO	P3 OUAB	P3 7273	P3 TINO	P3 VOLA	STAU	DMSO	P2 7648	P2 6244	P2 LNT1	P2 1390	H2O
H	H2O	P4 7648	P4 6244	P4 LNT3	P4 1392	P3 CURC	DMSO	STAU	P3 PALM	P3 DEXA	P3 BUTA	P4 1775	P4 AZD9	P4 BLU5	P4 OLAP	P4 PYRV	DMSO	P4 RAD5	P4 PAX	P4 DEBR	P3 PALM	P3 DEXA	P3 BUTA	H2O
I	H2O	P4 ALIS	P4 6738	P4 BLEO	P4 OUAB	P4 7273	P4 TINO	P4 CURC	DMSO	P4 VOLA	P4 ALIS	P4 6738	DMSO	P4 BLEO	P4 OUAB	P4 7273	P4 TINO	P4 VOLA	P3 CURC	P3 7648	P3 6244	P3 LNT2	P3 1391	H2O
J	H2O	P3 1775	P3 AZD9	P3 BLU5	P3 OLAP	P3 PYRV	P3 RAD5	P3 PAX	P3 DEBR	P4 PALM	P4 DEXA	P4 BUTA	P5 1775	P5 AZD9	P5 BLU5	P5 OLAP	P5 PYRV	P5 RAD5	P5 PAX	P5 DEBR	P4 PALM	P4 DEXA	P4 BUTA	H2O
K	H2O	P5 7648	P5 6244	P5 LNT1	DMSO	P5 1393	P6 PALM	P6 DEXA	P6 BUTA	P5 CURC	P5 ALIS	P5 6738	P5 BLEO	P5 OUAB	P5 7273	P5 TINO	P5 VOLA	P4 CURC	DMSO	P4 7648	P4 6244	P4 LNT1	P4 1392	H2O
L	H2O	P4 1775	P4 AZD9	P4 BLU5	P4 OLAP	P4 PYRV	P4 RAD5	P4 PAX	P4 DEBR	P6 7648	P6 6244	P6 1776	P6 AZD10	DMSO	P6 BLU6	P6 OLAP	P6 PYRV	P6 RAD6	P6 PAX	P6 DEBR	P5 PALM	P5 DEXA	P5 BUTA	H2O
M	H2O	P5 ALIS	P5 6738	DMSO	P5 BLEO	P5 OUAB	P5 7273	P5 TINO	P5 VOLA	P6 CURC	P6 ALIS	P6 6738	P6 BLEO	P6 OUAB	P6 7273	P6 TINO	P6 VOLA	P5 7648	P5 6244	P5 CURC	DMSO	P5 LNT1	P5 1393	H2O
N	H2O	DMSO	STAU	P5 PALM	P5 DEXA	P5 BUTA	P5 1775	P5 AZD9	P5 BLU5	P5 OLAP	P5 PYRV	P5 RAD5	P5 PAX	P5 DEBR	P6 LNT1	P6 1394	APHI	DMSO	P6 CURC	P6 PALM	P6 DEXA	P6 BUTA	STAU	H2O
O	H2O	P6 ALIS	P6 6738	P6 BLEO	P6 OUAB	P6 7273	DMSO	P6 TINO	P6 VOLA	P6 1776	P6 AZD10	P6 BLU6	P6 OLAP	P6 PYRV	P6 RAD6	P6 PAX	DMSO	P6 DEBR	P6 7648	P6 6244	P6 LNT1	P6 1394	DMSO	H2O
P	H2O	H2O	H2O	H2O	H2O	H2O	H2O	H2O	H2O	H2O	H2O	H2O	H2O	H2O	H2O	H2O	H2O	H2O	H2O	H2O	H2O	H2O	H2O	H2O

Figure 2.3 - Final V02 plate layout - Controls are colour coordinated negative control DMSO is highlighted in yellow, STAU (staurosporine) is highlighted orange and APHI (aphidicolin) is highlighted in grey. All compounds are labelled with P1-P6 prefix to determine the exact concentrations, these are specified previously in table 2.12. All outer wells are filled with water and are not used for any drug plate analysis.

2.5 Sample Collection and Processing

2.1.1 Summary of ex vivo screening pipeline

The project workflow is illustrated in figure 2.4. Prior to the surgical procedure, obtaining informed consent from the patient is essential to determine their willingness to allow the use of tumour tissue for research purposes. Once consent is granted, samples are collected immediately after surgical removal and transported to the laboratory at room temperature in sterile containers within 30 minutes of surgery. Under sterile conditions the sample is processed to create a single-cell suspension, the tumour samples undergo mechanical and enzymatic dissociation, followed by cultivation under specific conditions to isolate the GSC population, which represents the drug-resistant tumour population after surgery. The cells are subsequently counted and dispensed onto pre-coated 384-well drug plates at precise volumes using automated multidrop equipment to minimize human error. These plates are then left to incubate for 4-days at 37°C and 5% CO_2. Afterward, the plates are fixed and stained with fluorescently tagged antibodies, reflective of the entire tumour cell population (including GSCs, tumour bulk and healthy cells). This prepares them for downstream automated microscopy and image analysis. Furthermore, an additional sample is collected for further genetic, transcriptomic, and phenotypic analyses in our research laboratory.
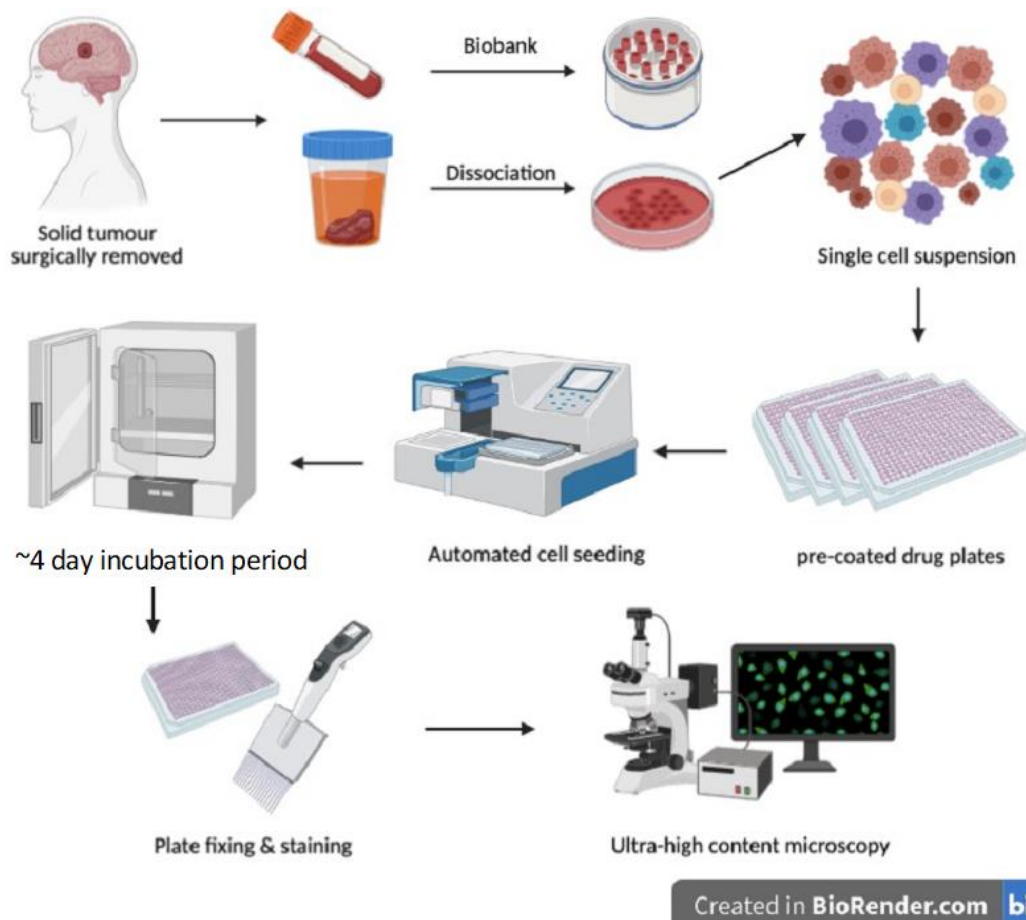
Figure 2.4 - Schematic representation of the ex vivo screening protocol for glioblastoma - Patient tumour samples are initially obtained from clinic; same day dissociation and cell seeding is performed onto pre-coated 384-well drug plates. Drug plates are then incubated for 4-days (37°C and 5% CO_2). Following this, plates are fixed and stained with appropriate fluorescent antibody markers ready for downstream microscopy and image analysis to evaluate treatment response.

2.5.1 Patient recruitment and sample transfer

Fresh treatment-naïve glioblastomas were collected from patients who provided written informed consent undergoing surgery at Sheffield Teaching Hospitals NHS Foundation Trust (Ethical approval: STH20854). The patient information sheet and consent form are provided within supplementary section 8.3. Fresh glioblastoma tissue surplus to histological requirements resected by the operating surgeon was collected intraoperatively whilst surgery was ongoing, pseudonymised/assigned a unique sample identifier and then rapidly transferred to the ex vivo laboratory within <30 minutes within a dry sterile specimen pot.

2.5.2 Sample processing and culture

Tumour samples were placed into 50-100mm petri dishes depending on the tissue size and washed thoroughly with pre warmed (37°C) PBS. All excess PBS was aspirated, and tissue specimens were measured, for larger samples multi region sampling was used to investigate intratumoural heterogeneity (e.g. GBM1 sample A, B, C). These we then further divided into smaller 2x2x2mm regions prior to dissociation. Depending on the size of the sample, 10-20ml of pre-warmed stem media, without growth factors (advanced DMEM F12 medium containing 1% B27, 1% L-glutamine, 1% Penicillin-streptomycin, 0.1% amphotericin B, 4ug/ml heparin) was added to immerse sample. Specimens were then mechanically dissociated using forceps and pipette tip, with more calcified solid tumours dissociated using scalpels. For smaller samples not modelling heterogeneity the total tissue homogenate was then divided equally into 4-6 15ml falcon tubes to give a maximum of ~0.5-1ml pellet of tissue per tube. Larger tissues modelling intratumoural heterogeneity were split into appropriately labelled 15ml falcon tubes (e.g. A, B, C) 4-6 tubes per sample. It is possible to derive smaller samples with 1-2 1ml pellets, however samples screened in this study are usually in excess, therefore we find it important to dissociate majority of tissue to give accurate representation of cells in entire the tumour. Following this 15ml tubes were then centrifuged at ~180 relative centrifugal force (RCF) for 3 minutes, after which the supernatant was carefully removed. If the residual pellet contained a large red blood cell (RBC) layer, pre-warmed PBS was added to each tube, agitated and left to settle for 10 mins. Subsequently, tubes were then centrifuged at 200 RCF for 30 seconds, and supernatant was carefully aspirated. Accutase™ (3ml) warmed to (37°C) was then added to each individual tube and the suspension was pipetted up and down to provide further disaggregation prior to agitated incubation using ThermoMixer C (Eppendorf) set at 37°C 750 rpm for 30 minutes. This enzymatic dissociation step was repeated until cells were well dissociated with the majority as single cells (typically 45-60 minutes). Dissociation was checked under brightfield using glass coverslips. Stem media (7ml) was added to each falcon tube and mixed well using a 10/5ml stripette. Cell suspensions were then centrifuged at ~180 RCF, the supernatant removed, and pellets resuspended in 3ml stem media, mixed well then filtered through a 70µM cell strainer. Cell solutions were then divided equally into 15ml falcon tubes (one per every 2x2mm tissue sample) and then centrifuged for 5 minutes. If a RBC layer was still present on the pellet, 5ml of ACK lysing

buffer was added and mixed well before leaving for 5 minutes before further centrifugation at ~180 RCF for 5 minutes. Following aspiration of the supernatant, cells were resuspended in 5ml PBS and mixed well and centrifuged again for 5 minutes, the supernatant aspirated and pellet resuspended in stem media including growth factors (EGF and FGF). Cells were then counted, viability tested with trypan blue using Cellometer Mini (Nexcelom Bioscience) cell counter, viability was typically between 20-40% however samples were used regardless. Using the live cell count, cells were further diluted in stem media containing growth factors into a 50ml falcon tube to give an appropriate density (usually 5-10k cells per well in 384 well). The pre-loaded drug plates were treated with Cultrex (1:20 dilution with plain DMEM F12) and allowed to polymerise for 30 minutes prior to cell seeding (5μL per well), Cultrex is a BME required to maintain GSC as adherent monolayers on plasticware. 40μL of the resulting suspension was dispensed to all but the outer wells of the 384-well drug plates, making the total volume 50μL.The empty outer wells of the plate were then filled with media (100uL) before sealing the plate with "breathe easy" sealing membrane (Sigma, MERCK) to help with any evaporation effects and placed within the incubator (37°C in 5% CO_2) for a 4-8 day incubation period, which was set based on previous publications using similar techniques (Arjonen *et al.*, 2020; Mäkelä *et al.*, 2020; Rantala *et al.*, 2020).

2.6 Irradiation of drug plates

All irradiation was performed using an experimental IR source within our research facility (^{137}Cs irradiator; CIS Bio International IBL437c). Drug plates were placed within equipment cannister at 45-degree angle, 1 hour after cell seeding (~2Gy/min). For irradiation of cell lysates for western blotting, when cells reached confluency, 6 well dishes were taped shut using autoclave tape and inserted into equipment cannister at 45-degree angle and were irradiated 1 hour prior to lysing (~5Gy/min).

2.7 Analysis of drug plate responses

2.7.1 Microscopy Imaging

All drug plates were imaged using a Cell Discoverer 7 (CD7) using Zen Blue 3.0 software. Prior to inserting the plate into the microscope, the bottom of the plate was wiped clean of any debris using lint free tissue. If the plate had been stored in the fridge it was left at room

temperature for half an hour prior to analysis to remove condensation. Once the specific brand of 384-well plate was selected from the plate list (Perkin Elmer 384 Cell Carrier Ultra), the plate could then be placed into the tray and loaded into the microscope.

Using the plate setup tab, the appropriate channels were selected for based on the excitation of the conjugated antibodies used, along with brightfield and DAPI as the reference channel. Next, the lens was set to a 10x magnification using the 0.5 lens. The plate was then calibrated using the brightfield channel as a reference to set the peripheral wells and ensure the plate is positioned correctly. Tile strategy was then selected for the plate, this determines how many images per well the microscope takes. This was usually set at a five-tile strategy however on plates with reduced numbers of cells (common with freshly dissociated cells) this number has been increased to 9-12 tiles per well to increase imaged area. Finally the focus was then set using DAPI as the reference channel, any of the additional antibody markers from this reference adding any offset values to the appropriate channels tab. Once this has all been completed the experiment would be started, usually taking between 2-4 hours depending on the number of channels and density of cells.

2.7.2 Image analysis

All image analysis was performed using Zeiss Zen Blue 3.0 analysis software. Using the processing tab an image subset from the initial image file was extracted selecting approximately 30 individual tiles, these included a selection of wells from positive, Staurosporine and negative DMSO control wells along with any wells containing significant debris such as hairs and fibres. This subset was then selected to train the software using the Zen Intellesis machine learning module, which allows segmentation of images based on the user training distinguishing between object and background, objects are then highlighted in yellow as shown by figure 2.5. The intellesis models used for drug plate analysis were trained using DAPI positive nuclei as an object, parameters included the 50 features setting. Once the Intellesis training model was completed an image analysis program was then created.
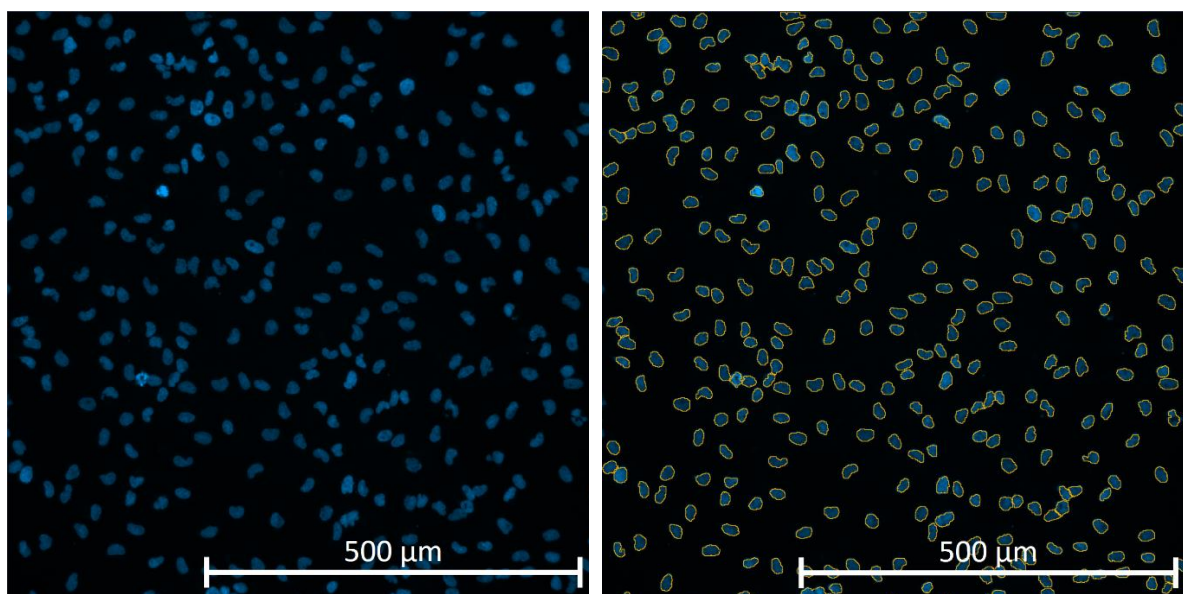
Figure 2.5 - Example of how the Zen Blue software images were obtained using the CD7 10x magnification - Example of how the Zen Blue software images were obtained using the CD7 10x magnification. Primary glioblastoma positively DAPI stained nuclei were identified as objects by the algorithm for scoring purposes (yellow outlines).

2.1.2 RStudio analysis

Plate layout templates were designed using excel which specified compound name, concentration and well number it corresponded to. Using RStudio software version 4.2.2 the output CSV files that were produced by Zen Blue analysis software were initially concatenated using the summarise function by dplyr (version 1.1.4) to obtain a DAPI frequency count per well. This file was then merged with the plate layout template by well number, so that each well corresponded to DAPI frequency, drug and concentration. Any drug response plots were generated using the graphical visualisation package, ggplot2 (version 3.5.0). In order to obtain cell metrics such as IC_{50} values, which is the concentration at which the relative cell count is equal to 0.5 (equation 2.1) and area under the curve (AUC) the area below the fitted dose response curve (equation 2.2), a package called GRmetrics was used (version 1.28.0).The output files generated from GRmetrics containing AUC values were imported back into RStudio, these values were then visualised as a heatmap using the pheatmap package (version 1.0.12).

$$y = \frac{a + (b - a)}{1 + (\frac{x}{c})^d}$$

Equation 2.1 – Four parameter logistic equation - Where 'y' represents the response, 'x' represents the concentration of the drug, a represents the bottom plateau of the curve, b represents the top plateau of

the curve, c represents the concentration of drug causing 50% of the maximum response (IC_{50}) and 'd' is the Hill slope which describes the steepness of the curve around the IC50 value.

$$AUC = \sum_{i=1}^{n-1} \frac{(x_{i+1} - x_i) * (y_i + y_{i+1})}{2}$$

Equation 2.2 - Equation for obtaining area under dose-response curve - Where 'n' represents the number of data points, *xi* and *xi*+1 are the concentrations corresponding to consecutive data points, *yi* and *yi* +1 are the response values corresponding to the concentrations of *xi* and *xi*+1 respectively.

2.7.3 Evaluating drug response

When evaluating drug response profiles, we have plotted both raw cell counts using DAPI as our positive cells (DAPI freq) and also normalised relative inhibition which is calculated using both positive and negative controls, as shown within the literature (Yadav *et al.*, 2014; Gupta *et al.*, 2020). Percent inhibition removes cross-plate effects by normalising the data to a specific percent score, however it does rely on quality of the data obtained from the positive and negative controls (equation 2.3).

$$\% \ Inhibition = 100 \ \times [1 - (x - \text{positive})/(negative - positive)]$$

Equation 2.3 - Percentage Inhibition - Where 'x' represents the individual data point, 'positive' represents the mean positive control count (staurosporine), 'negative' represents the mean negative control count (DMSO).

Whilst IC_{50} values are a commonly used statistic for drug screening data, it is not always possible to determine the IC_{50} as not all responses to drugs will fit within the canonical sigmoidal shape of a dose response, additionally lack of concentration data points can lead to an ill-fitting model. This therefore leads to gaps in results making IC_{50} as an endpoint statistic useless, when comparing an entire cohort of samples. Instead, we adopted the use of AUC statistic as it will always give a numeric value usually between 0 and 1. Additionally where IC_{50} only gives information regarding the concentration to achieve 50% inhibition, AUC values can capture increased sensitivities that beyond the IC_{50} values at higher drug concentrations.

2.7.4 Statistical Analysis

Shapiro-Wilk normality tests were performed to assess the datasets prior to statistical analysis to decide the correct tests to perform. In order to confirm differences between two

groups Mann-Whiney U-test was performed on non-parametric datasets or Students t-test on parametric datasets, p-values less than 0.05 would determine whether the differences in results were significantly different. All normality tests and statistical analysis was performed using R package *stats* version 4.2.2. As the current study is not comparing ex vivo drug responses to any clinical indications, normal power calculation or simulation studies were not used to determine the sample size at this time.

2.8 Stem marker optimisation

The GSC population is speculated to be the basis of tumour residual cells which gives rise to secondary foci with resistant characteristics. Using antibody markers specific to this GSC population e.g. CD133, nestin, SOX2 alongside tumour bulk cell populations e.g. GFAP, an astrocytic differentiation marker, it is hoped that we can investigate treatment response through multi-parameter, ultra-high content microscopy and sophisticated image analysis algorithms; for instance, comparing the counts of DAPI stained cells between drug and DMSO control wells. Suitable drugs would be those which could specifically target the GSC population, exploiting specific antibody markers for each it would be possible to assess the effect of the drug in multiple cell populations. Additionally, depending on the therapeutic identified, further analysis techniques would be performed; for instance, apoptosis would be measured for known cytotoxic agents using caspase markers and cell cycle arrest or cellular proliferation would be analysed for known cytostatic chemotherapeutics markers such as ki-67.

2.8.1 Optimization of conjugated antibodies

In order to optimise the concentration required for conjugated stem cell marker antibodies nestin and CD133 Ox5 edge cells were seeded at a density of 1,000 cells per well on a Perkin Elmer 384 well plate and incubated for 4 days at 37°C 5% CO_2. On day 4 the plate was fixed and stained using antibody concentrations of 1:1000, 1:500 and 1:250 in PBS containing 3% BSA and 0.05% TWEEN20, which was left overnight in the dark at 4°C and analysed using microscopy. Buffer only (PBS containing 3% BSA and 0.05% TWEEN20) was used as a control.

2.1.3 Quantitative PCR

For RNA extraction, Cx18 Bulk/stem cells were seeded into Cultrex coated 6-well plates and incubated until 70% confluent before harvesting. Qiagen RNeasy Mini Kits were used to extract RNA. Initially, media was aspirated from cultured cells and cells were washed twice with PBS. PBS was then aspirated and 350µL RLT buffer was added to each well and cells were then dislodged using a cell scraper and transferred to labelled QIAshredder columns before being centrifuged at 8000 RCF for 2 minutes. The purple columns were discarded and 350µl of 70% ethanol was added to the supernatant, this solution was then transferred to a RNeasy Minispin column and centrifuged for 15 seconds. The flow through was discarded and 700µl RW1 buffer was added to each column and centrifuged at 8000 RCF for another 15 seconds. This process was then repeated twice but with 500µl RPE buffer, the first instance centrifuged for 15 seconds and the second for 2 minutes, discarding the flow through for each step. Excess ethanol was then removed by centrifuging the column for 1 minute, before adding 50µl of RNase free water and centrifuging again for another 1 minute to elute the RNA. Total RNA was then quantified for each sample using Nanodrop 2000 spectrophotometer, which quantifies absorbance at wavelength at 260nm to establish the concentration of RNA in each sample, and the ratio of sample absorbance at 260/280 was used to confirm purity (absence of contaminants such as protein, which absorb strongly at/near 280nm) with ratios of ~2 deemed to represent 'pure' RNA. After quantification RNA samples were either used immediately or stored at -80°C. RNA samples were reverse transcribed using High-Capacity RNA-to-DNA™ Kit (Applied Biosystems™). The RT reaction was prepared on ice in order to obtain a 30µl sample of cDNA for downstream qPCR. Volumes of sample equivalent to 1µg of RNA were added to reagents in the kit after 15µl buffer and 3µl of enzyme and made up to 30µl using RNase free water. Samples were then reverse transcribed using a Biorad thermal cycler T100 using cycling parameters 37°C for 1 hour, 95°C 5 minutes to convert RNA into cDNA. Each resulting cDNA sample was analysed in triplicate for each individual probe within a 384-well PCR plate with GAPDH used as a control 'housekeeping' gene for each sample. Each reaction consisted of: 2µL cDNA, 5µL TaqMan™ Universal PCR Mastermix, 2.5µL ddH2O and 0.5µL of probes (provided in table 2.10). The plate was sealed using optical adhesive film (MicroAmp™) and loaded onto a 7900HT Fast Real-Time PCR System to perform quantitative PCR. The system was set to report FAM with repeats of 40 cycles. Cycling conditions involved an initial 95°C hold for 10 minutes followed by 40 cycles of 15 second 95°C denature step and

finally 60°C for 1 minute in order to anneal and extend. Double delta Ct (2-ΔΔCt) analysis was used to determine relative gene expression using an average Ct value from the triplicate runs. For example, to detect differences in expression between primary, patient derived GSCs grown in stem conditions and bulk differentiated cells: ΔCt = Mean Control (GAPDH) Probe Ct – Mean Gene Probe Ct, and ΔCt Expression = 2-ΔCt. Then, to calculate fold-change expression in GSCs relative to bulk cells: ΔΔCt = ΔCt Expression (Stem)/ ΔCt Expression (Bulk).

2.8.2 Immunoblotting

For immunoblotting glioblastoma cells were seeded into Cultrex-coated 6-well plates and incubated at 37°C in 5% CO_2 for 48 hours. Before media removal, cells were washed twice in ice-cold PBS. Cells were then lysed with the addition of 100µl lysis buffer (20 mM Tris-HCl pH 7.5, 150 mM NaCl, 1% Triton X-100, 1 mM DTT and 1 mM EDTA supplemented with 50 U/µl benzonase (Novagen), protease and phosphatase inhibitors (Sigma). Cells were immediately harvested using a cell scraper and transferred to labelled eppendorf tubes on ice. Each sample was then vortexed for 10 seconds before being placed on ice for 15 minutes. Samples were vortexed again following a final 15-minute incubation on ice and one final vortex. Samples were then centrifuged at 14,000 × g for 15 min at 4°C. Gel electrophoresis was performed using NuPage system (Invitrogen). Samples were resolved on 4-12% Bis-Tris gels in MOPS buffer, transferred to Protran® nitrocellulose membranes (0.1µm pore size) which were then probed for proteins of interest using antibodies diluted in 5% BSA (details of antibodies shown in table 2.4).

2.9 Flow Cytometry and analysis of cell cycle distribution

2.9.1 Sample Preparation

Cells were plated into 6-well dishes overnight, they were treated with WEE1 inhibitor for 1hour before being collected. Media was removed and cells were washed twice in PBS, before 500uL/well of Accutase. Both the media and PBS washes were retained. Following detachment, cells were collected into labelled 15ml falcon tubes. Each Falcon tube was then centrifuged at 1,200 rpm for 3 minutes. The supernatant was discarded, retaining a cell pellet, to this 1ml of ice cold 70% ethanol was added in a dropwise manner, ensuring even

distribution through gentle mixing on a vortex. Cells were left to fix overnight before excess ethanol was spun off and cells were washed twice in PBS, centrifuging at 1,200rpm for 3 minutes. To each sample 5uL of RNAseA (1µg/µl stock) was added to added to each sample and incubated at room temperature for 15 minutes to allow the degradation of RNA, whilst leaving DNA intact. After this, samples were protected from the light with foil and 200µl PI (50µg/ml stock) was added to each sample. Samples were incubated for at least 15 minutes (but typically overnight at 4°C) to allow the intercalation of PI with DNA, prior to flow cytometric analysis.

2.9.2 FACSCalibur Analysis

Samples were processed using a BD FACSCalibur system, the data was analysed using FlowJo (Version 10.8.1) software. In order to remove cell debris and doublet cells from single cell gating cells, the forward scatter and side scatter was analysed. A 488nm laser was utilised to excite PI, with emission detected using the FL-1 (530nm emission filter). A cumulative histogram based on PI emission data and the number of cell/events was plotted in FlowJo, each peak was then gated for each stage of the cell cycle.

Chapter 3 – Ex Vivo Optimisation

3.1 Drug Plate Optimisation

3.1.1 Introduction

Despite success within haematological cancers (Snijder *et al.*, 2017), the concept of ex vivo drug screening is relatively novel within solid glioblastoma tissue, and therefore required optimisation. Most of the optimisation work described within this chapter was carried out using the same low passage primary glioblastoma stem-like cell lines so as to be as representative of primary dissociated cells as possible (a list of these cells is available within Chapter 2 table 2.7). However, despite our best efforts, there were some instances due to COVID-19 disruptions that this was not possible, and therefore either different primary or established glioblastoma cell lines were also used during optimisation experiments. Initial work investigated; drug solvent effects, plate brand optimisation, seeding density optimisation, reducing plate variability through circumventing evaporation effects, comparing electronic hand vs plate cell seeding and centrifuging drug plates to minimise loss of cells through fixing and staining steps (figure 3.1).
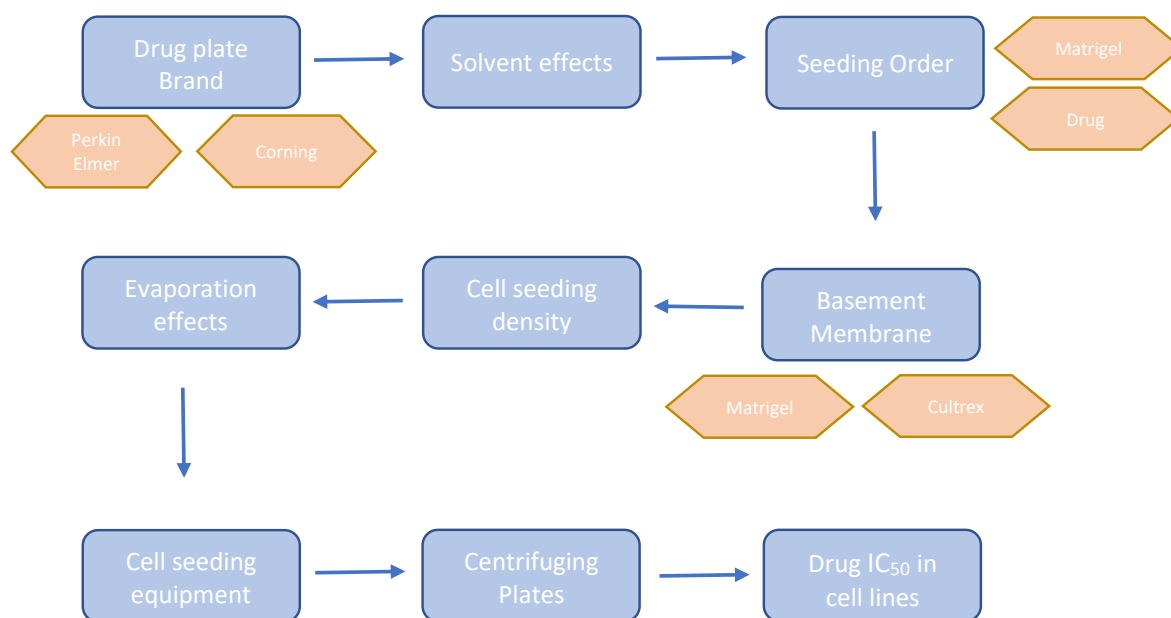
Figure 3.1 - Summary of optimisation steps required to develop ex vivo HTS for glioblastoma -
The plating efficiency and quality of microscopy images were compared between two different 384-well drug plate brands using a solvent (DMSO) titration assay. Additionally, the seeding order of BME (Matrigel), drug, and cells within the 384-well plate was examined. Drug responses of primary cell lines were compared using two different BME extracts (Matrigel and Cultrex), and optimal seeding densities for both primary cell lines and freshly dissociated patient samples were determined. The effect of a

breathable sealing membrane on reducing plate evaporation was evaluated by testing DMSO control coefficient of variation (COV) with and without the membrane. Furthermore, the impact of using a humidifier chamber during a 4-day incubation period on reducing plate evaporation effects was assessed by comparing drug responses of three patient samples. A comparison was made between two different cell seeding methods: handheld automated 16-channel E1-ClipTip electronic pipette and automated multidrop dispenser. Effect of centrifuging sample drug plates to minimize cell loss during fixing and staining steps was tested. Finally, IC50 values of the drug library within cell lines were investigated to design updated V02 plates.

3.1.2 Solvent sensitivity of glioblastoma cells

DMSO is an extensively used solvent in pharmacology and toxicology and is the solvent used to dilute the majority of the drugs within our ex vivo library. As part of initial optimisation of ex vivo screening methodology, the sensitivity of glioblastoma cells to increasing concentrations of DMSO was investigated using established LN18 cells across two brands of 384-well plates. From the data in figure 3.2 it was shown that there were no significant differences between the DAPI cell counts within growth media control and the lower 0.02% and 0.05% DMSO treated cell counts. There were however significantly higher (p value = <0.0001, one way ANOVA) cell counts within the DMSO wells 0.1%, 0.25%, 0.5% and 1% in comparison to normal growth media for both 384-well brand plates tested.
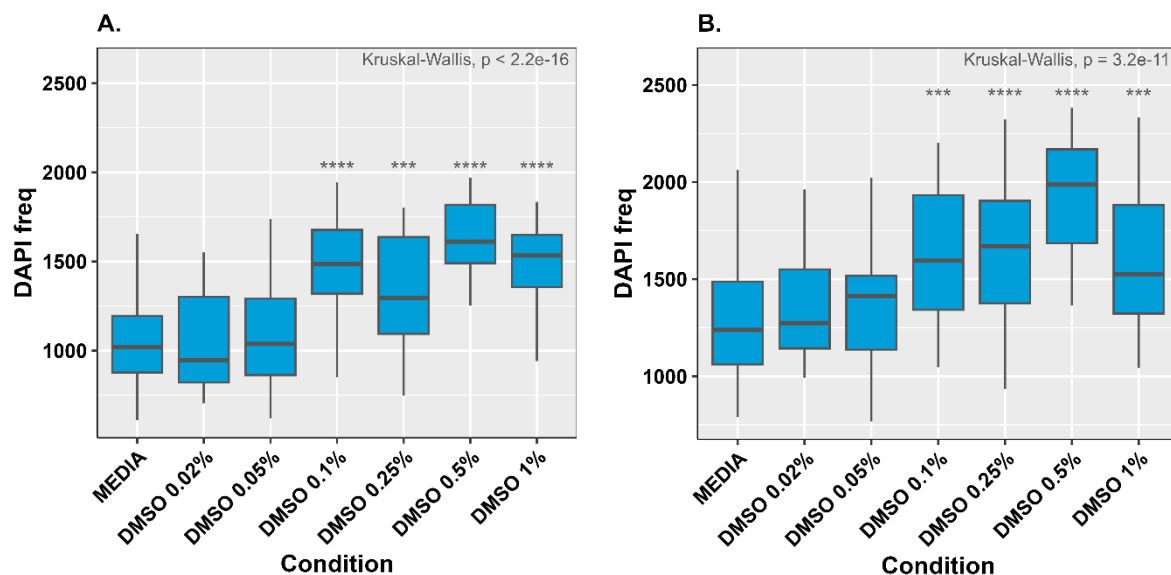
Figure 3.2 - DAPI cell counts of LN18 cells subjected to DMSO concentrations compared between two 384 well plate brands - **A:** Cell Carrier Ultra 384-well plate (PerkinElmer). **B:** CellBIND 384-well plate (Corning)**. LN18** cells were seeded onto both brand 384 well plates and incubated for 4 days, with corresponding media or DMSO condition. Plates were then imaged on a CD7 microscope, with 20x lens with 0.5 magnification using a 5-tile imaging strategy. The central box of the boxplot displays the interquartile range (IQR), where the lower boundary corresponds to the first quartile and the upper boundary corresponds to the third quartile, the horizontal line within the box represents the median

3.1.3 Seeding density Optimisation

The optimal seeding density of a primary GSC cell line (Cx18) and a patient sample (GBM10A) were investigated to determine a suitable range of seeding densities required for a 4-day incubation period to obtain drug response profiles. Raw AUC values were obtained for every drug at each seeding density, these individual values were then plotted using a linear correlation to give an R^2 value, values nearer to 1 represent good correlation between results.

Cx18 cells were seeded onto GBM drug plates at four different seeding densities of 250, 500, 1000 or 2000 cells/well. Plates were imaged to obtain DAPI counts, these counts were then used to determine AUC for each specific drug at each specific seeding density. Correlation analysis was then performed in relation to 1000 cells/well condition to test the consistency in results. The R^2 values depicted in figure 3.3A suggest that all seeding densities tested against the pre-established 1000 cells per well gave similar end point drug response results and therefore there is a suitable range in which cells can be seeded to get reproducible drug response profiles.

The behaviour of freshly dissociated cells from a patient sample however is quite different to primary cell lines, as following the dissociation steps of patient tumour samples the cell suspensions often have low viability counts (15-40%). Additionally, some of the cells counted in the analysis as 'dead' are immune or red blood cells, which do not adhere and subsequently get washed away during fixing and staining steps. For this reason, the cell counts used for dissociated tissue is much higher than that for cell lines, for this purpose a range of seeding densities was therefore compared from 5-20 thousand cells per well.

Ex vivo sample GBM10A was seeded on three identical drug plates at three different seeding densities 20,000, 15,000 and 10,000 cells/well as shown in figure 3.3B. When comparing to 20,000 cells per well an R^2 value of 0.846 and 0.944 for 10,000 cells and 15,000 cells respectively indicated there was a high degree of consistency between all three seeding densities and therefore suggesting that it is possible in future to seed a range of densities,

which is particularly important when dissociating smaller sized tumour samples, which achieve much lower viable cell counts.
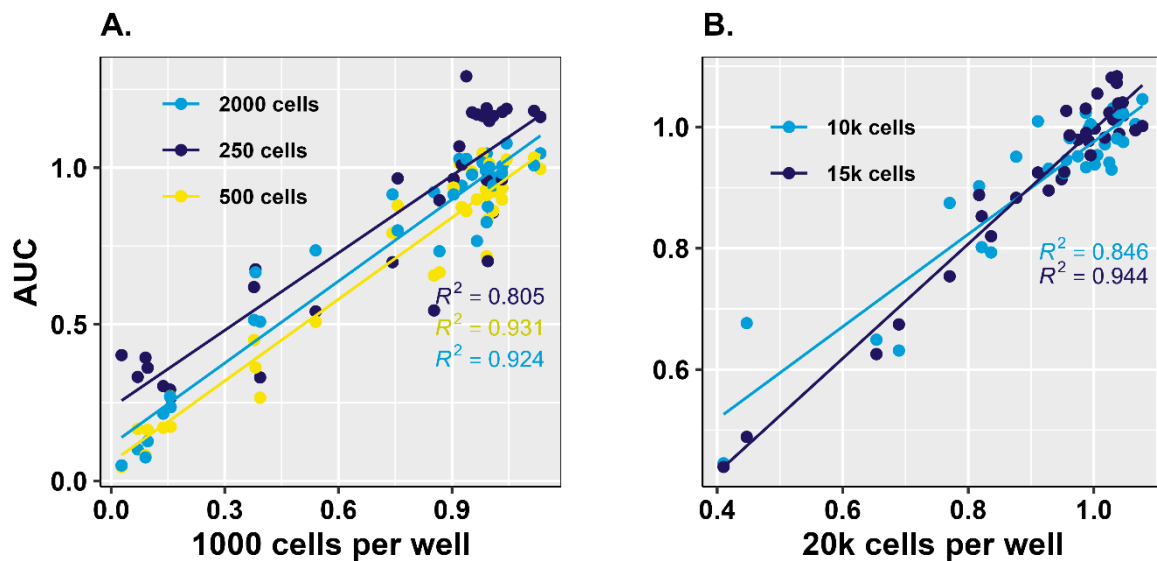
Figure 3.3 - Comparing the individual drug dose response AUC values at different seeding densities - **A:** AUC values for Cx18 cells seeded onto drug plates at 250, 500, 2000 cells per well relative to optimised 1000 cell per well plate. **B:** AUC values for GBM10A cells were seeded onto drug plates at 10,000 and 15,0000 cell per well compared to 20,000 cell per well plate. Plates were imaged on a CD7 microscope, with 20x lens with 0.5 magnification using a 5-tile imaging strategy.

3.1.4 Reducing Evaporation effects

To circumvent plate evaporation known as "edge effect', the outer most wells of the 384-well drug plates were not used for any experimental samples, instead they were filled with 100µL of media. To further avoid plate evaporation effects, breathe-easy sealing membranes were used as they had been shown previously to significantly reduce plate evaporation effects (Boehnke *et al.*, 2016). To investigate whether these membranes would help reduce evaporation effects and improve reproducibility on our drug plates we compared the cell counts of two different glioblastoma cell lines, LN18 (established) and G7 stem (long-term cultured primary stem-like) following a 4-day incubation period with and without breathable membranes. Figure 3.4 shows a comparison between the 24 DMSO control wells which are distributed evenly across 384-well drug plates. Due to a lack of biological repeats, it is not clear whether the membrane significantly aided the cell counts, however the membrane did reduce the coefficient of variation (COV) by 0.4% in the LN18 cells and 1.9% in G7 stem. Based

on the reduced COV across the DMSO wells when using the breathable membrane, it was decided that all further experiments would incorporate the breathable membrane.
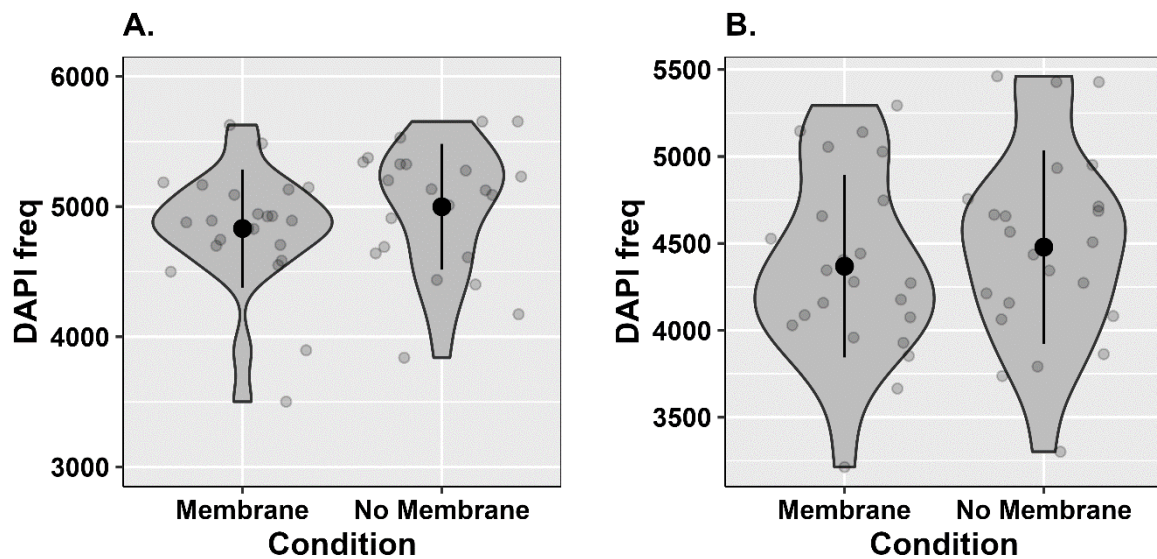
Figure 3.4 - Investigating the effects of cell counts using plates with and without a breathe-easy sealing membrane to circumvent evaporation - **A.** Comparing DMSO cell counts from drug plates seeded with G7 stem cells incubated with and without breathable membrane. COV with membrane = 9.4%, without = 11.3%. **B.** Comparing DMSO cell counts from drug plates seeded with LN18 incubated with and without breathable membrane. membrane = 11.8%, without 12.2%. Plates were imaged on a CD7 microscope, with 20x lens with 0.5 magnification using a 5-tile imaging strategy. Error bars represent standard deviation (SD) around mean. Biological repeat = 1, technical replicates 22.

To further prevent evaporation effects drug plates were also incubated within humidifier chambers. The TMZ drug response profiles of three primary cell lines (GBM18, GBM20, GBM21) were compared between plates incubated normally and within a humidifier chamber (figure 3.5 A, C and E). Additionally, the DAPI cell counts from the DMSO control wells were compared between plates (figure 3.5B, D and F). From the boxplot comparisons of the DMSO control wells it suggests that the DAPI frequencies are lower when cells have been subjected to humidifier chamber incubation. Nevertheless, there are multiple outliers within the data (figure 3.5 B and D) from cells GBM18 and GBM20 subjected to incubator only, this is most likely a factor of increased evaporation effects, within wells towards the outer circumference of plates. The use of humidifier chamber is used therefore to reduce variation between repeat measures across drug plates.
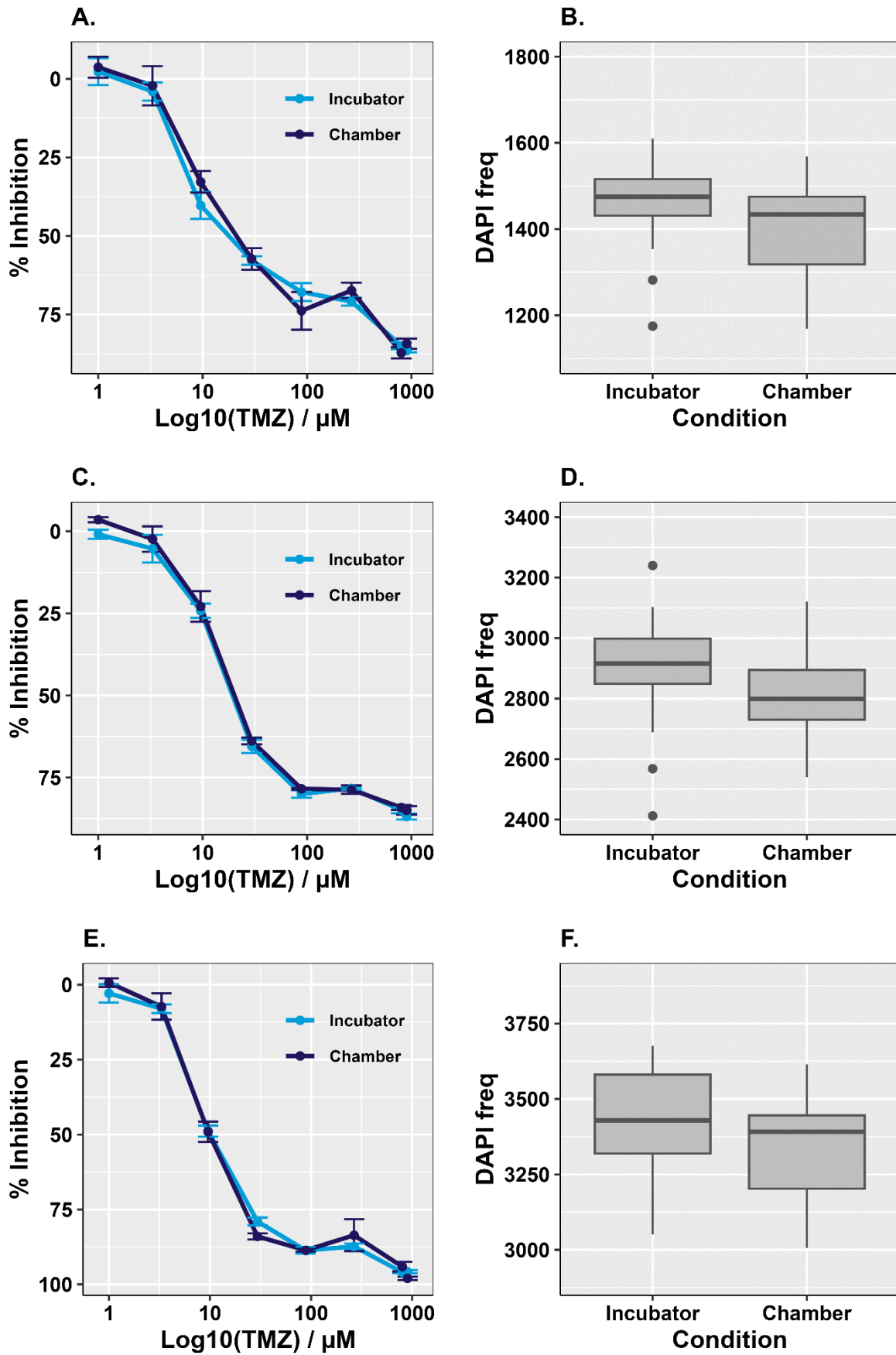
Figure 3.5 – Comparing the TMZ dose response curves with drug plates incubated with and without being placed in a humidity chamber - Three different primary samples were tested **A/B** corresponds to

GBM18, incubator COV= 8.6%, chamber = 8.1%. **C/D** corresponds to GBM20,   incubator COV = 6.6%, chamber = 4.8%. **E/F** corresponds to GBM21, incubator COV= 5.1%, chamber = 5.0%. Left hand dose response curves represent TMZ percent inhibition (calculated using equation 2.3), in both conditions, right hand boxplots compare the DAPI counts in 24 DMSO control wells for both conditions. The central box of the boxplot displays the IQR, where the lower boundary corresponds to the first quartile and the upper boundary corresponds to the third quartile, the horizontal line within the box represents the median and the whiskers extend to the minimum and maximum values within 1.5 times the IQR. Plates were imaged on a CD7 microscope, with 20x lens with 0.5 magnification using a 5-tile imaging strategy. Error bars on dose response curves respresent SEM, biological repeats n=1, technical replicates N=4.

3.1.5 Comparing Cell Seeding Methods

During the course of these optimisation experiments, it was noted that there was often a high variation within the DMSO control wells when using our Multidrop cell seeding equipment, therefore we compared this original method to seeding by hand using an automated E1-ClipTip electronic pipette. To compare these two methods LN18 cells were seeded onto blank 384-well plates, half of the plate using the traditional Multidrop cell seeder and the other half using 16 channel E1-ClipTip electronic pipette. Following 4-days the plate was imaged and DAPI cell counts were compared as shown in figure 3.6 below.

When comparing the Multidrop equipment to hand seeding using the 16 channel E1-ClipTip pipette, the COV was reduced from 14.07 % to 9.41% highlighting the multidrop equipment may have required calibrating or the dispenser heads replacing. A comparison between the two seeding conditions using an unpaired student t-test revealed significant differences between the two seeding conditions (figure 3.6). Whilst the DAPI count mean was higher using the multidrop, the variance of the replicates was significantly reduced seeding by hand. Further investigation of this by another lab member showed that the multidrop equipment was dispensing approximately 10% more volume, which can explain the increase in cell count (data not shown). As a result, it was decided that future experiments should be seeded by hand to avoid any unnecessary variation within results.
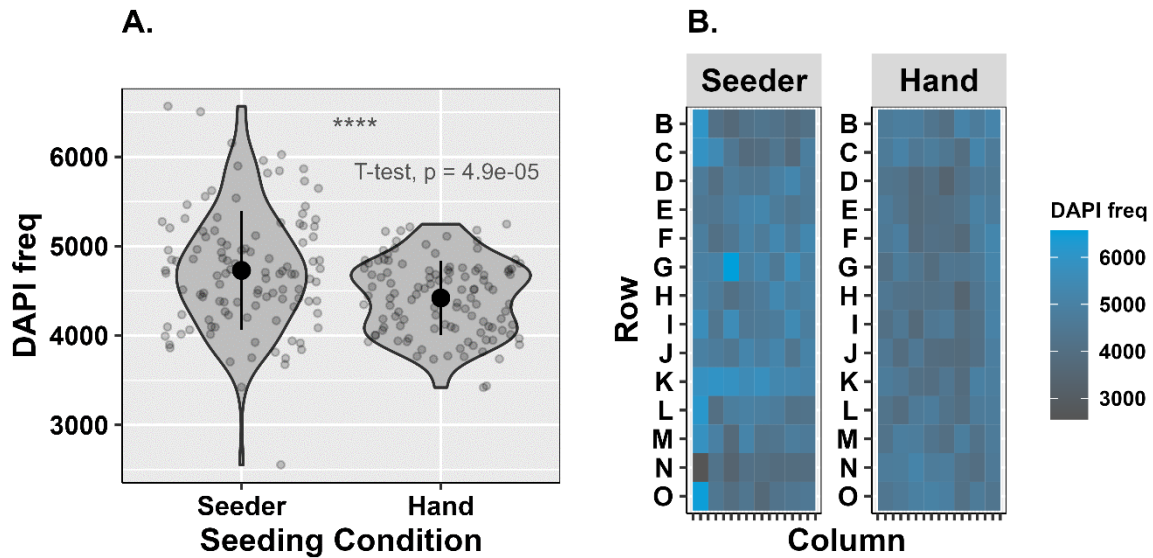
Figure 3.6 - DAPI cell counts of LN18 cells seeded by hand or using automated Multidrop cell seeder - LN18 cells were seeded both by hand using an E1-ClipTip electronic pipette and using automated Multidrop equipment at a density of 1,000 cells per well onto a 384 well plate. **A.** comparison between DAPI counts following the two different seeding methods, unpaired student t-test was performed p= <0.0001. Error bars represent SD. **B.** Heatmap showing the well specific DAPI frequencies of both seeding methods. Plates were incubated for a 4 day period following fixing and staining with DAPI, plates were then imaged on a CD7 with 20x lens with 0.5 magnification using a 5-tile imaging strategy. LN18 multidrop seeder (COV 14.07%) vs. hand seeded (COV 9.41%).

3.1.6 Centrifugation of drug plate

In order to avoid loosely adherent cells washing away we tested plate centrifugation during the fixation steps. GBM011 sample was seeded identically onto two drug plates, prior to any fixing and staining steps one of the plates was centrifuged @10,000G for 2 minutes halfway into 30-minute PFA fixation. To compare the two different methods percentage inhibition was calculated for each well and the data was plotted using a linear correlation to give an R^2 value of 0.862 (figure 3.7). This represents a good correlation between the results, showing that centrifugation of the plate may have little effect on the drug response profiles. Due to this good correlation between results, we believe most of the cells which were washed away are either dead or are immune cells and therefore do not adhere to the BME provided. As we are aiming towards using multiple IF antibody markers to target stem cell populations and evaluate treatment response, we decided to not adopt this centrifuge approach as following microscopic investigation, it showed to retain dead cells and debris, making themicroscopy images very dirty and difficult to analyse. When the DAPI counts for the DMSO control well

were compared there was much higher variation within the centrifuged plate repeats. To maintain the low COV on the drug plates the spin method was not adopted.

A.

B.
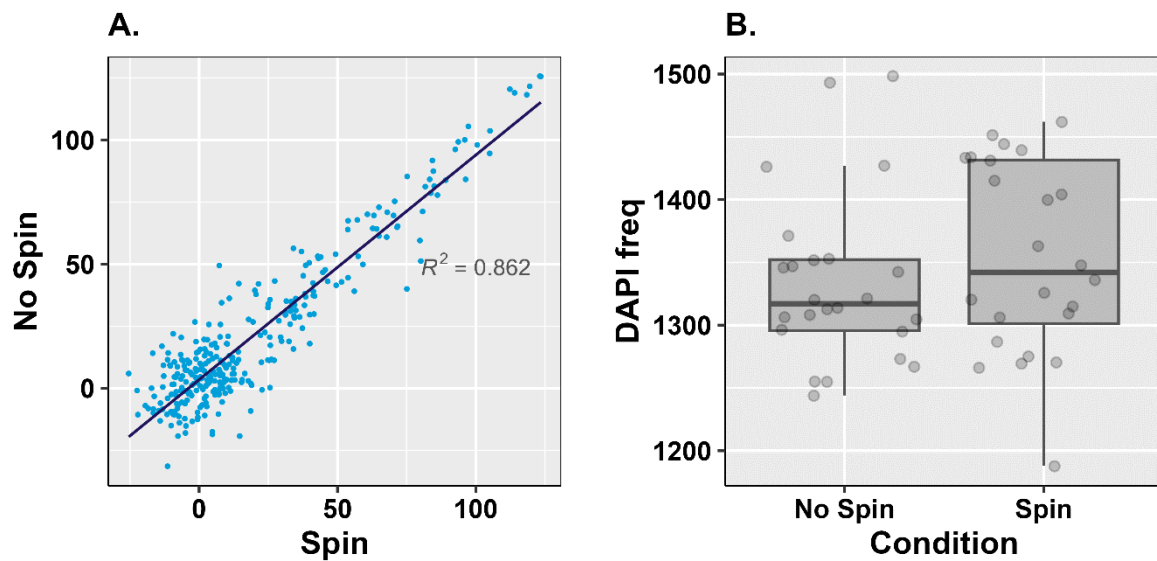
*Figure 3.7 - **Investigating spin steps to reduce washing away of cells** -* To retain whole cell population on plates following fixing and staining steps two identical drug plates were seeded with sample GBM11 freshly dissociated cells, following a 4-day incubation plates were removed from incubator and spun @10,000G for 2 minutes. **A:** Correlation coefficient comparing the individual well percent inhibition (calculated using equation 2.3), values from spin and no spin plates. R2= 0.862. **B:** Comparison of the DAPI frequencies from the 24 DMSO control wells. The central box of the boxplot displays the IQR, where the lower boundary corresponds to the first quartile and the upper boundary corresponds to the third quartile, the horizontal line within the box represents the median and the whiskers extend to the minimum and maximum values within 1.5 times the IQR. Biological repeats n=1, technical replicates N = 24.

3.2 Optimising Basement Membrane

Next, we wanted to assess the effect of plating alternations within out 384-wells. Due to not having direct access to plate printing machinery within our department, drug plates would need to be produced in large batches and stored within our lab at -80°C. Another factor to consider was that glioblastoma stem-like cells are non-adherent and will grow as spheroids without the presence of a BME on plasticware. We therefore wanted to investigate whether the seeding order of the drug, BME and cells had any effect on the efficacy of the drugs, as a result the three possible plating alternations were tested.. The three conditions are shown in figure 3.8. Out of the three possibilities, condition 1 is the ideal order as it would allow for a higher throughput process; drug plates would be printed in batches and stored at -80°C, once confirmation of a suitable clinical sample is then relayed to the ex vivo team, prior to surgery,

pre-printed drug plates would then be coated with BME (Matrigel) ready for downstream tumour cell seeding.
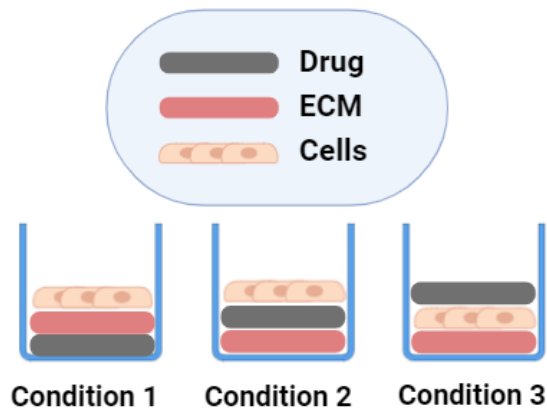
Figure 3.8 - Illustration of the three plating alternations which were tested to investigate effects on drug efficacy within 384-well drug plates - Condition 1 plating order (drug, ECM, cells), Condition 2 plating order (ECM, drug, cells). Condition 3 plating order (ECM, cells, drug).

3.1.1 Plating Order – Cisplatin Sensitivity

To investigate if the plating order of drug, BME (Matrigel) and cells affects drug efficacy, the sensitivity of Cx18 cells to cisplatin was investigated in the three different conditions, as shown by the dose response curves in figure 3.9. Using R package GR metrics IC_{50} values were calculated; Condition 1 IC_{50} = 1.21 ± 0.260 μM, condition 2 IC_{50} = 1.30 ± 0.315 μM, condition 3 IC_{50} = 1.20 ± 0.2.12 μM. There was complete overlap between the cisplatin IC_{50} values for all three conditions, this encouragingly suggests that condition 1 can be used successfully for the purpose of this drug screening project.
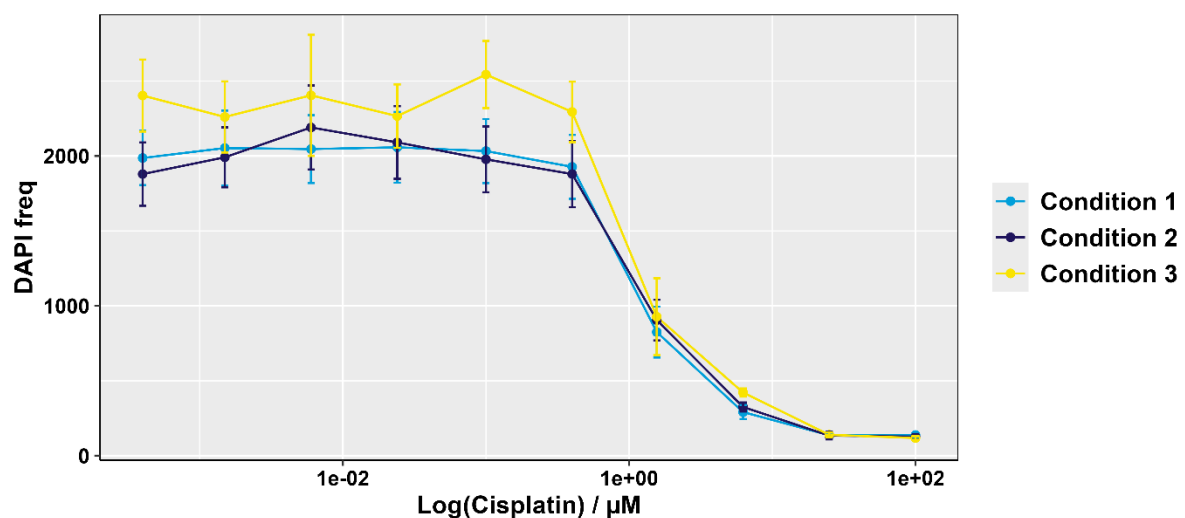
Figure 3.9 - Dose response curves for Cx18 cells treated with cisplatin for 4 days using three different plating conditions - Cx18 cells were seeded into 384 well plates at a density of 1000 cells per well and incubated for 4-days with 0 - 100 µM cisplatin. DAPI cell counts were obtained using the CD7 microscope with 20x lens with 0.5 magnification using a 5-tile imaging strategy. Condition 1 IC_{50} = 1.21 ± 0.260 µM, condition 2 IC_{50} = 1.30 ± 0.315 µM, condition 3 IC_{50} = 1.20 ± 0.2.12 µM. Error bars represent SEM. Biological repeats =3, technical replicates = 4.

3.2.1 Plating Order – Temozolomide Sensitivity

To further illustrate that condition 1 is suitable for drug screening, the SoC drug TMZ was tested using the three different alternations. As TMZ's mode of action works through futile cycling of MMR, multiple rounds of cell cycling are required for cells to undergo DNA damage resulting in cell death, therefore an 8-day incubation period was also tested alongside 4 days as shown below in figure 3.10.

The mean and SD of the IC_{50} values from three biological repeats for each condition are shown in figure 3.11.. Conditions 1 and 2 have the most consistent IC_{50} values across all three independent biological repeats within both the 4-day and 8-day incubation period, highlighted by smaller SD around the mean. This suggests that seeding TMZ above or below the ECM has similar effects on drug efficacy, and overall, it is improved within these 2 conditions shown by lower mean IC_{50} values within both incubation periods. Condition 3 showed the highest mean IC_{50} values with largest degree of variation within both the 4-day (28.8 ± 19.1µM) and 8-day (22.60 ± 12.5µM) incubation period. This high SD between repeats may be due to higher cell adherence and cell cycling, by allowing the cells to adhere to BME prior to drugging. Despite Condition 3 being the most representative model of patient tumour treatment, for logistical reasons described above around the critical need for ex vivo screening of clinical samples with short notice requiring the use of pre-printed drug plates, we therefore proceeded to adopt condition 1 for future ex vivo screening development.
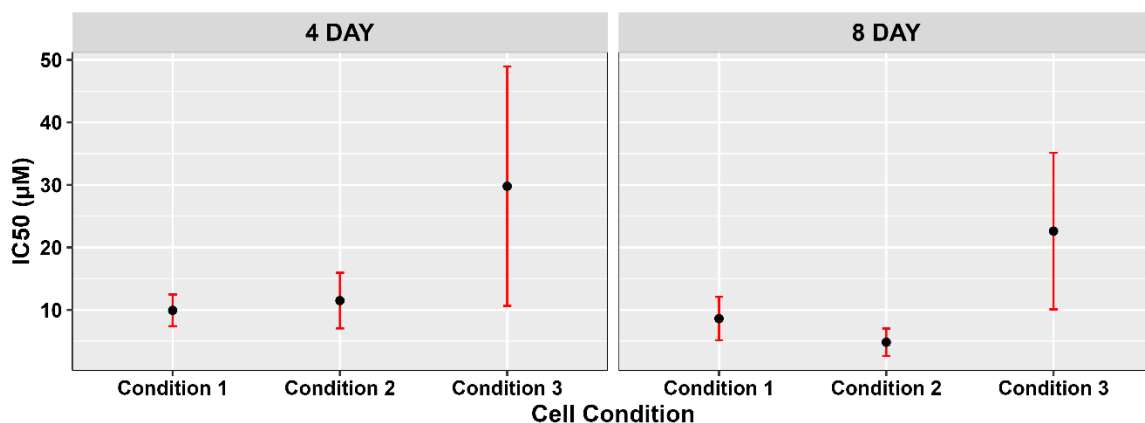
Figure 3.11 - Comparison of the IC_{50} response values comparing three different seeding conditions at two incubation periods 4-day and 8-days - Mean estimated IC_{50} values are represented by the black data points, with red error bars showing the standard error. Cells were incubated for 4 days. Condition 1 average IC_{50} = 9.94 ± 2.54 µM, condition 2 average IC_{50} = 11.5 ± 4.44 µM, condition 3 average IC_{50} = 28.8 ± 19.1 µM. Cells were incubated for 8 days. Condition 1 average IC_{50} = 8.62 ± 3.47 µM, condition 2 average IC_{50} = 8.84 ± 2.19 µM, condition 3 average IC_{50} = 22.60 ± 12.5 µM. IC_{50} values were calculated using the DRC package (Version 3.0-1) within R.

3.2.2 Comparing Basement Membrane Brands

As previously mentioned, a BME is required for primary glioblastoma stem-like cells to adhere as monolayers on plasticware. Initial work proceeded with the use of BME extract Matrigel, which had been previously optimised by the Collis laboratory for the culturing of glioblastoma primary cells. However, following the first year of this study there were Matrigel shortages within the UK due to Brexit and COVID-19, which resulted in our lab sourcing another BME alternative, Cultrex.

To evaluate the suitability of alternative BME, a direct comparison was performed between our already optimised BME Matrigel and the potential alternative Cultrex. To investigate the suitability to retain stem-like cultures on plasticware, DAPI cell numbers of Ox5 cells were compared following a 4-day incubation period cultured using the two different brand extracts (figure 3.12). This data demonstrated that Cultrex would be a suitable alternative to Matrigel, as both cell lines exhibited higher cell counts when cultured within Cultrex, measured through positive DAPI cell counts. This could have been due to different levels of BME components in the Cultrex, permitting more cells to adhere initially or alternatively higher levels of growth factors which caused the cells to divide faster. This data therefore confirms the ability of Cultrex to retain stem-like cultures, and be used as a suitable alternative to Matrigel.
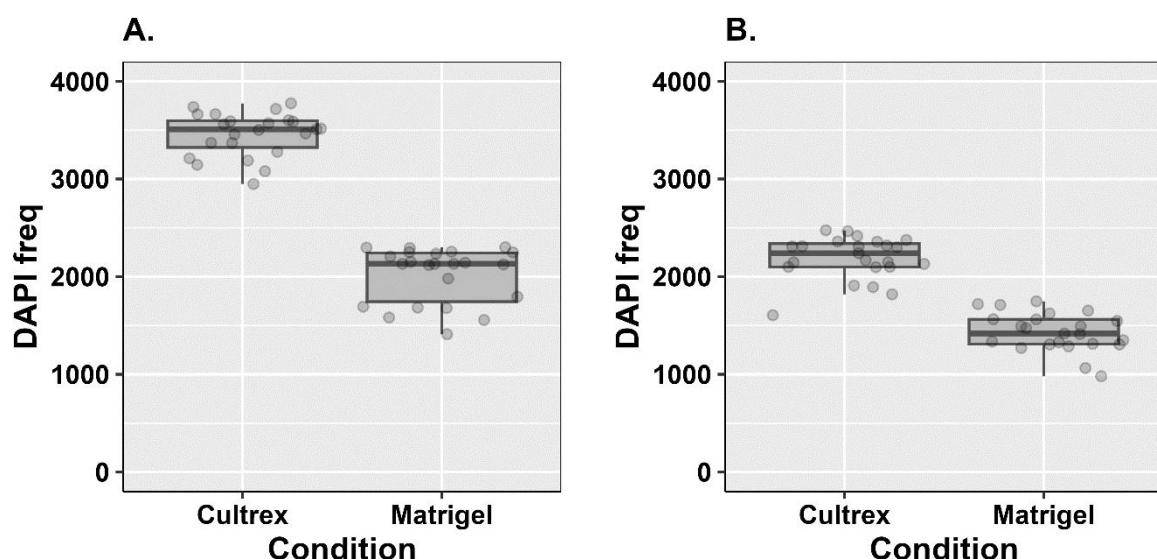
Figure 3.12 - Comparing the cell numbers of the DMSO control wells of plates coated with either Matrigel or Cultrex as a basement membrane - Cell numbers were obtained from DAPI cell counts within DMSO control wells. A: Ox5 Core. B: Ox5 Edge. The central box of the boxplot displays the IQR, where the lower boundary corresponds to the first quartile and the upper boundary corresponds to the third quartile, the horizontal line within the box represents the median and the whiskers extend to

In order to determine whether or not the different BME had any inadvertent effect on drug responses, the two different BME Cultrex and Matrigel were compared using Ox5 cells seeded on our V01 GBM drug plates. DAPI cell counts were obtained using microscopy and normalised using percent inhibition calculation (equation 2.3), to obtain the dose response curves depicted by figure 3.13. It was decided to test both the BME extracts on the entire drug library, rather than just controls to confirm the BME results were consistent over a large range of drugs. The data shown highlights identical inhibition dose curves for both Matrigel and Cultrex, within both the Ox5 Core and Edge cells, demonstrating that drug efficacy was not altered by brand of BME.
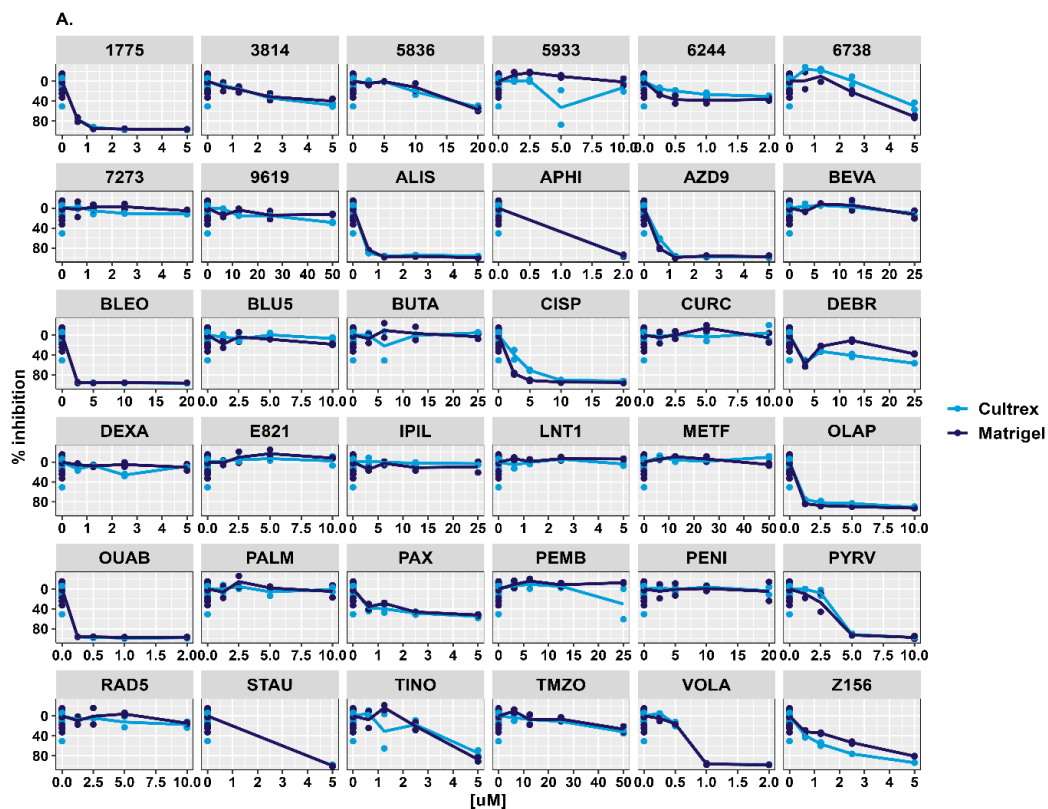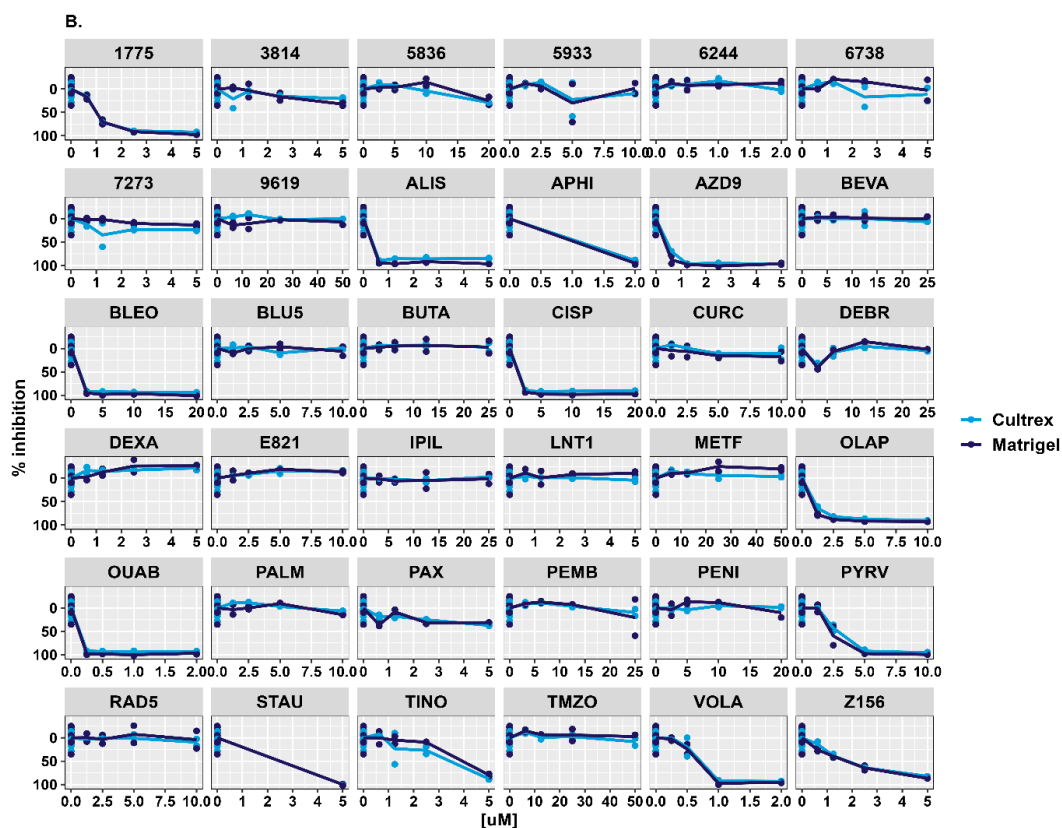
Figure 3.13 - Investigating the relative inhibition of Ox5 Core and Edge cells using two different brand basement membranes (Cultrex and Matrigel) to confirm drug efficacy is maintained - Ox5 cells were seeded onto V01 GBM plates at a density of 1000 cells per well and incubated for 4-days. DAPI cell counts were obtained using a CD7 microscope, with 20x lens and 0.5 magnification using a 5-tile imaging strategy. DAPI cell counts were used to calculate percent inhibition (calculated using equation 2.3). **A:** Ox5 core cells. **B:** Ox5 edge cells. Biological repeat =1, technical replicates =2.

3.3 Image Capture and Analysis Optimisation

3.3.1 Tile Strategy Comparison

To evaluate drug responses, multiple images of each individual well within a 384-drug plate must be captured using high content microscopy. To do this using the Zeiss CD7 microscope a 'tile' imaging strategy was followed, with each tile corresponding to a section of the individual well area captured. Two different number tile strategies were therefore evaluated: 5 image tiles per well or 9 image tiles per well, corresponding to 28.8% and 51.5% of total well area respectively, based off the dimensions of a PerkinElmer Cell Carrier Ultra 384-well plate. The locations of these tiles can be pre-selected using the Zeiss software either through a symmetrical arrangement or can be set randomly, for the purpose of this study all tile images were selected symmetrically to give even coverage within the well.

To test the consistencies between the results using these two different number tile strategies, four different patient sample drug plates were imaged using both a 5 tile and 9 tile strategy. The AUC values were then calculated for each individual drug for both strategies, the consistency of these results were compared using a correlation analysis as shown in figure 3.14. From the data shown samples GBM23 (graph B) and GBM24 (graph C) had R^2 values of 0.96 and 0.94 which signifies a high level of correlation between the AUC results from both tile strategies, therefore the much faster 5-tile strategy would be suitable to capture the whole well drug response.

This is not the case for every sample however, as from the data shown for samples GBM13 (graph A) and GBM25 (graph D), there is very poor correlation between the AUC results from both tile strategies (0.744 and 0.167). This is apparent when there are very low cell counts on the plates, and therefore a higher imaging strategy such as 12-tile or higher is required to achieve a higher percentage of well and therefore cell population imaged. Consequently, the tile strategy used is often reflective of the quality of sample, whilst it would be optimal to image the entire well of every single sample, it is often wasteful as the time and running costs of the microscope usually supersede the benefits. Therefore, it was decided that the imaging strategy should be selected on a case-by-case approach depending on the cell counts within the DMSO control wells, as shown in table 3.1 below. Here it was shown that increasing the tile imaging strategy from 5 to 9 led to improvement in the COV, apart from GBM24 where COV was increased by 2.7% using a larger 9-tile strategy. The DMSO control counts with the highest COV corresponded to samples with lowest mean cell count, GBM25 5-tile (142 cells, COV 30%) and GBM13 5-tile (315 cells, COV 15.8%). The data from table 3.1 supports the notion that lower cell counts lead to higher COV therefore we decided it was important to set a threshold for our imaging pipeline. It was therefore decided that if the DAPI counts from the DMSO control wells displayed a COV above the threshold of 15%, the plate would be re-captured at a larger tile strategy.
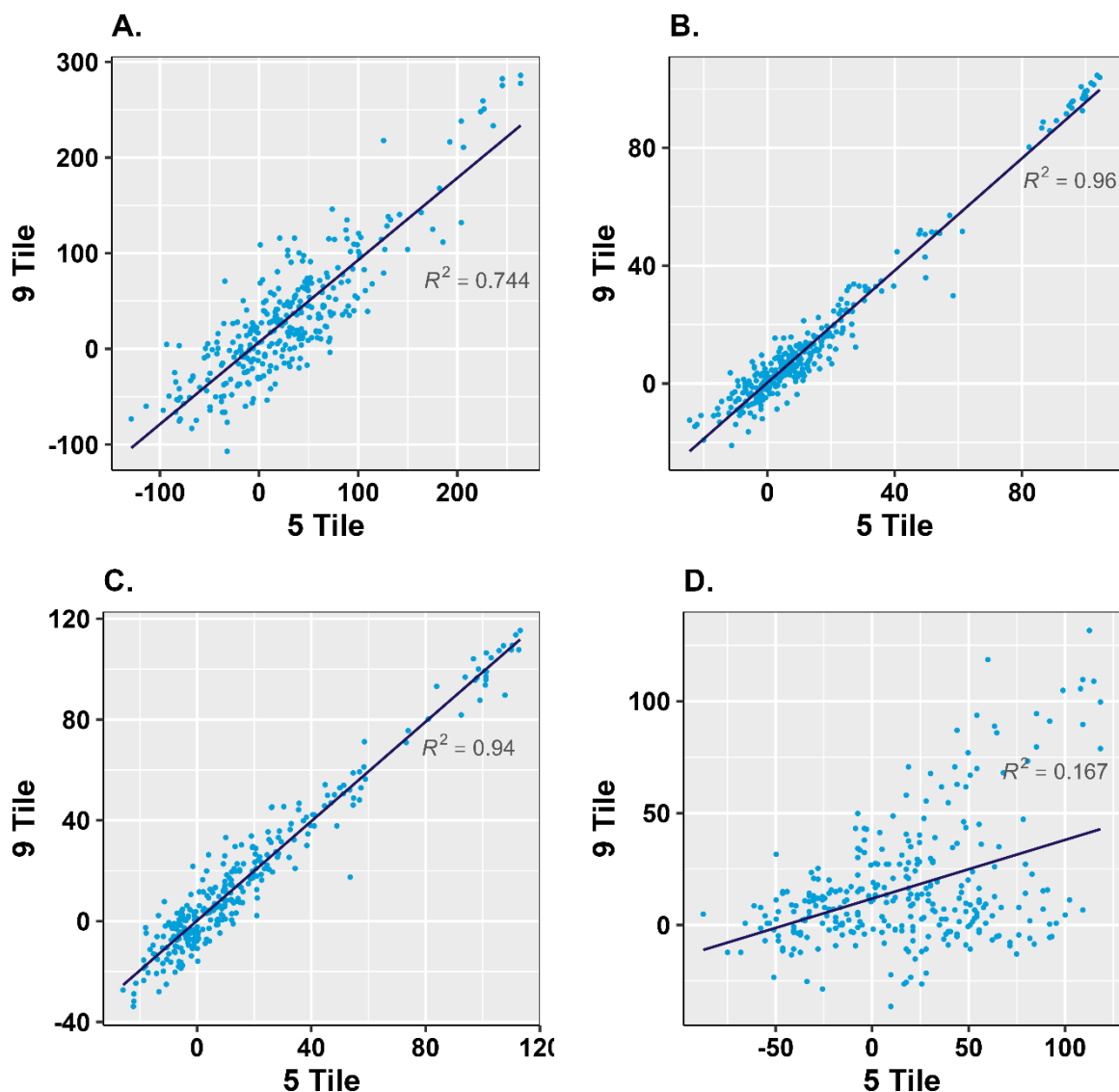
Figure 3.14 - Correlation analysis using relative inhibition calculated from DAPI cell counts from 5-tile and 9-tile imaging strategy for 4 primary samples - **A:** GBM13, **B:** GBM23, **C:** GBM24 and **D:** GBM25. Correlation analysis using calculated percentage inhibition values between two independent tile strategy settings. For the majority of samples, a 5-tile strategy was sufficient to capture the whole enough cells to generate a dose response, however on less densely populated samples such as GBM25 where the correlation in dose response is low between 5 and 9 tile, a higher 9 or 12 tile image strategy was adopted.

Table 3.1 - Comparison of DMSO counts and COV for different tile imaging strategies.

Sample Name	Tile Strategy	Mean DMSO count	COV
GBM25	5	142	30%
GBM25	9	372	8.1%
GBM24	5	681	6.8%
GBM24	9	1246	9.7%
GBM23	5	517	7.0%
GBM23	9	961	6.1%
GBM13	5	315	15.8%
GBM13	9	609	10.6%

3.2 Drug plate response optimisation

3.3.2 Sample End-Point analysis

Various metrics are available for defining a positive drug response to treatment. Two of the most commonly used metrics are IC_{50} and EC_{50}. IC_{50} denotes the dose necessary for a 50% inhibition in enzyme activity or cell count compared to controls, while EC_{50} represents the dose that corresponds to the midpoint of the sigmoidal dose-response curve (Brooks *et al.*, 2019). An alternative measure is the AUC, which exhibits greater resilience against experimental fluctuations compared to IC_{50} and EC_{50}. AUC condenses the complete dose-response relationship into a single numerical value between 0 and 1, making it much easier to compare and rank different drug responses (Pozdeyev *et al.*, 2016). IC_{50} and EC_{50} on the other hand only provide information about a specific point on the curve, for highly resistant cultures it is not aways possible to obtain dose for 50% viability and therefore is less reliable as requires extrapolation of dose response curve. In summary AUC offers a comprehensive, standardised and less noise-sensitive perspective in overall drug responses, making it the preferred choice when comparing and evaluating multiple sample drug responses across a library of different compounds (Fallahi-Sichani *et al.*, 2013).

For the first batch of glioblastoma specific drug plates, drug concentration ranges were selected based upon IC_{50} values from the literature. This approach was taken in order to conserve time and allow optimisation of ex vivo screening within solid glioblastoma tissue. Using these drug plates, a total of 18 samples were successfully screened, of these samples two were multiple region samples, modelling heterogeneity. Our initial heatmap generated using AUC values is shown in figure 3.15. We were able to retrospectively annotate each tumour sample based on their *MGMT* gene methylation status, this highlighted the issue with SoC drug TMZ as we saw no response despite differential *MGMT* statuses. This led to further investigation of TMZ within chapter 5.
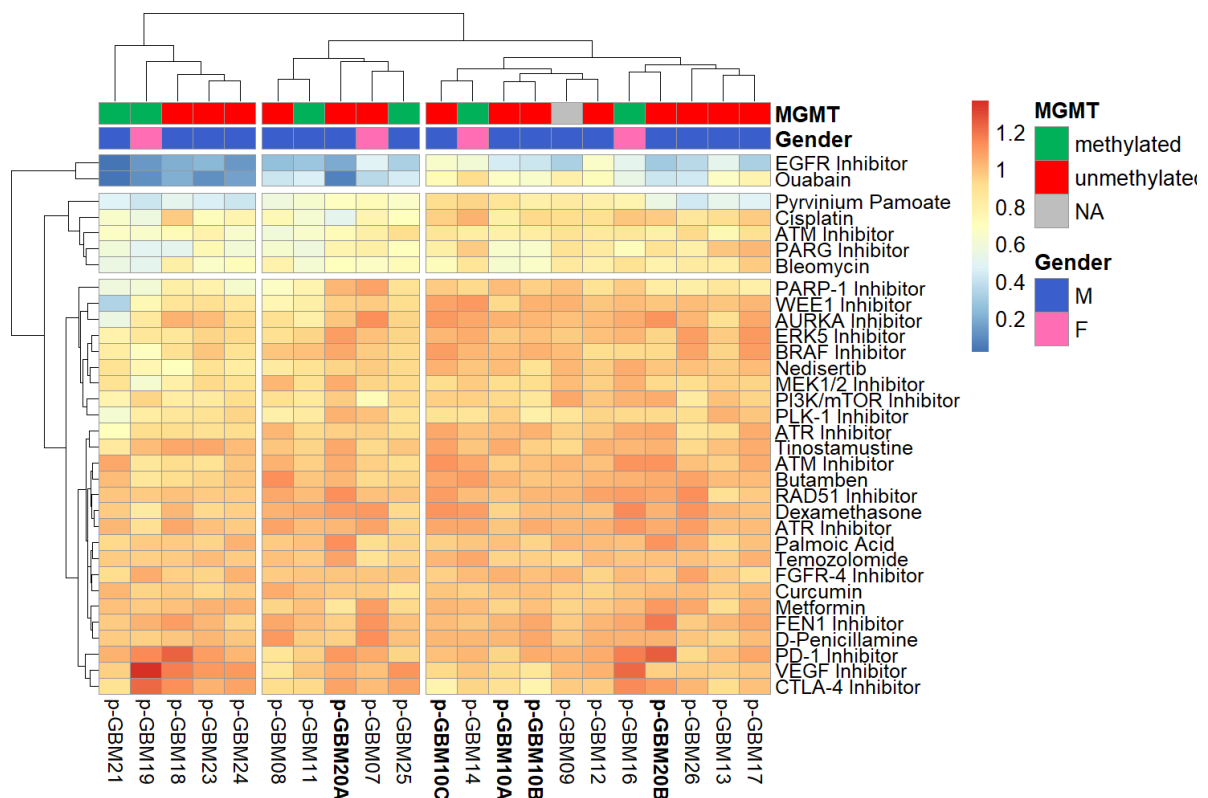
Figure 3.15 - GBM sample heatmap depicting raw AUC drug response for primary GBMs dissociated from 18 individual tumours - Scale shown represents cell death as 0 (blue) and cell survival as 1 (red). Larger samples such as GBM10 (A, B and C) and GBM20 (A and B; indicated in bold) were sectioned into multiple regions and screened independently in order to model the intertumoral heterogeneity of the disease. AUC values were calculated from 2 technical replicates following 96hr drug incubations using R package GR metrics and the heatmap was constructed using R package pheatmap as detailed in the methods section. Note, due to the fact that this was performed on limited fresh clinical material, biological repeats were not performed. Hierarchical clustering is explained in the text below.

The 'pheatmap' package used to generate these heatmaps in R utilises a hierarchical clustering function. This function initially calculates a Euclidean distance matrix, based on all the observations and variables within the data frame matrix. Agglomerative clustering is then performed on the distance matrix, whereby each drug response is separated out then clustered iteratively to merge the closest clusters, until one single cluster remains. The dendrogram allows visualisation of these observations how they are grouped and their relative distances. Despite limited drug concentration optimisation for these plates, it was still possible to identify differential responses through multiple drug signatures.

Two different samples (GBM10 and GBM20) were sub-sectioned into multiple regions and screened individually to model intratumoral heterogeneity. GBM20 appears to be the most heterogenous sample of the two, shown by the large distance between A and B sample

responses. Of the two GBM20A appears the most sensitive sample, especially to EGFR and ouabain, it also shows a response to cisplatin treatment unlike the GBM20B sample. GBM10 samples A, B and C appear less heterogeneous as they are clustered together, however it does appear than GBM10C is more resistant than the other two samples in particular to EGFR inhibitor, whilst GBM10A and B show very similar drug response profiles, suggesting that they were from spatially similar regions within the original tumour tissue.

3.2.1 Identifying resistant and sensitive tumours

In order to differentiate between resistant and sensitive tumour samples, we investigated the AUC drug response data for each individual drug, shown in figure 3.16A below. For each drug we used a Shapiro wilk test for normality, mean AUC values were used for drugs which had a normal distribution, median AUC values were used for non-normal data. This allowed us to determine patient tumour sensitivity or resistance for each drug, based on their AUC value being below or above the mean/median. From the drug library 5/34 drugs AZD1775, AZD6244, AZD6738, Palmoic acid and Alisertib were not normally distributed, therefore the median AUC value was used.

Another common way to compare drug AUC values is to standardise the datapoints using a Z-score normalisation, this method measures how many SDs above or below the group mean each data point is (Malo *et al.*, 2006). Normalising using this method makes the sample responses easier to compare as all the data points are plotted on a common scale therefore removing plate variation (figure 3.16B). One of the issues with this method is that it assumes the data is normally distributed, we know from table 3.2 there are 5 drugs that do not follow this trend. We therefore tested another method known as the modified z-score, which can be used for non-parametric data sets as it utilises the median and median absolute deviation (MAD) to calculate a z-score.

A.

B.

C.
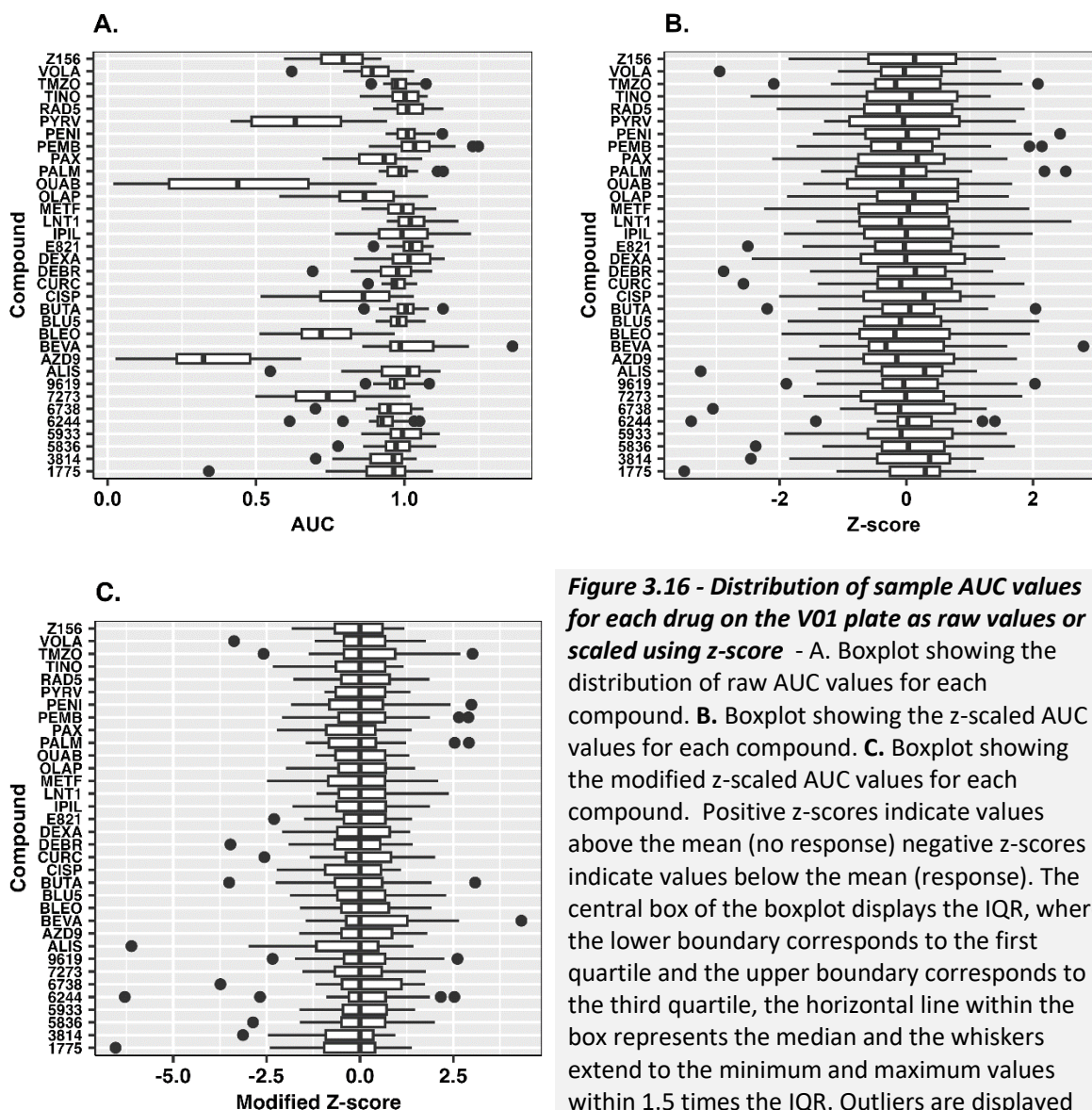
Figure 3.16 - Distribution of sample AUC values for each drug on the V01 plate as raw values or scaled using z-score - A. Boxplot showing the distribution of raw AUC values for each compound. **B.** Boxplot showing the z-scaled AUC values for each compound. **C.** Boxplot showing the modified z-scaled AUC values for each compound. Positive z-scores indicate values above the mean (no response) negative z-scores indicate values below the mean (response). The central box of the boxplot displays the IQR, where the lower boundary corresponds to the first quartile and the upper boundary corresponds to the third quartile, the horizontal line within the box represents the median and the whiskers extend to the minimum and maximum values within 1.5 times the IQR. Outliers are displayed by data points outside the whiskers.

The z-score normalised AUC data from V01 drug plates was calculated and plotted as a heatmap shown (figure 3.17). By normalising the data, it is much easier to distinguish between responders and non-responders for each drug, also clustering of more resistant (left hand side) and more sensitive (right hand side) samples can be useful.
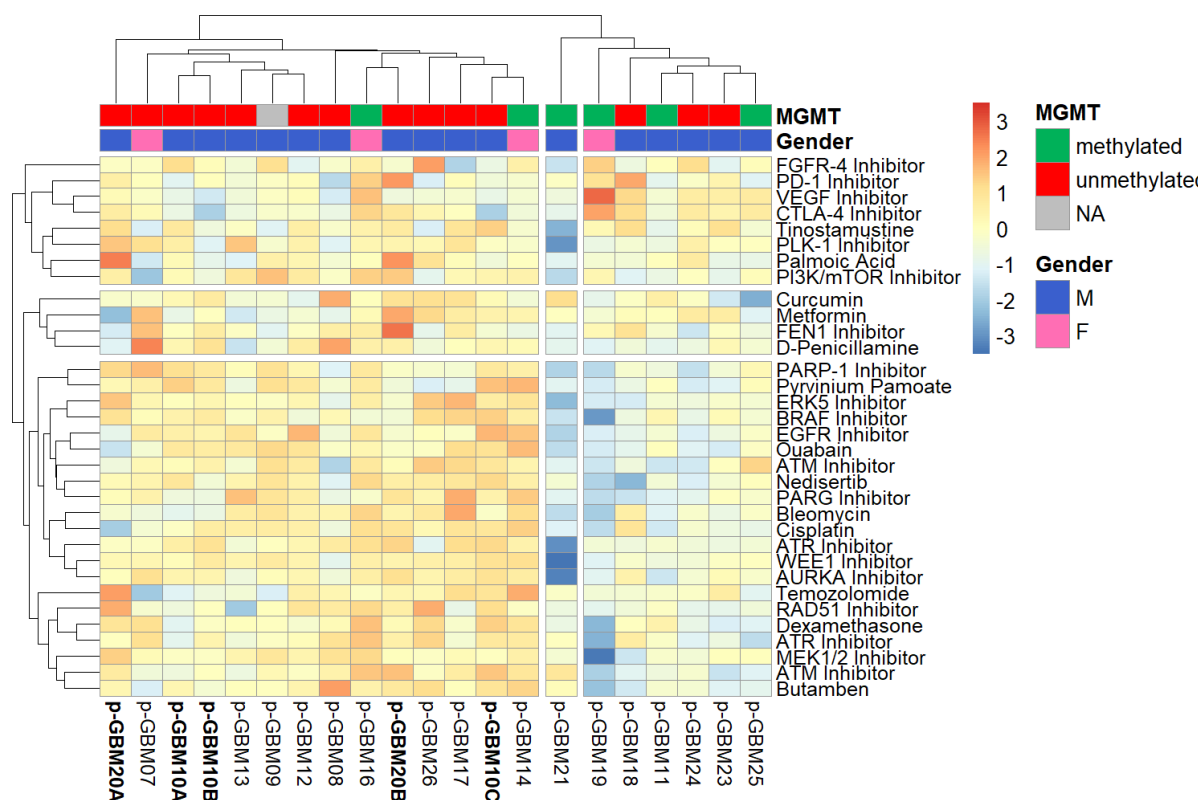
Figure 3.17 - GBM sample heatmap depicting z-scaled AUC drug response for primary GBMs dissociated from 18 individual tumours - Scale shown represents cell death as -3 (blue) and cell survival as 3 (red). Larger samples such as GBM10 (A, B and C) and GBM20 (A and B; indicated in bold) were sectioned into multiple regions and screened independently in order to highlight the intertumoral heterogeneity of the disease. AUC values were calculated from 2 technical replicates following 96hr drug incubations using R package GR metrics and the heatmap was constructed using R package pheatmap as detailed in the methods section. Note, due to the fact that this was performed on limited fresh clinical material, biological repeats were not performed. Hierarchical clustering is explained in the text below.

Out of the 32 drugs on the plate, figure 3.16A highlighted the majority of AUC values residing around 1, highlighting no response. Therefore, to distinguish between active and redundant compounds we investigated the AUC values in more detail. We first performed a Shapiro Wilk test for normality which revealed that the dataset was not normally distributed with a median IQR AUC of 0.961 (0.871-1.01; figure 3.18). Any compounds which had a mean/median AUC greater than 0.961 were deemed as inactive and were subsequently removed from drug hit and phenotype analysis, as shown in table 3.2 highlighted in red. The 13 active compounds were then plotted as a heatmap, shown below in figure 3.19.

131

Table 3.2 - Determining active drugs based on the thresholds generated by mapping AUC distributions for all 18 glioblastoma samples screened.

Compound	Normal Distribution?	Mean/Median	Activity
AZD9291	YES	0.3493	Active
Ouabain	YES	0.4577	Active
Pyrvinium Palmoate	YES	0.6401	Active
Bleomycin	YES	0.7397	Active
PDD00017273	YES	0.7428	Active
AZD0156	YES	0.7800	Active
Cisplatin	YES	0.8193	Active
Olaparib	YES	0.8475	Active
Volasertib	YES	0.8938	Active
Paxalisib	YES	0.9156	Active
AZD6244	NO	0.9250	Active
M3814	YES	0.9280	Active
AZD6738	NO	0.9479	Active
Dabrafenib	YES	0.9629	Inactive
AZD1775	NO	0.9635	Inactive
AX15836	YES	0.9687	Inactive
TH9619	YES	0.9723	Inactive
Curcumin	YES	0.9736	Inactive
Temozolomide	YES	0.9803	Inactive
BLU-554	YES	0.9827	Inactive
Palmoic Acid	NO	0.9850	Inactive
Metformin	YES	0.9904	Inactive
Ipilimumab	YES	0.9916	Inactive
Tinostamustine	YES	0.9976	Inactive
KU55933	YES	0.9994	Inactive
Butamben	YES	1.0018	Inactive
D-Penicillamine	YES	1.0086	Inactive
Alisertib	NO	1.0131	Inactive
Dexamethasone	YES	1.0161	Inactive
RAD51	YES	1.0178	Inactive
VE-821	YES	1.0233	Inactive
Bevacizumab	YES	1.0247	Inactive
LNT1	YES	1.0254	Inactive
Pembrolizumab	YES	1.0444	Inactive
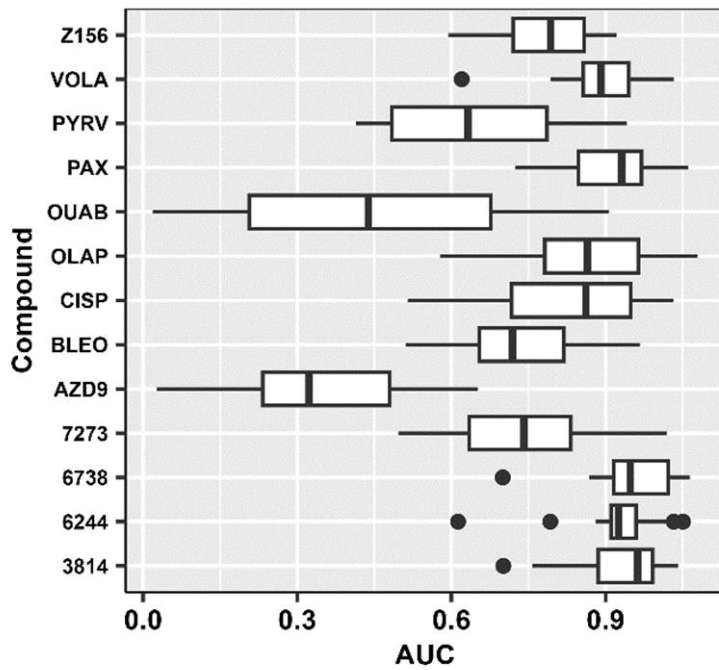
Figure 3.18 - Active compound AUC boxplot - Active compounds were selected for based on their mean/median AUC, if it was below the median IQR of 0.961 compounds were deemed as active. The central box of the boxplot displays the IQR, where the lower boundary corresponds to the first quartile and the upper boundary corresponds to the third quartile, the horizontal line within the box represents the median and the whiskers extend to the minimum and maximum values within 1.5 times the IQR.

B.
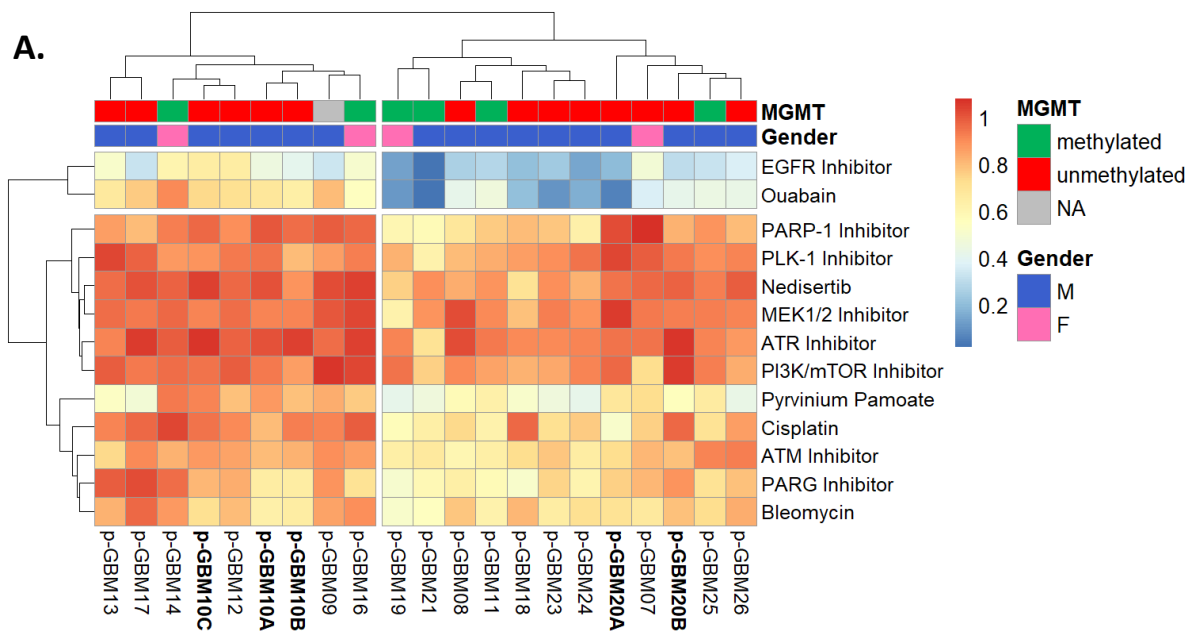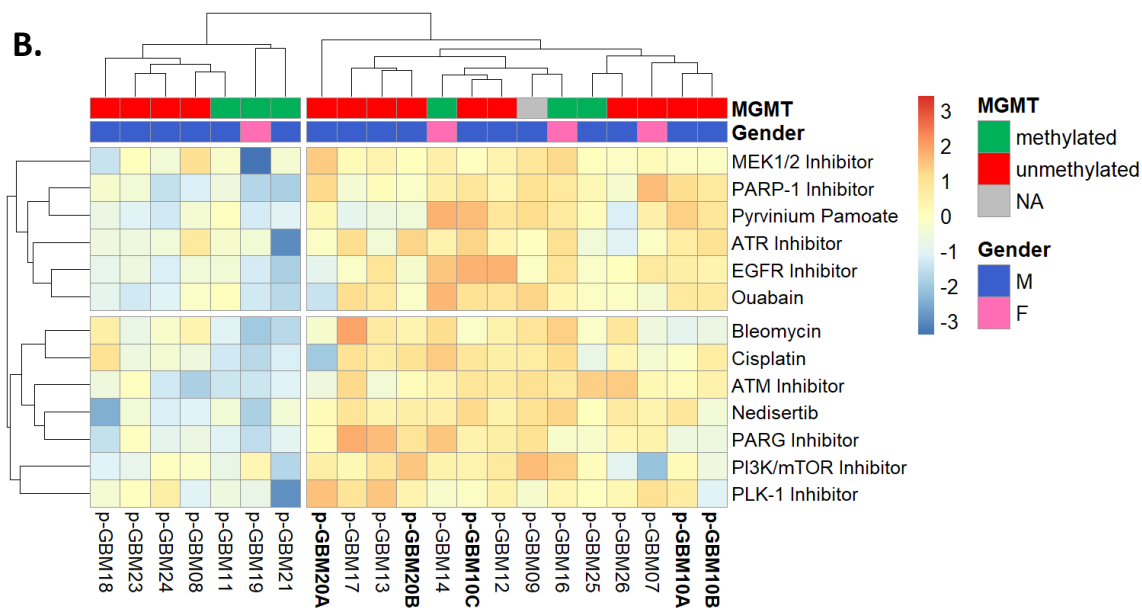
Figure 3.19 - GBM sample heatmap depicting raw AUC values (A) and z-scaled AUC (B) obtained from active drugs in ex vivo screens of primary GBMs dissociated from 18 individual tumours - Scale shown represents cell death as -3 (blue) and cell survival as 3 (red). Larger samples such as GBM10 (A, B and C) and GBM20 (A and B; indicated in bold) were sectioned into multiple regions and screened independently in order to highlight the intertumoral heterogeneity of the disease. AUC values were calculated from 2 technical replicates following 96hr drug incubations using R package GR metrics and the heatmap was constructed using R package pheatmap as detailed in the methods section. Note, due to the fact that this was performed on limited fresh clinical material, biological repeats were not possible. Hierarchical clustering is explained in the text below.

We then plotted the positive drug responses for each sample using raw mean and median AUC values (based on results of a normality test) or using calculated z-scores, data shown in figure 3.20. Using the raw AUC values, a median threshold value of 5 was calculated and set as threshold for sensitive (green) and resistant (red) tumour samples, giving a total of 12 sensitive tumours and 9 resistant. Whilst for the z-score standardised data, the median number of drug responses was 6, resulting in 11 sensitive and 10 resistant tumours. The two approaches do lead to similar results, apart from whether GBM07 is classed as either a resistant or sensitive sample.
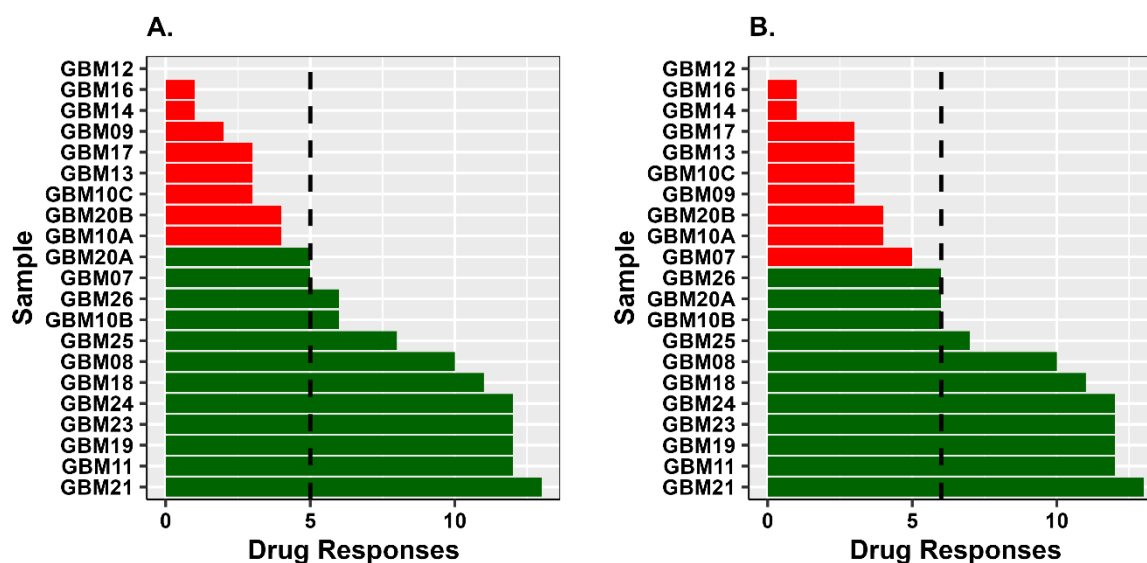
Figure 3.20 - Segregating multi hit sensitive (green) and resistant (red) tumors based on their active drug responses - **A**: Segragating based on mean/median AUC of single data value relative to group AUC. **B:** Segragating following z-score normalisation (formula = (x-mean)/standard deviation, where x = the single data value.

3.4.3 Measuring assay quality using z-prime

The typical HTS process involves a primary screen to identify potential hits, followed by a secondary screen to further confirm the initial findings (Malo *et al.*, 2006). However, the use of freshly dissociated tissue hinders our ability to obtain biological replicates and perform secondary screens. We therefore need to be confident that our HTS assay can detect real reproducible drug hits. One way to do so is to investigate the technical replicates on each individual drug plate, low SD and COV would indicate that the measurements are consistent and reproducible.

A more comprehensive way to determine the robustness of our HTS drug plates is through calculation of a z-prime number. This was deemed a desirable quality control measure as it quantifies the separation between controls, which we have used throughout to calculate percentage inhibition (Mpindi *et al.*, 2015). Z-prime was calculated for each sample drug plate using the mean and SD values of positive control (staurosporine) and negative control (DMSO) (the equation used is shown below). The raw data used to calculate the z-prime values are depicted by table 3.3, for long term primary cell line cultures and table 3.4 for freshly dissociated patient samples. A z-prime value greater than 0.5 reflects good robustness and reproducibility, values between 0-0.5 shows a marginal but acceptable assay, whilst a score

135

less than 0 is poor and is unable to distinguish between positive and negative controls (Bray, Carpenter and Imaging Platform, 2017).

$$Z - prime = 1 - \frac{3(SD \text{ of } DMSO \text{ control values} * SD \text{ of } staurosporine \text{ values})}{Mean \text{ of } DMSO \text{ values} - mean \text{ of } staurosprine \text{ values}}$$

Equation 3.1 - Calculation of z-prime - Where SD represents standard deviation calculated as the square root of variance relative to the mean

Z-prime calculations rely on the mean and SD of positive and negative controls, which statistically assumes that these both follow a normal distribution. Skewed data and outliers in the data can disrupt this assumption giving misleading Z-prime values. For each sample and cell line which was screened using V01 GBM drug plates we calculated the z-prime value, which are plotted below in figure 3.21. When investigating the mean DMSO and staurosporine counts for samples with Z-prime values <0, they have complete overlap between the controls, partly due to higher staurosporine counts and reduced DMSO counts, both with large SD. Therefore, samples drug responses with z-prime values <0 should not be used and were therefore removed from any further analysis.
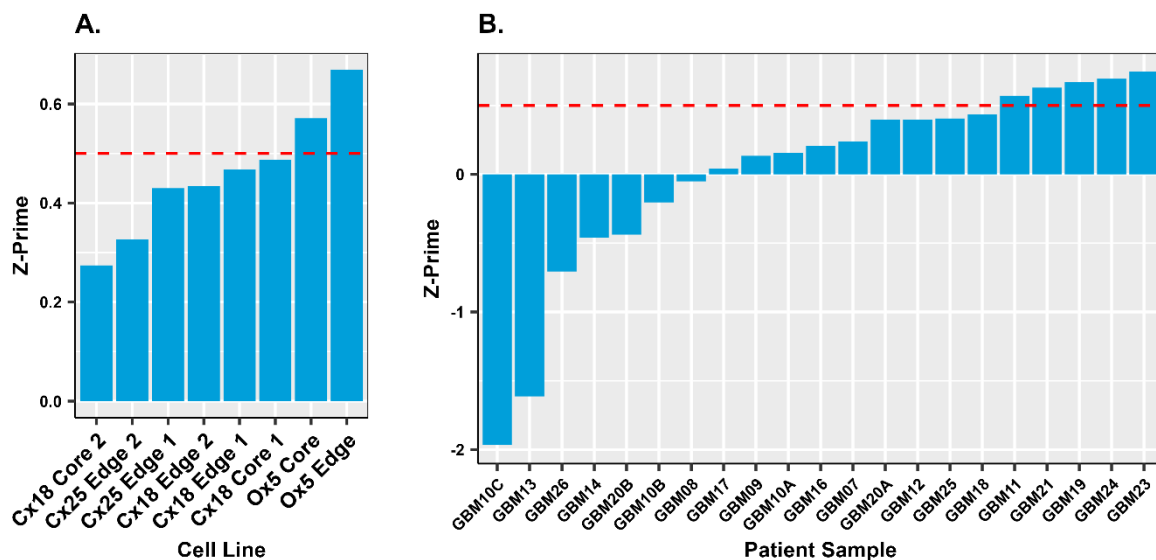
Figure 3.21 – Comparison of Z-prime scores for samples screened using GBM V01 drug plates - A: Long term primary cell line cultures. Cells were plated at a density of 1000 cells per well for 96 hours. **B:** Freshly dissociated patient samples. All seeded at 5000 cells per well. The red dashed line indicates a z-prime value of 0.5 which traditionally is used as a cut off value for assay quality.

Table 3.3 – Control means and SD values used for calculation of z-prime scores for long term primary cell line cultures screened using GBM V01 plates

Cell Line	Mean DMSO	DMSO SD	Mean STAU	STAU SD
Cx18 Core 2	879	193	18	15
Cx25 Edge 2	429	88	8	6
Cx25 Edge 1	615	112	9	3
Cx18 Edge 2	757	140	7	1
Cx18 Edge 1	733	128	5	2
Cx18 Core 1	2247	367	24	13
Ox5 Core	3386	408	193	49
Ox5 Edge	2185	215	100	15

Table 3.4 – Control means and SD values used for calculation of z-prime scores for freshly dissociated patient samples screened using GBM V01 plates

Patient Sample	Mean DMSO	DMSO SD	Mean STAU	STAU SD
GBM10C	667	66	495	103
GBM13	609	64	467	59
GBM26	573	87	258	91
GBM14	820	99	537	38
GBM20B	395	93	126	35
GBM10B	247	34	136	9
GBM08	176	32	64	7
GBM17	407	56	202	8
GBM09	830	59	338	82
GBM10A	219	21	122	5
GBM16	943	123	322	41
GBM07	235	31	61	12
GBM20A	344	50	36	11
GBM12	1624	88	885	59
GBM25	372	30	103	23
GBM18	529	76	69	10
GBM11	1353	75	421	57
GBM21	1383	164	4	5
GBM19	362	32	25	5
GBM24	681	46	100	12
GBM23	961	59	78	15

3.4.4 Comparing freshly derived and established GSC drug responses

To investigate the differences in drug responses between patient derived samples and primary cell lines a direct comparison was performed. The drug responses of two patient samples (GBM21 and GBM25) were compared with their matched cultured primary stem-like cells order to evaluate whether drug sensitivities are maintained. The heatmap shown in figure 3.22 highlights cell cycle inhibiting drugs such as Wee1i and AURKAi showing increased effects on both of the low passage cells in comparison to the freshly dissociated tissue. One cause of the increased sensitivities shown in the cultured cells may be because these cells have been in culture for several weeks post-surgical resection and are therefore stable and dividing, making them more susceptible to cell cycle inhibiting drugs. Whereas the dissociated patient tissue cells may be in a slow dividing, quiescent state due to having undergone significant stress including complete change of environment, dissociation into a single cell suspension and then drugging in a duration of 3-6 hours.

Another possible explanation for differential drug responses between the primary sample and matched primary cultures could be the selectivity process of culturing on plasticware with the supplementation of stem cell media and growth factors. The surviving cells within the culture might exhibit heightened sensitivity to specific drugs. Additionally, it was observed that both GBM21 and GBM25 cultured cells became increasingly sensitive to both bleomycin and cisplatin treatment compared to freshly dissociated tissue. This heightened susceptibility could be attributed, in part, to elevated levels of cell division, rendering them more susceptible to DNA-damaging agents. Notably, the primary cells from GBM25 became more sensitized to EGFR inhibitor Osimertinib. While this may be linked to culturing with the growth factor EGF, the validity of this assumption is uncertain, especially considering that this trend was not observed in the responses of GBM21.
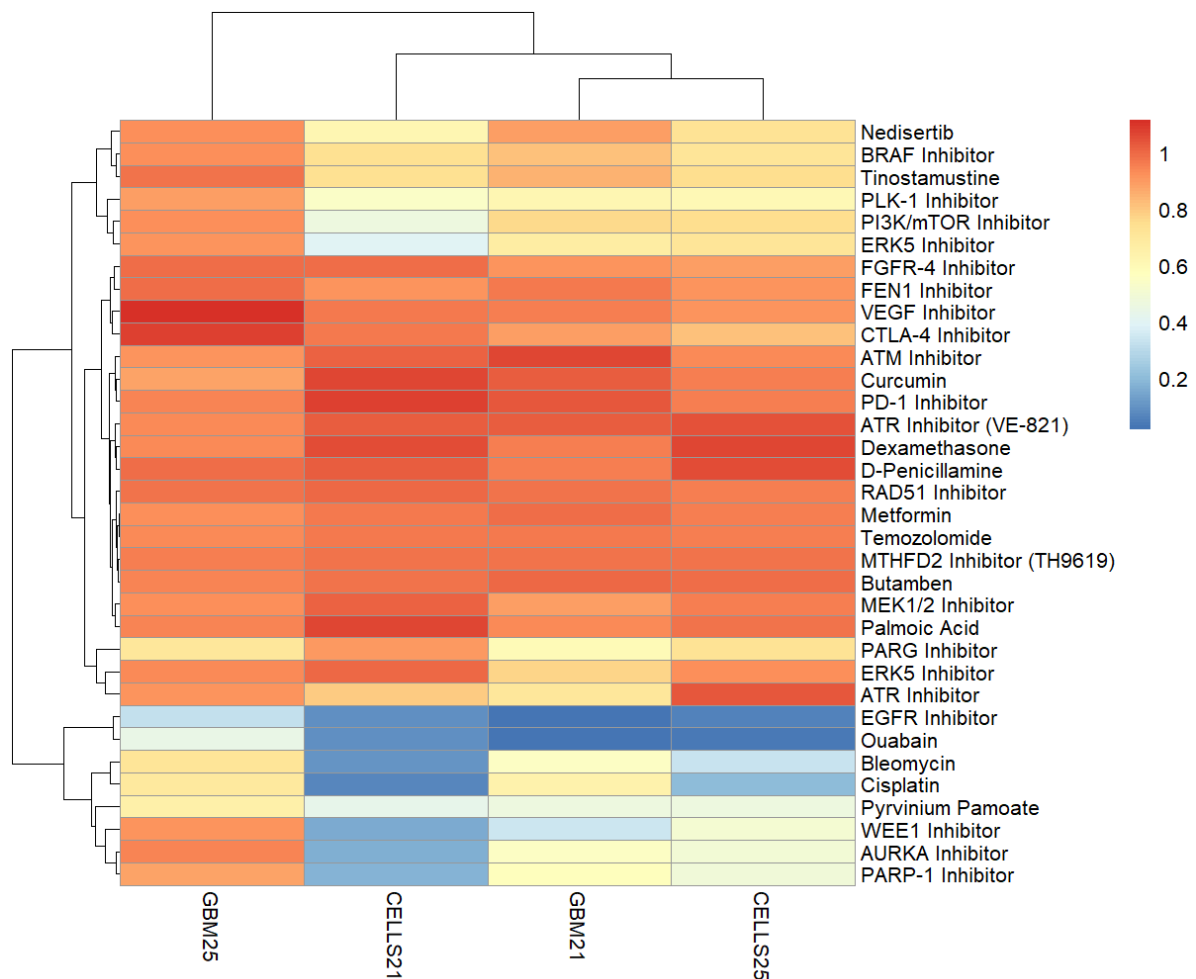
Figure 3.22 - Comparing the AUC responses of the freshly dissociated sample and corresponding primary cell lines for GBM21 and GBM25 - The scale shows blue as cell death and red is no response. AUC values were generated from GR metrics package in R, pheatmap package was used to generate the heatmap.

Aphidicolin is a DNA polymerase inhibitor that is often used as a negative control for cytostatic drugs, but also can be used to estimate the growth rates of samples, when compared to positive DMSO control wells. For patient samples GBM21 and GBM25 and their matched primary cell lines we proceeded to compare the cell counts obtained from both the DMSO and aphidicolin control wells, as depicted in figure 3.23. For sample GBM21, both the fresh tumour cells and the primary culture cells exhibited notable differences in the cell counts between the two controls. This suggests that both the cells screened from the original sample and primary culture demonstrated growth over the 4-day assay period. Conversely, in the case of sample GBM25, there was no significant difference observed between the cell counts for the two controls. However, there was a slightly significant difference between the cell counts between the controls for the matched primary cells.
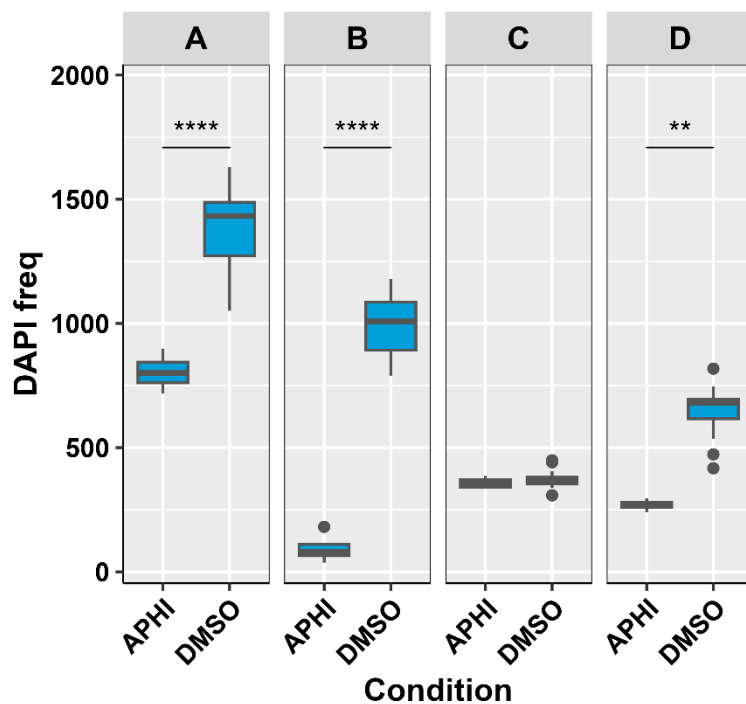
Figure 3.23 - Comparison of the DAPI cell counts within the DMSO and Aphidicolin wells for samples GBM21 and GBM25 and their respective primary cell lines - A. GBM21 primary sample, B. GBM21 cell line, C. GBM25 primary sample, D. GBM25 cell line. Unpaired t-test was performed on normally distributed data and Mann Whitney U test was performed on non-normally distributed data. Normality testing was performed using Shapiro wilks. Each sample drug plate contained 4 aphidicolin repeats and 24 DMSO repeats. **ns: p > 0.05, *: p <= 0.05, **: p <= 0.01, ***: p <= 0.001, ****: p <= 0.0001.**

Upon comparing the DAPI cell counts from DMSO and Aphidicolin treatments for the entire cohort of patient samples using the V01 drug plates, 60% (13/21) samples showed no significant differences as depicted by figure 3.24. This demonstrates that most samples are not exhibiting significant growth over the 4-day period. However, among the samples, 8 did show a significant difference in the counts between DMSO and Aphidicolin control wells. The most significant being GBM21, GBM11 and GBM19. Interestingly GBM21 and GBM19 clustered together within the figure 3.17 & 3.19 heatmap and showed increasing sensitivity to the drug library.
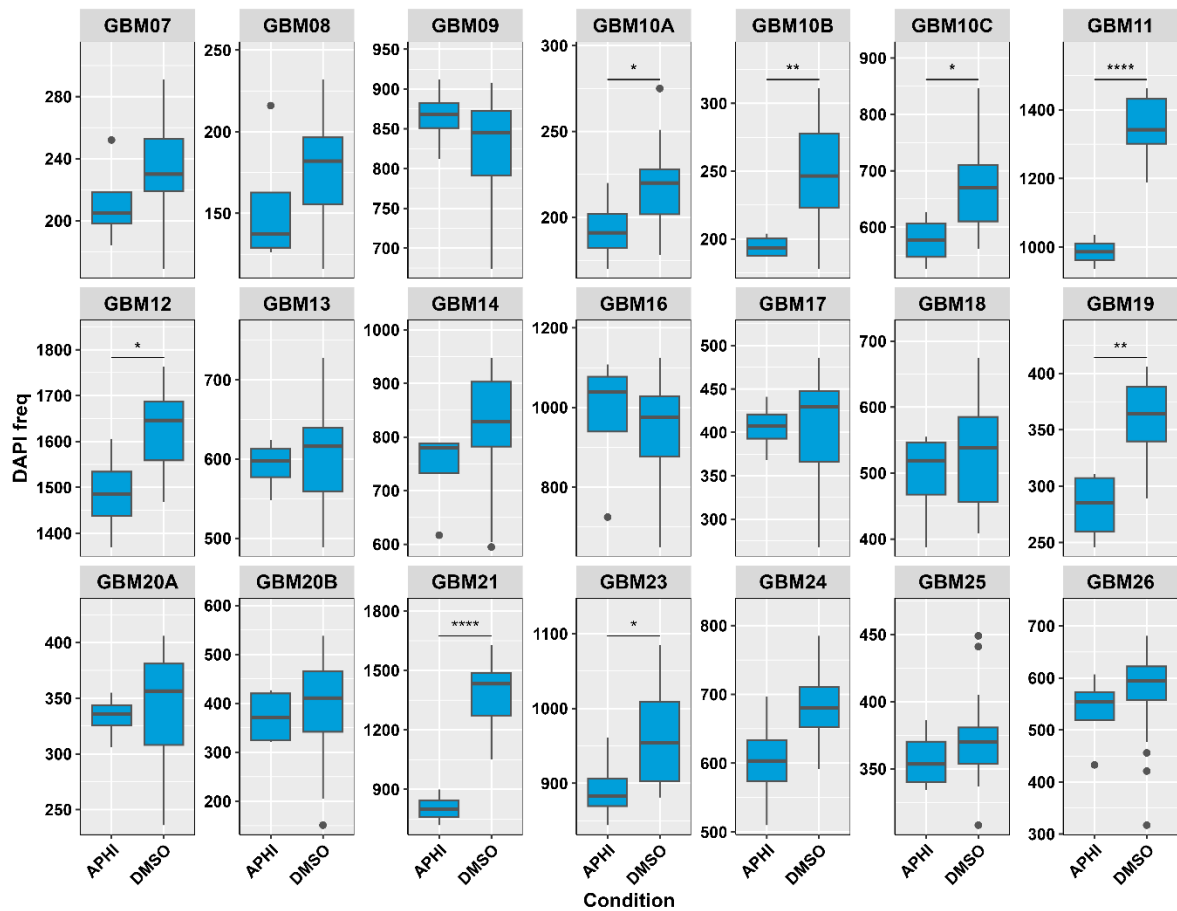
Figure 3.24 - Comparison of the DAPI cell counts within DMSO and Aphidicolin wells for each *sample -* Aphidicolin is a cell cycle inhibiting drug, therefore the relationship between the counts of these control wells can be used to estimate whether the sample cells are actively dividing within this 4-day incubation period. The central box of the boxplot displays the IQR, where the lower boundary corresponds to the first quartile and the upper boundary corresponds to the third quartile, the horizontal line within the box represents the median and the whiskers extend to the minimum and maximum values within 1.5 times the IQR. Unpaired t-test was performed on normally distributed data and Mann Whitney U test was performed on non-normally distributed data. Normality testing was performed using Shapiro wilks. Each sample drug plate contained 4 aphidicolin repeats and 24 DMSO repeats.

3.4 Summary points

- DMSO concentrations used on these drug plates had no significant effects on the DAPI cell counts of established LN18 cells relative to media controls.

- Investigating the optimal seeding densities to show similar drug responses – within cells a range of 500 – 2000 was suitable for obtaining similar end point results. Within primary patient samples 10k, 15k, 20k were all suitable at obtaining high correlation and therefore similar dose responses.

- Evaporation effects can cause high COV across drug plates control wells. Breathable membranes were adopted to reduce this COV.

- Humidifier chambers were also able to reduce COV within DMSO control wells.

- Variation in results were seen when using different cell seeding equipment, highlighting the importance of using properly calibrated equipment. Moving forward, hand-held electronic pipettes were used for seeding drug plates with cells to reduce variability.

- It was hypothesised that fixing and staining steps could be washing away non-adherent cells, however the high correlation between drug responses and analysis of images revealed centrifugation of drug plates caused retaining of cell debris and dead cells, which would hinder quality of future IF imaging, therefore this centrifugation approach was not adopted.

- Investigated drug, cells and Matrigel plating order to confirm seeding drug underneath Matrigel still maintained drug efficacy.

- Shortages in Matrigel due to COVID-19 and Brexit led to replacement with the alternative BME reagent Cultrex. This extract showed identical drug response profiles when compared to Matrigel, but showed improved cell count numbers, suggesting that it was better at maintaining primary GSC populations ex vivo.

- Analysis of image capture revealed that suitable tile strategy of microscopy is dependent on sample quality. Samples with lower cell count require higher imaging strategy to capture more percent of well area.

- Initial V01 drug plate analysis of 18 samples revealed that despite requiring further drug concentration optimisation this tool was able to highlight tumoral heterogeneity based on differential responses of multiple region samples. This

heatmap also highlighted the issues with SoC drug TMZ which were circumvented in chapter 5.

- Primary and matched long-term GSC cultures dose responses were compared. The long-term cultured cells showed increasing sensitivities to the drug library, this would be expected partly due to their higher rates of cell division due to selection pressures of long-term ex vivo culture and highlights the need to screen tumour samples rapidly following surgical resection in order not to introduce any growth selection bias.

3.5 Discussion

As DMSO is the primary solvent used within this study to dissolve our drug compounds we initially performed a titration assay to investigate its individual effect on glioblastoma cells. This data highlighted none of the concentrations of DMSO tested displayed toxicity to LN18 cells, however an increase in cell numbers was measured in wells containing 0.1-1% solvent. Several studies have reported DMSO to effect multiple cellular functions such as inflammation, lipid metabolism, apoptosis, cell cycle, protein expression, differentiation, molecule binding, enzyme activity, reactive oxygen species scavenging, cell polarisation, radioprotection and autophagy (Tunçer *et al.*, 2018). Previous work by Tunçer and colleagues showed that low doses of DMSO (0.1-1.5%) can cause alterations in the membrane lipids of epithelial cells, some of which may be responsible for the cells ability to adhere to plasticware (Tunçer *et al.*, 2018), which may be one possible explanation of the higher cell counts in the higher % DMSO wells. Previous work by others has also reported cell viability increasing above controls in low doses of DMSO (< 0.5%), with antioxidative properties reducing cellular reactive oxygen species (ROS) levels, however high DMSO exposure (3.7%) enhanced apoptosis, accelerated through mitochondrial dysfunction and oxidative stress (Sangweni *et al.*, 2021).

In another study, 3D microtissues modelling cardiac and hepatic tissue were exposed to medium with and without DMSO (0.1%) for two weeks, following this the proteome, full transcriptome and whole-genome methylation was measured (Verheijen *et al.*, 2019). The results demonstrated that DMSO induces large changes in microRNAs and epigenetics

especially within the cardiac model, while its obvious high concentrations of DMSO are toxic, low doses of DMSO are commonly regarded as being inert, however this is not the case. While DMSO remains the universally used solvent in numerous research settings it is clear from this data and the literature that its influence on cellular processes remains an area requiring further investigation. Due to lack of suitable alternatives to solubilise the compounds within our initial drug plates, the use of DMSO was unavoidable and was therefore used as the primary solvent for solid drug dilutions. Fortunately, the concentration of DMSO used on the drug plates (0.05%) showed no significant differences in the cell counts compared to the control media wells.

The experiments performed within this chapter have facilitated optimisation of ex vivo screening for solid glioblastoma tissue. Following this, we have successfully highlighted how ex vivo HTS of glioblastoma cells can be used to explore individual patient responses, to highlight novel compound hits, of particular importance is our ability to highlight differential responses within multi region samples to model the heterogenous nature of glioblastoma. The total sample cohort consisted of 30 tissue specimens, 2 of which were muti region samples (GBM20A & B and GBM10A, B & C). The first 6 specimens were used for early tissue dissociation optimisation, prior to designing V01 drug plates. Of the samples screened 21/23 were successful using the V01 plates failure was due to no attachment of dissociated cells.

To measure the robustness of the assay we used a z-prime score, which calculates the difference between positive and negative controls using the means and SD. From the analysis of our primary cell lines screened (figure 3.21A) 100% showed a z-prime score above zero, whilst the freshly dissociated samples, 66% (14/21) of samples were above zero (figure 3.21B), indicating the 7 samples with a z-prime score below 0 should be removed from the analysis, as they showed no separation between controls. It is important to note that not every patient sample will be suitable for ex vivo screening, for instance some tumours are highly necrotic, and others do not grow well on plasticware, which is consistent with the literature and our findings when separately propagating adherent primary glioblastoma cell lines (Grube *et al.*, 2021).

The process of screening freshly dissociated patient tissue removes the ability to perform biological repeats, and therefore any directly comparable follow up experiments. For all patient samples the propagation of a primary cell line was attempted using any leftover cell suspension, however these do not always expand and culture successfully. When successful, we have been able to compare the drug responses between freshly dissociated patient tissue and their corresponding primary derive cell lines. From these analyses, we observe differential responses between the two matched populations despite the low passage number of primary cells. One way to circumvent this is increasing the number of technical repeats on the plate, however, this then reduces the number of drugs that can be screen within a single plate, therefore limiting the likelihood of identifying potential hits.

Upon comparison of drug responses between freshly dissociated cells and matched low passage primary cells, one cause of the increased sensitivities shown in the cultured cells may be a result of several weeks of cell culture, within growth promoting media post-surgical resection and are therefore stable and dividing, making them more susceptible to cell cycle inhibiting drugs. Whereas the dissociated patient tissue has undergone significant stress including complete change of environment, dissociation into a single cell suspension and then drugging in a duration of 3-6 hours.

Another factor contributing towards the differential drug responses between the primary sample and matched long-term GSC cultures could be the selectivity process of culturing on plasticware with the supplementation of stem cell media and growth factors. Stem cells which have survived and multiplied faster (thus making up a larger population) within culture may be more sensitive to these specific drugs. It also appeared that both GBM21 and GBM25 cultured cells became increasingly sensitive to both bleomycin and cisplatin treatment compared to freshly dissociated tissue, which again may be partly due to higher rates of cell division, making them more vulnerable to DNA damage agents. Interestingly the GBM25 primary cells became more sensitized to EGFR inhibitor Osimertinib, this may be an artifact of culturing the cells with growth factor EGF, however this assumption is unconfirmed as this trend was not seen in the GBM21 responses. Another ex vivo screening study within glioblastoma compared the transcriptome data between cultures and patient matched tissue. The results of this study revealed that cell culture samples exhibited elevated expression

levels of genes associated with cell cycle replication, including those related to G2/M, E2F, and MYC targets (Ntafoulis *et al.*, 2023). The discovery of heightened expression of cell cycle-related genes in cell lines further corroborates our drug response data, specifically the increased sensitivity to drugs like WEE1 and AURKAi.

When comparing the cell counts between the DMSO and aphidicolin controls for samples screened using V01 drug plates, we were able to estimate the extent of proliferation during the 4-day assay. The most significant differences in counts were observed in samples GBM21, GBM19 and GBM11. Interestingly when we investigate at the active compound heatmap (figure 3.19B), we observed hierarchical clustering of these specific samples within the samecluster. Suggesting the similarities in drug responses, could be attributed to increased proliferation, potentially enhancing the efficacy of specific drugs.

Whilst it is useful having this estimate of growth rate using aphidicolin and DMSO controls, it is important to note that there will be different aphidicolin sensitivities between samples based on pre-existing molecular abnormalities and therefore other more reliable markers of proliferation could be used, for instance ki-67 staining which is a stapple use within histology. This will also help us to indicate whether the assay has affected sample proliferation or if this was pre-existing of original tumour. Collectively, this data highlights the importance of ex vivo screening, using freshly dissociated tissue we can recapitulate the whole tumour cell population, which is more clinically relevant to the patient in comparison to using patient derived cell lines which have undergone weeks of selection through multiple passages on plasticware.

When culturing primary/established cell lines, it is crucial to maintain optimal conditions to promote growth. Typically, these cells exhibit much shorter doubling times, in comparison to cancer cells in vivo. This phenomenon was observed during the derivation of our tumour samples into primary cell lines. A large proportion of the samples screened using the V01 drug plates displayed poor Z-prime values, indicating inadequate separation between controls and minimal or no growth. Without sufficient cell growth, many drugs within the library will appear inactive. For instance, SoC drug TMZ relies on futile cycling of MMR to exhibit DNA damage. One approach to circumvent this issue is the addition of an 8-day assay to

complement the 4-day, not only will this allow more time for cells to divide but will also act as an additional biological repeat, enhancing the reliability of results.

Matrigel/Cultrex are BME's derived from Engelbreth-Holm-Swarm mouse sarcoma, they have been a popular choice over the last 40 years for a multitude of cell culture purposes. However, due to their animal derived nature they have a poorly defined composition, with large batch-to-batch variability (Aisenbrey and Murphy, 2020), additionally, specific pathways may be influenced by unknown cell signalling factors present in the matrix, and may disrupt stem cell phenotype and drug screening responses (Koutsopoulos and Zhang, 2013). For the initial optimisation steps, it was believed that the ease of use, availability and lower cost associated with animal derived ECM outweighed the benefits of optimising a synthetic ECM. Therefore, for the purposes of this project, following Matrigel shortages it was ensured that a single batch of Cultrex was purchased that would last the entire duration in order to maintain reproducibility. Moving forward with this project, a synthetic BME alternative would be desirable (costs permitting). This will allow for highly reproducible, more clinically relevant tuneable synthetic scaffolds, which display similar peptide sequences derived from brain ECM. Hydrogel scaffolds have been shown to improve cell survival and differentiation properties when compared to Matrigel or collagen scaffolds (Koutsopoulos and Zhang, 2013).

Investigating the IQR of the AUC values for each drug revealed most of the compounds upon the V01 plate were not within the correct IC_{50} range to see a response, or alternatively the samples screened did not contain the relevant mutations for targeted therapy response. We therefore investigated the IC_{50} values of primary cell line cultures following long-range dose response to advise for the second batch of drug plates. At the initial stages of development, the IC_{50} values were not essential, we were mainly focused on the proof-of-concept that ex vivo screening was possible using freshly dissociated glioma tumour tissue. The IC_{50} data obtained from these long range dose response curves depicted within supplementary chapter 8 figure 8.1, were essential for the design of the updated V02 drug screening plates.

Chapter 4 – Molecular Analysis of Ex Vivo Data

4.1 Introduction

To further corroborate our ex vivo drug screening findings and gain insights into the differential drug responses, molecular analysis was carried out where matched primary cell lines were available. For instance, our V01 drug screen highlighted differential responses against PAR glycohydrolase (PARG) inhibitor for our multi-region Cx18 sample cells. To further investigate we performed immunoblotting of the key proteins involved with PARP-1 mediated repair. Additionally, we explored the sensitivity of GBM21 to WEE1 inhibition by examining key G2/M checkpoint proteins and through cell cycle analysis using FACS. Finally, we aimed to understand the underlying differential response to ouabain of Cx18 STEM and BULK cultures, through investigation of key DDR protein expression within these populations.

4.2 Cx18 Heterogeneity PARGi Sensitivity

Multimodal therapies are often used to overcome therapy resistance or induce synthetic lethality. One promising target to potentiate the cytotoxicity of drugs is the use of inhibitors which target DNA damage repair pathway enzymes such as PARP and PARG. PARP is a critical enzyme involved in the regulation of several DNA repair pathways, including BER SSB repair, and DSB repair. Both PARP-1 and PARG are attractive drug targets as both are shown to be upregulated in most glioblastoma cell lines compared to healthy astrocytes (Braidy *et al.*, 2019). PARP inhibitors have been approved for the treatment of BRCA1/2 mutated ovarian and breast cancers, working via synthetic lethality. Due to BRCA1/2 mutations, these cancer cells exhibit defective HR repair, and subsequent inhibition of PARP activity causes an induction of collapsed replication forks due to defective HRR leading to efficient killing of tumour cells (Bryant *et al.*, 2005; Farmer *et al.*, 2005).
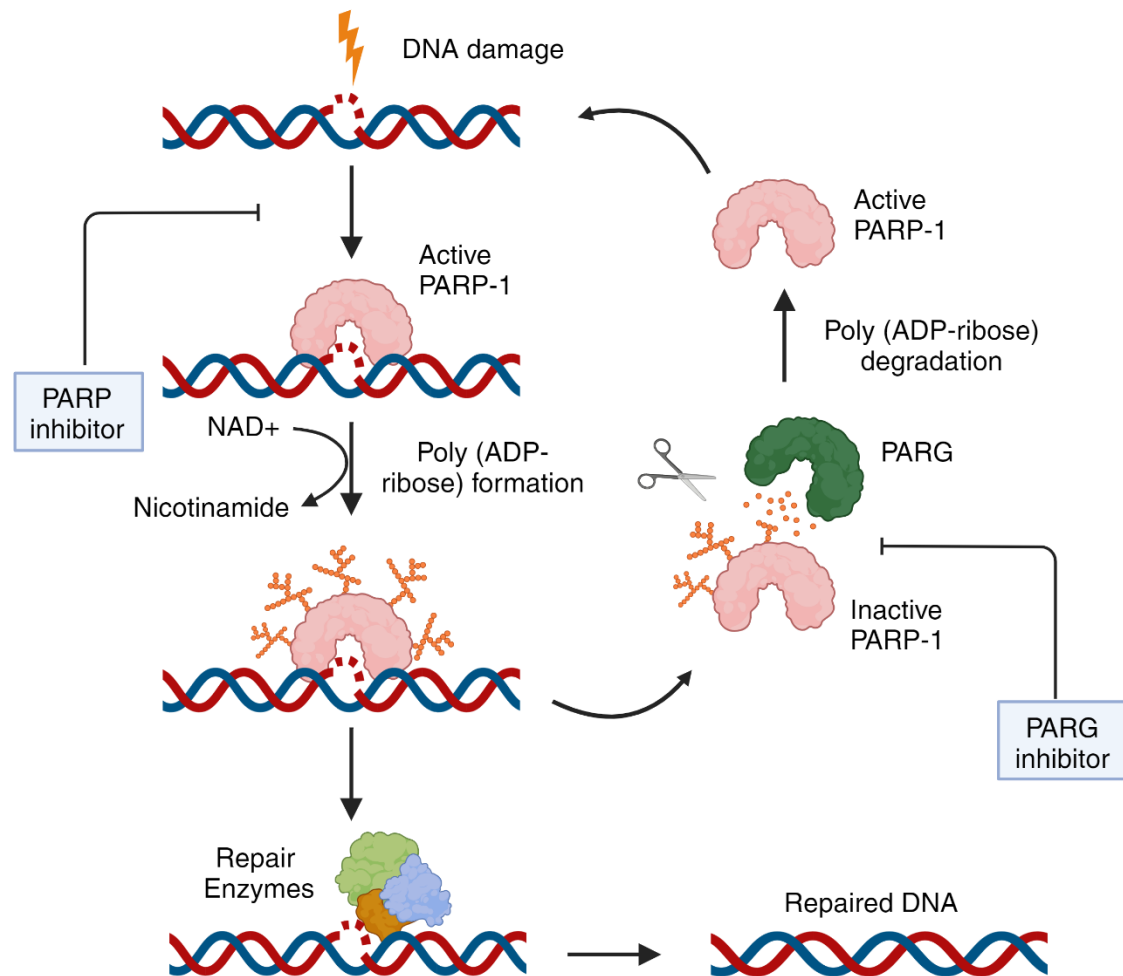
Figure 4.1 – Overview of PARP mediated DNA repair - Following DNA damage, PARP-1 is recruited to the strand break, here it utilises NAD+ as a substrate to catalyse the transfer of ADP-ribose onto itself and other target proteins. Nicotinamide is cleaved off during this reaction. This permits the localisation and activity of essential DNA repair enzymes. To reactivate PARP-1, PARG activity is essential for PAR chain catabolism. Figure created using Biorender (https://biorender.com/).

PARP mediated DNA repair is summarised in figure 4.1. Mechanistically, upon DNA damage PARP-1 is recruited to the strand break where it induces the synthesis of PAR subunits, PARP-1 is the main target of this PARylation, it is essential for its activation and recruitment of other downstream repair factors. PARylation is completely reversible through the degradation activity of PARG de-ribosylation allows PARP-1 to be recycled at additional sites of DNA damage (Fathers *et al.*, 2012; Pascal and Ellenberger, 2015). Cellular cofactor NAD+ plays a crucial role in PARP-1 mediated DNA repair pathways. PARP-1 enzymes require NAD+ as a substrate to add ADP-ribose to target proteins, these PAR chains are essential for the recruitment of essential DNA repair factors (Wilk *et al.*, 2020). Following severe DNA damage, PARP-1 overactivation can lead to depletion of cellular NAD+, cells can overconsume ATP in

efforts to restore NAD+ however this often leads to energy crisis and has shown to lead to necrotic cell death off the cell (Braidy *et al.*, 2019). The regulation of PARP-1 is critical for maintaining cellular homeostasis and preventing excessive DNA damage. A recent report by Li *et al.*, (2022) showed increasing cellular NAD+ through addition of precursor dihydronicotinamide riboside (NRH) strongly increased the toxicity of TMZ and PARGi combination treatment. They summarised that TMZ treatment induces the activation of PARP, and therefore the synthesis of PAR chains. Subsequently, the administration of NHR increases cellular NAD+ which further enhances PARP activity and PAR chain formation. Bulky PAR adducts accumulate onto the site of DNA damage, but their degradation is blocked by PARGi. This obstruction causes trapping of DNA repair factors, resulting in the accumulation of unrepaired DNA damage. inconsequently, there is an upsurge in cell death signalling, marked through increased levels of cleaved caspase 3 and suppression of survival signalling evidenced by reduced p-AKT signalling (Li *et al.*, 2022).

Interestingly PARGi have been shown to exhibit single agent activity in a number of different GBM primary cell lines, showing robust radiosensitizing activity (Jackson, Gomez-Roman and Chalmers, 2019) and similar to PARPi, PARGi have also shown to potentiate TMZ treatment (Murai *et al.*, 2014; Gogola *et al.*, 2018). It is hypothesized that PARGi single agent therapeutic ability is a result of existing HR repair deficiencies, thus PARGi treatment results in accumulation of collapsed replication forks, without the proper HR repair machinery (BRCA deficiencies) this damage is synthetically lethal (Fathers *et al.*, 2012).

4.2.1 The effect of PARG inhibition on GSCs

As described in Chapter 3, initial drug plate optimisation was carried out using low passage primary glioblastoma cell line models, to investigate whether our ex vivo screening plates could detect tumour heterogeneity displayed through differential drug response profiles. Patient sample Cx18 was sub sectioned into multiple CORE/EDGE regions to generate Cx18 heterogeneity cell line model, (total of 4 cell lines x2 CORE x2 EDGE) each of which was processed using ex vivo. The complete dose response profiles for drug plate V01 are shown in figure 4.2, and the associated AUC heat map in figure 4.3.
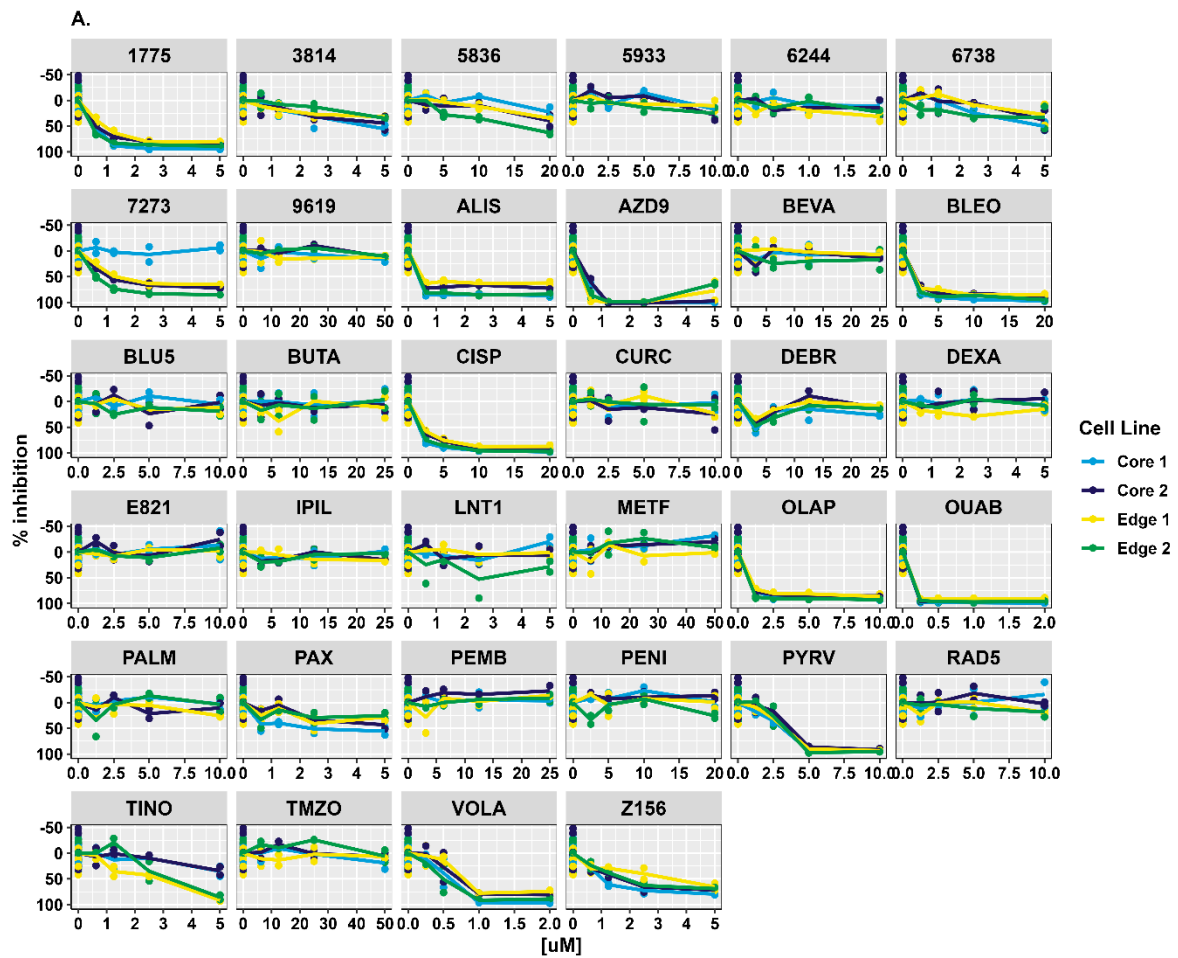
Figure 4.2 - Percentage growth inhibition drug response profiles to V01 drug plates for the 4 Cx18 primary GSC cell lines derived from multi region sampling - DAPI counts were collected using automated IF microscopy, the counts were normalized using positive and negative controls on each dose plate to provide the response measure (relative inhibition %). Each colour line is representative of individual CORE or EDGE cell line. Biological repeat = 1, technical replicates = 2.

151
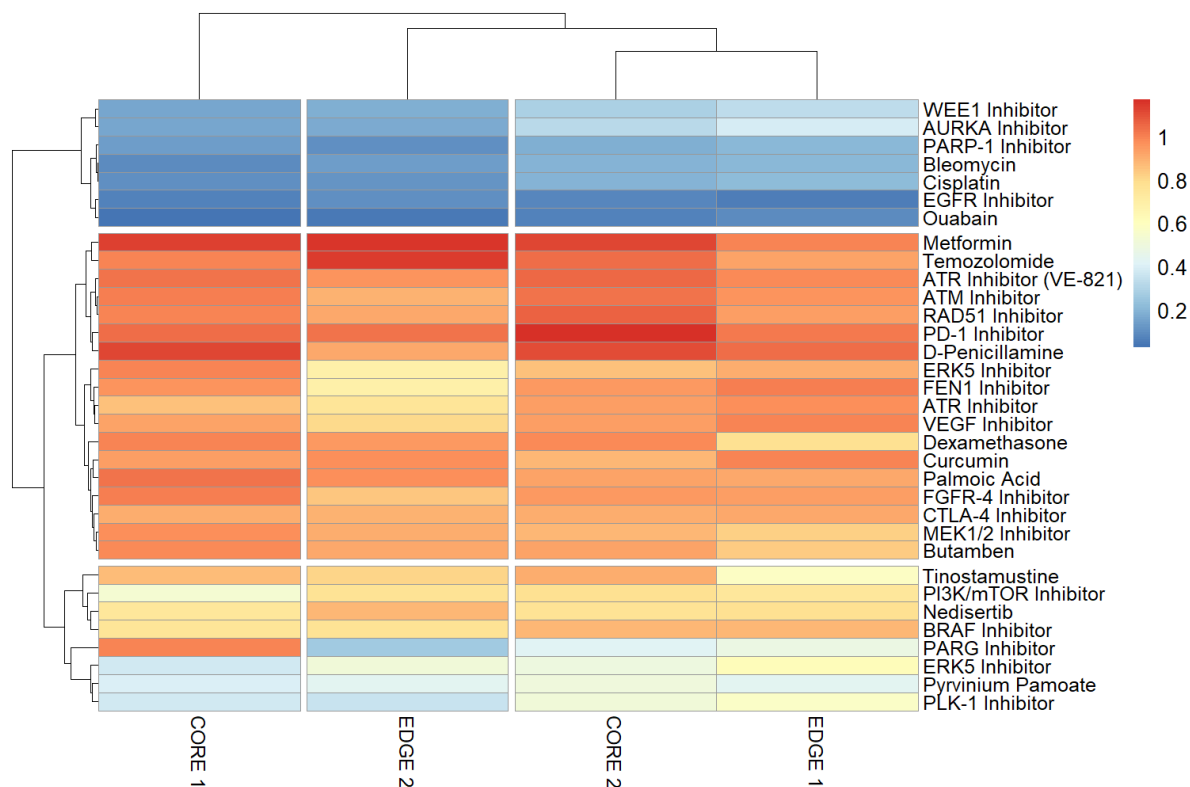
Figure 4.3 - Raw AUC heatmap for the 4 matched Cx18 primary GSCs cell lines calculated from the dose response curves (Figure 4.1) - Scale shown represents cell death as >0.1 (blue) and cell survival as >1 (red). AUC values were calculated from 2 technical replicates following 96hr drug incubations using R package GR metrics and the heatmap was constructed using R package pheatmap as detailed in the methods section. Biological repeat = 1, technical replicates = 2.

Of particular interest was the dose response curve to the PARG inhibitor denoted 7273 on figure 4.2 (and further highlighted in figure 4.4A). The Cx18 CORE 1 (blue) dose response in figure 4.2 appeared increasingly resistant to PARGi, while the other three cell lines showed increasing sensitivity to the drug, the most sensitive being the EDGE 2 cell line (the spatially furthest away from the CORE 1 sample based on dissection of the original tumour mass from core to invasive edge). To elucidate the mechanisms underlying this differential response to the PARG inhibitor, further investigation was conducted on the most sensitive and resistant cell lines (CORE1 and EDGE2).

Initially CORE 1 and EDGE 2 cells were incubated with incremental doses of PARGi for 24 hours, before being lysed and prepared for western blotting: blots were probed for PARG, a-PAR and PARP-1. As shown in figure 4.4B the levels of PARG appears lower in the EDGE 2 cells compared to the CORE 1, this itself may cause less drug required to inhibit PARG and initiate a response in the EDGE 2 cells, making them more sensitive to PARGi treatment. It also

appeared that EDGE 2 cells exhibit an induction in a-PAR in a PARGi dose dependent manner, while CORE 1 a-PAR accumulation appeared relatively consistent across the three PARGi dose points. Additionally, untreated levels of PARP-1 in the CORE 1 cells appeared slightly higher than that of the EDGE 2, which may be a factor of higher PARP-1 activity thus more efficient PARP-1 mediated repair and therefore decreased sensitivity to PARG inhibition.
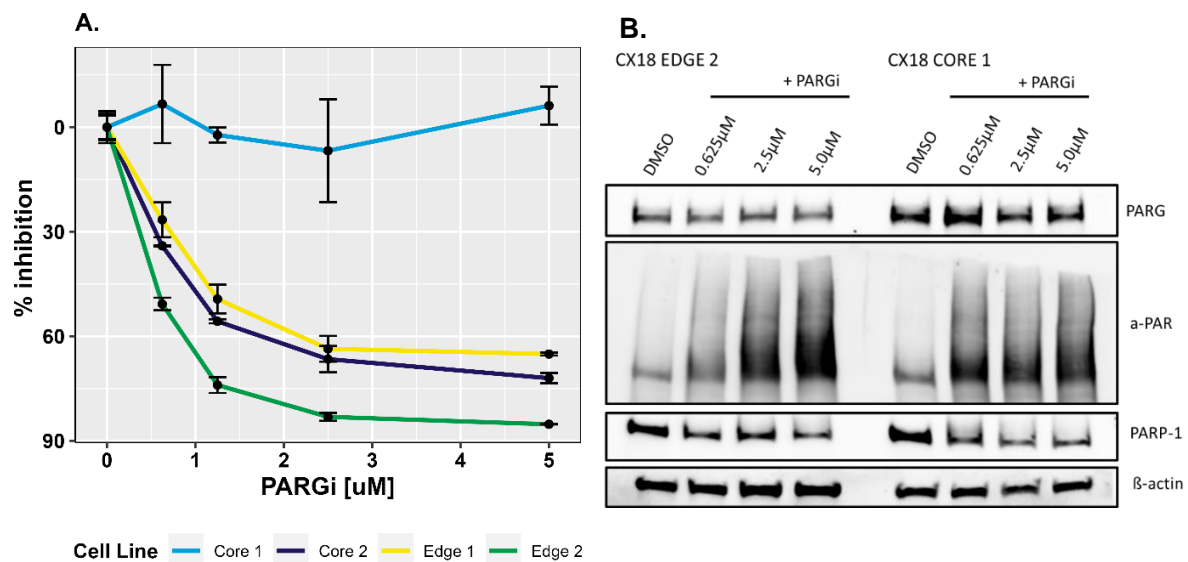
***Figure 4.4 - PARG inhibition of Cx18 cell lines - A.** Cx18 CORE 1, CORE 2, EDGE 1 and EDGE 2 differential dose PARGi % inhbition dose response. Error bars represent SEM **B.** Western blot for poly(ADP-ribose)(PAR), PARP-1, PARG and β-actin in Cx18 CORE 1 and EDGE 2 cells. PARG inhibition increased cellular levels of poly(ADP-ribose) in Cx18 cells untreated (DMSO) and treated with PARG inhibitor (0.625, 2.5 and 5μM). Biological repeat = 1.*

4.2.2 Rescuing PARGi using β-Nicotinamide mononucleotide

NAD+ serves as a crucial substrate for PARP enzymes, as it undergoes decomposition and splitting into ADP ribose and nicotinamide, which can subsequently be recycled (Navas and Carnero, 2021). To try and further understand the mechanisms behind the increased PARGi sensitivity exhibited by EDGE 2 cells compared with their matched CORE 1 counterparts, we questioned whether they possess a potential PARP-1 deficiency. We therefore used β-Nicotinamide mononucleotide (NMN), a precursor of NAD+ in an attempt to rescue these cells from PARGi treatment. Initially we performed a NMN titration assay to ensure that supplementing the cells with NMN would not exhibit any stimulatory or inhibitory effects on the cells and therefore bias our results, which is depicted in figure 4.5. From this data we did not observe any significant differences between the different cell populations Cx18 CORE 1

(figure 4.5A) or Cx18 EDGE 2 (figure 4.5B.) as determined by one-way ANOVA, CORE p= 0.18, EDGE p=0.1.
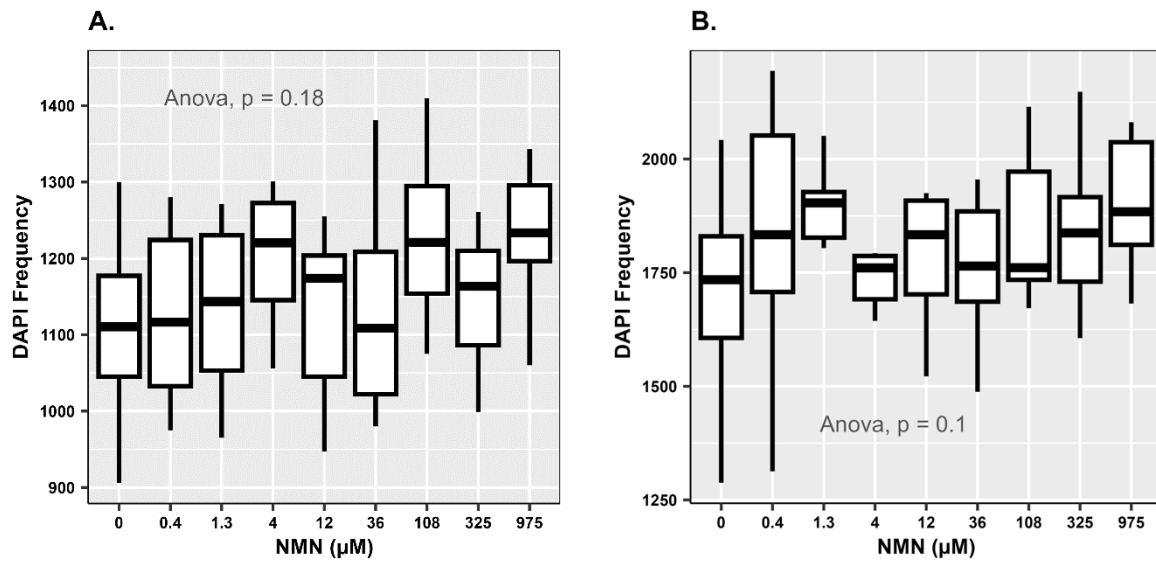
Figure 4.5 - Titration of NMN supplement on DAPI counts of CORE (A) and EDGE (B) Cx18 Cells. - DAPI cell counts of CORE and EDGE Cx18 cells were measured following 4-day exposure to incremental doses of NMN supplement. One-way ANOVA revelated no significant differences between group means. The central box of the boxplot displays the IQR, where the lower boundary corresponds to the first quartile and the upper boundary corresponds to the third quartile, the horizontal line within the box represents the median and the whiskers extend to the minimum and maximum values within 1.5 times the IQR. Biological repeat =3, technical replicates = 4.

Prior to seeding onto PARGi specific drug plates Cx18 CORE 1 and EDGE 2 cells were incubated with 500 µM NMN treatment, as recommended by the Bryant group based on their previous experience of working specifically with PARP and PARG inhibitors. The dose response curve displaying percentage inhibition (figure 4.6A), displayed pre-treatment with NMN slightly rescuing the EDGE 2 cells from PARGi treatment suggesting they may lack efficient PARP-1 activity. Further investigation of the inhibition values from individual PARGi concentration points for the EDGE 2 cells (figure 4.7) revealed that there were significant differences between the NMN and normal cell responses, for 2.5µM (p=0.028), 5 µM (p=0.00018) and 10µM (p=8.3e-07). The Significance increased in a dose dependent fashion, revealing that supplementing with NMN was able to rescue Cx18 EDGE 2 cells from increasing doses of PARGi. Comparing the individual concentration points within the CORE 1 cells showed no significant differences between NMN treated and normal cells.

Subsequently CORE 1 and EDGE 2 cells were incubated with NMN with and without 5μM PARGi for 24 hours, before being lysed and prepared for western blotting: blots were probed for PARG, a-PAR and PARP-1 (figure 4.6B). Again, this blot confirms that EDGE 2 cells have lower basal levels of PARG compared to CORE 1 cells, possibly making them more sensitive to smaller increments of PARGi. Whilst the PARG levels appeared consistent in CORE 1 cells across all conditions, the levels of PARG in the EDGE 2 cells appeared to increase following NMN treatment, which may help explain why they become slightly more resistant to PARGi inhibition following NMN pre-treatment (figure 4.6A). Following treatment with 5μM PARGi there was a reduction in PARP-1 levels within both the cell lines (figure 4.6B.), which would be expected as PARGi causes accumulation of parylation and therefore causes trapping of PARP-1 onto sites of DNA damage. Within the EGDE 2 cells it appeared that co-treatment with NMN and PARGi causes PARP-1 levels to increase higher than PARGi alone, this may therefore result in the slight rescue to PARGi treatment we observed within the dose response in figure 4.5A. Additionally, the a-PAR levels within the CORE 1 cells appeared to increase to a larger extent within both the DMSO controls and the PARGi condition following NMN treatment, compared to EDGE 2, possibly suggesting these cells are more efficient and reliant at this PARP-1 mediated repair. Within the CORE 1 cells NMN & PARGi treatment appeared to increase a-par accumulation but caused a complete depletion of available PARP-1, due to excessive a-par chain accumulation. This suggests that the PARGi is effective in these CORE 1 cells at inhibiting the removal of a-par chains, however the CORE 1 cells are more effective at repairing the damage this inhibition causes. It may be possible that CORE 1 cells are more proficient at HRR to mediate this damage, which would be interesting to assess in future studies.
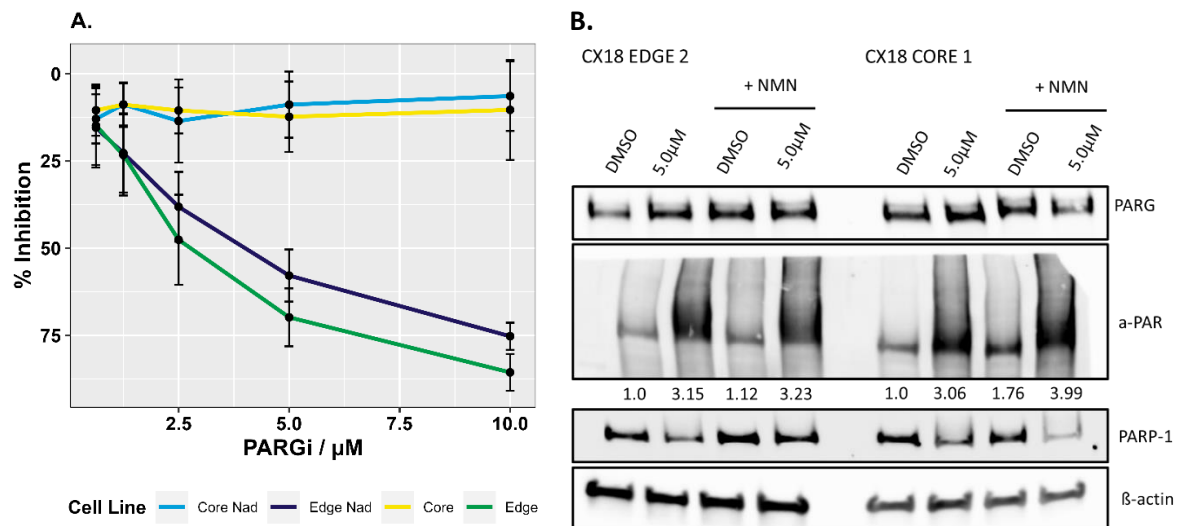
Figure 4.6 - Cx18 CORE 1 and EDGE 2 response to PARG inhibition following NMN pre-treatment - A. Cx18 CORE 1 and EDGE 2 cells PARG dose response curves with and without NMN pre-treatment. Error bars represent SEM. Technical replicates = 4, biological repeats =3. **B.** Immunoblot for poly(ADP-ribose)(PAR), PARP-1, PARG and β-actin in Cx18 CORE 1 and EDGE 2 cells following PARG drugging (5µM) with and without NMN pre-treatment. Numbers below a-PAR, represent intensity of treated a-PAR signals relative to each cell lines DMSO intensity. Biological repeat = 1.
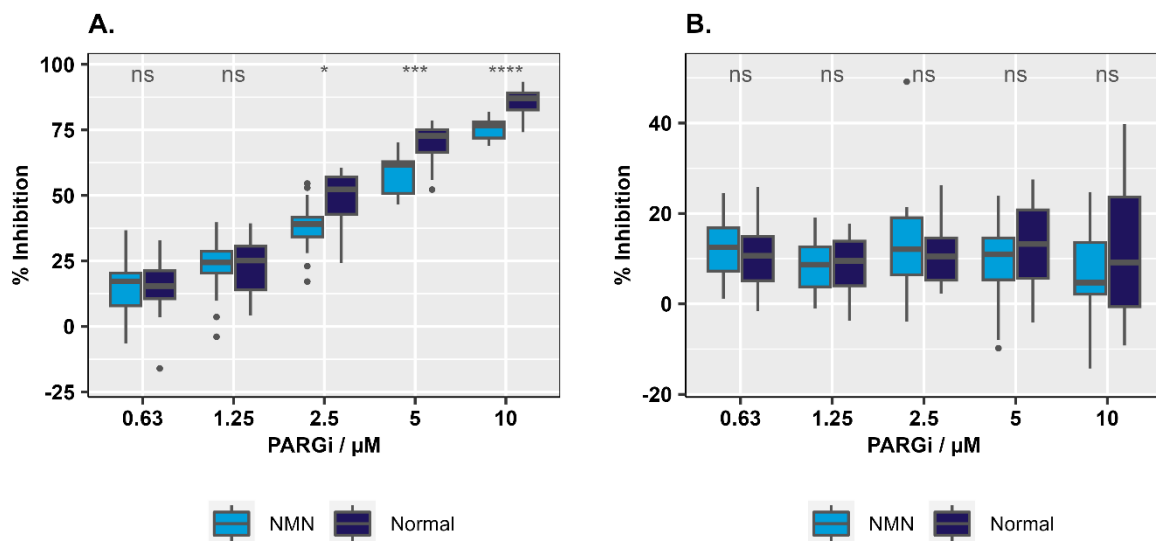
Figure 4.7 - Comparing % inhibition at each PARGi concentration point from NMN treated and normal cells - A. Comparison of Cx18 EDGE 2 cells. **B.** Comparison of Cx18 CORE 1 cells. The boxplot visualises the median, the upper and lower hinges correspond to first and third quartiles and the two wiskers correspond to largest value within the 1.5* IQR from the hinges. Any data beyond the whiskers are outliers. Unpaired t-test was performed to evaluate significance. The central box of the boxplot displays the IQR, where the lower boundary corresponds to the first quartile and the upper boundary corresponds to the third quartile, the horizontal line within the box represents the median and the whiskers extend to the minimum and maximum values within 1.5 times the IQR. Outliers are displayed by data points outside the whiskers a. Biological repeats = 3, technical replicates = 4.

156

Following this the levels of DNA damage were investigated between the two different CORE 1 and EDGE 2 cell lines following PARG inhibition, using fluorescent γ-H2AX foci staining/quantification: an established marker of cellular DNA damage levels. The EDGE 2 cells exhibited significantly higher levels of γ-h2AX foci compared to CORE 1 within the control samples and following treatment with 2µM and 5µM PARGi (figure 4.8). The respective images for the data are depicted by figure 4.9. When comparing each cell lines levels of γ-H2AX foci individually, treatment with PARGi had no significant effect on the CORE 1 cells γ-H2AX foci relative to the DMSO control whilst the EDGE 2 cells showed significantly higher levels of γ-H2AX following both 2 µM (p=<0.0001) and 5 µM (p=<0.0001) PARGi treatment relative to DMSO control. There was no significant difference between the two drugged conditions (p=0.19), showing that the increase in PARGi dose did not effect γ-H2AX foci. When comparing the γ-H2AX foci between the cell lines within each condition, EDGE cells displayed significantly higher foci in the DMSO (p=0.02), 2 µM PARGi (p = 1e-11) and 5 µM PARGi (p= 3.9e-10). These data therefore suggest that PARGi within the EDGE 2 cells causes an induction of DNA damage, possibly due to the inability of stalled DNA replication forks to restart, causing persistent replication stress.
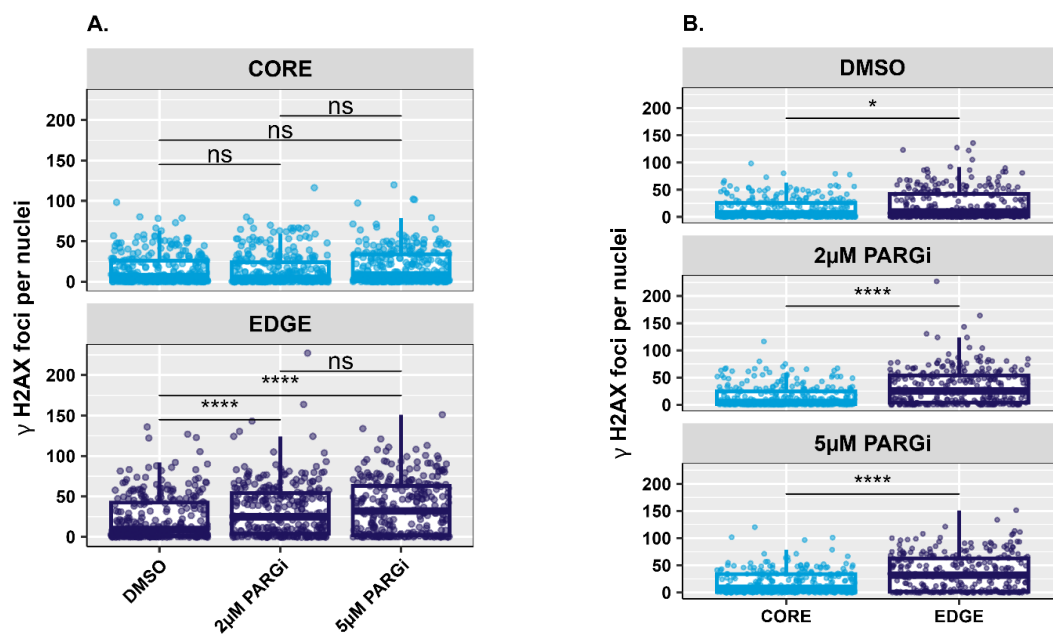
Figure 4.8 - Comparing the levels of γ-H2AX between the Cx18 CORE and EDGE cell lines following PARGi treatment - **A.** Comparing γ-H2AX foci following increasing PARGi dosing within each cell line. **B.** Comparison of the two cell lines γ-H2AX foci at each dose. The central box of the boxplot displays the IQR, where the lower boundary corresponds to the first quartile and the upper boundary corresponds to the third quartile, the horizontal line within the box represents the median and the whiskers extend
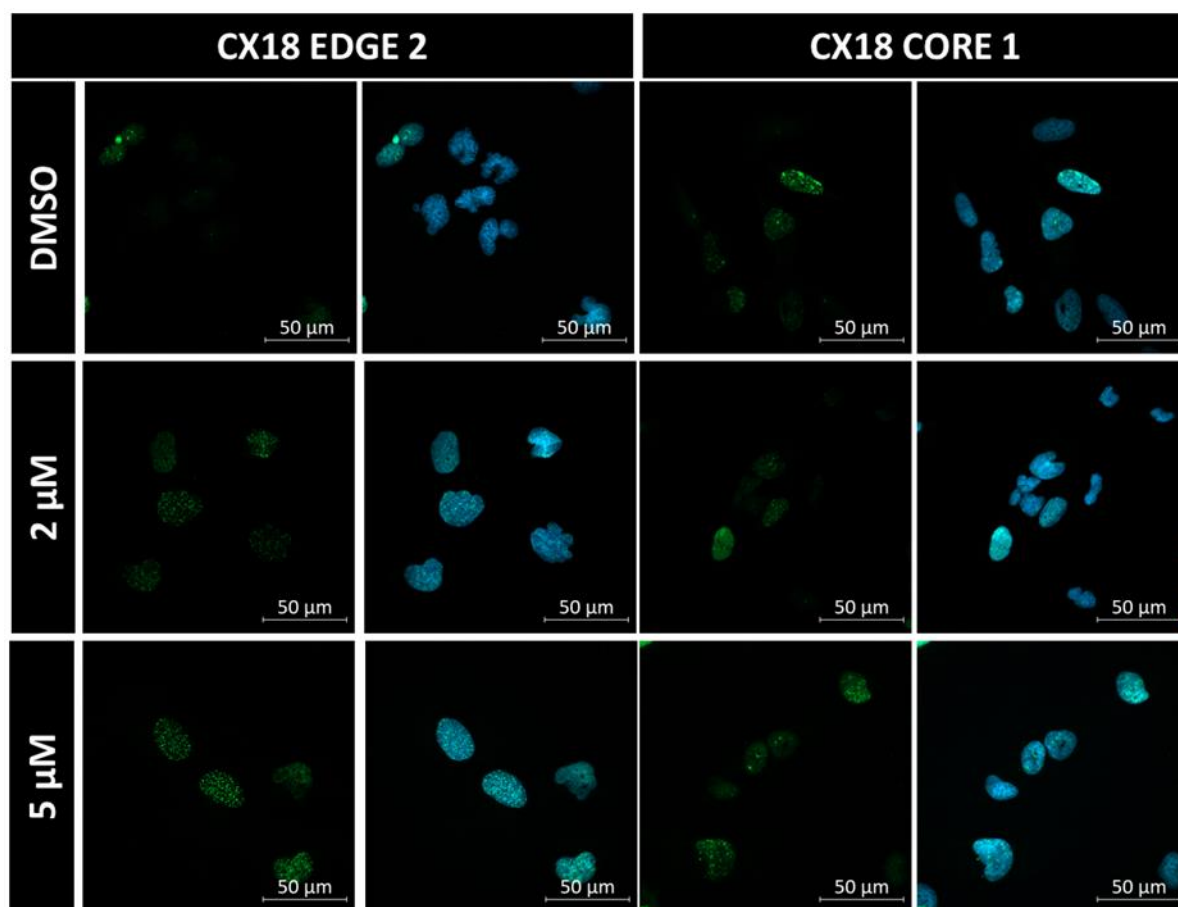
Figure 4.9 - Respective IF images of the Cx18 CORE 1 and EDGE 2 cells following PARGi treatment - Respective IF γ-H2AX staining images for both cell lines, untreated and following 2 and 5 μM PARGi. Images were taken using Zeiss LSM 980 Airyscan confocal microscope. Technical replicates = 100 cells, biological repeats = 3.

We next investigated the γ-H2AX levels of Cx18 CORE 1 and EDGE 2 cells following NMN pre-treatment and PARG inhibition (figure 4.10), the representative images are depicted by figure 4.11. Akin to the previous results there was no differences between the CORE 1 cells γ-H2AX foci after PARG & NMN treatment. Within the EDGE 2 cells there was no significant difference between the γ-H2AX foci levels within the DMSO and 2 μM PARGi treated cells, however in the previously shown PARGi alone treatment (figure 4.8) this difference was statistically significant. Furthermore, upon comparing the EDGE 2 DMSO and 5 μM PARGi treated cells, a decrease in significance was observed (p=0.00073), in contrast to the comparison with PARGi treatment alone (p=<0.0001). This observation implies that NMN treatment may have the capacity to reduce DNA damage levels in EDGE 2 cells by enhancing PARP-1 levels and activity.

Notably, a slightly significant difference in γ-H2AX foci was detected between the 2 μM and 5 μM drug-treated conditions (p=0.02), compared to the PARGi-alone condition (p=0.19). This suggests a potential role for NMN in reducing γ-H2AX levels at lower PARGi doses. Similarly, when comparing conditions across different cell lines (figure 4.10B), the levels of γ-H2AX within the DMSO and 2 μM conditions were no longer significantly different between the CORE 1 and EDGE 2 cells, however a statistical difference was maintained within the 5 μM dose (p=<0.0001).
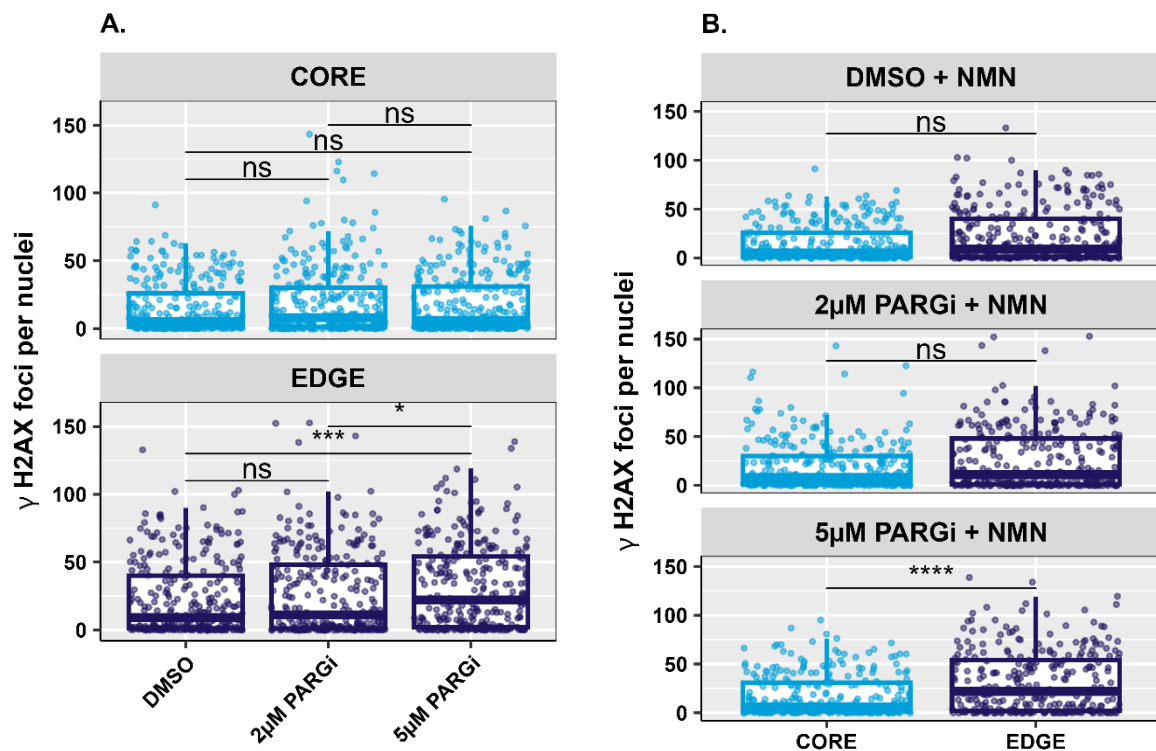
Figure 4.10 - Comparing the levels of H2AX between the Cx18 CORE 1 and EDGE 2 cell lines following PARGi + NMN treatment - **A**. Comparing γ-H2AX foci following increasing PARGi dosing within each cell line. The central box of the boxplot displays the IQR, where the lower boundary corresponds to the first quartile and the upper boundary corresponds to the third quartile, the horizontal line within the box represents the median and the whiskers extend to the minimum and maximum values within 1.5 times the IQR. **B.** Comparison of the two cell lines H2AX foci at each dose. Unpaired Man Whitney U test was performed. Technical replicates = 100 cells, biological repeats = 3.
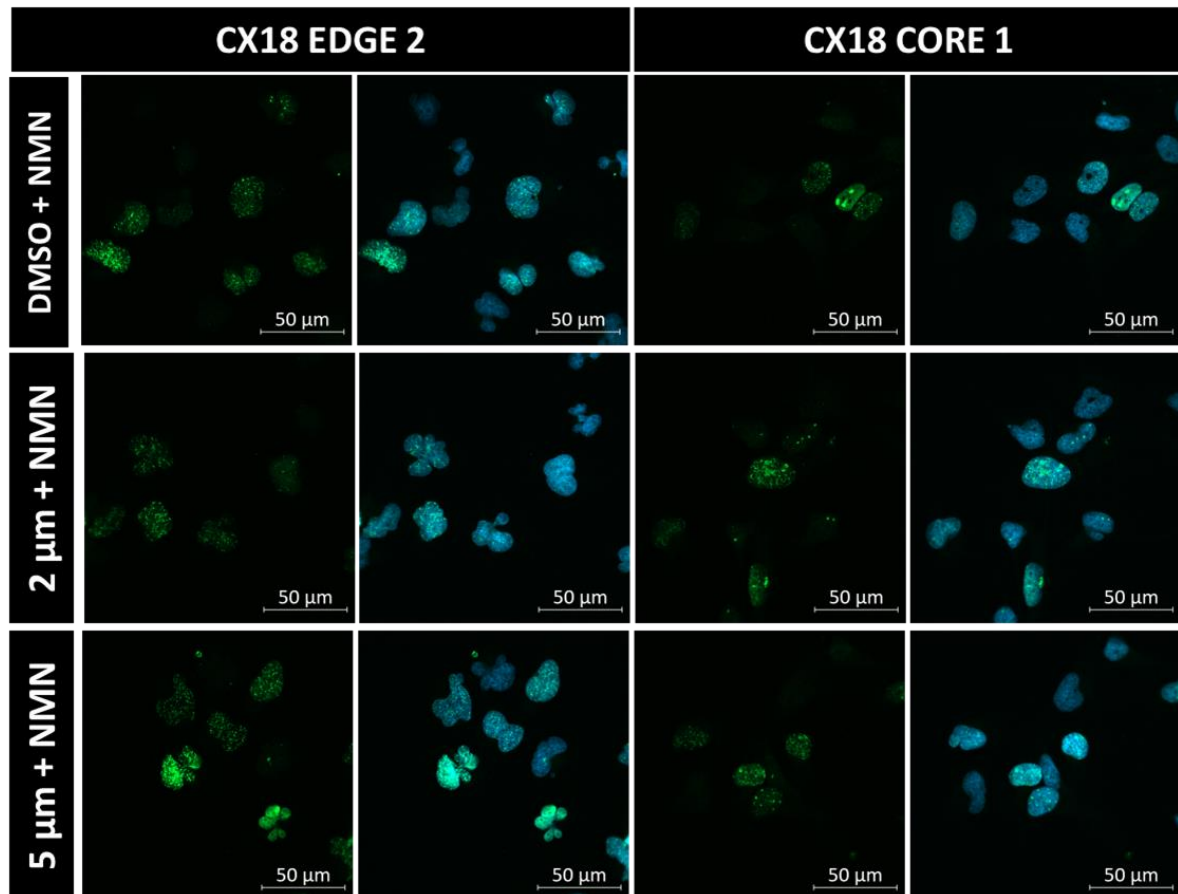
Figure 4.11 - Respective IF images of the Cx18 CORE 1 and EDGE 2 cells following NMN & PARGi treatment - Respective IF γ-H2AX staining images for both cell lines, untreated and following 2 and 5 µM PARGi. Images were taken using Zeiss LSM 980 Airyscan confocal microscope. Technical replicates = 100 cells, biological repeats = 3.

4.3 GBM21 and WEE1i sensitivity

Following DNA damage, CHK1 is activated through phosphorylation via either ATM or ATR depending on the type of genotoxic stress. CHK1 then simultaneously phosphorylates WEE1 and CDC25C, thus activating WEE1 kinase activity and inactivating CDC25C phosphatase activity. WEE1 initiates cell cycle arrest through inactivation of CDK1/CDC2-bound cyclin B via phosphorylation on the tyrosine15 residue, this causes cells to arrest in the G2 phase until the DDR machinery sufficiently restores the damage, preventing premature mitosis (Rowley, Hudson and Young, 1992). WEE1 is also involved in the timing of cell division, through stabilizing replication forks during the S-phase (Esposito *et al.*, 2021). Inhibition of WEE1 therefore reduces the level of inactivated phosphorylated CDC2 resulting in cells entering into premature entry to mitosis with unresolved DNA damage, increased replication stress and

ultimately cell death via mitotic catastrophe (Aarts *et al.*, 2012), and as such, WEE1 inhibitors are currently being developed as oncology therapeutics (Curtin, 2023).

Work by (Mir *et al.*, 2010) performed in silico analysis of microarray data and identified overexpression of WEE1 in glioblastoma, and analysis of IHC tissue sections also showed consistency with the gene expression data, whereby glioblastoma cell nuclei contained much higher levels of WEE1 protein compared to non-neoplastic brain regions. Additionally, the correlation of mRNA of WEE1 and patient survival highlighted that high expression of WEE1 corresponded with worse patient survival therefore highlighting it as a potential therapeutic target in glioblastoma. The resistance of glioblastoma cells to DNA damaging agents may partly be due to the ability to overexpress specific checkpoint kinases such as WEE1 which prolong cell-cycle arrest and therefore allow time to repair the damage. Contradictory to this, work by Music *et al* (2016) found WEE1 correlating with poor patient survival in lower grade gliomas, in higher grade IV tumours WEE1 levels correlated with improved patient survival, additionally WEE1 protein levels correlated with better survival in *MGMT* methylated patients, whilst survival benefit in un-methylated patients with high WEE1 expression was less pronounced, suggesting a role for WEE1 in tumour response and patient survival requires further investigation (Music *et al.*, 2016).

p53, which is a key regulator of the G1 checkpoint is commonly mutated in many malignancies including glioblastoma, causing these cells to be defective at arresting cells in G1. As a result, these cells become more reliant on the G2/M checkpoint (Wang *et al.*, 2001; Li *et al.*, 2002). *In-vitro,* the use of WEE1 inhibitors supersedes the G2 checkpoint and sensitized p53 deficient cells to DNA damaging agents such as gemcitabine, carboplatin and cisplatin (Hirai *et al.*, 2009, 2010). *In-vivo* WEE1 inhibitors have shown to inhibit tumour growth (Hirai *et al.*, 2009). Despite this, Van Linden demonstrated that sensitising p53 deficient acute myeloid leukaemia (AML) cell lines to antimetabolite chemotherapeutics using WEE1 inhibitors was not possible, suggesting not all cancers and/or chemotherapeutics are suitable when using p53 mutation as a predictive biomarker for WEE1 induced chemo sensitisation strategies (Van Linden *et al.*, 2013)

From the V01 drug screening sample data, GBM21 appeared increasingly sensitive to the WEE1 inhibitor AZD1775 in comparison to all the other patient samples (Chapter 3, figure 3.15). One possibility for the enhanced sensitivity to WEE1 inhibition may be a result of combined deficiencies in cell-cycle regulation. To investigate this, immunoblot analysis was performed to investigate the G2/M checkpoint within GBM21 alongside GBM11 (figure 4.12). We selected GBM11 as a comparative sample as it displayed a modest response to WEE1 on our V01 heatmap and exhibited a significant difference between DMSO and aphidicolin cell counts, suggesting the original sample cells were actively dividing. As aphidicolin is a DNA polymerase inhibitor, it arrests cells at the entrance to S-phase blocking cell cycle progression. Interestingly GBM21 displayed the higher levels of p-CDC2/CDK1 than GBM11, suggesting that this protein may be more active in these cells, causing increasing sensitivity to WEE1i. Similar, for the mitotic-associated Aurora kinase proteins, GBM21 displayed significantly higher Aurora B, but similar levels of Aurora A than GBM11.
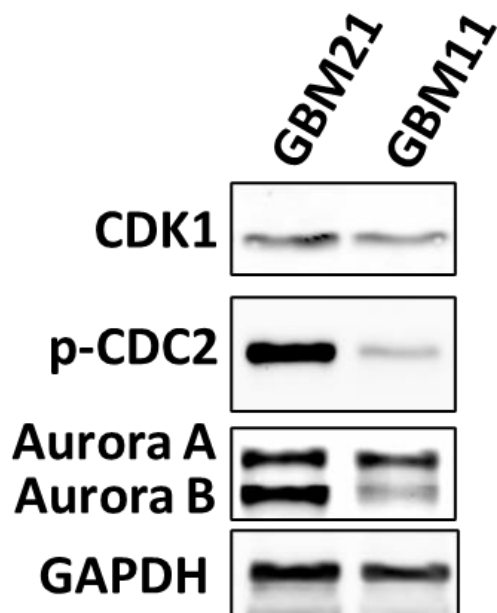
Figure 4.12 - Immunoblot analysis of G2/M checkpoint in primary GSC cells cultured from GBM21 and GBM11 - Cell lysates from the indicated GSC primary cell line were probed with the indicated antibody. Biological repeat = 1.

To further investigate the potential mechanism(s) for the observed WEE1i sensitivity in GBM21, FACS-based cell cycle analysis was performed on the primary cells derived from GBM21 and GBM11 patient sample cells, following 1-hour WEE1i treatment (figure 4.13). As expected treatment with the WEE1 inhibitor AZD1775 caused both cell lines to exhibit an increase in the mitotic fraction (M) compared to untreated (UT) cells. The cell cycle profiles

of both cell lines appeared similar apart from the subG1 population, where the GBM11 cells exhibited a higher fraction of cells in both UT and WEE1i conditions, indicating higher levels of cell death. However, the short drug incubation period (1 hour) prior to analysis likely did not allow enough time to detect large amounts of mitotic-induced cell death, which would have otherwise been highlighted by the sub G1 fraction in the treated cells. Therefore, from this FACS data, it has to be concluded that there is no indication that the GBM21 cells are more sensitive to WEE1i compared to the GBM11 cells.
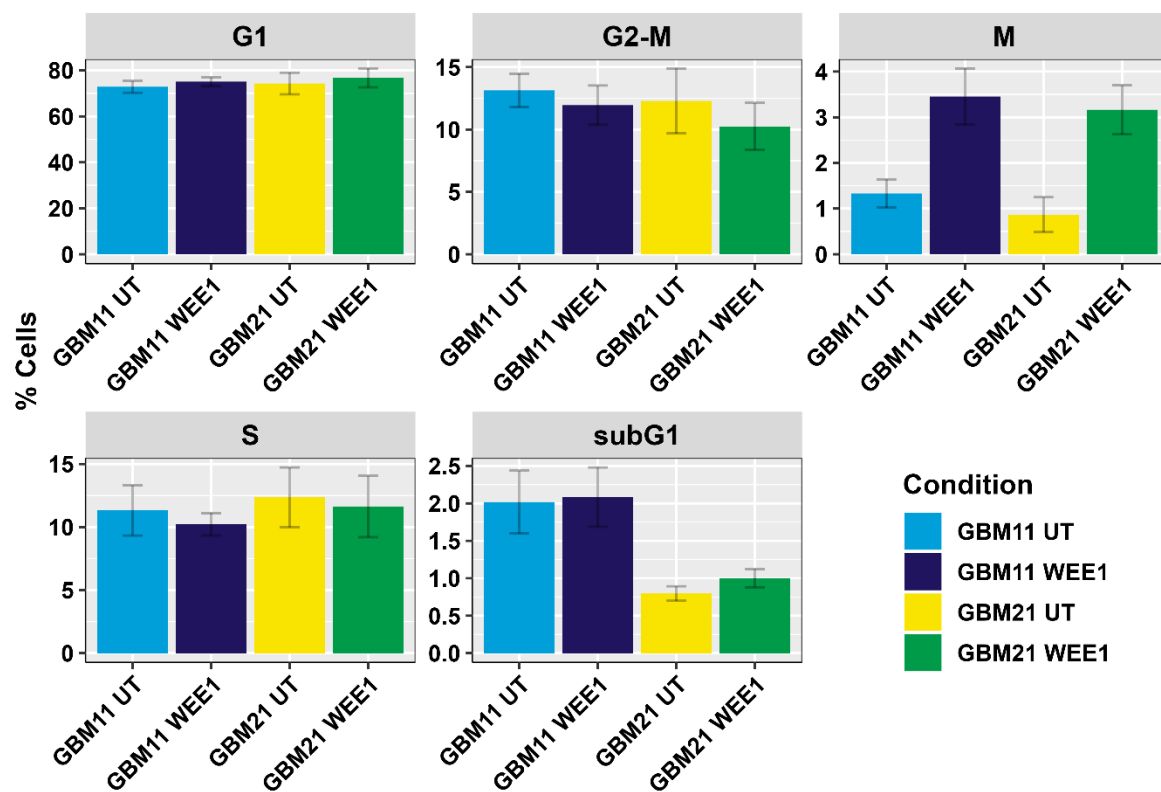
Figure 4.13 - Quantification of accumulation of cells within specific phases of the cell cycle following treatment with the WEE1i AZD1775 - GBM11 and GBM21 cells were either treated with DMSO (UT) or 0.1μM of WEE1i and analysed for cell cycle stage using FACS analyses. Biological repeats = 3, technical replicates =1. Error bars represent standard error.

Based on these findings it was difficult to decipher the reasoning behind the identified AZD1775 (WEE1i) sensitivity for GBM21 within the V01 ex vivo screen. Consequently, a follow up AZD1775 dose response experiment was performed using both GBM21 and GBM11 primary cells, to validate these as *bone fide* hits. This data shown below (figure 4.14) revealed GBM11 primary cells to be more sensitive than GBM21, with IC$_{50}$ values of 0.013 and 0.23 μM

respectively, suggesting that the initial plate screening on V01 was unable to pick up on this GBM11 sensitivity to WEE1 inhibition.
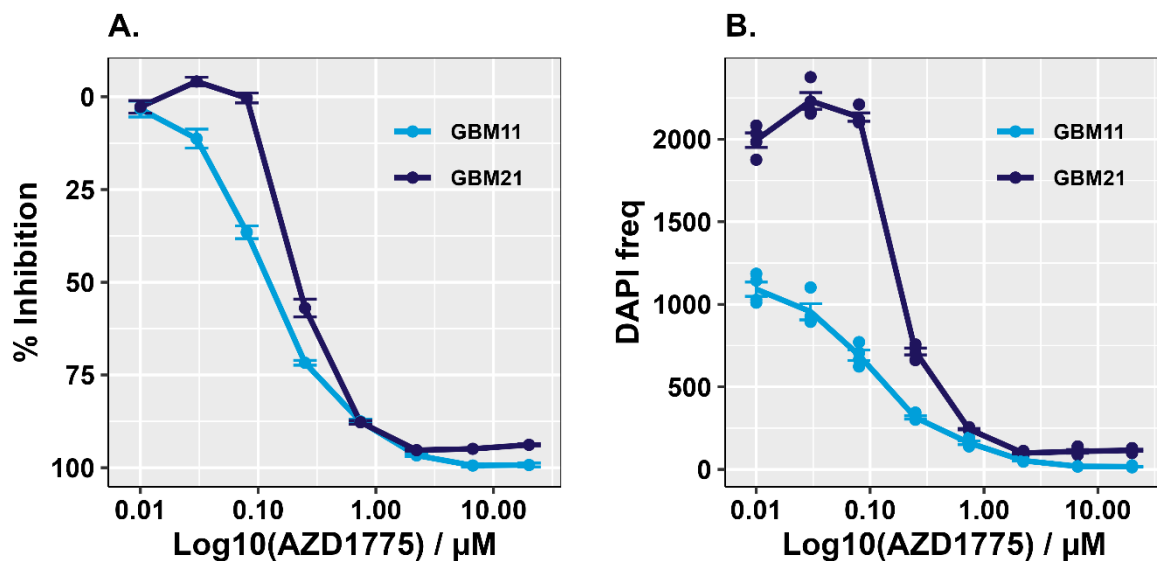
Figure 4.14 - GBM21 and GBM11 dose response to WEE1i AZD1775 showing both calculated percentage inhibition and cell frequency measured using DAPI positive cells - **A.** WEE1i sensitivity represented by % inhibiton. **B.** WEE1i sensitivity using raw DAPI cell counts. The response readout (DAPI count) was collected using automated IF microscopy, the counts were normalized using positive and negative controls on each dose plate to provide the response measure (relative inhibition %). GBM11 IC_{50} = 0.13 μM, GBM21 IC_{50} = 0.23μM. Biological repeats = 3, technical replicates =4. Error bars represent standard error.

As specified previously, GBM11 was selected to compare with GBM21 as it showed modest WEE1 sensitivity on the V01 drug plate heatmap (Chapter 3, figure 3.15), but also displayed evidence of cell division through differences between cell counts obtained from DMSO and aphidicolin wells on drug plate (Chapter 3, figure 3.23). We therefore could not suggest the lack of WEE1 response on the drug plate was a factor of minimal cell division, thus allowing WEE1 to exert an effect.

One of the issues with these follow up experiments is the use of primary cell lines which have been derived from the original patient tumour, despite being low passage, they have still undergone selection through passaging on plasticware with media favouring the GSC population. When the drug responses of freshly dissociated patient sample cells were compared to their cultured primary cell lines (Chapter 3, figure 3.22) it was observed that the primary cell lines exhibited increased drug sensitivities, in particular the response to WEE1 inhibitor. Within the GBM21 sample vs its matched primary cells we saw an increase in the

sensitivity to WEE1i through a lower AUC value, additionally GBM25 sample which showed no response to WEE1i on the drug plate showed increasing sensitivity within the corresponding cell line. It may be possible these sensitivities are induced through primary culturing.

4.4 Bulk vs Stem Ouabain Sensitivity

Ouabain is a cardiac glycoside, traditionally used in the clinic to treat heart failure. It causes rapid inhibition of Na+/K+-ATPase enzymes, therefore elevating levels of cytosolic Ca2+ resulting in increased myocyte contractility. The therapeutic efficacy of cardiac glycosides on neoplastic cells was first reported in 1967, a decade later, breast cancer patients who had taken digoxin (another cardiac glycoside) showed tumour reduction, alongside lower risk of recurrence (Stenkvist *et al.*, 1979). The anti-cancer mechanisms by which cardiac glycosides work remains to be fully elucidated, however there are multiple mechanisms of actions reported within the literature. Some of these mechanisms include; Inhibition of Na+/K+-ATPase enzymes, activated oncogenic Ras pathways which induces ROS (Prassas and Diamandis, 2008), inhibiting the PI3K pathway (Yang *et al.*, 2018), activating endoplasmic reticulum stress, inhibiting the hypoxia inducible factor 1 alpha (HIF-1α) and ERK1/2 signalling pathway (D. H. Lee *et al.*, 2017). There are multiple reports involving the DDR, linking cardiac glycosides with reduced expression of DNA repair proteins and kinases (Bao *et al.*, 2016; Yang *et al.*, 2021).

The radiosensitizing ability of ouabain was first reported over 30 years ago, despite no insight to the exact mechanisms; the therapeutic index of IR within lung adenocarcinoma cells was enhanced following ouabain treatment, with no effect to normal lung fibroblasts (Lawrence and Davis, 1990). Another study highlighted ouabain as a novel inhibitor of the FA/BRCA pathway, via a small molecule chemical library screen (Wha Jun *et al.*, 2013). The FA/BRCA pathway is a DNA repair pathway which is activated in response to ICLs, which are highly toxic legions induced by chemotherapeutic agents such as mitomycin C and platinum-based compounds such as cisplatin and carboplatin, thus inhibition of this pathway can potentiate ICL-inducing agents. The chemical screen study also went on to reveal that ouabain treatment was able sensitise U2OS osteosarcoma cell line to MMC, supporting the idea that ouabain can

serve as a chemosensitizer towards ICL-inducing anticancer drugs (Wha Jun *et al.*, 2013). Additionally, work by Ola Rominiyi within the Collis lab has shown the ability of ouabain to inhibit the FA/BRCA pathway through reduction in FANCD2 levels leading to radiosensitisation of both established and primary GSCs (unpublished). To investigate whether our growth media conditions could influence drug responses, we investigated the differences in dose responses between Cx18 CORE 1 cells which had been cultured in both stem cell enriching 'STEM' media and serum containing differentiating 'BULK' media, containing FBS. Shown below is heatmap depicted using drug response AUC values (figure 4.15), which were calculated from DAPI cell counts. From the heatmap we can see that cells grown in STEM promoting media are increasingly sensitive to BRAFi (dabrafenib), TMZ and ouabain whilst the BULK cells are more sensitive to MEK1/2 inhibitor (selumetinib) and bleomycin.
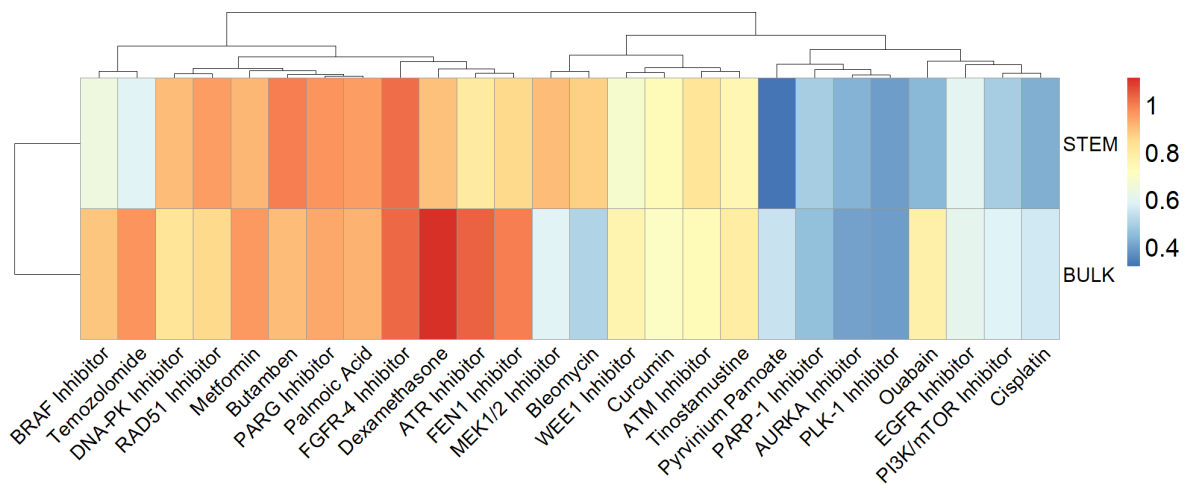
Figure 4.15 - Comparing the AUC drug responses calculated using DAPI cell frequency of the primary Cx18 cell line cultured in both STEM and BULK promoting media - The scale represents blue as cell death and red as survival. AUC values were generated from GR metrics package in R, the heatmap was generated using the pheatmap package. Biological repeat =1, technical replicates = 4.

Of the differential responses, we were particularly interested in the ouabain sensitivity, and therefore selected this for further investigation. The data in figure 4.16 below shows the dose response curves which the AUC values in the heatmap above (figure 4.15) were calculated from, again highlighting the increasing sensitivity which STEM cultures show in comparison to BULK.
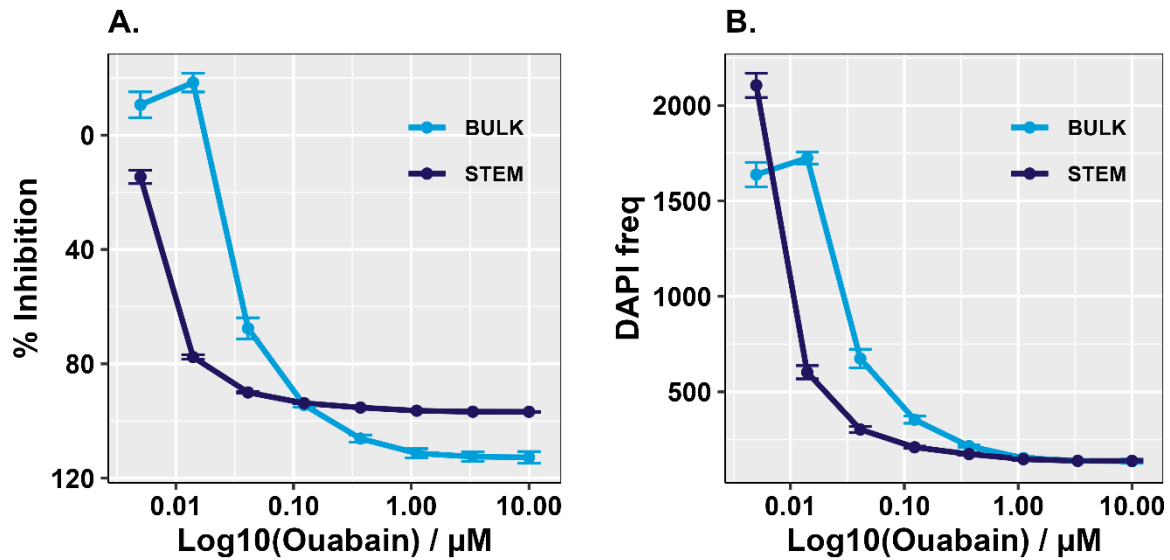
Figure 4.16 - Cx18 BULK and STEM cultures dose response curves to ouabain showing both calculated percentage inhibition and cell frequency measured using DAPI positive cells *- A. Ouabain sensitivity represented by % inhibiton. B. Ouabain sensitivity using raw DAPI cell counts. The response readout (DAPI count) was collected using automated IF microscopy, the counts were normalized using positive and negative controls on each dose plate to provide the response measure (relative inhibition %). STEM IC$_{50}$ = 0.0095μM, BULK IC$_{50}$ = 0.047μM. Biological repeats = 3, technical replicates =4. Error bars represent standard error.*

Previous studies have shown the ability of ouabain to inhibit NHEJ activity (Du *et al.*, 2018). DNA-PKcs is a serine/threonine kinase, during NHEJ, it phosphorylates repair proteins and itself to allow completion of DSB repair (Curtin, 2023). We therefore initially investigated the levels of DNA-PKcs foci between the resistant and sensitive cell cultures using IF microscopy as a marker of NHEJ activity (figure 4.17), the respective images are depicted by figure 4.18.

When we compared the levels of DNA-PK foci between the untreated BULK and STEM cultures, there were statistically significant differences, which was consistent within the IR and combination (IR & OUABAIN) treatment (figure 4.17 and table 4.1). However following ouabain treatment alone there was no significant difference between the foci counts of the two cell lines. Investigation of the mean foci per nuclei revealed that following ouabain treatment the levels of DNA-PK foci increased nearly 5-fold higher in the STEM in comparison to 1.5-fold increase within the BULK relative to UT control, corroborating the initial drug response profiles, that stem cultures are more sensitive to Ouabain treatment (figure 4.17 and table 4.1).

When comparing the DNA-PK foci levels for each cell line individually (figure 4.17B), following treatment with Ouabain, the levels of DNA-PK foci was significantly higher compared to the untreated cells generating p values of <0.0001 for both the STEM and BULK cultures. Treatment with IR and the combination also generated statistically significant results relative to the untreated control, again p values of <0.0001.
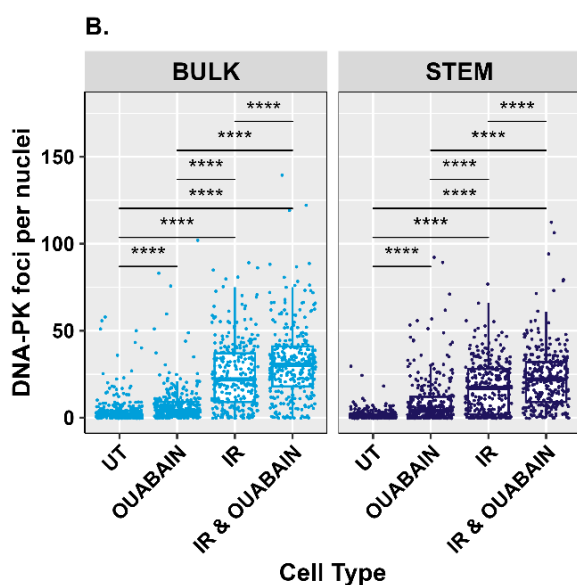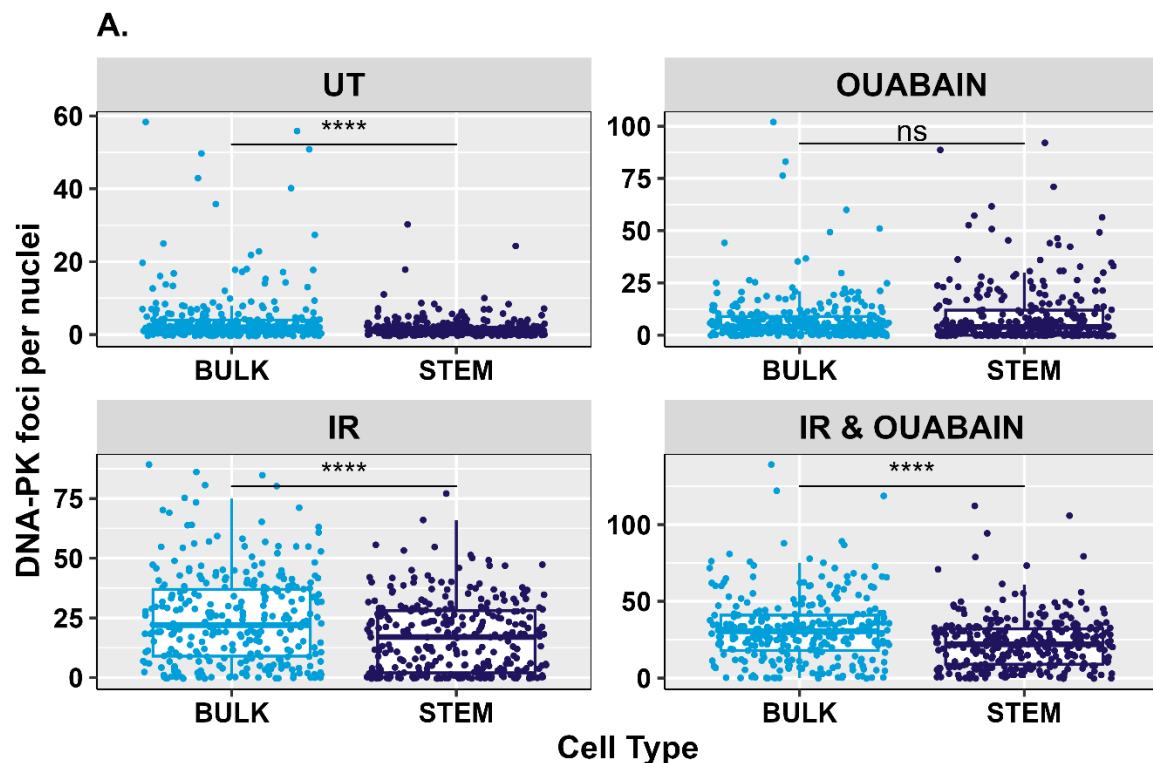
Figure 4.17 - Investigating the DNA-PKcs foci levels within STEM and BULK cultures following ouabain, IR and combination therapy - A. Comparison between the BULK and STEM DNA-PK (Thr-2609) foci counts for each condition. B. Comparison between the conditions within both of the STEM and BULK cell line cultures. The central box of the boxplot displays the IQR, where the lower boundary corresponds to the first quartile and the upper boundary corresponds to the third quartile, the horizontal line within the box represents the median and the whiskers extend to the minimum and maximum values within 1.5 times the IQR. Biological repeats = 3, technical repliates = 100 cells per condition.

Table 4.1 - Mean DNA-PKcs foci counts and their standard deviation within the STEM and BULK cultures.

Condition	Stem mean foci (± SD)	Bulk mean foci (± SD)
UT	1.87 ± 2.79	4.99 ± 12.9
Ouabain	9.17 ± 14	7.63 ± 11.5
IR	16.8 ± 15	24.6 ± 19.2
IR + Ouabain	22.9 ± 17	31.8 ± 21.3
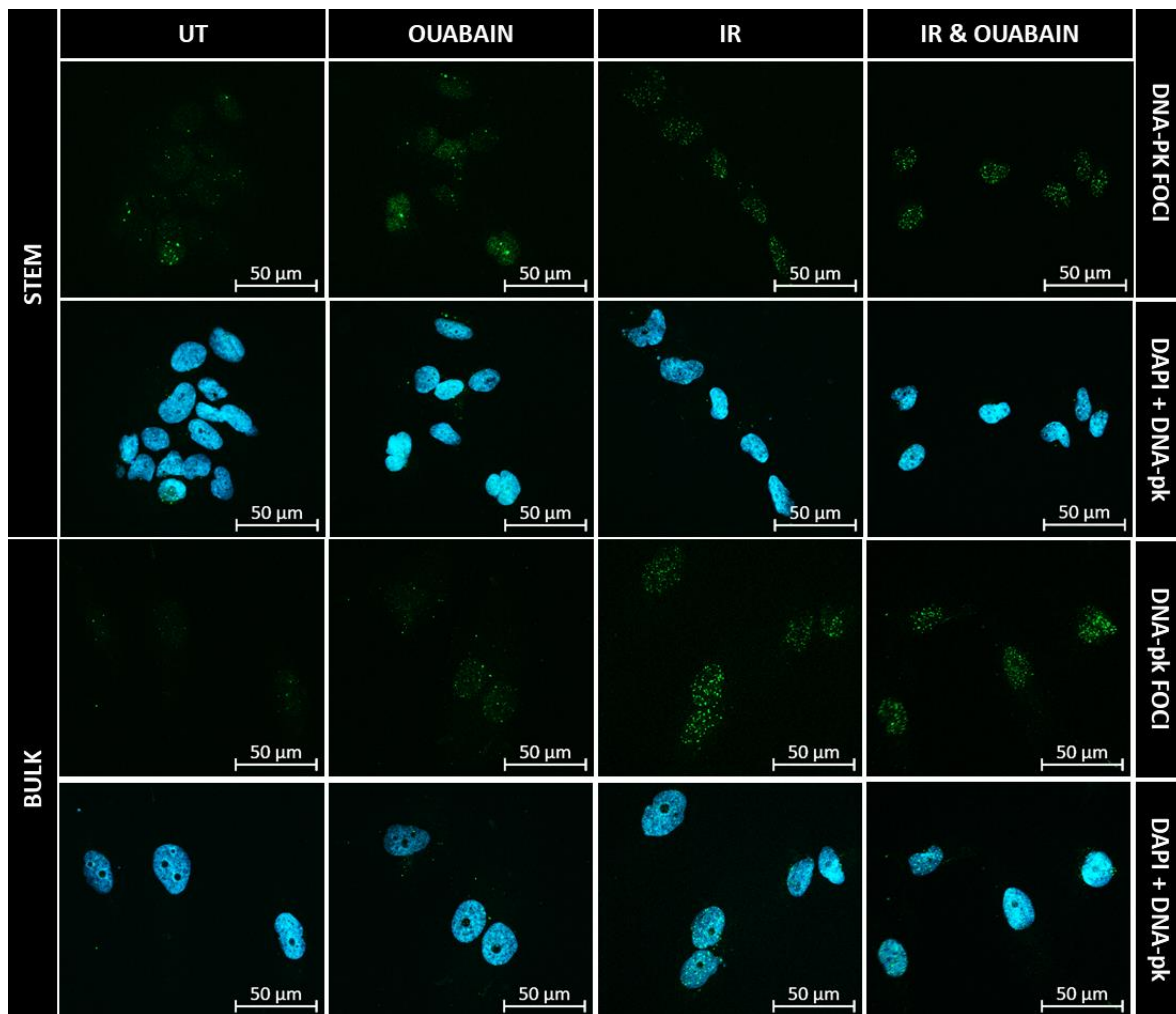
Figure 4.18 - Respective IF images of the Cx18 BULK and STEM cells following, Ouabain, IR and combination treatment - Images were taken using Zeiss LSM 980 Airyscan confocal microscope. Cell nuclei is detected using DAPI (blue), DNA-Pk foci (green). Biological repeats = 3, technical replicates = 100 individual cells.

As mentioned previously, multiple reports have indicated that cardiac glycosides have the ability to reduce expression of DNA repair proteins and kinases (Bao *et al.*, 2016; Yang *et al.*, 2021), we therefore investigated the levels of multiple DDR proteins within the BULK and STEM cultures following ouabain and IR treatment through immunoblotting (figure 4.18).

DNA damage repair is activated to maintain genomic integrity of cells following DNA damage, inhibiting the DDR is an attractive target in cancer due to overreliance on cancer cells of DDR to alleviate effects of replication stress.

Surprisingly immunoblotting data revealed higher levels of DNA-PKcs within the STEM cultures, as apposed to the IF data which revealed higher DNA-PKcs foci within the BULK populations. Data shown revealed evidence of an upregulated DDR in Cx18 STEM cultures, suggesting these cells may be more primed to respond to DNA damage due to heightened levels of associated proteins. For instance, a radiation dose of 5Gy induced phosphorylation of ATM at serine 1981 to a larger degree in the STEM cultures than the BULK. Additionally, the BULK cultures exhibited higher levels of a-PAR and γ-H2AX suggesting increase in SSB and DSB, consistent with lack of active DDR. Our findings are further substantiated by existing literature, which has pointed out that GSC populations exhibit an increase in phosphorylated DNA damage response proteins and higher G2/M, activation that matched BULK tumour cell populations (Carruthers *et al.*, 2015).
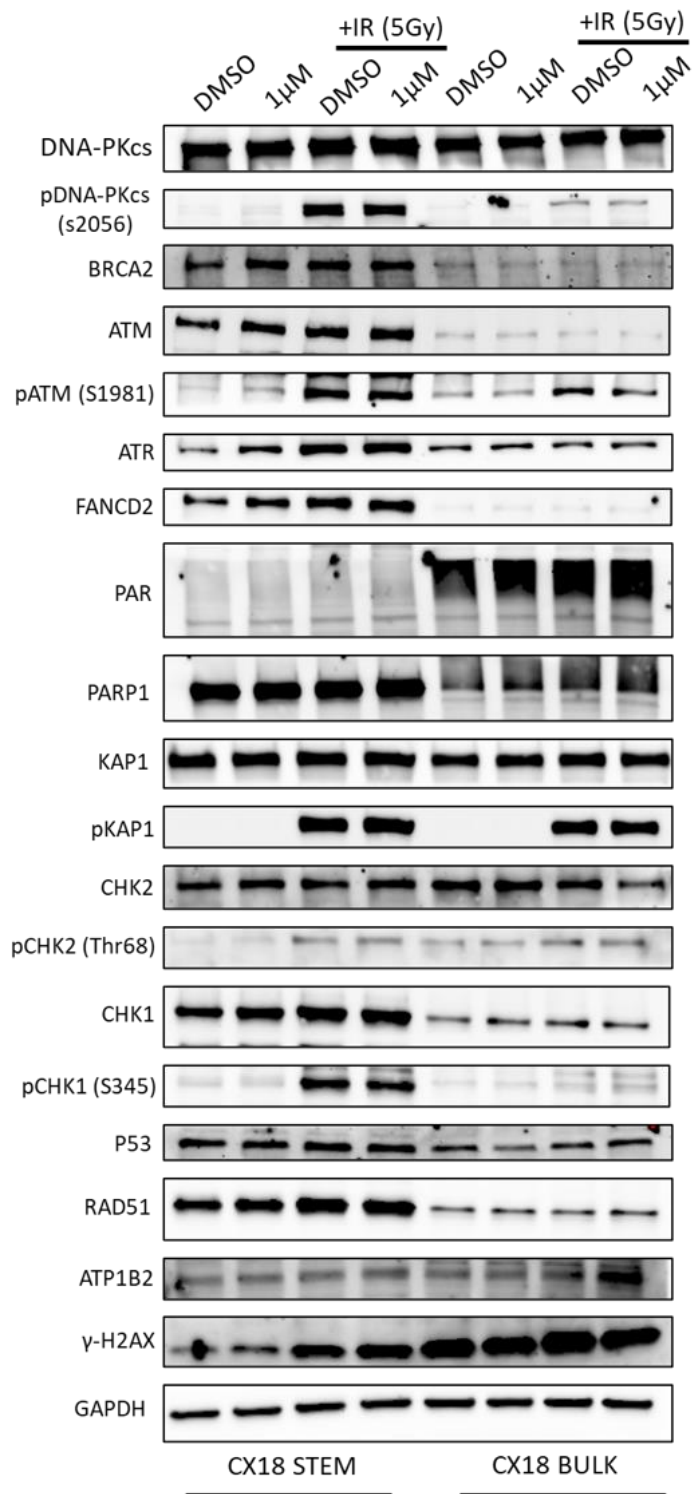
Figure 4.19 - Immunoblot analysis of multiple DDR associated proteins within BULK and STEM cultures following ouabain and IR treatment - The left four lanes correspond to STEM treated cells and the right four lanes correspond to BULK treated cells. Cells were plated into 6 well dishes for 24 hours prior to exposure to the indicated doses of ouabain or DMSO, then IR therapy (5Gy) 1 hour later. Cells were then incubated for an additional hour prior to lysis and western blotting.

171

4.5 Summary Points

- Our ex vivo screening platform can highlight differences within drug responses for multi region samples.

- The nature of screening freshly dissociated tissue means it is not possible to obtain biological repeats, follow up experiments with low-passage cell lines can often give misleading results as culture conditions have enriched for a rapid growing phenotype.

- The differential responses for cultures growth in STEM and BULK media suggests it may be important to screen samples within both media conditions, as growth factors within the media may influence the upregulation of certain pathways.

- The plasticity of these STEM cells highlighted later in chapter 5 indicates that these cells can flip between GSC and differentiated like states depending on external stimuli, therefore it makes sense to find combinatory therapies to target both tumour BULK and STEM cell populations.

4.6 Discussion

4.6.1 Cx18 differential responses to PARG

Unlike with PARPi and HR deficient tumours, the mechanism behind PARGi synthetic lethality has not yet been fully elucidated, with contradictory findings reported in the current literature. For instance multiple papers investigating MCF7 breast cancer cell lines showed that depletion of HR proteins BRCA 1/2 , PALB2, ABRAXAS and BARD1 provoked synthetic lethal interaction with PARGi (Fathers *et al.*, 2012; Gravells *et al.*, 2017). However, another study looking at BRCA1 mutations in multiple cancer cell lines, showed no synthetic lethality with PARGi (Noll *et al.*, 2016). It has also been shown that it is possible to kill BRCA-proficient cancer cell lines using the small molecule PARGi JA2131 (Houl *et al.*, 2019). Whilst only 1/6 ovarian cancer cells harbouring the BRCA 1/2 mutation showed PARGi sensitivity towards PDD00017273, instead they showed that synthetic lethality using PDD00017273 was linked with replication associated genes such as TIMELESS, HUS1 and RFC2 (Pillay *et al.*, 2019).

Immunoblot analysis from another lab member (data not shown) demonstrated that Cx18 EDGE 2 cells express reduced p-ATM, p-CHK1 and p-CHK2 levels compared to the CORE 1 cells

following IR treatment. This suggests that they have reduced checkpoint activation, making them less primed to respond to DNA damage. ATM activation is critical at maintaining genome integrity, responding to DSB and other lesions. If either of the CHK1 and CHK2 signalling pathways are defective, this will lead to accumulation of DNA damage and eventual cell death. Futhermore, the EDGE 2 cells also expressed lower levels of interfilament protein nestin and transmembrane protein CD133, both markers of GSCs, suggesting the CORE 1 cells have an increased stem phenotype which is associated with therapy resistance through heightened levels of DNA repair mechanisms.

Overall, these data suggests that the differences between CORE 1 and EDGE 2 sensitivities are a multitude of factors. Firstly, immunoblotting revealed EDGE 2 cells expressing lower levels of PARG, thus requiring less PARGi to exert a inhibitory effect compared to CORE 1 cells. Secondly, the supplementation of NMN to the EDGE 2 cells was able to significantly rescue them from PARGi. This suggests they may also have lower PARP-1 activity, possibly because of lower basal levels of cellular NAD+ compared to the CORE 1 cells. Subsequent avenues for exploration may include quantifying the cellular NAD levels of these cell lines before and after treatment, to further confirm this hypothesis. Finally, we believe that the lower levels of DDR proteins in the EDGE 2 cells will heighten sensitivity to PARG as these cells lack the ability to efficiently respond to DNA damage, in comparison to CORE 1 cells.

Although there are currently no ongoing clinical trials investigating the use of PARG inhibitors for glioblastoma, we anticipate that this may evolve in the coming years due to promising developments in preclinical research. For instance, PARG inhibition has shown to strongly potentiate the DNA damage induced through TMZ (Tang *et al.*, 2011). Additionally administration of PARGi alongside precursor NHR has shown S-phase arrest and apoptosis specific to GSC, with minimal toxicity in normal astrocytes (Li *et al.*, 2021), this study also demonstrated PARP1 and PARG protein levels are significantly elevated in glioma derived cells and GSCs, in comparison to normal astrocytes. Similar to our findings Jackson et al has found PARGi, PDD00017273, to exert single agent therapeutic activity on clonogenic survival within a panel of glioblastoma cell lines in a dose-dependent manner. Interestingly they also reported PARGi, to sensitize glioblastoma cells to IR treatment (Jackson, Gomez-Roman and Chalmers, 2019)

4.6.2 GBM21 WEE1 sensitivity

While it is useful to culture GSCs derived from the primary ex vivo screening sample for follow up experiments, we have shown previously (chapter 3, figure 3.22) that low passage primary cells often display heightened sensitivity to most drugs on the plate. This therefore makes it difficult to make any direct comparisons to follow up experiments performed post-screen; this is emphasized by the WEE1 sensitivity data shown previously within this chapter. Original screening data within the V01 plates revealed GBM21 and GBM11 to be the most sensitive and resistant samples to WEE1 inhibition, however upon follow up analysis of both primary culture cell lines, it became apparent that GBM11 was in fact more sensitive to WEE1i than GBM21. Upon analysis of DMSO and aphidicolin cell counts, both original screened sample and matched primary cells underwent cell division during the 4-day assay. This therefore rejects the idea that GBM11 was unable to respond to WEE1i, because it underwent no cell division during the assay timeframe. It does however suggest that the stem promoting growth conditions, is enriching for a population of cells which are sensitive to specific drugs (see chapter 5 for further analysis of drug responses within stem-specific sub-populations).

Upon examining the clinical trials database, we found that there are presently only two ongoing studies focused on the utilization of WEE1 inhibitor AZD1775, both of which are specifically targeted at recurrent glioblastoma. Previous pre-clinical data from a xenograft model reported poor brain penetrance of AZD1775 (Pokorny *et al.*, 2015), however the results from the phase 0 trial revealed that AZD1775 has excellent brain penetrance in humans, achieving pharmacologically relevant tumour concentrations (Sanai *et al.*, 2018). This study also unveiled checkpoint disruption marked by increased DNA damage, cell-cycling and programmed cell death. The second investigation is a phase I trial dedicated to assessing the side effects and optimal dose of AZD1775 when administered together with RT and TMZ within both newly diagnosed and recurrent glioblastoma. Collectively whilst still in its early stages, this data emphasizes the considerable promise of WEE1i, AZD1775 within glioblastoma.

4.6.3 Cx18 BULK vs STEM Ouabain responses

Upon investigation of the DNA-PKcs foci counts between the BULK and STEM, the BULK cells displayed higher levels of foci within the untreated cells compared to the STEM. This data is supported by the immunoblot analysis of the DDR proteins which reveal much lower levels of proteins within the BULK, suggesting they are less primed to respond to accumulated DSB and therefore display higher levels of NHEJ associated kinase p-DNA-PKcs. Following ouabain treatment the levels of foci between the BULK and STEM cultures was no longer statistically significant, STEM cultures foci numbers increased 5-fold higher than the untreated levels, whilst the bulk only increased 1.5-fold. One possible reason for the larger increase in the STEM population may be their increased reliance on NHEJ repair, which consistent with previous reports that ouabain inhibits NHEJ, thus leading to a build-up DSB and foci in the treated cells.

Due to antibody suitability, we probed our immunoblot using a DNA-PKcs (Ser2056) specific antibody. There were marginal levels of the DNA-PKcs (Ser2056) within both the untreated and ouabain controls for both BULK and STEM, however following IR the STEM cultures displayed much higher levels of DNA-PKcs. One possible reason for the differences between the levels of DNA-Pkcs between the IF and western blot data could be the different phosphorylation sites targeted for each assay (serine S2056 used for western blot and threonine 2609 for IF). These two phosphorylation sites are within distinct regions of DKA-PK corresponding to the ABCDE (threonine) and PQR cluster (serine). Studies have shown that these two sites can be differentially phosphorylated. The ser-2056 phosphorylation is a an autophosphorylation event while thr-2609 phosphorylation can occur via DNA-PK and ATM following IR (Chen *et al.*, 2005, 2007). This could therefore explain some of the differences observed between the IF and western blot datasets.

From the collective ouabain data, we believe the variances in the Ouabain sensitivities are a result of growth differences between the fast-dividing STEM and the slower growing BULK cultures. Akin to the ouabain responses, we also observed STEM cultures having increased resistance to TMZ, AZD6738 (ATRi) and 1775 (WEE1i); figure 4.15. We therefore propose a model where the STEM population of cells are cycling quicker, accumulating more DNA damage and therefore are encountering more cell cycle checkpoints resulting in cell death, whereas the BULK cells are still accumulating DNA damage (supported through increased

levels of γ-H2AX and a-PAR) but are dividing much slower, have lower checkpoint activation possibly due to cell residing in G0 phase, and therefore are appearing more drug resistant.

Intriguingly from the BULK/ STEM heatmap (figure 4.15) we observed increased sensitivity of BULK culture cells to MEK1/2 inhibition by selumetinib, alongside reduced sensitivity to BRAFi by dabrafenib. Ouabain has been shown to inhibit levels of p-Akt and mTOR in established glioblastoma cells (Yang *et al.*, 2018), making both selumetinib, dabrafenib and ouabain possible inhibitors of both Ras/Raf/MEK/ERK and PI3K/PTEN/Akt/mTOR pathways respectively, which are both frequently deregulated in cancer. Within melanoma approximately 50% of patients harbour a BRAF mutation, selective BRAFi such as dabrafenib were developed for the treatment of the most common BRAFV600E mutation (Akbani *et al.*, 2015). Initially these BRAFi showed promising results, however this remained short lived due to drug resistance. One mechanism in which these tumour cells develop resistance is through overactivation of alternate PI3K pathway (Shi *et al.*, 2014; Van Allen *et al.*, 2014).

It has been suggested patients with brain metastases can develop resistance to BRAFi through ERK and PI3K activating extrinsic factors in cerebral spinal fluid (CSF). A study demonstrated that the *in-vitro* efficacy of BRAFi is dramatically reduced in the presence of CSF, suggesting CSF contains various growth factors and cytokines, some of which are reported to activate ERK/MAP kinase signalling in a Ras-dependent manner (Seifert *et al.*, 2016). In addition, cotreatment with PI3K kinase inhibitor was able to restore the cell killing. The observed differences in BULK/STEM survival could therefore also be a factor of increased reliance on individual pathway, promoted through growth factors specific to the BULK and STEM cell enriching media. Future work could investigate signalling pathways following selumetinib (MEK1/2 inhibition), dabrafenib (BRAF inhibition) and ouabain treatment, or similar to the study by Seifert et al investigate the possibility to induce cell death via drug co-treatment, targeting both pathways.

Previous studies have shown ouabain to induce DNA damage within osteosarcoma cell line, comet assay and DNA electrophoresis revealed that ouabain induced DNA breaks and fragmentation. Authors reported the dose dependent increased phosphorylation of several DDR proteins such as ATM, ATR, p53, γ-h2ax, mediator of DNA damage checkpoint (MDC-1),

PARP and BRCA1 following ouabain treatment (Chou *et al.*, 2018; Yang *et al.*, 2021). The issue however with this study is the long-time frame (48 hour) in which the cells were incubated with ouabain before being analysed. It is difficult to assume these effects were a direct result of ouabain, and more likely an indirect effect on DNA and altered DDR due to chronic ouabain exposure. Following our 1-hour incubation with ouabain we saw minimal DDR effects, there was only a slight induction in γ-H2AX, Rad51 and p-ATM (within the STEM cells). Future work would be useful to investigate the DDR following an extended time course experiment with ouabain. Additionally, as the heatmap in figure 4.15 highlights, the BULK cultures are increasingly sensitive to the radiomimetic drug bleomycin, it would also be interesting to assess the radiosensitivities of the BULK and STEM cultures following IR treatment and whether low doses of ouabain could sensitize either of the BULK or STEM towards IR treatment, as previous studies have highlighted the radiosensitizing ability of cardiac glycosides not only within glioblastoma but also NSCLC (J. Y. Lee *et al.*, 2017).

Difficulties in treating the highly drug resistant and plastic GSCs has led to other strategies, such as promoting GSCs into differentiation, thus making them easier to treat through loss of proliferative potential and self-renewal capacity. Multiple studies have demonstrated this is possible using ouabain and other cardiac glycosides, promoting the inhibition of HIF-1. HIF is a heterodimeric transcription factor that consists of HIF-1α, HIF-2α and HIF-1β subunits. HIF regulates the expression of hundreds of genes in response to hypoxic environments including VEGF, essentially promoting angiogenesis, cell survival and motility (Kaur *et al.*, 2005). A study by Lee et al demonstrated the ability of cardiac glycoside digoxin to inhibit HIF-1α protein expression, but also dramatically reduce GSC marker expression (CD133, nestin, Bmi-1 SOX2, Olig-2 and Oct4) and increased differentiation marker expression (GFAP and Tuj1) both at the protein and mRNA level (D. H. Lee *et al.*, 2017). Another study using ouabain (Yang *et al.*, 2018) has shown that as a monotherapy, it can repress AKT/mTOR signalling and expression of HIF-1α and its treatment resulted in reduced cell viability and cell migration within established U87 glioblastoma cells, however no causative link was made. This data suggests that ouabain may be inhibiting the STEM population via inhibition of HIF-1 pathway, which the differentiated BULK cultures are less reliant upon, as inhibition of HIF-1α promotes differentiated cell phenotype.

What initiated the investigation into comparing the drug responses of the STEM and BULK cultures is the lack of agreed culture media and supplementation standard for glioblastoma cultures, this absence of consistency is reviewed by Ledur et al (Ledur *et al.*, 2017). This review highlighted animal origin serum, FBS, as the most commonly used growth factor supplement. The clinical relevance of FBS is questionable when working with glioblastoma, firstly the protein composition of FBS is very distinct and most serum proteins are unable to cross the BBB (Reiber, 2001), secondly it is animal derived, and similar with Matrigel/Cultrex it is notorious for large batch variation of its components. Following the identification of GSCs, it raised questions regarding suitability as it induces the differentiation of NSCs. Similar to our findings comparing drug responses of cells exposed to serum-media and NSC promoting media, studies comparing the latter and oligodendrocyte promoting media have also highlighted differential drug responses, including sensitivity to SoC TMZ (Ledur *et al.*, 2016). Whilst we believe it is important to study the drug responses in all glioblastoma cell populations alternatives to FBS are required, one possible alternative is the patient's own serum obtained from blood samples, whilst it is not a perfect model of CSF *in-vivo*, it is still more clinically relevant than FBS.

Finally, hypoxia has been described as essential for the maintenance of GSC, promoting cell survival, motility and angiogenesis. Glioblastoma tumours frequently exhibit elevated oxygen levels in proximity to the perivascular space, in contrast to hypoxic, nutrient-deprived, necrotic regions (Calabrese *et al.*, 2007; Mohyeldin, Garzó N-Muvdi and Quiñ Ones-Hinojosa, 2010). Evans et al measured oxygen levels within glioblastoma and defined mild hypoxic regions ranging from 0.5-2.5%, moderate ranging from 0.1-0.5% and severe as 0.1% oxygen or less, they also showed severity of hypoxia was associated with increasing tumour grade (Evans *et al.*, 2004, 2008). This highlights another potential path for future development of our glioma ex vivo screening platform, as our current incubation involves oxygen levels at 20%, much higher than *in-vivo* levels. It may therefore be useful to explore differential drug responses within much lower, more clinically relevant oxygen levels aimed at specifically targeting GSC niches that are believed to be responsible for drug resistance and tumour recurrence. Targeting of such niches within our ex vivo drug screening platform is further explored in the following chapter.

Chapter 5 - Further optimisation of ex vivo drug screening for glioblastoma

5.1 Introduction

To provide proof of concept for ex vivo screening, it is important we can predict treatment response from patients using our screening platform. Depending on the age and health of the patient they will receive maximal resection surgery, followed by RT and concomitant and adjuvant chemotherapy with TMZ, which was approved in 2005 when it showed to increase patients median OS from 12.1 months to 14.6 in multi-centre clinical trials (Stupp *et al.*, 2005). Patients with glioblastoma can be separated into two main cohorts based on the *MGMT* gene promoter methylation status present within the tumour. Patients whose tumour presents with epigenetic silencing of the *MGMT* DNA repair gene through promoter methylation, respond better to TMZ treatment leading to improved survival rates (Hegi *et al.*, 2005). Despite this knowledge, patients are treated with TMZ irrespective of *MGMT* gene methylation status, and as such, it is important that other treatment regimens are designed for patients who have proficient *MGMT* expression as they do not statistically benefit from SoC drug TMZ. Additionally, there are issues regarding the poor localization of TMZ to the brain. Microdialysis techniques have been used to quantify the tissue concentration of systemically administered therapeutic agents in human brain tumours. Only 20% of SoC drug TMZ plasma concentration was shown to reach the brain tissue (around 1-5mM) with multiple factors including the permeability of the BBB, circulation of the brain tumour and short half-life affecting localised bioavailability (Pitz *et al.*, 2011). Again, this emphasizes the importance of ex vivo screening to find more suitable effective treatments for all glioblastoma patients, irrespective of *MGMT* promoter methylation.

Given that the GSC population is inherently drug resistant and responsible for tumour recurrence, it is important to try and identify potential GSC-specific compound cytotoxicity. Therefore, it is necessary to identify robust IF markers to discern microscopically between cancerous and healthy tissue, to identify compounds that exhibit GSC-specific cytotoxicity. With respect to glioblastoma this is challenging, primarily due to the lack of definitive cell markers. Both normal NSCs and GSCs share the same biological characteristics including their expression of neuronal or glial markers such as CD133, CD15 and intergrin-a6 (Brescia,

Richichi and Pelicci, 2012). The overlap between NSC and GSC suggests that GCS are a result of malignant mutations within NSCs. Therefore, precaution should be made when selecting drugs which target the stem cell population.

Additionally glioblastoma cells are highly plastic, differentiation is reversible and differences between these GSC-like states and differentiated-like states is minimal (Yabo, Niclou and Golebiewska, 2022). GSCs use environmental cues to adapt to dynamic microenvironmental conditions, essentially, they can act like a switch going back and forth from a stem like state to differentiated. The 'Go or Grow' theory stipulates that these GSCs can alter their behaviour to either highly proliferative or highly infiltrative depending on external stimuli (Oliveira *et al.*, 2017). Indeed, we have demonstrated this within our Cx18 differentiated 'BULK cells which have shown the ability to re-express stem cell markers based on their culture conditions (see figure 5.18 later in this chapter).

Another factor leading to irregularities within glioblastoma research is the universal agreement on cellular growth conditions. Ideally a growth media is required which best recapitulates the tumour environment and reduces genetic drift. Neurobasal media was developed for the culturing of neurones, similar to DMEM however contained lower levels of glutamine and reduced osmolarity, it also contains specific growth factors (EGF & FGF) which have been evidenced to enrich for cancer stem cell populations. Whilst growth media containing serum can induce differentiation of these stem-like cells. As mentioned above, there is no universally established marker for these GSC populations, therefore the most used markers within the existing literature were tested within both GSC promoting 'STEM and serum containing 'BULK growth conditions to show that either cell state can be enriched for based on the growth conditions. The data presented in this chapter builds on the initial set up of the ex vivo glioma screening platformed detailed in Chapter 3, in order to further develop and refine this tool as part of future NHS-based proof-of-concept observational trials and eventual interventional ex vivo trials.

5.2 Recapitulating Irradiation Response

In order to replicate irradiation in the clinic we have optimised both our caesium irradiation source up to 10Gy and correlated this with the radiomimetic drug bleomycin (figure 5.1). This can be used as a replacement when an experimental IR source is unavailable, which may be the case for a large number of research laboratories, and thus broadens the potential use of our ex vivo screening platform to other centres as part of our efforts to reduce/replace the use of murine PDX models. Additionally, bleomycin use as an alternative to IR in an ex vivo screening format is also beneficial as it can be added as a combination drug to specific drug wells, rather than irradiating the entire drug plate when using a caesium source. Investigation of Cx18 dose responses to both IR and bleomycin showed 2Gy (clinically relevant dose) is equal to 1.25 µM bleomycin (figure 5.1).
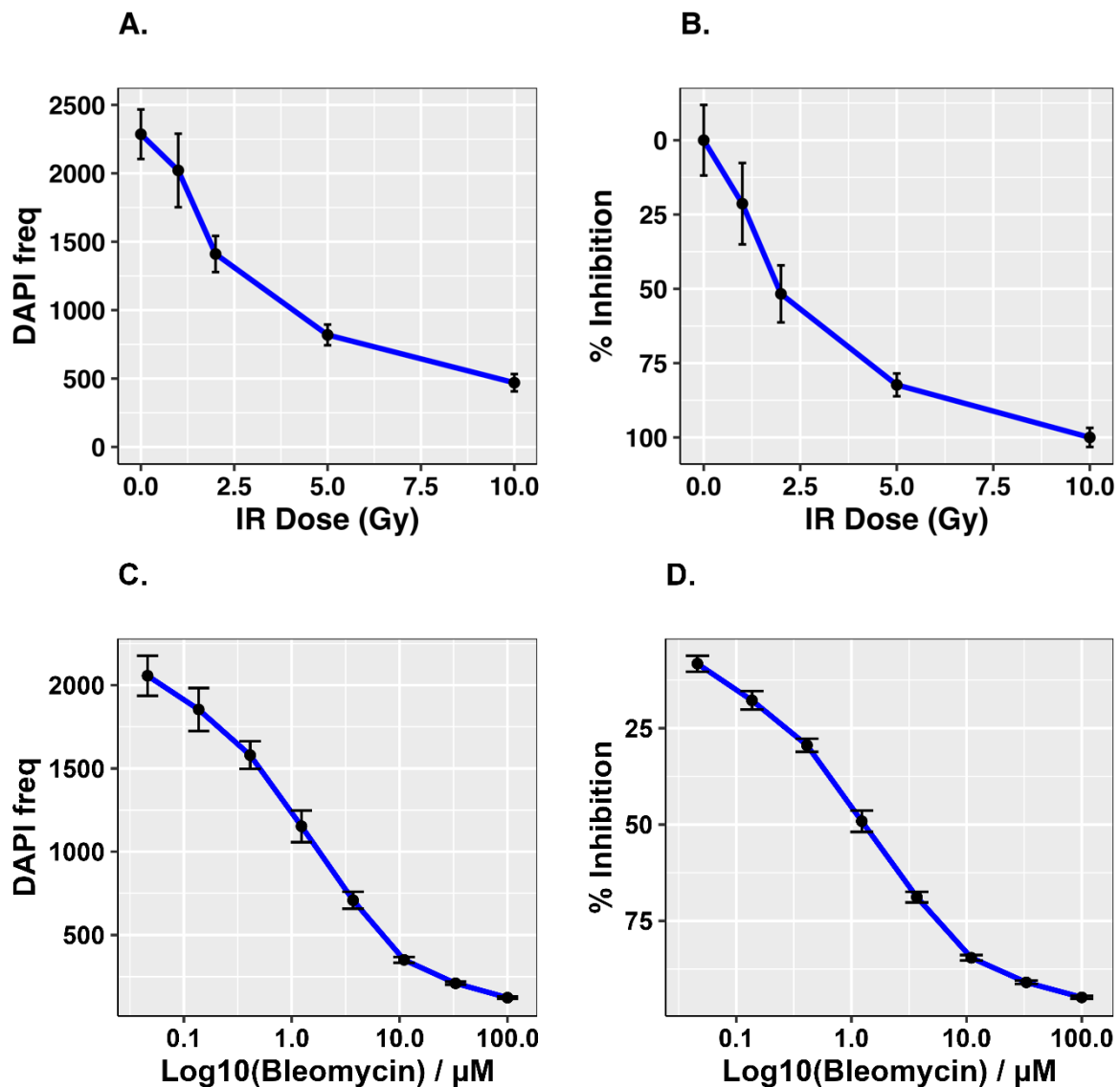
Figure 5.1 - Cx18 dose response curves for IR and bleomycin showing both cell frequency measured using DAPI positive cells and calculated % inhibition - **A.** IR sensitivity using raw DAPI cell counts **B.** IR sensitivity represented by % inhibition **C.** Bleomycin sensitivity using raw DAPI cell counts **D.** Bleomycin sensitivity represented by % inhibition. The response readout (DAPI count) was collected using automated IF microscopy, the counts were normalized using positive and negative controls on each dose plate to provide the response measure (relative inhibition %). Bleomycin IC_{50} = 1.25 µM equal to 2Gy IR. Error bars represent standard deviation. Biological repeats = 3, technical replicates = 4.

5.1 Investigating Temozolomide half life

Initial analysis of ex vivo screening data revealed the SoC drug TMZ exerting no effect on the cell counts of samples (Chapter 3, heatmap figure 3.15). Figure 5.2 shows the GBM sample responses to TMZ for 18 different clinical samples and two multi-regional matched primary GSC cell lines, Cx18 and Ox5 (derived from an *MGMT* +ve and an *MGMT* -ve tumour) depicted through AUC values. The samples are colour coordinated based on their *MGMT* methylation status which in theory should predict treatment response, showing methylated (green) with

lower AUC vales than unmethylated (red) samples, however this was not observed using the initial V01 GBM drug plates.
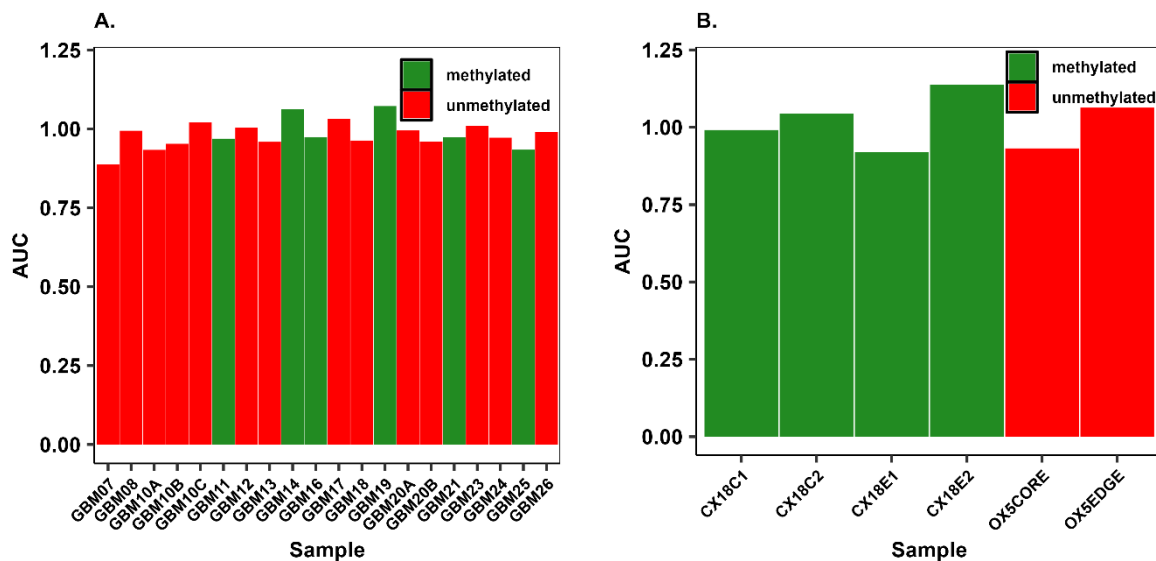
***Figure 5.2 - Evaluating the significance of MGMT methylation status on TMZ AUC response using V01 GBM drug plates -* A.** Freshly dissociated patient sample screening AUC data **B.** Primary GSC cell line screening AUC data. *MGMT* status was not correlated with response to TMZ treatment.

Previous work treating Cx18 cells with TMZ under different plating conditions confirmed that the doses used are within the correct dose range required to see a response to TMZ (chapter 3). To check whether the issue was regarding the TMZ potency on the original GBMV01 drug plates, fresh TMZ specific drug plates were made to screen cell lines Ox5 and Cx18 again, as shown in figure 5.3. It was possible to distinguish between the *MGMT* unmethylated Ox5 and methylated Cx18 C1 cell lines based on their differential responses to TMZ.

As noted above, only 20% of the TMZ concentration found in the blood plasma is transferred to CSF. It is postulated this is due to its short half-life, during its absorption within the gastrointestinal track and distribution within blood plasma, it has a half-life of 1.8h, when it spontaneously hydrolyses under physiological pH to MTIC it had an ever shorter half-life of 2 min (Beale *et al.*, 1999). It is known from the literature that TMZ used in experimental systems is used at physiologically high range of 100 – 4000 µM (Strobel *et al.*, 2019), which is not in the clinical range estimated between 14.95-34-54 µM (Rosso *et al.*, 2009). However, the dosing regimens within *in-vitro* experiments often use a single dose of TMZ, as a surrogate for multiple doses used in the clinic.

A. | **B.**
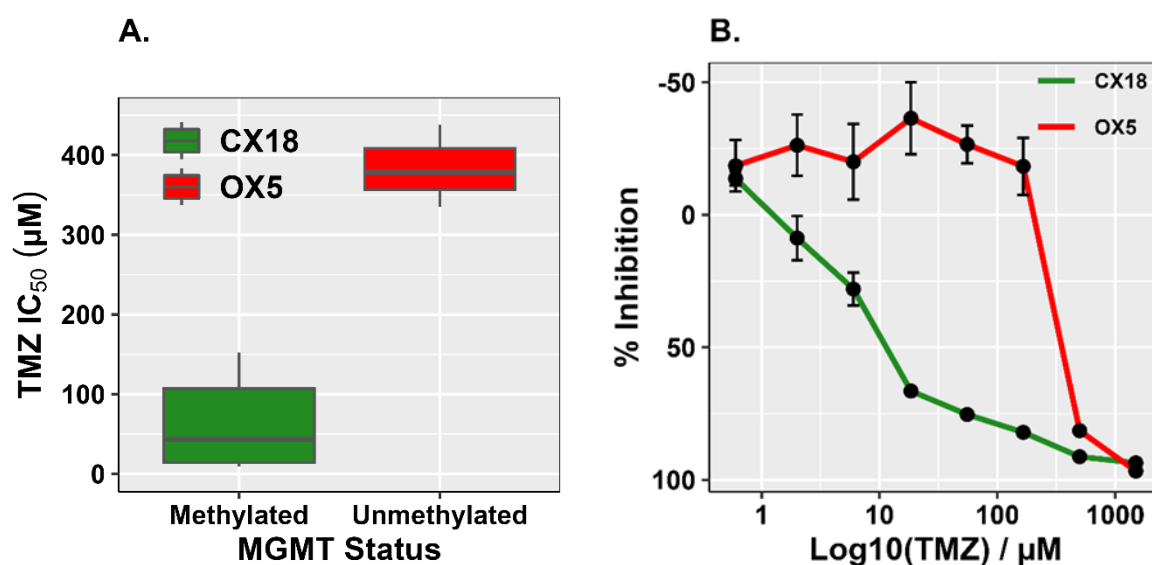
*Figure 5.3 - MGMT status was able to predict TMZ treatment response in MGMT methylated and unmethylated cell lines Cx18 and Ox5 - **A.** Boxplot depicting IC$_{50}$ values generated from Cx18 (green, *MGMT* methylated) and Ox5 (red, *MGMT* unmethylated) response to temozolomide. The central box of the boxplot displays the IQR, where the lower boundary corresponds to the first quartile and the upper boundary corresponds to the third quartile, the horizontal line within the box represents the median and the whiskers extend to the minimum and maximum values within 1.5 times the IQR. **B.** Temozolomide sensitivity represented by % inhibition. Error bars represent SEM. Mean ± SD IC$_{50}$ Cx18 = 63.5 ± 61.2 µM, Ox5 = 383.9 ± 51.8 µM. Biological repeats =3, technical replicates = 4.

Given the data shown in figure 5.3, it was postulated that the lack of TMZ response observed on the V01 drug plates was due to degradation of TMZ, because of its short half-life. When making up the batch of GBM V01 plates, drugs were thawed and reconstituted at the appropriate concentration in the evening and stored at 2-8°C ready for drug plate printing the following morning. To test this idea, TMZ specific drug plates were made fresh, one plate was seeded with cells immediately, the other two plates were seeded after overnight storage at 2-8°C or at -80°C, the drug response data for each of these plates is shown below (figure 5.4). Drug responses from plates stored at 2-8°C showed significantly higher IC$_{50}$ values (121.8 ± 16.0 µM) with increased standard deviation between repeats in comparison to the fresh (IC$_{50}$ = 14.4 ± 4.1 µM) and at -80°C (IC$_{50}$ 11.8 ± 1.9 µM) drug plates (figure 5.4). This showed that adding an extra freeze thaw cycle to stored drug plates long term had no effect on the efficacy of TMZ, as no significant difference between fresh and at -80°C storage IC$_{50}$ values. Storing plates at 2-8°C did however significantly affect the potency of TMZ and therefore should be avoided when storing drugs and drug plates for ex vivo screening.
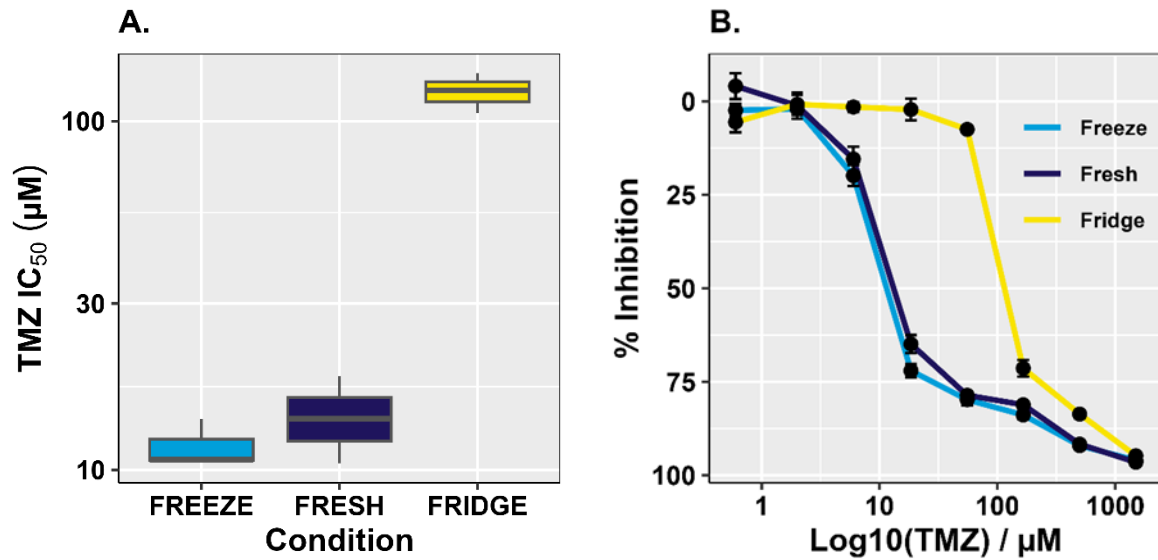
Figure 5.4 - Investigating the efficacy of temozolomide on Cx18 cells following different drug plate storage techniques, fresh, fridge or freezer - **A.** Boxplot depicting IC_{50} values generated from different plate storage techniques; Fresh, fridge, freeze. The central box of the boxplot displays the IQR, where the lower boundary corresponds to the first quartile and the upper boundary corresponds to the third quartile, the horizontal line within the box represents the median and the whiskers extend to the minimum and maximum values within 1.5 times the IQR. **B.** Temozolomide sensitivity represented by % inhibition. Mean ± SD IC_{50}: Freeze IC_{50} = 11.8 ± 1.9 µM, fresh IC_{50} = 14.4 ± 4.1 µM, fridge IC_{50} = 121.8 ± 16.0 µM. Error bars represent SEM. Biological repeats =3, technical replicates =4.

5.3 Correlating clinical data with ex vivo Temozolomide responses

Once the issues regarding TMZ had be resolved our aim was to correlate clinical data and ex vivo responses, to highlight the predictive power of ex vivo screening. To address this, we screened all available biobanked primary GSC cell lines using SoC drug TMZ with and without 2Gy IR. The dose response curves are shown in figure 5.5A and AUC values are summarised by the boxplot in figure 5.5B. When looking at TMZ monotherapy there was a distinct separation of patient sample responses, and upon adding *MGMT* methylation status retrospectively we observed separation of samples with regards to TMZ sensitivity as determined by *MGMT* gene methylation. Within the combination therapy there was not an obvious separation between the samples in the AUC, as individual patient radiosensitivity is now a contributing factor and thus masking TMZ sensitivity differences.
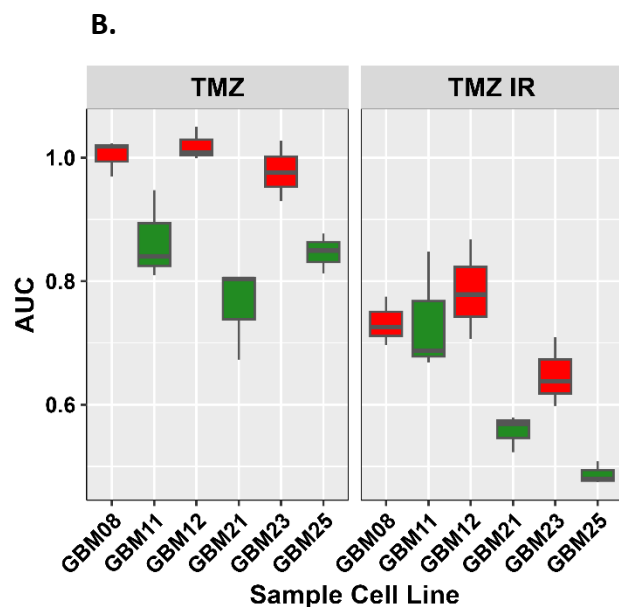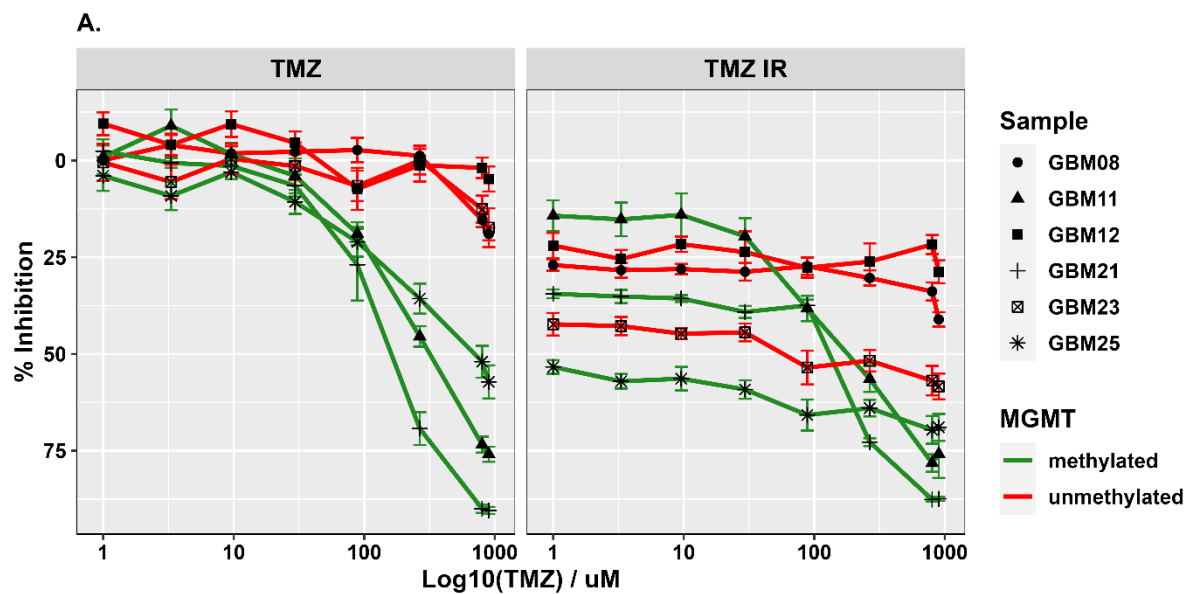
Figure 5.5 - Dose response profiles of patient sample derived cell lines following TMZ ± (2 Gy) IR treatment - A. Percent inhibition curves (calculated using equation 2.3), for 6 patient derived cell lines following treatment with TMZ monotherapy and TMZ & IR combination therapy. Error bars represent SEM. **B.** Boxplot displaying the AUC values generated from the repeated dose response curves for TMZ and TMZ & IR. The central box of the boxplot displays the IQR, where the lower boundary corresponds to the first quartile and the upper boundary corresponds to the third quartile, the horizontal line within the box represents the median and the whiskers extend to the minimum and maximum values within 1.5 times the IQR. Biological repeats = 3, technical replicates = 4.

5.4 Optimising Drugs for V02 plates

As mentioned above, the initial V01 drug plates were designed prior to any optimisation of drug IC_{50} values. For the second batch of drug plates (GBM V02), long range dose response analysis was performed for each individual drug which was not in the correct IC_{50} range on the original V01 plates, using cell lines Ox5 core and edge, (supplementary chapter 8, figure 8.1). This highlighted which drug concentration ranges needed to be adjusted for the second version of drug plates. Additionally, the issues with SoC drug TMZ efficacy was also investigated and amended (shown in previous section).

5.4.1 Sample end point analysis drug plate V02

For the second batch of updated GBM V02 drug plates three separate patient samples were screened, one of which was a model of heterogeneity GBM26 (A, B and C), the other was a single sample screened using both normal and extended incubation period GBM30 (4-day and 8 day) and finally a single GBM27 sample. The AUC values obtained from two technical replicates are shown in the heatmap diagram in figure 5.6. It is evident from the heatmap data, that hierarchical clustering is separating out GBM30 (8-day) drug responses from the other sample profiles.
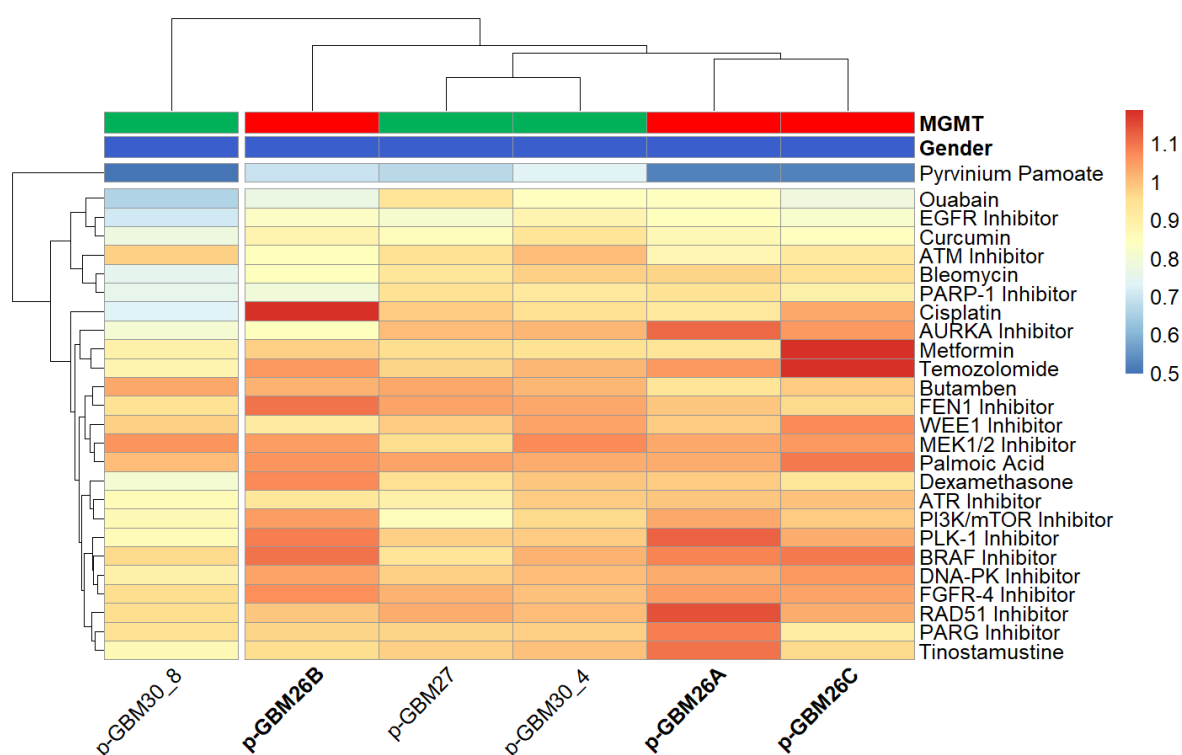
Figure 5.6 - GBM sample heatmap depicting raw AUC drug responses based on DAPI cell counts for primary GBMs dissociated from 3 individual patient tumours - Scale shown represents cell death as 0 (blue) and cell survival as 1 (red). Larger sample GBM26 (A, B and C) was sectioned into multiple regions and screened independently in order to highlight the intertumoral heterogeneity of the disease. AUC values were calculated from 2 technical replicates following 96hr drug incubations using R package GR metrics and the heatmap was constructed using R package pheatmap as detailed in the methods section. Note, due to the fact that this was performed on limited fresh clinical material, biological repeats were not performed.

Next, we normalised the AUC values by drug using pheatmap package built in z-scale feature, as this allows easier interpretation and comparison between the samples. As anticipated the *MGMT* methylated samples GBM30 and GBM27 show a heightened inhibitory response to TMZ treatment, in comparison to the other *MGMT* unmethylated samples (figure 5.7).
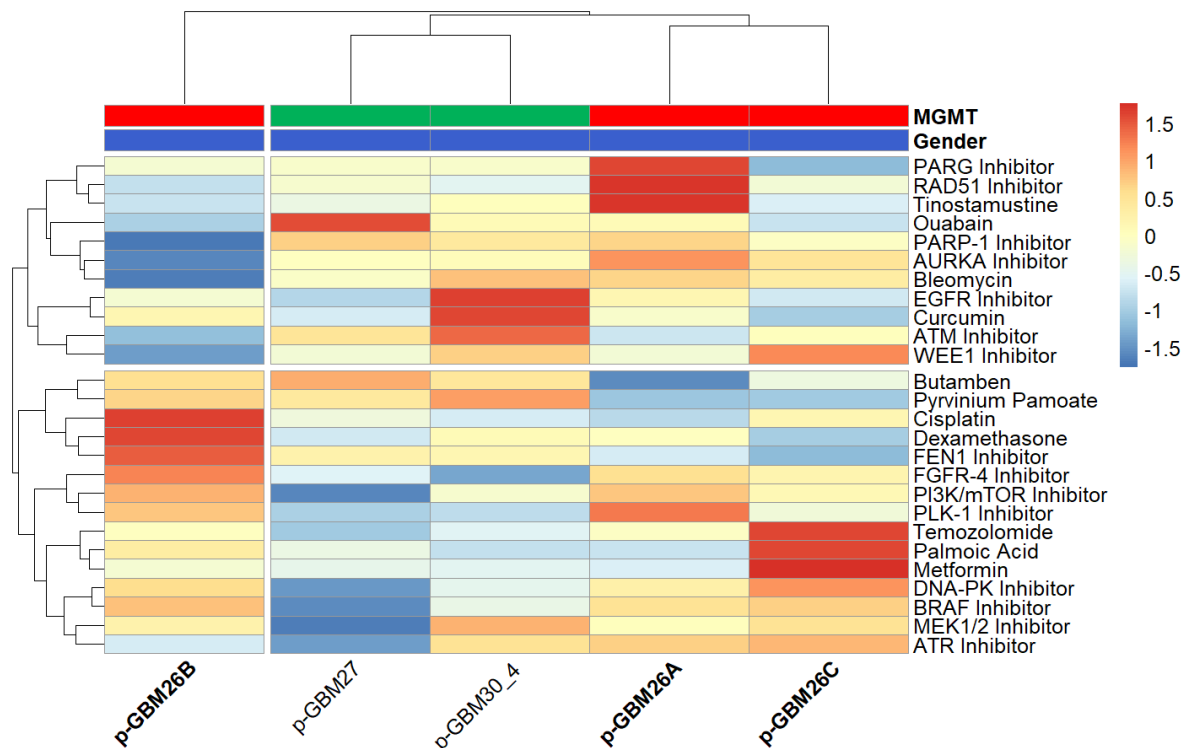
Figure 5.7 - GBM sample heatmap depicting scaled AUC drug responses based on DAPI cell counts for primary GBMs dissociated from 3 individual patient tumours - Scale shown represents cell death as 0 (blue) and cell survival as 1 (red). Larger sample GBM26 (A, B and C) was sectioned into multiple regions and screened independently in order to highlight the intertumoral heterogeneity of the disease. AUC values were calculated from 2 technical replicates following 96hr drug incubations using R package GR metrics and the heatmap was constructed using R package pheatmap as detailed in the methods section, values were scaled using the in-built z-scale function. Note, since this was performed on limited fresh clinical material, biological repeats were not performed.

Following this, the AUC responses of GBM30 following a 4-day and 8-day incubation period were compared, shown in figure 5.8 below. From this heatmap we can see much lower AUC values for over half of the drugs within the library. Of particular importance is the response to TMZ, despite being a methylated *MGMT* sample, the GBM30 4-day response is minimal, however when we extend the assay to 8-days we can see TMZ exerting a larger killing effect. We know that these samples have minimal growth over the 4-day period and therefore by doubling this time it allows drugs to exert more cell death through cell cycle-mediated mechanisms. Conversely, we observed that the cells are not dying as a result of the prolonged incubation period, we can see drug responses from MEK1/2 down to BRAF, AUC values are 1 and above suggesting the cells are proliferating within these drug wells, relative to DMSO control wells. Moving forward we will carry on trialling both incubation periods in parallel, as

not all samples may be suitable for the prolonged 8-day protocol depending on the mechanism of action and cell growth/doubling rates.
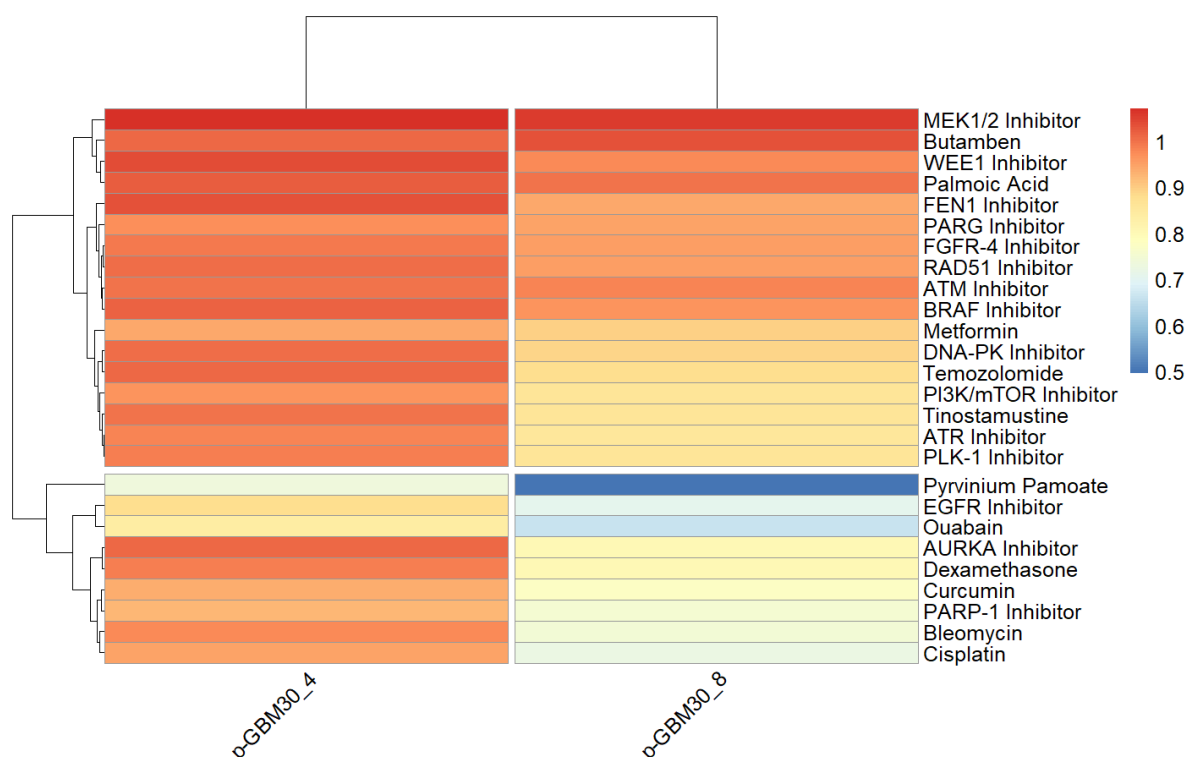
Figure 5.8 - GBM sample heatmap depicting raw AUC drug response for primary GBM30, testing a 4-day and 8-day incubation period - AUC values were calculated from 2 technical replicates following 96hr drug incubations using R package GR metrics and the heatmap was constructed using R package pheatmap as detailed in the methods section. Note, since this was performed on limited fresh clinical material, biological repeats were not performed.

5.4.2 Measuring assay quality using z-prime

Next, the z-prime values for our V02 GBM drug plates were calculated and assessed, the raw data from which these z-prime values were calculated are shown within table 5.1 for long term primary cell line cultures, and table 5.3 for freshly dissociated patient samples. Investigation of the z-prime values highlighted that 10/11 of primary GSC models screened using updated V02 plates had Z-prime values above 0.5, highlighting these drug plates are robust (figure 5.9A). Figure 5.9B shows a comparison between 6 primary GSC models screened both using V01 and updated V02 drug plates, with 5/6 of these cell lines exhibiting an improvement in the z-prime value using the V02 plates. Similar to data shown in chapter 3 for the V01 drug plates, the z-prime values for the freshly dissociated samples are not as robust as the cell lines (figure 5.9C), 3/6 of these samples had z-prime values about zero. Promisingly, extending the assay timeframe from 4-day to 8-days using GBM30 increased the

z-prime value. Upon investigation of the raw data from both version plates (data shown in table 5.2 below) either the standard deviations for both positive and negative controls are reduced or the DMSO counts are significantly higher than staurosporine for the V02 plates.

A.

B.

C.
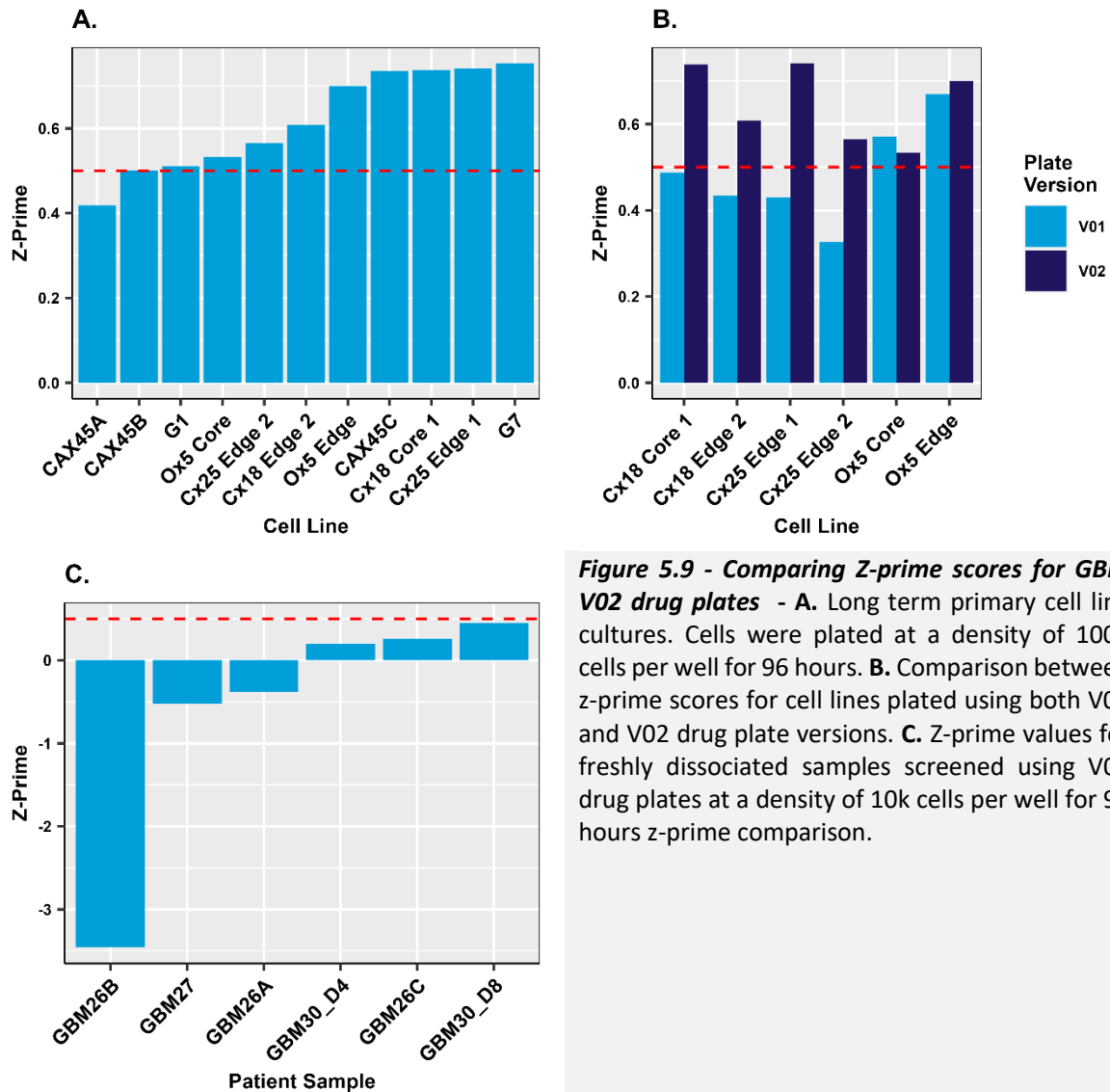
Figure 5.9 - Comparing Z-prime scores for GBM V02 drug plates - **A.** Long term primary cell line cultures. Cells were plated at a density of 1000 cells per well for 96 hours. **B.** Comparison between z-prime scores for cell lines plated using both V01 and V02 drug plate versions. **C.** Z-prime values for freshly dissociated samples screened using V02 drug plates at a density of 10k cells per well for 96 hours z-prime comparison.

Table 5.1 - Control means and SD values used for calculation of z-prime scores for long term primary cell line cultures screened using GBM V02 plates

Cell Line	Mean DMSO	DMSO SD	Mean STAU	STAU SD
CAX45A	1265	238	13	5
CAX45B	663	77	39	27
G1	1751	278	20	5
Ox5 Core	900	129	44	4
Cx25 Edge 2	915	124	17	6
Cx18 Edge 2	858	103	43	4

Ox5 Edge	1077	98	16	9
CAX45C	1239	97	29	10
Cx18 Core 1	2092	168	43	11
Cx25 Edge 1	1548	128	21	4
G7	1906	154	9	2

Table 5.2 - Comparing the z-prime and COV values for cell lines screened using V01 and V02 plates.

Cell Line	Plate Version	Z-prime	DMSO COV (%)
Ox5 Core	V01	0.57	12.0
Ox5 Core	V02	0.53	14.4
Ox5 Edge	V01	0.67	9.8
Ox5 Edge	V02	0.70	9.1
Cx18 Core 1	V01	0.49	16.3
Cx18 Core 1	V02	0.74	8.1
Cx18 Edge 2	V01	0.43	18.5
Cx18 Edge 2	V02	0.61	12.0
Cx25 Edge 1	V01	0.43	18.2
Cx25 Edge 1	V02	0.74	8.3
Cx25 Edge 2	V01	0.33	20.5
Cx25 Edge 2	V02	0.57	13.6

Table 5.3 - Control means and SD values used for calculation of z-prime scores for freshly dissociated patent samples screened using GBM V02 plates

Patient Sample	Mean DMSO	DMSO SD	Mean STAU	STAU SD
GBM26B	220	57	133	73
GBM27	354	62	170	32
GBM26A	832	193	187	104
GBM30_D4	3494	388	1506	145
GBM26C	694	107	140	31
GBM30_D8	2187	194	682	83

5.5 Bulk vs Stem Cell Marker Expression

5.5.1 RNA & Protein Expression

We initially investigated the levels of commonly used stem cell markers CD133, nestin and SOX2 and differentiation marker GFAP between 'BULK and 'STEM cultured cell lines at the RNA level using RT-qPCR. To confirm that the most commonly used stem cell markers can be enriched for using specific growth conditions, and as a validation for our IF data, RT-qPCR was performed on bulk and stem cell populations to assess the levels of RNA of each individual marker (figure 5.10). It was hypothesised that we would see elevated levels of all GSC markers at the protein and RNA level in cells cultured in STEM promoting media, versus those cultured

in BULK media which promotes differentiation. As anticipated, the data shows significant increases in the RNA expression levels of all three GSC markers in the STEM cell populations relative to the BULK. This confirms that the *in-vitro* culture conditions we have adopted are sufficient to enrich and maintain GSC populations based on these markers and is consistent with previous findings from other groups (Gomez-Roman *et al.*, 2017). Unexpectedly, the expression of GFAP, a marker of differentiation, which we therefore would predict to be more highly expressed in the serum containing BULK cell populations, also showed increased expression levels in STEM populations (figure 5.10).
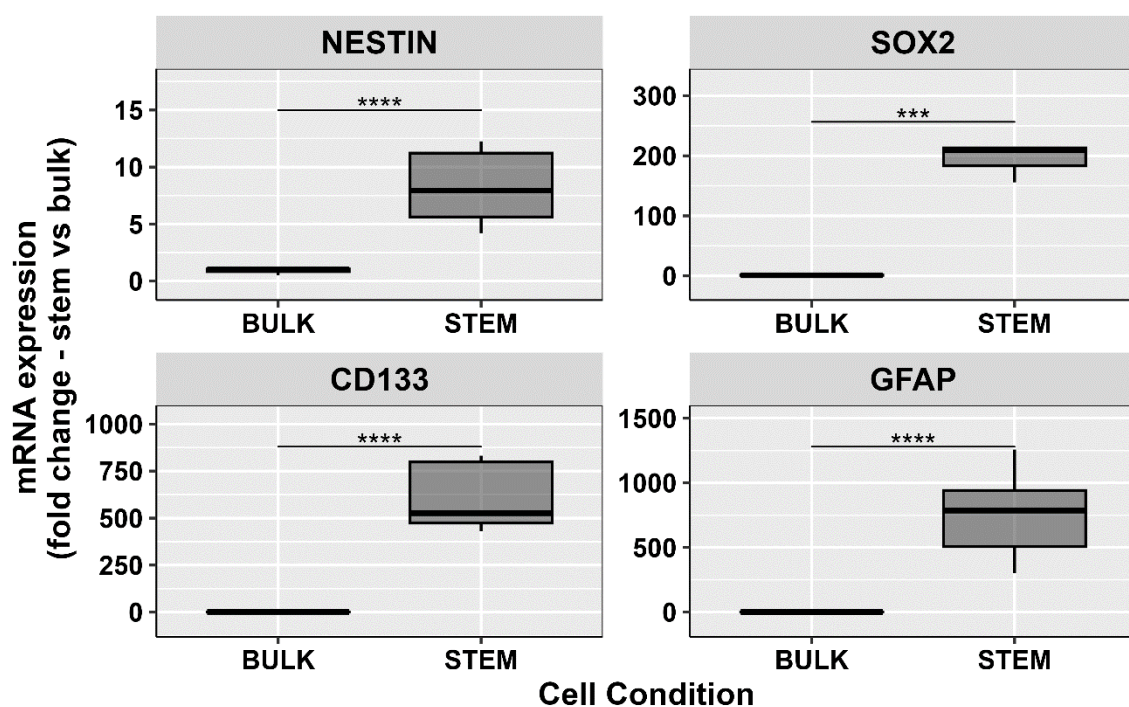
Figure 5.10 - Cx18 mRNA expression of GSC markers nestin, SOX2 CD133 and differentiation marker GFAP within two model growth conditions STEM and BULK - Expression levels of all three GSC markers mRNA were higher within the Cx18 model STEM cell populations compared to the BULK. The central box of the boxplot displays the IQR, where the lower boundary corresponds to the first quartile and the upper boundary corresponds to the third quartile, the horizontal line within the box represents the median and the whiskers extend to the minimum and maximum values within 1.5 times the IQR. Data represents mean ± SEM (***P<0.0005). Significance was calculated using the Mann-Whitney-U test. Biological repeats = 3, technical replicates per biological repeat = 3.

To further corroborate the RT-qPCR data shown above, immunoblot analysis was performed on the cell lysates growth in both BULK and STEM media. . Analysis of the protein expression of GSC markers nestin, SOX2 and differentiation marker GFAP are show in figure 5.11. The levels of both GSC markers (nestin and SOX2) were elevated within the STEM cultures versus the BULK, suggesting these may be robust markers for GSC expression. Unexpectedly we also

saw higher levels of the differentiation marker GFAP in the STEM cultures versus the BULK. We were unable to measure the CD133 protein levels through western blotting due to nonspecific antibody binding.
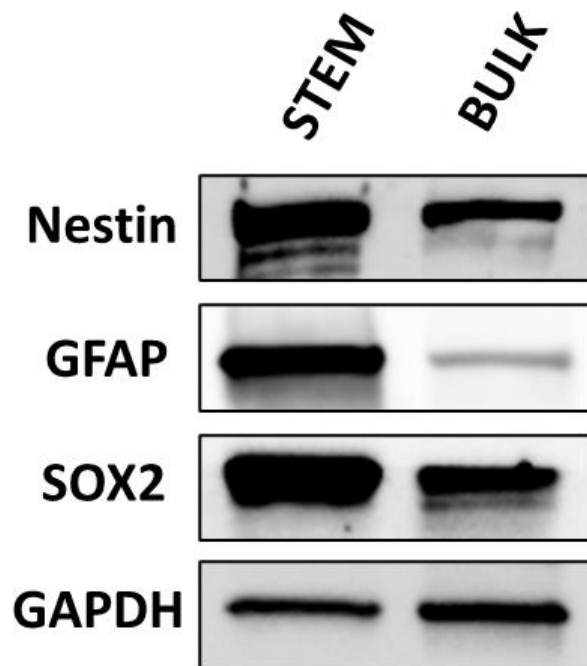
Figure 5.11 - Analysis of GSC and differentiation makers via Western blotting - Cx18 CORE 1 cells cultured in both STEM and BULK media for a minimum of 5 passages were lysed for western blotting. Membranes were probed for the GSCs markers nestin and SOX2 and differentiation marker GFAP. GAPDH was used as a loading control. Biological repeat = 1.

5.5.2 Immunofluorescence Antibody Optimisation and staining

In addition to the RT-qPCR data shown above, Ox5 edge cells which have previously been shown by the Collis laboratory to exhibit high levels of GSC marker expression (unpublished), were used to optimize conjugated GSC marker antibody staining protocols for CD133 and nestin. Such staining is planned for future ex vivo procedures to determine drug efficacy specificity in GSC niches (the population strongly suspected to drive tumour resistance and regrowth fowling current treatment regimens). Conjugated antibodies were used as opposed to sequential primary and secondary protocols to reduce washing steps following fixing of drug plates, to retain the whole cell population.

Three concentrations (1:1000, 1:500, 1:250) of both antibodies alongside DAPI 1:1000 was added to fixed OX5 edge cells and left overnight in the dark at 4°C. Figure 5.12 displays from left to right the merge image of both nestin (displayed in red) and CD133 (displayed in green), CD133 alone, nestin alone, DAPI alone, nestin and DAPI merged and finally all three merged. There was a more noticeable change in intensity for the CD133 at the different dilutions,

1:500 was selected for further experiments as 1:1000 was not as distinct whilst the 1:250 dilution was too intense. There was a less noticeable change in the intensity of the stains for the nestin antibody at all concentrations, despite this a 1:500 concentration was also selected as the staining appeared more distinct compared to the other dilutions tested (figure 5.12), based on viewing the images.
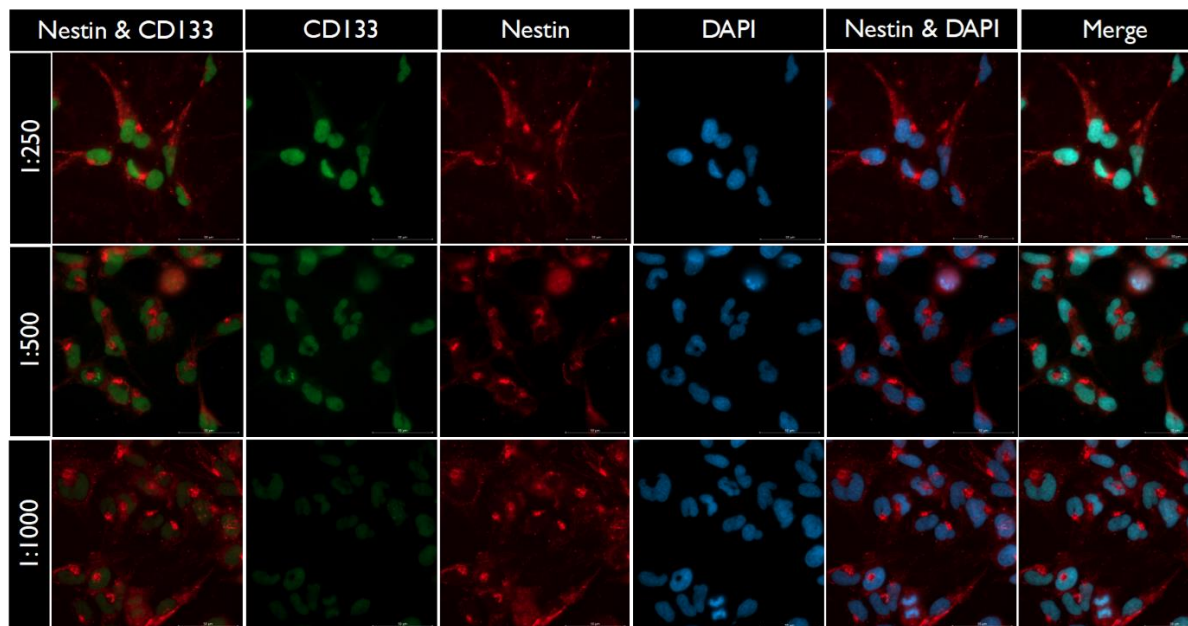
Figure 5.12 - Concentration optimisation of conjugated Nestin and CD133 IF cell markers using Cx18 stem cells - Representative images are shown for the indicated antibody staining at three different concentrations (1:1000, 1:500 and 1:250).

Using these optimised conditions, we then performed IF microscopy to compare GSC and differentiation marker expression within BULK and STEM cell cultures (figure 5.13-5.17). Staining of intermediate filament protein nestin within Cx18 BULK and STEM cultures is shown in figure 5.13. Nestin is expressed in NSCs and is a commonly used marker for GSCs (Bernal and Arranz, 2018). Nestin staining was present in both BULK (differentiated) and STEM (GSC) cell cultures, but to a lesser extent within the BULK, with lower staining intensity (figure 5.13). This supports the data from both RT-qPCR and immunoblotting whereby nestin expression was still present in the BULK cultures.
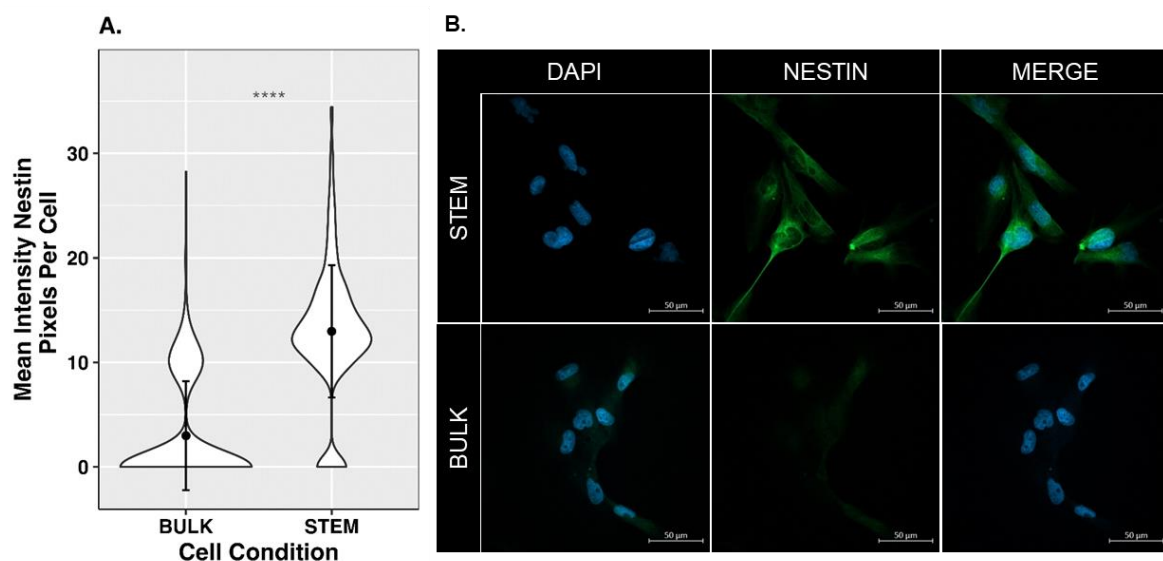
Figure 5.13 - IF expression of neuroepithelial stem cell protein nestin in Cx18 cells cultured in either BULK and STEM cell media - **A.** Comparing the mean intensity of nestin staining within both bulk and stem populations. **B.** Analysed IF images from BULK and STEM populations showing nuclear marker DAPI (blue), nestin (green) and merge channel image. Error bars represent SD around the mean. Statistical analysis was performed using Man-Whitney U test. Biological repeats = 3, each consisting of 100 cell images.

SOX2 is a transcription factor essential in the maintenance of embryonic and NSCs, it is involved in regulating cell fate decisions and is considered a robust marker for GSCs (Maria *et al.*, 2009). The SOX2 staining of Cx18 cells cultured in both BULK and STEM conditions is shown below in figure 5.14. Similar to nestin, SOX2 was also present in both cell culture conditions, however the intensity of the staining was much lower in the BULK population of cells.
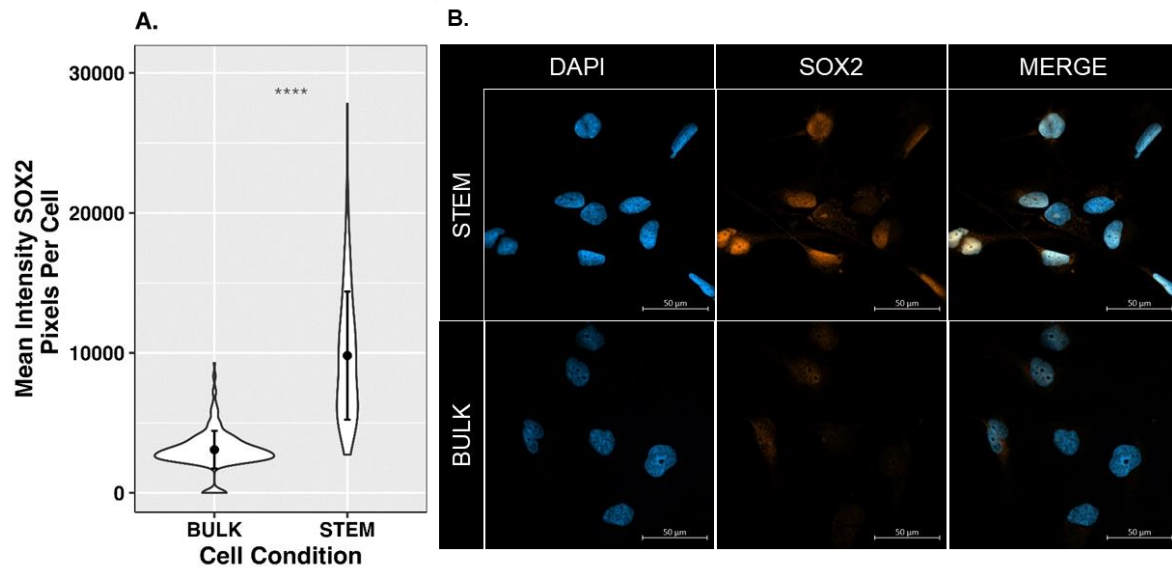
Figure 5.14 - IF expression of transcription factor SOX2 in Cx18 cells cultured in either BULK and STEM cell media - **A.** Comparing the mean intensity of SOX2 staining within both BULK and STEM populations. **B.** Analysed IF images from BULK and STEM populations showing nuclear marker DAPI (blue), SOX2 (orange) and merge channel image. Error bars represent SD around the mean. Statistical analysis was performed using Man-Whitney U test. Biological repeats = 3, each consisting of 100 cell images.

CD133 is a transmembrane protein, despite being a commonly used markers for GSCs, there remains lots of controversy regarding its use. Some studies have questioned the suitability of CD133 as an appropriate marker for GSC as they have found CD133 negative cells to also possess tumour initiating ability (Ludwig and Kornblum, 2017), suggesting CD133 is only a positive marker for a subset of GSCs. Staining of CD133 also known as prominin-1 (PROM1) or AC133 is shown in figure 5.15 below. Expression of this stem marker was evident in both culture conditions however, the STEM cell populations exhibited more staining within the nuclear and cytoplasmic regions, whereas the BULK cells exhibited less nuclear staining.
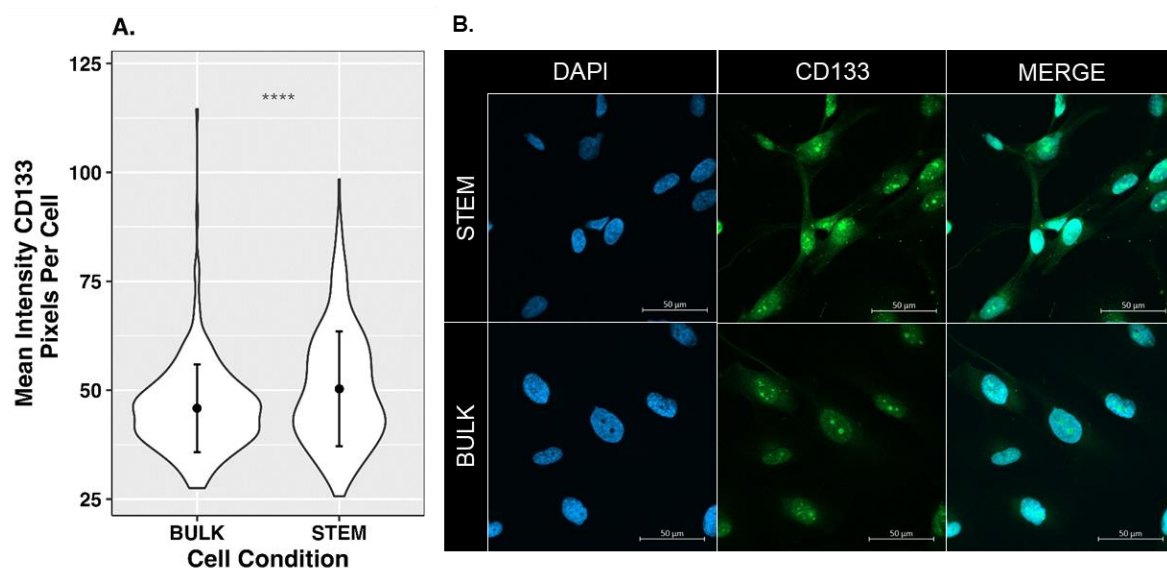
Figure 5.15 - IF expression of stem cell protein CD133 in Cx18 cells cultured in either BULK and STEM cell media - **A.** Comparing the mean intensity of CD133 staining within both BULK and STEM populations. **B.** Analysed IF images from BULK and STEM populations showing nuclear marker DAPI (blue), CD133 (green) and merge channel image. Error bars represent SD around the mean. Statistical analysis was performed using Man-Whitney U test. Biological repeats = 3, each consisting of 100 cell images.

Vimentin is a type III intermediate filament protein which is widely expressed within mesenchymal and undifferentiated cells and is involved in various cellular processes including migration, adhesion and signalling. Over recent years it has emerged as a potential marker for glioblastoma, as several studies have reported abundant expression in such cell populations (Nowicki *et al.*, 2019). It has also been reported that vimentin expression in glioblastoma cells correlates with poor patient outcomes (Zhao *et al.*, 2018). The vimentin staining of Cx18 BULK and STEM cultures is shown by figure 5.16, again there is not a complete depletion of this marker within the BULK cells, with the only difference is the intensity of the vimentin staining is slightly (albeit significantly) more pronounced in the STEM cell populations.
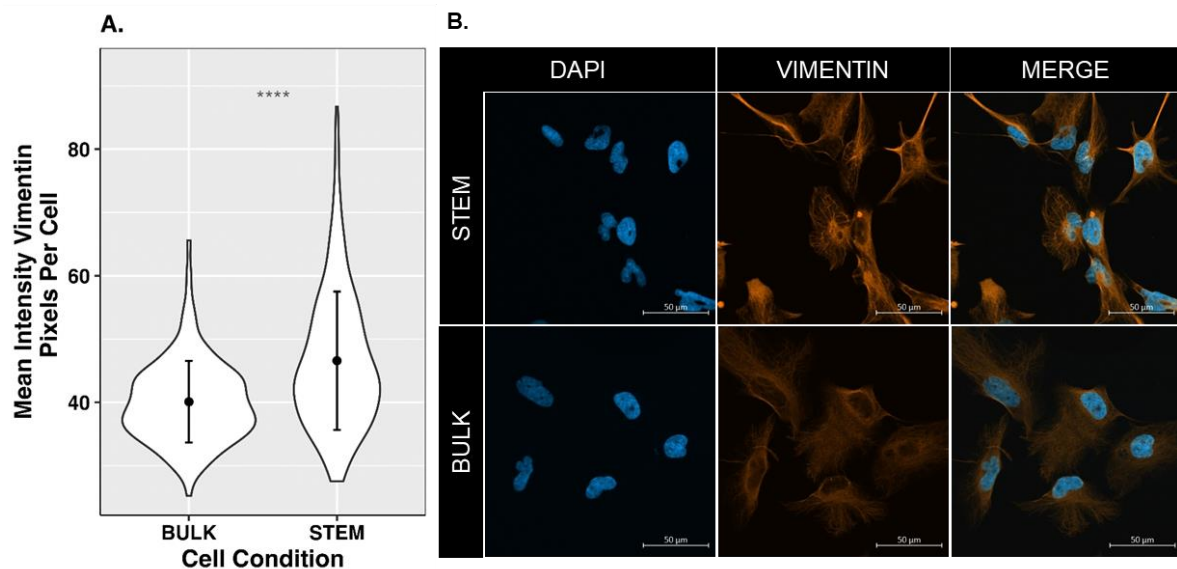
Figure 5.16 - IF expression of intermediate filament vimentin in Cx18 cells cultured in either BULK and STEM cell media - **A.** Comparing the mean intensity of vimentin staining within both BULK and STEM populations. **B.** Analysed IF images from BULK and STEM populations showing nuclear marker DAPI (blue), vimentin (orange) and merge channel image. Error bars represent SD around the mean. Statistical analysis was performed using Man-Whitney U test. Biological repeats = 3, each consisting of 100 cell images.

Similar to vimentin, GFAP is also a type III intermediate filament protein specific to mature astrocytes, but has also found to be expressed in foetal and adult NSCs (Hol and Capetanaki, 2017). Reactive gliosis also known as glial scar formation is an inflammatory response characterised by the overabundance of microglia and astrocytes characterised through GFAP overexpression, this reactive gliosis is usually following damage or disease of the CNS such as a patient suffering from neurodegenerative diseases, acute brain injuries, epilepsy and lower

grade astrocytoma. With regards to cancer, GFAP is commonly used to identify malignancies of glial cell origin such as astrocytoma or glioblastomas (Duffy, Huang and Rapport, 1982). Subjecting Cx18 cells to BULK media resulted in a complete depletion in the expression of GFAP, measured through IF staining depicted in figure 5.17.
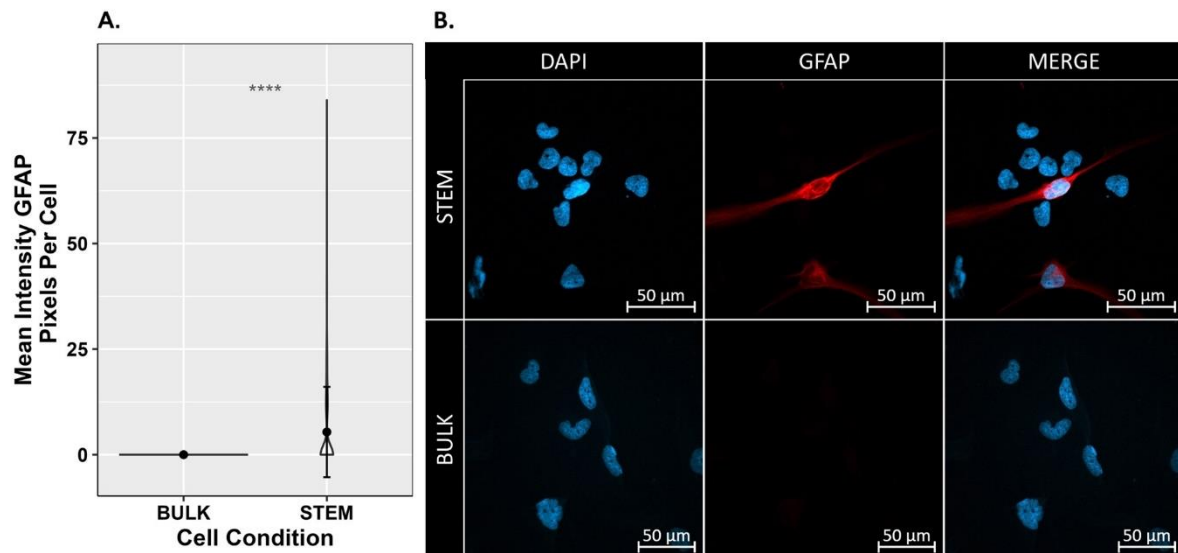
Figure 5.17 - IF expression of intermediate filament GFAP in Cx18 cells cultured in either BULK and STEM cell media - **A.** Comparing the mean intensity of GFAP staining within both BULK and STEM populations. **B.** Analysed IF images from BULK and STEM populations showing nuclear marker DAPI (blue), GFAP (red) and merge channel image. Error bars represent SD around the mean. Statistical analysis was performed using Man-Whitney U test. Biological repeats = 3, each consisting of 100 cell images.

In conclusion this data supports our hypothesis that STEM promoting media maintained the expression of commonly used GSC markers, we also showed this occurred at a higher in the STEM cultured cells when compared to matched BULK cultures. We confirmed this initially at the RNA level using RT-qPCR, and at the protein level through immunoblotting and IF staining. We did not however obtain expected results for the RNA and protein expression of the differentiation marker GFAP, which we saw at higher levels in the STEM culture cell populations. Suggesting this marker may not be a robust and suitable marker for differentiated GSC cultures.

5.5.3 Plasticity in GSCs

To highlight the highly plastic and interchangeable nature of these GSCs, investigation into the culture conditions was carried out. Cx18 BULK cells which had been subjected to minimum of 5 passages in BULK media, were switched back into their original STEM growth media for a minimum of 5 passages before being lysed for western blotting (named RE-STEM).

The western blot and RT-qPCR analysis of GSC and differentiation markers is shown in figure 5.18. Despite multiple passages in differentiating BULK medium, nestin protein expression was lower, but still present in the BULK cell populations. Reintroducing the cells back into STEM media allowed nestin expression to restore, almost back to its original level at the protein level (figure 5.18A). Whilst the mRNA levels of nestin between the BULK and RE-STEM cells showed no significant difference (figure 5.18B). Looking at the expression of SOX2 and GFAP, the western blotting data showed protein levels to be higher in the RE-STEM populations compared to the BULK, the mRNA levels further corroborated this data, as of both markers were significantly higher (both $p= 0.00379$) in the RE-STEM population of cells compared to the BULK.
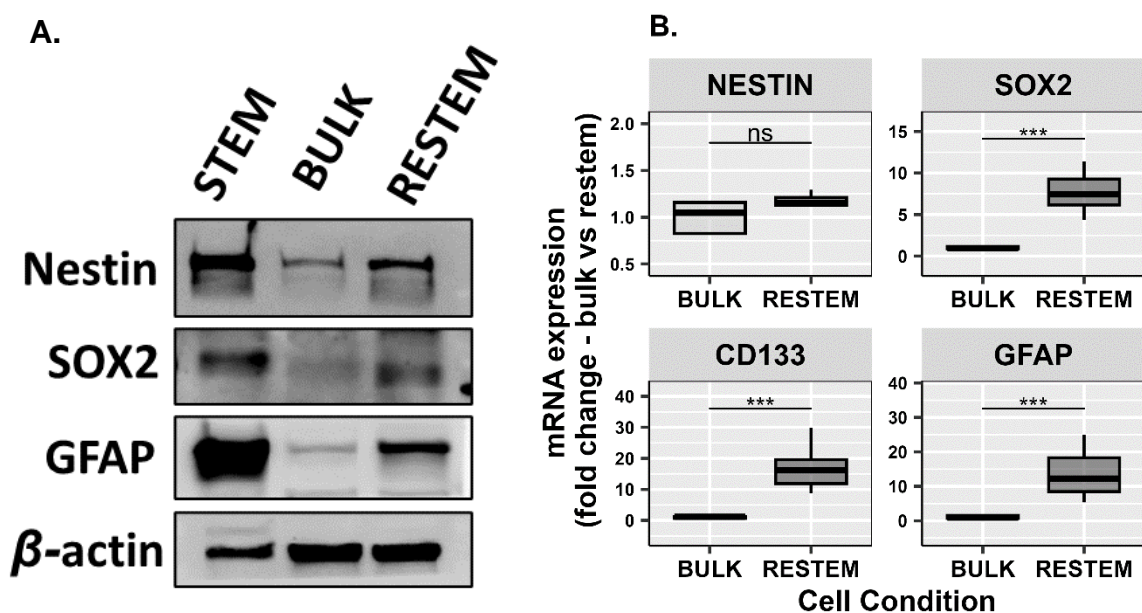
Figure 5.18 - Comparison of protein and mRNA expression levels of GSC markers (nestin, SOX2 and CD133) and differentiation marker (GFAP) in STEM, BULK and RE-STEM cultures - **A.** Comparison of protein expression levels between STEM, BULK and RE-STEM cells measured using immunoblotting. Biological repeat =1. **B.** Comparison of mRNA expression levels between stem, bulk and restem cells measured using RT-qPCR. Statistical analysis was performed using Man-Whitney U test. Biological repeat =3, technical replicates =3.

5.5.4 GSC marker expression within our ex vivo screening assay

To ensure the expression of these markers is maintained over the ex vivo screening assay period we investigated the mean intensity of CD133, nestin, SOX2, GFAP and vimentin within 2-day increments over 8 days and compared the mean intensities to the previously adopted 4-day incubation (figures 5.19 & 5.20). Despite adopting a 4-day incubation period initially, investigation into an 8-day exposure may be necessary to determine cytotoxicity levels for certain compounds within our ex vivo screening platform (see figure 5.18 above), therefore we wanted to ensure the expression of these markers are maintained throughout this extended drug dosing period.

The intensity of nestin staining showed the highest degree of variation within each incubation group, with the largest standard deviations of all IF markers used. The numbers of nestin positive cells also increased within the 4-day and the 8-day incubation. When comparing the levels of nestin from the 4-day to the 8-day there was no significant differences in the mean intensity or the numbers of nestin positive cells. Out of all the IF stains tested, CD133 showed no reduction in the positively stained cells over the 8-day incubation period. There were however significant differences in the mean intensities of cells. The intensity of CD133 increased from 2-day to 4-day incubation, this however decreased back down to previous levels at 6-day and 8-day. The standard deviation of CD133 was minimal. The mean intensity of SOX2 remained constant between the 4-day and 2-day incubation period, it did however reduce significantly within the 6-day relative to the 4-day control. Interestingly the mean intensity of SOX2 increased significantly higher within the 8-day incubation period. Again, similar to CD133 the levels of cells expressing SOX2 were high within these Cx18 cells, the levels of SOX2 positive cells remained constant over the 8-day period. The mean intensity levels of GFAP were slightly lower within the 4-day incubation group compared to the 2-day, these levels dropped even further within the 6-day incubation. Like SOX2 expression we saw an induction in GFAP expression within the 8-day incubation period relative to the 4-day control. Looking at the total positive cell numbers, GFAP is not expressed abundantly within these Cx18 cells compared to the previous markers. The 8-day group has the highest levels of GFAP positive cells 53/300, in total (table 5.4).

A.
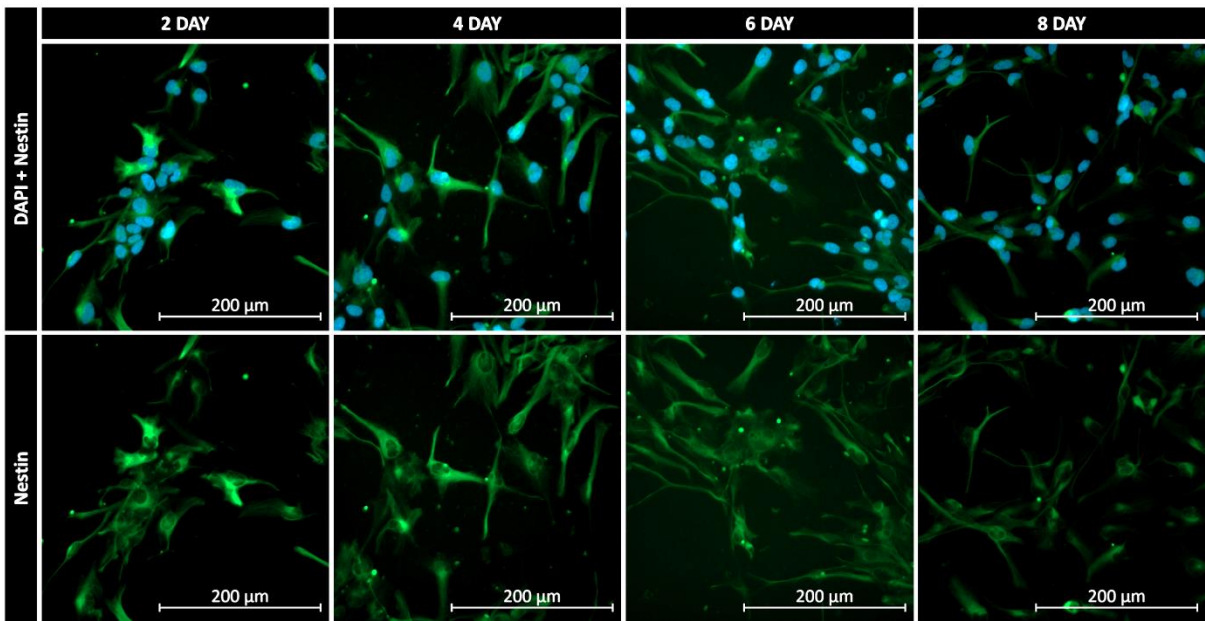
B.
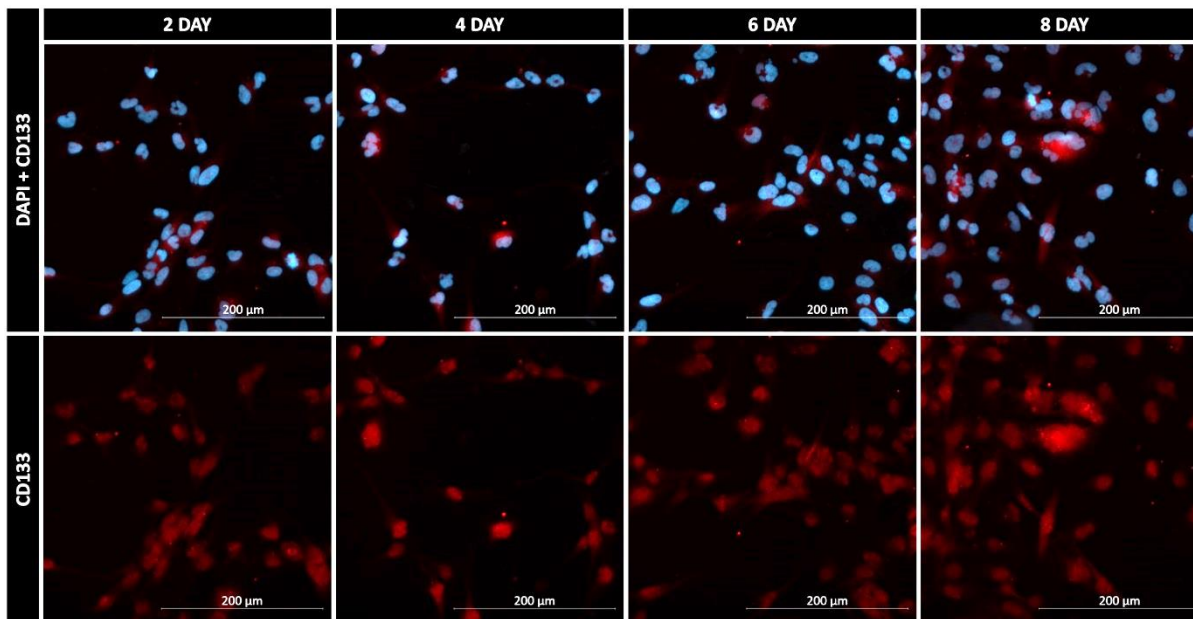
C.
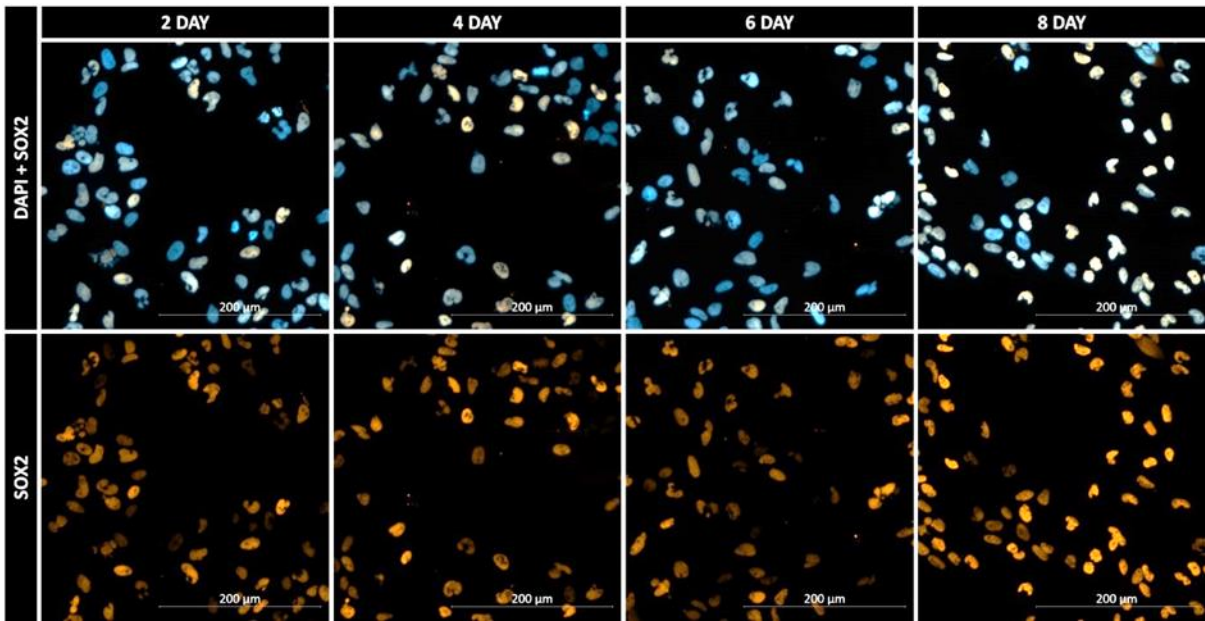
D.
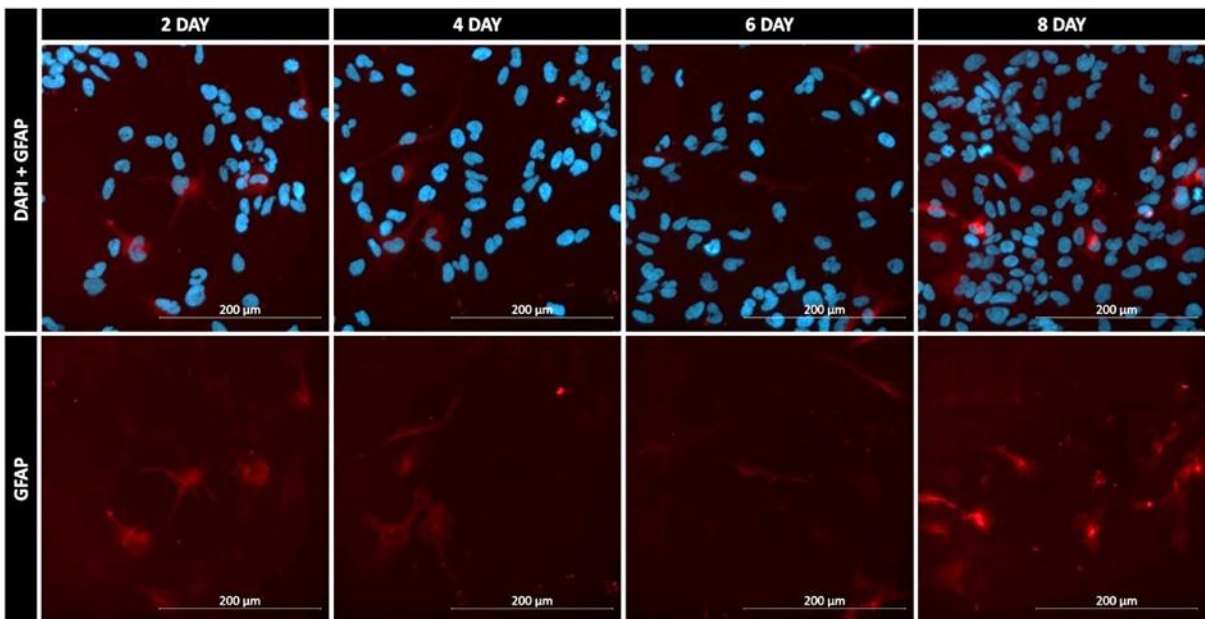
Figure 5.19 - Representative microscopy images investigating the effect incubation time has on the expression of commonly used GSC and differentiation markers within Cx18 cells - **A.** Depicts Nestin (green) and DAPI (blue), **B.** Depicts CD133 (red) and DAPI (blue), **C.** Depicts SOX2 (orange) and DAPI (blue) **D.** Depicts GFAP (red) and DAPI (blue).
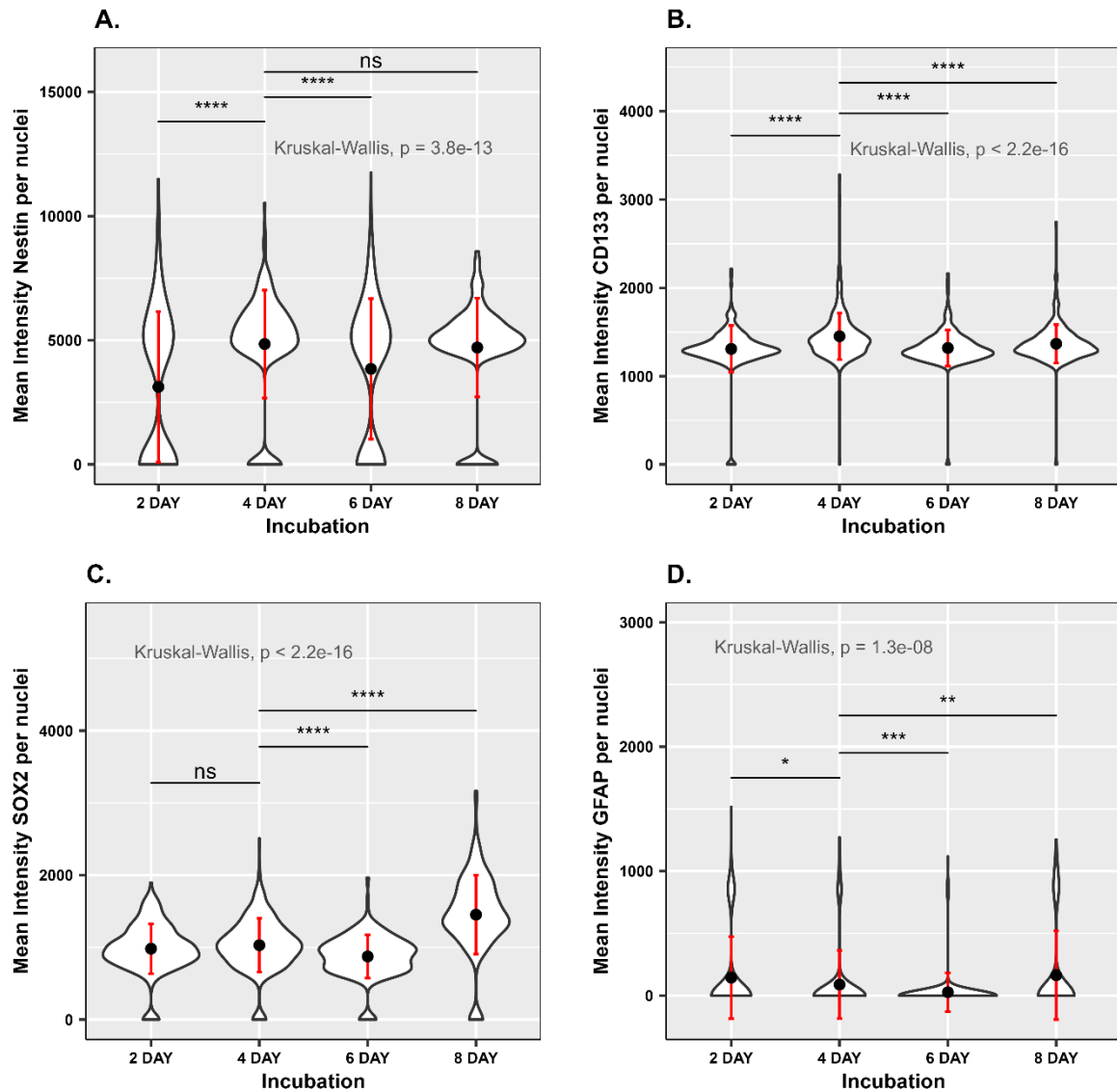
Figure 5.20 - Quantification of the effect of incubation time on marker expression by measuring mean intensity per nuclei - **A.** Nestin, **B.** CD133, **C.** GFAP, **D.** SOX2. Comparing the mean intensity of marker staining within Cx18 stem cells, following extended incubation time. Error bars represent SD around the mean. Statistical analysis was performed using Man-Whitney U test. Biological repeats = 3, each consisting of 100 cell images (technical replicates).

Table 5.4 - Comparing the levels of marker positive cells for each IF stain within each incubation period.

Marker	Incubation	Positive Cells (%)
Nestin	DAY 2	54
	DAY 6	86
	DAY 6	68
	DAY 8	87
CD133	DAY 2	97
	DAY 4	99
	DAY 6	99
	DAY 8	99
SOX2	2 DAY	95
	4 DAY	89
	6 DAY	95
	8 DAY	93
GFAP	2 DAY	19
	4 DAY	9
	6 DAY	3
	8 DAY	17

5.6 Ex vivo responses using GSC Immunofluorescence markers to determine GSC-specific drug cytotoxicity

5.6.1 Primary GSC cultures

Glioblastoma is an extremely heterogenous disease, exhibiting both inter- and intra-tumour heterogeneity. By screening freshly dissociated samples, ex vivo approaches have the advantage of maintaining tumour heterogeneity (through lack of long-term culture selection) and capturing drug response of multiple cell populations. Using fluorescent microscopy to evaluate treatment response, it could be possible to stain a single sample with multiple florescent markers, ideally, aiming to discover drugs which can specifically target and kill the GSC populations and have minimal/no toxicity to normally cells.

We therefore tested the suitability of these markers on a primary sample cell line Cx18 which had been screened using GBM V01 drug plates. The markers used were stem cell markers CD133, nestin, vimentin and reported differentiation marker GFAP, the latter two staining protocols have been previously optimised by another lab member (data not shown). Figure 5.21 shows the expression of each of these markers, images were captured from a single image acquired from a DMSO control well within the plate. This data confirmed it would be

possible to use multiple stem cell markers on a single sample drug plate, without overlap of fluorescent detection channels (figure 5.21). To investigate the intra assay reproducibility of these markers, we next compared these across the 24 DMSO wells across the 384 well drug plate to determine any variation (table 5.3), highlighting the median count, COV and SD. Just under half of the total cell numbers (DAPI) were also expressing the stem cell marker CD133, which was the most abundant marker, followed by nestin, vimentin and GFAP being the lowest. There was a large amount of variation within the control wells for cells expressing these markers as highlighted by the COV and SD columns, particularly cells expressing nestin, CD133 and GFAP. The levels of vimentin across the 24 DMSO control wells displayed the least amount of variation.
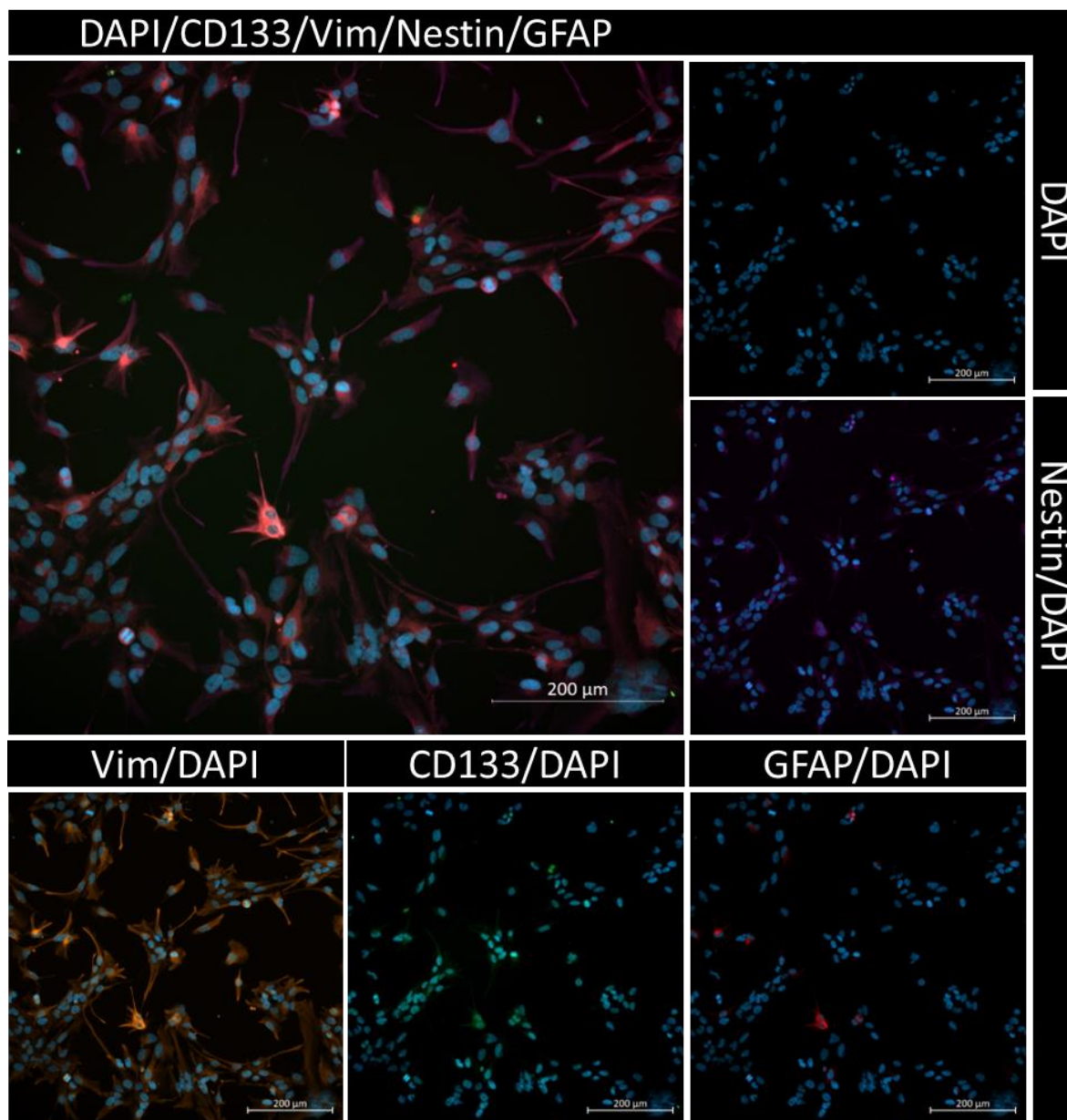
Figure 5.21 - Immunofluorescence expression of stem cell markers CD133 (green) and nestin (purple), vimentin (orange) and differentiation marker GFAP (red) merged with nuclei stain DAPI in Cx18 stem cells - Images were obtained from a DMSO control well captured using a V01 GBM drug plate.

Table 5.3 - Marker median, coefficient of variation and standard deviation across 24 DMSO control wells for each IF marker.

IF Marker	Median DMSO count	DMSO COV	DMSO SD
DAPI	2259	16.3%	366
NESTIN	951	31.9%	312
CD133	1037	29%	306
Vimentin	907	19.4%	175
GFAP	260	27.1%	73

We then investigated the dose responses for each drug using the relative fraction of each florescent marker used. Nuclei stain DAPI was used as a marker of total cell population, nestin, CD133 and vimentin as markers of GSC populations and GFAP as a marker of differentiated populations. Marker positive fractions (Nestin, CD133, GFAP and Vimentin +VE) were calculated as the fraction of marker positive viable cells after drug treatment divided by the average fraction of appropriate viable marker cells in the DMSO containing control wells, similar to methods performed by Snijder (Snijder *et al.*, 2017). We then calculated AUC from these fractions using GR metrics package in R, these AUC values were then plotted using pheatmap for each sample to compare drug responses within the marker positive and negative fractions. For cell line Cx18 this analysis is shown in figure 5.22 for GSC markers nestin, CD133 and vimentin and figure 5.23 for differentiation marker GFAP.
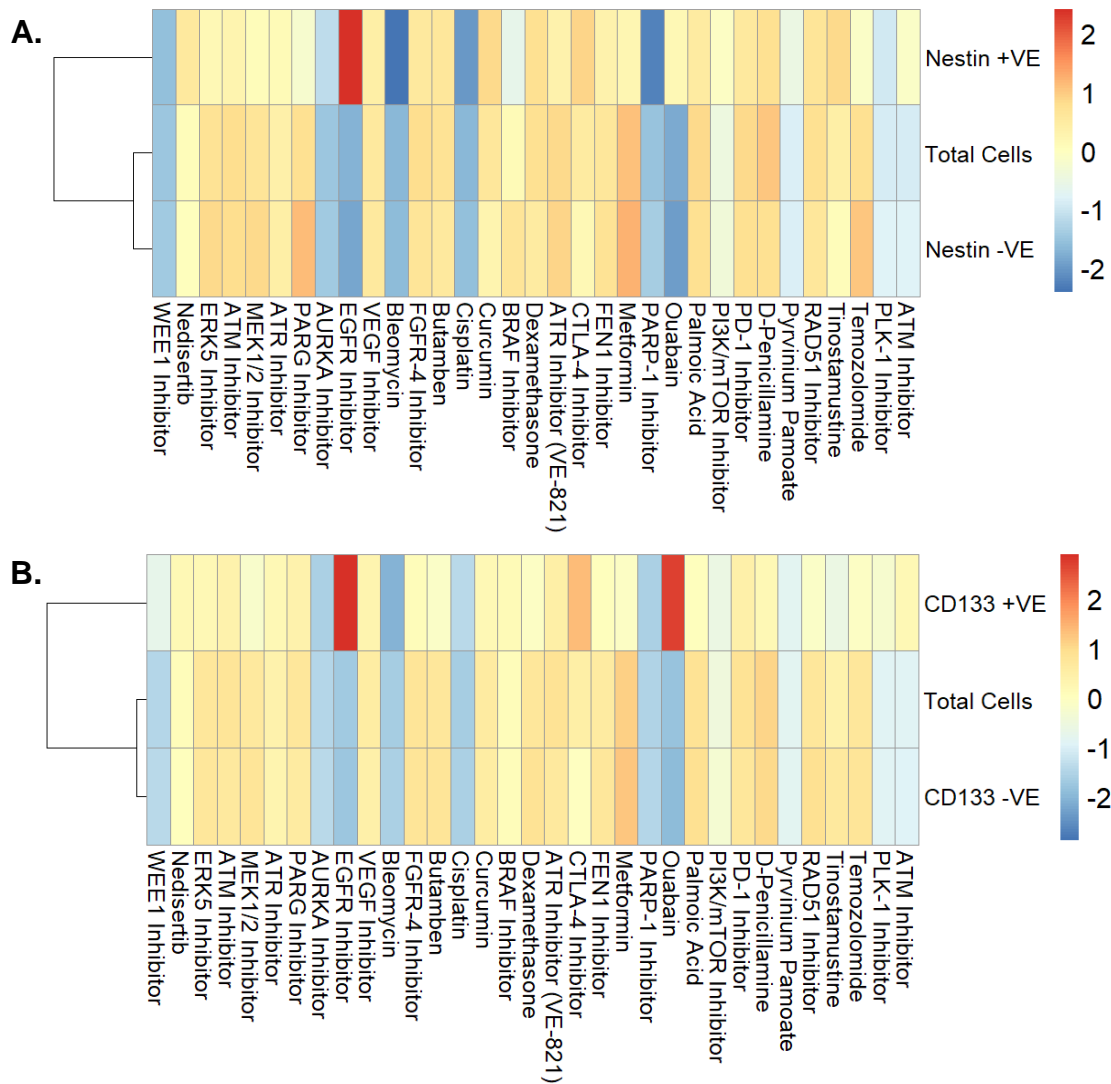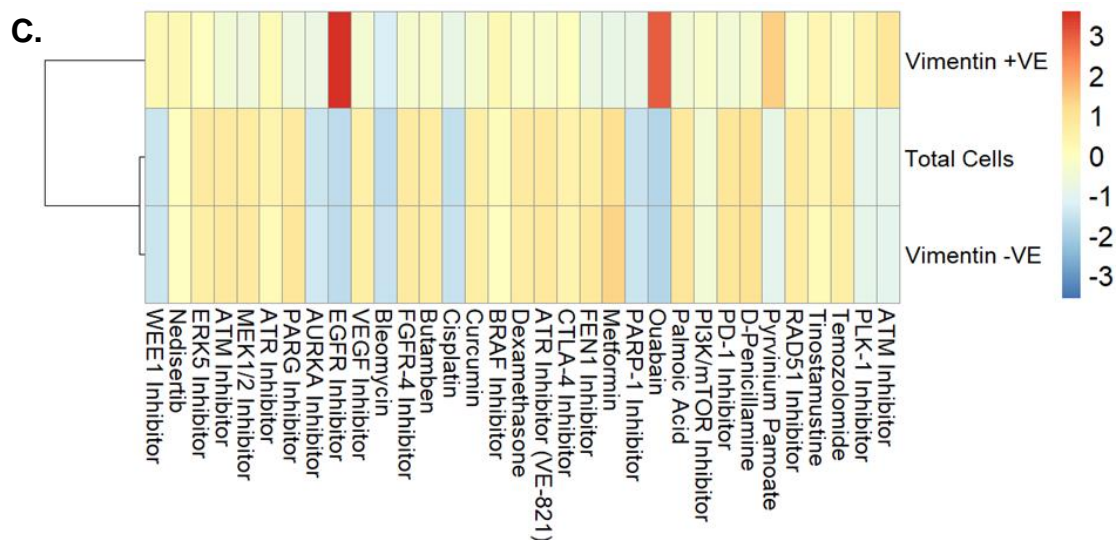
Figure 5.22 - Cx18 AUC dose responses within multiple stem marker fractions relative to DMSO control - **A.** Nestin positive fractions. **B.** CD133 positive fractions. **C.** Vimentin positive fractions. Relative fractions were calculated using the positive/negative stem marker and DAPI count of cells within drugged wells relative to positive count in DMSO control wells. Relative fractions were then used to calculate AUC values which were z-score normalised and plotted within pheatmap package in R.

We observed similar drug response profiles within both Nestin +VE and CD133 +VE fractions. In particular the EGFR inhibitor, which caused a proliferative increase in the fraction of both nestin and CD133 positive cells. Similarly, we see that ouabain also exerts a killing effect in the total cell population, however, causes a significant growth stimulus in the CD133+ fraction, and to a lesser extent in the Nestin +VE fraction. Drugs such as WEE1i, AURKAi, bleomycin, cisplatin, PARPi, pyrvinium palmoate and PLK-1i also display similarities within the responses between both markers, however these would be potentially unfavourable due to the reduction the total cell population. This would only be suitable if the drug demonstrated a significantly pronounced cytotoxic impact on the GSC populations compared to the non-GSC cells. Within the Nestin +VE fraction, drugs of particular interest appear to be PARGi, BRAFi, metformin and TMZ, whilst within the CD133 +VE fraction MEK1/2, FGFR-4i, butamben, curcumin, dexamethasone, FEN1i, Metformin, palmoic acid, RAD51i, tinostamustine and TMZ appear to specifically reduce the fraction of CD133 positive cells.
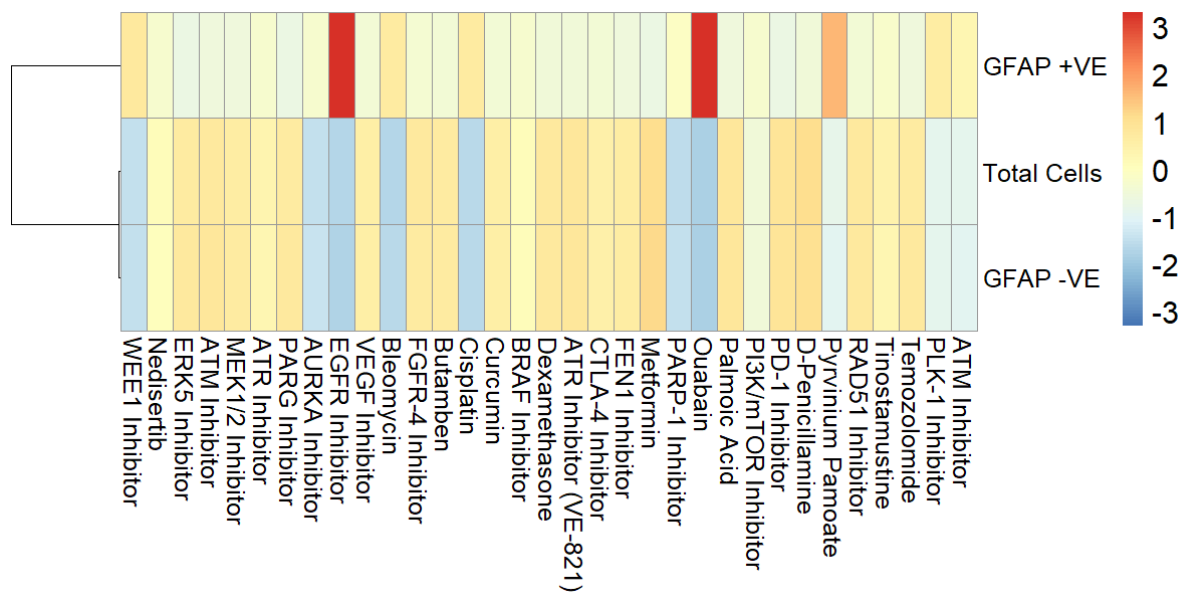
Figure 5.23 - Cx18 long-term culture AUC dose responses within differentiation marker GFAP fraction relative to DMSO control - Relative fractions were calculated using the positive/negative GFAP stained cells and DAPI count of cells within drugged wells relative to positive/negative counts in DMSO control wells. Relative fractions were then used to calculate AUC values which were z-score normalised and plotted within pheatmap package in R.

Interestingly when the dose responses of the GFAP +VE cell fractions were examined, we observed a couple of similarities with the GSC population such as resistance to EGFRi and ouabain. There are however distinct differences, such as resistance to WEE1i, AURKAi, bleomycin, cisplatin, PARPi, pyrvinium palmoate and PLK-1i, when comparing the GFAP +VE fractions to the previously shown GSC fraction drug responses (figure 5.23). This data confirms the heterogeneity of the disease reported in the literature. It also highlights the advantage of using multiple cell markers to differentiate between multiple cell population drug responses, and the importance of using multimodal therapies to suitably treat this disease.

5.6.2 Patient derived samples

We next stained two suitable ex vivo V01 sample plates seeded with patient sample cells GBM20A and GBM24 with the fluorescent GSC marker nestin and nuclei marker DAPI. These two sample plates were chosen for this analysis as they had good cell coverage of the wells, with good clear images and z-prime scores above 0.25 indicating good separation between positive and negative controls. Furthermore, among the various markers used for staining these samples, nestin staining was chosen for further analysis due to its elevated abundance.

The heatmap generated for GBM20A following nestin staining is shown in figure 5.24. From analysis of the Total Cells data, the majority of drugs are deemed to be exerting no killing effect on this sample, apart from EGFR inhibitor and ouabain. However, when we investigate the Nestin +VE fraction we see that some of these compounds are specifically reducing the GSC fraction, for instance responses from cisplatin, BRAFi, CTLA-4i, and metformin all show a reduction, specifically in nestin positive cells. Supporting the Total Cell fraction data, we can see that ouabain also exerts a killing effect on the Nestin +VE fraction, conversely we can see that EGFR inhibitor exerted an increase in the Nestin +VE fraction, whilst reducing the Total Cell fraction. As the ultimate aim is to identify therapeutic drugs that specifically target GSC populations with little or no damage to normal/ healthy cells, EGFRi and Ouabain would not be desirable drug options. The 11 drugs from cisplatin – metformin which only exert a killing effect on the Nestin +VE fraction would be suitable drug candidates based on this data.
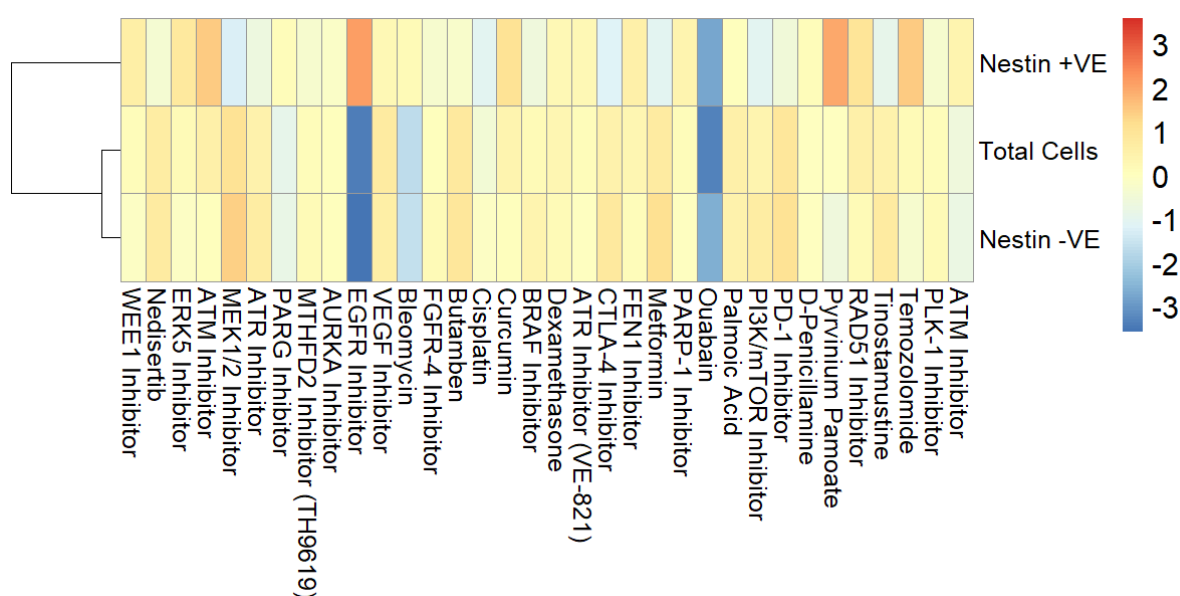
Figure 5.24 - GBM20A AUC dose responses within the total cell fraction (DAPI) and Nestin positive and negative fractions - Relative fractions were calculated using the positive/negative nestin and DAPI count of cells within drugged wells relative to positive counts in DMSO control wells. Relative fractions were then used to calculate AUC values which were z-score normalised and plotted within pheatmap package in R.

The heatmap generated for GBM24 following nestin staining is shown in figure 5.25. Compared to GBM20A, this sample appeared to have more Total Cell drug responses, again including EGFR inhibitor and ouabain but additionally PARG inhibitor, Pyrvinium Palmoate,

PARP-1 inhibitor and ATM inhibitor. Interestingly the Nestin +VE fraction in GBM24 appears to be generally more drug resistant, with only a slight killing effect from drugs between VEGF inhibitor and CTLA-4 inhibitor. Similar to GBM20A we also see the similar response within the Total Cell and Nestin +VE towards ouabain and EGFR inhibitor.
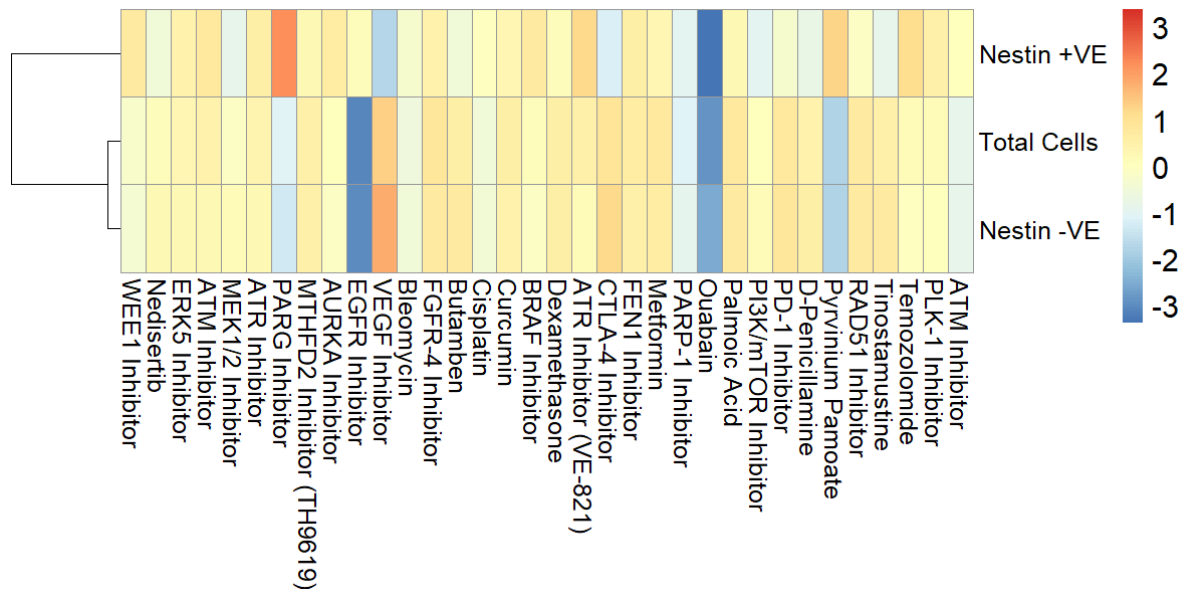
Figure 5.25 - GBM24 AUC dose responses within the total cell fraction (DAPI) and Nestin positive and negative fractions - Relative fractions were calculated using the positive/negative nestin and DAPI count of cells within drugged wells relative to positive counts in DMSO control wells. Relative fractions were then used to calculate AUC values which were z-score normalised and plotted within pheatmap package in R.

5.6.3 Extended drug incubation

As demonstrated earlier in this chapter, we conducted a comparison between the drug plate responses seeded with GBM30 cells for 4 days and 8 days. This analysis revealed not only an augmentation in drug hits but also an amplification of pre-existing hits. We therefore aimed to explore the consistency of these effects within the GSC population. The drug responses of sample GBM30 following a 4-day and 8-day incubation period using V02 drug plates with respect to nestin as a surrogate for GSC fraction is shown below (figure 5.26 A & B respectively). Evaluating the 4-day drug response heatmap (figure 5.26A), pyrvinium pamoate exerts a killing effect specific to the Nestin -VE fraction, whilst causing an increase in the Nestin +VE cell fraction, similar to GBM20 and GBM24 responses shown previously. However, unlike the previous samples, GBM30 Nestin +VE cells responded to EGFR inhibition in the 4-day assay, however, in the 8-day assay, the EGFRi is more effective towards the nestin -VE

cells. This suggest that over time this EGFRi may not be effective at specifically targeting the GSC cell population.

Drugs which specifically target the Nestin +VE fraction in the 4-day assay include MEK 1/2 inhibitor (AZD6244/selumetinib), butamben (calcium channels), palmoic acid (targeting Pol beta), tinostamustine (Pan-HDACi & alkylating agent) and cisplatin (lower (blue) AUC values depicted in figure 5.26A). Of these, MEK 1/2 inhibitor, butamben, palmoic acid and tinostamustine remain specifically toxic to only the Nestin +VE fraction within both the 4-day and 8-day assays. Additionally, figure 5.26B suggests that the FEN1 inhibitor and BRAF inhibitor (dabrafenib) specifically target the Nestin +VE fraction within the 8-day assay. These data therefore suggests that these may be suitable drugs which can exert long-term killing effects on the nestin stem cell population within this patient tumour.
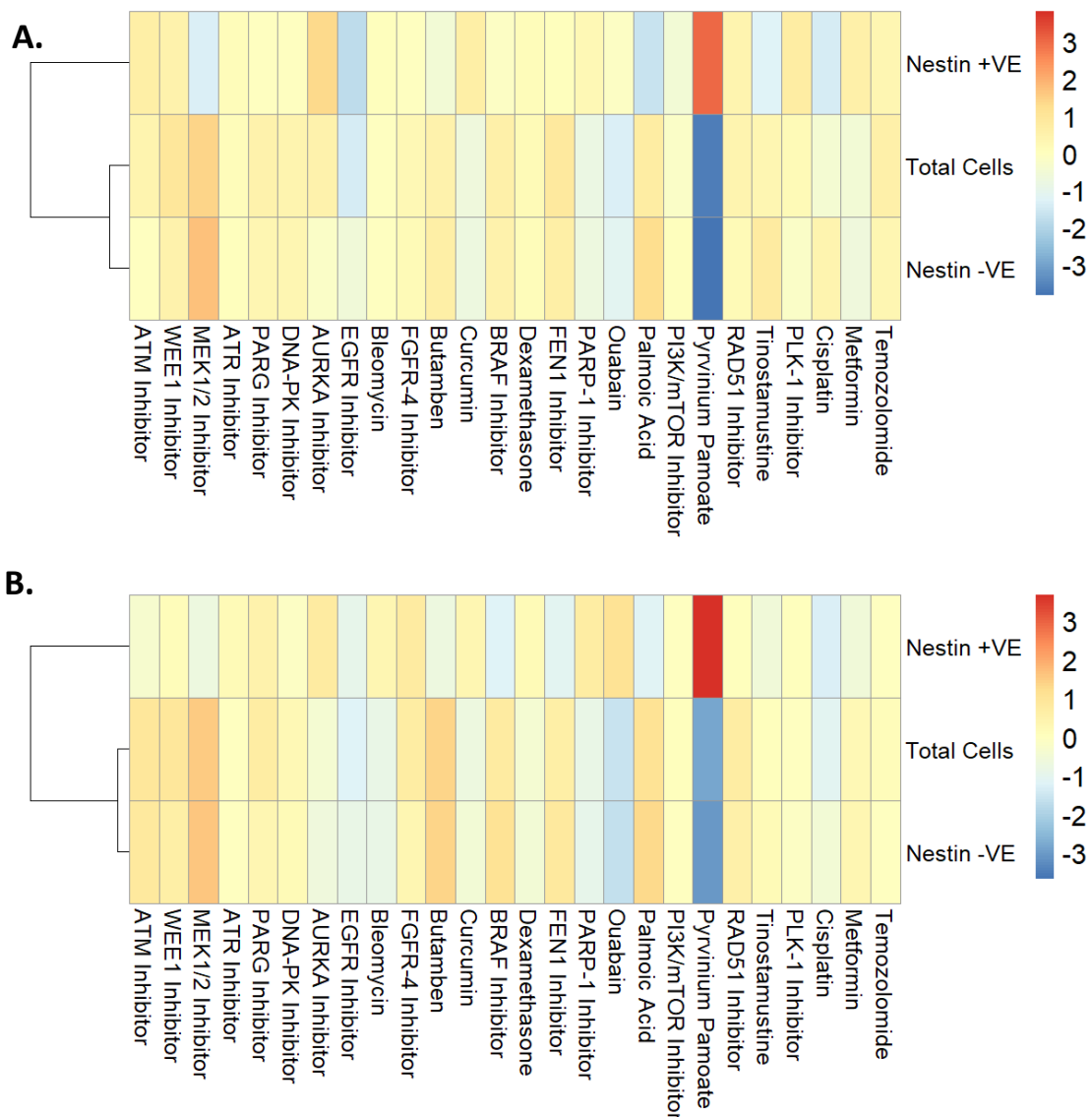
Figure 5.26 - GBM30 AUC dose responses within the total cell fraction (DAPI) and Nestin positive and negative fractions - **A.** Represents drug responses following a 4-day incubation period. **B.** Represents the drug responses following an 8-day incubation period. Relative fractions were calculated using the positive/negative nestin and DAPI count of cells within drugged wells relative to positive counts in DMSO control wells. Relative fractions were then used to calculate AUC values which were z-score normalised and plotted within pheatmap package in R.

5.7 Summary of Key Findings

- We have replicated radiotherapy in the clinic using both an experimental caesium IR source and correlated this with a radiomimetic drug bleomycin, where access to experimental irradiator is not possible.

- Issues with TMZ half-life have been highlighted through lack of efficacy, moving forwards all drug plates should be used fresh, avoiding any drug degrading through refrigerating or additional freeze thaw cycles.

- We were able to predict *MGMT* methylation status of long-term culture primary cell lines (Ox5 and Cx18) and also lower passage primary sample cell lines through TMZ ex vivo response.

- Our updated GBM V02 drug plates were able to differentiate between *MGMT* methylated and unmethylated tumours based on their TMZ response and showed improved z-prime values when comparing cell line data.

- Extending the incubation period from 4-day to 8-day showed improvement in drug responses in over half of the drug library, however, this still needs to be validated in more samples.

- We were able to confirm that our neurobasal media promotes stem cell phenotype through expression of commonly used markers nestin, CD133, SOX2 and vimentin at both the mRNA and protein level.

- Use of differentiation marker GFAP not suitable as a marker of differentiated/healthy cell due to higher expression levels in the stem cell cultures.

- We were able to culture glioma bulk populations back into stem conditions to re-populate expression of stem like cells, highlighting the inherent plasticity of glioblastoma

- Overall total levels of positive stained cells did not alter significantly when extending incubation time from 4-day to 8-day, however the intensity mean of the marker staining was variable.

- Highlighted similarities between the dose responses within the different GSC fractions of IF stained Cx18 drug plates, which also demonstrated it was feasible to stain drug plates with 6 IF markers corresponding to six separate channels.

However, staining of sample cells highlighted that not all samples will stain sufficiently or if at all to the GSC markers optimised within Cx18 cell lines.

- Addition of an 8-day assay results in increase in drug hits and an amplification of pre-existing hits, thus 8-day assay can serve as an additional biological repeat to support initial 4-day findings.

5.8 Discussion

5.1.1 Optimisation for V02 plates

To generate important proof-of-concept data for our glioma ex vivo screening platform, we wished to correlate our TMZ response with the *MGMT* status of the patient. Eventually, in the longer term the clinical response. Disappointingly, on our original GBM V01 drug plates, none of the samples responded to SoC drug TMZ, which was later discovered to be a factor of drug degradation, as indicated within this chapter. This highlights the importance of handling drugs and plates rapidly and avoiding any fridge incubation and freeze thaw cycles to increase reproducibility. Taking this into account, we therefore switched the drug printing machinery for the updated plates to a more streamline faster dispenser which required minimal human interaction.

Once we had circumvented the TMZ efficacy issue, we were able to screen low-passage primary cell lines (derived from samples previously screened using V01 plates). From this data shown in figure 5.5, we can see a clear separation between the *MGMT* methylated and unmethylated samples based on their TMZ monotherapy response. When we combined TMZ and IR at lower doses of TMZ, the separation was not as obvious however, at the highest dose of TMZ we also observed separation of samples based on their percent inhibition. If replicated in patient sample tissues this in theory could predict how well a patient will respond to SoC without waiting for histology and genetic screening data. It could also dictate whether patients with unmethylated *MGMT* promoter should be consented for ex vivo guided therapy, as these patients do not statistically benefit from TMZ treatment.

Using the updated V02 drug plates we successfully screened 3/5 patient samples, one of which was a multi-region sample (GBM28 A, B & C), another compared increased assay

timeframe (GBM30, 4-day and 8-day). Examining the raw AUC heatmap (figure 5.6) we can see hierarchical clustering between the two *MGMT* methylated samples GBM27 and GBM30 (4-day). Additionally, we notice that sample GBM30 (8-day) exhibited a higher amount of drug sensitivities, and hierarchical clustering is completely distinct from the other sample drug responses. When we include this GBM30 (8-day) to the heatmap it is able to mask some of the other sample sensitivities as it alters the scale due to decreased AUC values. We therefore removed this sample from the z-score scaled heatmap (figure 5.7), here of particular interest is the response to TMZ, which we see within the *MGMT* methylated samples has a blue and therefore lower AUC value. This shows that the new updated V02 plates can distinguish between methylated and unmethylated samples based on their TMZ response.

When we compared the z-prime values from the cell lines screened both using the V01 and V02 plates 5/6 lines exhibited an increase z-prime value, signifying improvement in assay robustness. These improvements in z-prime values are more than likely a factor of using different plate printing equipment. The Plate Mate liquid handler dispenser used for V01 drug plates required prior drug preparation involving suspending in media and dispensing into 4 serially diluted base plates, whereas the ECHO used for V02 drug plates only required the transfer of drug stock solutions into a master plate. The former equipment therefore increased the opportunity for human error and variation between repeats, possibly contributing to z-prime differences.

As the drug dispensing equipment is not owned by our group, we had to book out a suitable time slot and to travel to a separate department. To save time on the day, the evening before using the V01 Plate Mate equipment drugs were thawed, seeded onto base plates and stored in the fridge. As we have previously shown that refrigerating TMZ reduces its efficacy, this could also be an issue with the positive control staurosporine, if it has degraded slightly, we would see less cell death and therefore less difference between the mean cell counts of positive and negative controls, also causing lower z-prime values. Additionally, the ECHO dispenser is much faster than the Plate Mate equipment, as such, it may be possible that the prolonged time from printing to freeze storing the plate also caused degradation of drugs in V01, leading to much higher variation in repeats. Out of the freshly dissociated patient samples screened using the V02 plates only 50% showed a z-prime value above zero, again

evidencing one of the caveats with this project, not all samples are suitable for ex vivo screening. This is supported by the literature and our findings when separately propagating adherent primary glioblastoma cell lines (Grube *et al.*, 2021). Encouragingly there was an improvement in the z-prime value when we extended the assay to 8-days within the GBM30 sample, supporting the idea of two separate incubation plates for specific drugs.

5.1.2 GSC marker expression

Overall, the mRNA and protein expression data between the BULK and STEM Cx18 cultures was as expected, with heightened mRNA levels of GSC markers nestin, SOX2 and CD133 in GSC-enriched culture media conditions which corroborated with both the immunoblotting and IF data. We show our STEM enriching media can maintain expression of widely adopted GSC cell markers, whilst the serum containing BULK media reduced these levels most likely due to differentiation of progenitor GSC cells. Examining the IF staining data, both nestin and SOX2 appeared to be the most robust for the purpose of determining patient drug response and discerning microscopically between normal and GSC populations, due to obvious differences between staining intensity. Whilst the staining of CD133 and vimentin being less robust. Additionally, as mentioned previously, there is some controversy within the literature as to the suitability of CD133 as a *bone fide* GSC marker. The data obtained regarding GFAP expression was unexpected. Following incubation in non-GSC selective media, Cx18 cells exhibited a reduction in GFAP (rather than an expected increase) both at the mRNA level measured through RT-qPCR (figure 5.10), at the protein level measured through immunoblotting (figure 5.11) and IF staining (figure 5.17). One possible explanation for this could be due transformation into other non-astrocytic cell lineages such as oligodendrocytes or neuronal cell types, which would not typically express GFAP.

Astrocytes were originally divided into two distinct groups by Cajal in 1897: fibrous astrocytes and protoplasmic astrocytes, which have since been identified to reside in distinct brain white matter and grey matter regions respectively. The fibrous astrocytes found in the white matter show to preferentially express GFAP (Mishima and Hirase, 2010). The alternative explanation of this data may be a consequence of heterogeneity within astrocytes, as not all cells of astrocytic lineage express GFAP (Bushong *et al.*, 2001; Giffard and Swanson, 2005; Cahoy *et al.*, 2008; Tatsumi *et al.*, 2018). A previous report by Xu showed that when specific astrocytes

were exposed to serum containing media, the amount of GFAP they expressed gradually decreased, which supports our notion that GFAP is unable to stain for the specific types of astrocytes within our BULK cultures (Xu, 2018). The use of GFAP as a suitable marker for 'differentiated' astrocytes is therefore questionable, other alternatives are required.

Despite showing reduced levels of each GSC marker in the BULK culture conditions, either one condition is not a pure representative sample and therefore cultures which have been enriched for GSCs will also likely contain some differentiated cells and BULK cultures grown in serum containing media will also possess a subpopulation of GSCs. The purpose of the work carried out in this chapter was to demonstrate if we can discern microscopically between glioblastoma cell populations. The cells used in these experiments were primary glioblastoma cultures which have been cultured long-term using GSC enriching media, which undoubtedly gives an unrepresentative picture of the cell environment of original patient tumour, hence why most cells in each image are expressing each marker, but at variable intensities. When relating this back to ex vivo screening this does come with its limitations, as the freshly dissociated cells used have not been cultured in either STEM or BULK enrichment media, they have only been plated for the assay duration (4 days) in STEM media and therefore the numbers of these GSCs will most likely vary between each patient sample.

5.1.3 Plasticity of GSCs

The data in figure 5.18 highlights the ability of these highly plastic GSCs to differentiate and revert back to a de-differentiated state dependent on their culture conditions. The differences between the levels of protein and mRNA for SOX2 and GFAP shown may be due to BULK serum conditions having a block on the translation of RNA into protein, however when we place these BULK cells back into GSC cell enriching media to de-differentiate it causes the re-expression of the protein and therefore the mRNA levels deplete. The expression of CD133 was performed solely using RT-qPCR and not IF or immunoblot due to high levels of non-specific binding of antibody, however like SOX2 and GFAP, CD133 mRNA levels are significantly reduced once cells are reintroduced to STEM cell media, suggesting that its protein expression may also increase. This data demonstrates that these cells never fully differentiate, they can flip in between the two states like a switch based on their environmental stimuli.

5.1.4 GSC Marker Expression through prolonged incubation

The evaluation of marker expression over time revealed that nestin was the only marker which displayed no significant differences in the mean intensities when comparing the 4-day and the 8-day incubation period. There were however significantly lower levels of nestin within both the 2-day and the 6-day relative to the 4-day control, which could this be a factor of cell cycle expression of nestin. A study by Sunabori *et al.*, (2008) shows nestin gene expression upregulated during G1/S phase but declines during G2/M phase. Nevertheless, the point remains whether we are quantifying these cells on our ex vivo drug plates based on intensity staining threshold or do we use a binary positive or negative based counting intensity value as 0 and 1. Overall if we are just adopting a positive and negative staining approach comparing the 4-day incubation positive cells to the extended 6-day or 8-day, CD133 and SOX2 appear to be the most robust at maintaining the positive cell numbers. However, if we are wanting to use a mean intensity threshold, only the nestin 8-day incubation showed no significant differences to the 4-day.

This chapter overall has revealed GFAP as a questionable 'differentiation' marker, due to lack of its expression when cells were subjected to serum containing media. Interestingly within the mean intensity expression assay the levels of GFAP positive cells are highest within the 8-day incubation period, possibly because stem promoting growth factors have been depleted, however the increase was not apparent in a time dependant manner, in fact the highest conditions were both 2-days (49/300 positive cells) and 8-days (53/300 positive) therefore it is difficult to draw any conclusions regarding the expression of this marker.

5.1.5 Dose responses within GSC marker fractions
As there is no singularly definitive marker for GSC populations, we employed multiple stains per plate. This approach was demonstrated to be feasible within the Cx18 cells, where we assessed the utility of three distinct stem marker stains alongside one differentiation marker. Promisingly, we saw similarities between the drug responses between the three GSC markers used: Nestin, CD133 and vimentin. We aim to use multiple GSC marker stains on our sample plates, which would help select multiple drug combinations, some displaying higher

sensitivity to certain GSC fractions than others. One of the issues we noticed with the IF markers when staining the Cx18 drug plates was the high degree of variation within the DMSO control wells, as shown in table 5.4, we see almost double the COV compared to the DAPI cell counts. However, we know from previous optimisation experiments that we can minimise this issue, for instance prioritising a larger imaging strategy or increasing the incubation time.

The drug responses within the primary cell line and patient sample drug plates highlights the importance of having multiple stains, as just examining the DAPI counts can lead to overlooking potential drug hits. Unlike within the Cx18 cell lines, the numbers of cells expressing markers was much lower within the freshly dissociated GBM20A, GBM24 and GBM30 samples, naturally as they have not undergone weeks of stem promoting cell culture. For this reason, only the nestin fraction was quantified. This further outlines the importance of using multiple stains upon a single sample drug plate as not every sample will express similar levels of each GSC marker, and therefore may need to be selected for case by case.

Due to EGFR's high mutational burden in glioblastoma, it is a desirable drug target, however, most EGFR targeting strategies have shown disappointing clinical results. The EGFR inhibitor used for this study is osimertinib (AZD9291), which is a 3rd generation EGFR-TKI that binds irreversibly to EGFR proteins, with 200 fold higher affinity towards those which possess the T790M mutation (Hirano *et al.*, 2015). EGFR induces pro-survival and anti-apoptotic signals through downstream target pathways such as RAS/RAF/MAPK and PI3K/AKT. Complimentary to the cell line data, we showed similarities in responses to EGFRi for samples GBM20A and GBM24, exhibiting cell death within only the Nestin -VE fraction, however sample GBM30 exhibited a different response, showing sensitivity to EGFRi within both the Nestin +VE and Nestin -VE cell fractions. One possibility behind the Nestin +VE fractions resistance to EGFR treatment may be due to under reliance towards for EGFR for survival/proliferation, they may have adapted compensatory reliance on other RTK families. Target compensation is common in glioblastoma where upon EGFR activation, other RTKs can be activated such as erythroblastic leukaemia viral oncogene homolog (ERBB2/3), hepatocyte growth factor receptor (HGFR), platelet derived growth factor receptor (PDGFR), insulin-like growth factor receptor (IGFR-1) and proto-oncogene tyrosine kinase (ROS1) (Stommel *et al.*, 2007; Padfield, Ellis and Kurian, 2015). With respect to GSCs, there have been reports of intrinsic resistance

to EGFR inhibition, through the compensatory activations of ERBB family, such as ERBB2 and ERBB3. Work by Clark in 2012 showed a dual inhibitor of EGFR and ERBB3 lapatinib was significantly better at preventing GSCs proliferation (Clark *et al.*, 2012).

Double minutes are extrachromosomal DNA molecules which are exclusive to cancer, recent reports revealed that glioblastoma has the highest incidence in double minutes out of all cancer types at approximately 60% (Kim *et al.*, 2020). Double minutes have shown to harbour resistance to certain drugs, which can be passed on nonuniformly to daughter cells (Sanborn *et al.*, 2013). Evidence within the literature shows that the *EGFR* oncogene was most frequently associated with double minutes in glioblastoma (Bigner, Mark and Bigner, 1990; Vogt *et al.*, 2004; Sanborn *et al.*, 2013). The highly adaptive nature by which glioblastoma can confer adaptive immunity was demonstrated by Nathanson et al, insights revealed that resistance to EGFR inhibitor was shown to occur through elimination of the mutant EGFRvIII through extrachromosomal DNA (Nathanson *et al.*, 2013). This may contribute towards the lack of stem fraction killing by EGFRi osimertinib, within our drug screen.

Upon comparison of GBM30 sample responses between a 4-day and 8-day assay overall, the 8-day assay appears superior, we observed an augmentation in drug hits and an amplification of pre-existing hits, in particular drugs which are specifically targeting and reducing the Nestin +VE fraction of cells. These analyses also highlighted that EGFRi which appeared suitable within the 4-day assay at targeting the Nestin +VE fraction exerted a negative effect on the Nestin -VE cell fraction within the 8-day assay. These samples are a heterogenous mix of multiple cell types, all with differential growth rates and potential actionable mutations, extending the assay time allows for cells to divide, allowing drugs such as TMZ to exert a larger killing effect. Based on these data and those presented elsewhere within this thesis, we conclude that it would be appropriate (sample size permitting) to proceed with seeding ex vivo samples for both a 4-day and an 8-day drug incubation assay. This approach aims to demonstrate the suitability of an 8-day incubation period, enabling the capture of diverse drug responses and the killing of GSCs across various sub-types and growth rates within heterogeneous GSC populations.

Chapter 6 - Conclusions and future work

6.1 Conclusions

Despite efforts involving surgery, RT, and chemotherapy the median survival for glioblastoma patients has remained a stagnant 14 months for nearly two decades. This lack of progress led Cancer Research UK to identify glioblastoma as one of the "cancers of unmet need" in their 2014 Research Strategy. Glioblastoma presents several challenges that hinder effective treatment. One prominent challenge is the difficulty in delivering potential therapeutics to the brain due to the BBB. Even the current SoC, TMZ, has limited brain localization, with only 20% of its plasma concentration reaching brain tissue (Pitz *et al.*, 2011). Another significant challenge is the resistance exhibited by GSCs, which display self-renewal capabilities, whilst harbouring the ability to differentiate into multiple cell lineages. The exceptional resistance of GSCs is attributed to their increased activation of the DDR (Bao *et al.*, 2006; Carruthers *et al.*, 2015). Additionally, extensive inter and intratumoural heterogeneity between spatially and/or temporally distinct regions of the same tumour, making it highly unlikely for a single therapeutic to successfully target and kill all the functionally distinct brain tumour regions within every single patient, thus highlighting the importance of personalised drug screening approaches (McLendon *et al.*, 2008; Barthel *et al.*, 2019). Moreover, there exists a deficiency of appropriate pre-clinical models capable of faithfully replicating the heterogeneous tumour microenvironment (Aldape *et al.*, 2019; Rominiyi, Al-Tamimi and Collis, 2019).

Personalised medicine signifies a shift away from conventional one-size-fits-all approaches to treating cancer, instead, raising the idea of tailoring treatments based on the unique characteristics of an individual's tumour. Over the last few years, the analysis of a patient's tumour genome has proven valuable in identifying actionable mutations that can lead to susceptibility towards specific therapies. For instance, the success of EGFR inhibitor gefitinib within NSCLC patients harbouring specific EGFR mutations such as L858R substitutions or deletions in the exon 19 (Maemondo *et al.*, 2010). Nevertheless, the connections between one's genetic makeup, biological functionality, and response to treatment often remain unclear, one example of this is the clinical failure of EGFR inhibitors within glioblastoma (Lee *et al.*, 2020). Increasingly, researchers are turning to PDX models to make more precise predictions about how a particular patient will respond to a drug. This typically involves the

transplantation of tumour tissue from patients into immunocompromised mice. For each patient, the tumour taken from a successfully engrafted mouse is further cultivated in a subsequent cohort of mice before any therapeutic interventions are carried out in yet another group of murine subjects. Consequently, even limited studies using these mouse avatars may necessitate around 40 such mice and several months of research to provide customized treatment recommendations from a shortlist of five therapy options for an individual patient.

Considering the principles of our NC3RS funders (Replacement, Reduction, Refinement), the ex vivo approach holds the potential to serve as a pre-clinical alternative, offering a way to replace and reduce the need for murine avatars in the evaluation of experimental therapeutics, not only for glioblastoma but also for numerous other solid tumours. Our initial drug plates encompass 35 distinct therapeutic agents that have been employed to assess 18 different patient samples. Creating the necessary number of avatars per patient to evaluate all 35 unique drug response profiles, which through conventional PDX models would be practically unfeasible. On average, testing a single treatment regimen requires 5-10 mice, and *in-vivo* replication of this work would necessitate a minimum of 3,150 PDX models (with 175 models per patient). This would represent an exceptionally large and impractical sample size, with the associated costs and time commitments for serial transplantation into multiple cohorts of mice being prohibitively high. Furthermore, when factoring in the typical duration required for successful PDX engraftment (spanning 4-8 months) and the average life expectancy of patients with glioblastoma (which falls within the range of 12-18 months), it becomes challenging to clinically validate any potential drug candidates. (Rubio-Viqueira *et al.*, 2006; Zhang *et al.*, 2018). Further to this, recent legislation in the United States has ushered in a significant change in drug approval protocols. The FDA no longer mandates animal testing as a prerequisite for clinical trials. Instead, innovative alternatives such as computer modelling, organ chips, and organoids are being encouraged (Wadman, 2023). This development holds great promise for the future of ex vivo drug screening and bodes well for the funding body's NC3Rs replace, reduce and refine mission.

The lack of suitable pre-clinical models to effectively recapitulate the tumour environment in glioblastoma has led to the development of this project. As such, we hypothesise that freshly dissociated glioblastoma tumour tissue would be the most suitable pre-clinical model for high

throughput drug screening. We believe screening cells directly following dissociation of fresh tumour tissue avoids selection for faster growing media enriched cell populations, thus obtaining drug response profiles for individual patients which recapitulate the original tumour environment, more so than traditional PDX and primary cell line models. Furthermore, combination of this approach together with the use of advanced high-content automated microscopy techniques will surpass traditional luminescent assays like CellTiter-Glo (CTG), primarily because we can quantify the presence of distinct cell populations through IF staining at single cell resolution. Our primary aims of this project were therefore to:

1) Successfully develop an ex vivo screening platform within solid glioblastoma tissue.

2) Decipher molecular mechanisms behind sensitive drug responses.

3) To optimise the use of appropriate imaged-based GSC markers to decipher between GSC, tumour bulk and healthy cell population drug responses to identify tumour selectivity.

6.1.1 Project achievements

Initially concerns arose regarding patient recruitment, mainly due to the impact of the COVID-19 pandemic, which led to a significant reduction in the numbers of surgeries and the availability of staff to recruit. Nonetheless, we are pleased to report substantial progress, including the 18 samples successfully screened using V01 and 3 samples for V02 drug plates. In addition, we have also contributed to the field by publishing a comprehensive review on ex vivo technology, emphasising its strengths and weaknesses compared to other widely used cell based models (Williams *et al.*, 2022). Furthermore, we have successfully published a methods/data manuscript in F1000 Research within the NC3Rs gateway. This publication provides in-depth insights into the techniques developed and employed for ex vivo screening of glioblastoma during the course of these PhD studies. These methods are now readily publicly accessible, and we are confident that they have the potential for adoption in the study of other cancer types by other research groups around the world (Gagg *et al.*, 2023).

6.1.2 Predicting patient response

Our initial drug plates were primarily designed for optimization purposes. Nevertheless, the absence of TMZ response raised concerns, as it is one of the mainstay SoC therapies used to

treat glioblastoma, and its efficacy was crucial for demonstrating that the screening platform could accurately predict clinical responses. Further investigations led to the discovery that its short half-life within our initial ex vivo methodology was contributing to its lack of efficacy, which we demonstrated was further attenuated through plate storage at 2-8°C. Moving forward with developing our second batch of drug plates, we adopted the use of a different liquid dispenser, the Echo 550. This dispenser eliminates the need for pre-mixing the drugs; instead, they are dispensed in their original stock concentrations directly from a base plate using acoustic technology. Therefore, removing the risk of any human error whilst serially diluting drugs, but also significantly reducing the handling time, which will have been contributing factor to the degradation of TMZ. Promisingly, using this equipment, we were able to distinguish between the tumours on our updated V02 drug plate based on their *MGMT* methylation status and TMZ response, however the sample size was minimal (3 samples), therefore a larger patient cohort would be required for increased confidence. For instance a recent similar ex vivo screening study showed that within their 66 screened GSC cultures an intermediate TMZ response group existed, which contained an almost equal distribution of *MGMT* methylated and unmethylated patients (Ntafoulis *et al.*, 2023). Resistance to TMZ in the *MGMT* methylated samples can be explained through mutations within the DNA MMR pathway (McFaline-Figueroa *et al.*, 2015), in addition HOX signature, EGFR expression and BER enzymes have showed a link with TMZ resistance (Migliavacca, Gorlia and Regli, 2008; Agnihotri *et al.*, 2012). This demonstrates how a functional screening test alongside our ex vivo screening platform may be useful as will be able to explain the reasoning behind lack of TMZ response in *MGMT* methylated patients.

Culturing residual patient sample cells alongside the assay allowed us to not only perform follow up experiments but has also aided towards developing our Sheffield Living Biobank (https://bit.ly/3yFF8WP). Despite the lack of efficacy of TMZ on the V01 drug plates, we were still able to discern varying responses to drugs between CORE 1 and EDGE 2 cells derived from the multi-region heterogeneous Cx18 GSC model. This underscores the fact that our 4-day assay is capable of preserving the intra-tumoral diversity found within tumours and is proficient at revealing differences in drug sensitivities/responses. This data also underlines the significance of examining multiple regions of patient samples (if possible), to capture the diverse molecular profiles present within the tumour. This, in turn, can lead to the exploration

of combination therapies which we are aiming towards within future directions (see below for details).

Analogous to our data shown in Chapter 4, where tumour cells were screened under conditions promoting both STEM and BULK growth, a recent study has adopted a similar approach. Named ChemoID assay, the chemosensitivities of GSCs and bulk tumour cells were screened to determine the most effective drug combinations, which were later confirmed in PDX models (Howard *et al.*, 2017). Where ChemoID assay results revealed sensitivity within both GSCs and bulk tumour cells, prolonged tumour regression was observed in PDX models. However, within patients whose tumour bulk cells showed sensitivity, but GSCs displayed resistance, the PDX models displayed initial tumour regression followed by regrowth following therapy termination. This study highlights the importance of targeting both the tumour bulk (representing the majority of the surgically excised tumour mass), and more importantly the GSC population as these cells are responsible for treatment resistance and repopulation of the tumour from the inevitable residual post-surgical tumour cells.

6.1.3 Comparable clinical trials

There are currently two interventional and five observational clinical trials being conducted using individual glioblastoma patient tumour specimens, or biopsies to help guide treatment decisions and improve patient care (see Table 6.1). Trials CSCRGBM and 3D-PREDICT are the only two which have published results. The former study is from the same group who created the ChemoID assay mentioned previously. They cultured stereotactic biopsy tissue to enrich for GSC and tumour bulk populations, these cultures were then drugged with 9 single agents and 5 drug combinations. Patients were then treated with chemotherapeutics which were predicted most effective by the ChemoID assay. The results showed that 6/14 patients had a complete response, 6/14 had a partial response and 2/14 showed progressive disease. More recently they have published the results of their clinical trial (NCT03632135), which demonstrated improved median survival in the ChemoID assay-guided group (12.5 months), compared to the physician choice group (9 months) (Ranjan *et al.*, 2023).

The 3D-PREDICT study initially identified potential targets for glioblastoma patients through investigation of their transcriptomics data, they then validated the findings within ex vivo patient derived organoids using their (3D-PREDICT) drug screening assay (Reed *et al.*, 2021). Using this model this group has also predicted clinical response to TMZ within 17/20 newly diagnosed glioblastoma patients (Shuford *et al.*, 2021). Despite both being further advanced than our current EVIDENT study (NCT05231655), we believe that our methodology is significantly superior for the following reasons: both the studies mention by the other groups incorporate the use of colorimetric/luminescence assays; 2,5-diphenyl-2H-tetrazolium bromide (MTT) and CTG to quantify drug responses. These approaches are rather rudimental and lack the ability to delve into the drug responses at single-cell resolution. Furthermore, it is worth noting that our multiregional CORE/EDGE cell models exhibit varying metabolic levels, which could potentially impact the results of these enzymatic assays, although the data is not presented here. In contrast, our study allows for the investigation of drug responses within individually stained/imaged glioblastoma specific populations. Furthermore, the scale of these drug screens is significantly smaller when compared to our approach, which currently utilises 32 drugs with plans to expand further (see Future Directions section).

Table 6.1 - Summary of clinical trials using ex vivo methodology in glioblastoma.

Identifier	Title	Sponsor	Status	Study type	Estimated Enrolment
NCT03632135	Standard Chemotherapy vs. Chemotherapy Guided by Cancer Stem Cell Test in Recurrent Glioblastoma (CSCRGBM)	Cordgenics, LLC	Active, Not recruiting	Intervention	150
NCT05231655	Ex VIvo DEtermiNed Cancer Therapy (EVIDENT)	Sheffield Teaching Hospitals NHS Foundation Trust	Recruiting	Observational	600
NCT03561207	3D Prediction of Patient-Specific Response (3D-PREDICT)	KIYATEC	Active, Not recruiting	Observational	570
NCT05380349	Combination Drug Therapy for Personalized Cancer Stem Cell High-Throughput Drug Screening for Glioblastoma	Swedish Medical Center	Not yet recruiting	Interventional	10
NCT03896958	The PIONEER Initiative: Precision Insights On N-of-1 Ex Vivo Effectiveness Research Based on Individual Tumor Ownership (Precision Oncology) (PIONEER)	SpeciCare	Recruiting	Observational	1000
NCT05556382	Glioblastoma Evaluation for Heterogeneity In RadioseNsitivity (GEHIRN)	Istituto Clinico Humanitas	Recruiting	Observational	30

| NCT06038760 | Prospective Evaluation of AI R&D Tool in Adult Glioma and Other Primary Brain Tumours (PEAR-GLIO) (PEAR-GLIO) | Ourotech, Inc. | Not Yet Recruiting | Observational | 50 |

6.2 Future Directions

While we have made exciting progress with proof-of-concept studies, it is essential to recognize that the development of our ex vivo screening platform, particularly for solid tumours, is still in its early stages (Williams *et al.*, 2022). Although we successfully distinguished the *MGMT* methylation status in the latest three samples by assessing their response to TMZ on the V02 drug plates, we had envisioned the opportunity to enhance this study by including a larger sample cohort. Furthermore, we were eager to introduce the utilization of combination plates in conjunction with SoC therapy into our research protocol as our work progressed. The following subsections details some of the other important factors which would like to consider for the future success of our ex vivo screening platform.

6.2.1 Developing more clinically relevant assay conditions

A limitation of this approach is the loss of the 3D tumour architecture when the tumour is dissociated into a single-cell suspension. The Chalmers group conducted a study comparing the radiosensitising effects of TMZ, bevacizumab, and erlotinib within patient derived GBM lines cultured as both 2D monolayers and 3D Alvetex scaffold models. Their research revealed varying responses, with the 3D model demonstrating greater reliability in predicting clinical efficacy (Gomez-Roman *et al.*, 2017). Whilst seeding dissociated cells onto 2D monolayers allows for fast and straightforward drug response analysis, the 3D approach may be something to consider in the future if we are wanting to develop a more clinically relevant screen. Another important culture condition which we have mentioned previously in Chapter 4, is the assay oxygen level. Hypoxia is a common characteristic of glioblastoma tissues, and is essential for the maintenance of GSC populations (Kolenda *et al.*, 2011; Mathieu *et al.*, 2011). A recent study by Ibrahim *et al.* displayed that in prostate, liver and breast cancer cell lines four chemotherapeutic agents: cisplatin, cyclophosphamide, doxorubicin, and 5-fluorouracil, showed reduced activity within cells exposed to hypoxic conditions, measured through higher IC_{50} values (Ibrahim *et al.*, 2022). Suggesting that the drug responses at atmospheric oxygen are not directly comparable to *in-vivo* tumour responses, as hypoxia

creates a state of treatment resistance. Experimental hypoxic chambers are used within our institute, as such, it would be interesting to compare an ex vivo drug plate response in normoxic vs hypoxic conditions.

6.2.2 Investigating other suitable GSCs markers

Prior to surgical resection, glioblastoma patients will often be administered an oral solution containing 5-ALA, also known also as the 'pink drink' in order to perform fluorescence guided surgery (FGS). The natural metabolite has excellent penetration of the BBB, where it is readily taken up by malignant brain tumours and infiltrating cells surrounding the tumour bulk. Upon penetration into malignant glioma cells it is metabolised into a fluorescent metabolite known as protoporphyrin IX (PpIX) (Walter Stummer *et al.*, 1998; Duffner *et al.*, 2005). Elevated production of this metabolite can be visualised trough the excitation with 405nm blue light, this therefore allows surgeons to accurately remove florescent glioma tissue sparing any adjacent healthy brain. As we process our tumour samples straight from surgery, we could utilise the fluorescence of this porphyrin to distinguish microscopically between GSCs and healthy cell populations on our drug plates, as an alternative to IF staining with commonly used GSC markers. This would significantly reduce the amount of washing steps and interference with the drug plates, hopefully retaining the cellular composition.

6.2.3 Combining ex vivo screening and next generation sequencing

Over the last two decades advances in next-generation sequencing (NGS) technology has made a significant impact on cancer diagnosis, management, and treatment. NGS has revolutionised the field of oncology by enabling researchers and clinicians to decode the genetic underpinnings of cancer, thereby paving the way for personalised therapies and more accurate prognostic assessments. NGS is a powerful tool which allows for the rapid and cost-effective sequencing of millions to billions of DNA fragments simultaneously, to elucidate the genetic mutations and alterations which drive the initiation and progression of cancer. NGS is an umbrella term for multiple different sequencing approaches, including whole genome sequencing (WGS), whole exome sequencing (WES), whole transcriptome sequencing (RNA-seq) and single cell RNA-seq. WGS is the most comprehensive NGS approach, it is highly detailed specifying all the genetic information within both coding and non-coding regions.

Whilst WES details all the genetic information strictly within the protein coding exon regions of DNA, because most known disease causing mutations usually occur in exons, it is thought to be the most cost-effective and efficient method (Bertier, Hétu and Joly, 2016).

Genomics has transformed cancer diagnosis. Genetic testing of liquid biopsies had enabled the detection cancer-related genetic alterations in circulating free DNA from blood samples, this is often much less invasive than scans or biopsies. It can often detect any cancer prior to patients displaying any symptoms, a multi-cancer early detection test called Galleri has recently shown to correctly identify two thirds of cancers in more than 5,000 patients with non-specific symptoms. It was also able to pinpoint the cancer site in 85% of those successful cases (Aldea *et al.*, 2023). NGS has also enabled the detection of certain biomarkers which can be used to diagnose specific cancer types, estimate prognosis and guide treatment, for instance the testing for variant *BRCA* genes in ovarian and breast cancer. These defective genes have later have been targeted through synthetic lethality, using drugs known as PARP inhibitors which initiate defective HR repair (Tutt *et al.*, 2021).

Additionally, advances in NGS have aided in improving the success of clinical trials, genetic information can help to decide eligible patients leading to more chance of drug success and therefore drug approvals. The identification of such targetable mutations has led to the development of 'basket trials', whereby patients are selected on the basis of a specific targetable mutation rather than tumour type (Cunanan *et al.*, 2017), with BRAF, EGFR and neurotrophic tyrosine receptor kinase (NTRK) inhibitors being some of the therapeutics that have shown promise across multiple cancer types. There is evidence emerging from umbrella trials that treating on genetic biomarkers alone is not sufficient to predict response. One such example is the National Lung Matrix Trial, where 22 different actionable biomarkers were used to direct patients into 8 treatment arms. Unfortunately, only 2 arms demonstrated a durable clinical benefit (Middleton *et al.*, 2020). Subsequent analysis of this trial suggested high mutation burden and lack of clinically relevant models played a role in the lack of efficacy observed. However, basket/umbrella trials are of particular importance for rare cancers, where clinical trials are not widely accessible due to lack of suitable candidates. Trials such as the recently initiated DETERMINE (NCT05722886) is trying to address this, utilising genetic biomarkers in rare cancers, but the results are still a few years away.

Personalised medicine is the emerging concept of analysing patient specific genetic mutations, to help tailor treatment plans. Genetic profiling has led to the development and approval of highly targeted treatments such as imatinib (Gleevec) which is used to treat chronic myloid leukemia (CML) through targeting of *BCR-ABL* fusion gene and trastuzumab a monoclonal antibody used to treat patients with HER2-amplified metastatic breast cancer (Ennis S Lamon *et al.*, 2001; Rian *et al.*, 2001). In comparison to traditional chemotherapeutics, these targeted treatments offer the advantage of much lower off target toxicity. In relation to glioblastoma, a genomics based personalised treatment pilot study, named Minderoo Precision Brain Tumour Programme (MPBTP) has been initiated in Cambridge whereby NHS patients with glioblastoma will have their tumour samples sequenced, hopefully to help identify actionable mutations which will enable more targeted effective care for brain tumours.

Advances in NGS have also allowed researchers to comprehensively profile the genomic landscape of glioblastoma tumours. TGCA is a large-scale genomics study which has molecularly characterised over 20,000 primary and normal matched samples in 33 cancer types. Glioblastoma was the first cancer type to be systematically studied, the initial publication investigated the genomic and transcriptomic results of 206 glioblastomas (McLendon *et al.*, 2008). The work led to the classification of glioblastoma into four different subtypes; proneural, neural, classical and mesenchymal (Verhaak *et al.*, 2010), however further comprehensive analysis has actually revealed there is only three, where neural classification was removed as it was believed to be an artifact of healthy brain tissue.

In the context of glioblastoma, the application of NGS has not yielded significant improvements in patient outcomes. When NGS is utilized in isolation, its primary function is to provide supplementary data for disease categorization rather than definitively confirming an individual's direct suitability for a targeted therapy that can be effectively leveraged. The sheer volume of genetic alterations within tumour cells introduces considerable complexity in the endeavour to differentiate the most critical, cancer-specific driver mutations and pathways from the multitude of genetic changes which have no known effect, described as passenger mutations. Even when we do identify genetic abnormalities with clinical

significance, there may not necessarily be actionable pharmaceutical treatments available for them, In fact, only about 20% of them can be matched to a pharmaceutical target (Massard *et al.*, 2017). Consequently, we have chosen an alternative approach where individual patient tumours are initially screened, and subsequent sequencing is performed retrospectively.

In addition to the research conducted in preceding chapters, we extended our efforts by submitting DNA extracted from residual tissue in 14 patient samples for WES. Among these samples, 11 were subjected to screening on the V01 drug plates, while the remaining three were sourced from multiregional sections of sample GBM26, and they underwent screening using the V02 drug plates. Regrettably, due to time constraints, we were unable to process and analyse the data necessary to create an additional chapter solely dedicated to WES. Had we completed this analysis, our aim would have been to examine the tumours in relation to clinical parameters such as age, sex, *MGMT* status, and to correlate these findings with our ex vivo determined drug sensitivities, both collectively and for each individual drug. This approach could have provided valuable insights into specific drug responses, the identification of novel biomarkers, or the discovery of new genes associated with drug sensitivities. As such, this is something that we are planning to do beyond these PhD studies.

6.3 Concluding remarks

The findings from this project have shown promising prospects for our ex vivo assay as a valuable tool in the future of precision medicine, applicable to both newly diagnosed and recurrent glioblastomas. In the case of newly diagnosed glioblastoma, our ex vivo platform has now demonstrated its ability to predict the patient response to TMZ treatment. This predictive capability helps determine whether patients would derive clinical benefits from the SoC treatment, making it a more favourable option for guiding therapy decisions. It is worth noting that research has indicated that patients with the unmethylated *MGMT* gene typically do not statistically benefit from such treatment (Hegi *et al.*, 2005). Furthermore, in the context of recurrent glioblastoma, our ex vivo assay aims to provides clinicians with a valuable tool for identifying more suitable treatment regimens that could be applied to recurrent disease. This is especially critical as the current prognosis in terms of PFS (5.5 months) and OS (8-9 months) rates remains suboptimal (van Linde *et al.*, 2017). Notably, the completion of

the ex vivo assay takes approximately one week following the receipt of the patient's tumour specimen post-surgery. This timeframe allows for the patient to recover adequately from surgery and for clinicians to make well-informed decisions regarding the most appropriate treatment pathway to pursue. Compared to similar precision oncology screens in the realm of glioblastoma, our ex vivo screening tool holds a distinct advantage. It encompasses a substantially larger drug library and is capable of analysing drug responses at the single-cell resolution through the utilization of ultra-high-content microscopy.

To the best of our knowledge, the research presented here marks the initial efforts to establish a robust high throughput ex vivo drug screening system for gliomas, utilizing freshly dissociated tumour tissue. We have worked diligently to optimize the seeding protocols, growth conditions, imaging techniques, and analysis procedures, enabling us to assess nearly all glioma samples from the clinic against custom drug plates or current SoC treatments. We are now able to integrate drug plate screening with SoC therapies, like radiation (comparing untreated plates with those exposed to 2Gy radiation), to mimic the clinical treatment approach and clinical trial conditions, especially if TMZ can be excluded from the treatment regimen for identified *MGMT* unmethylated tumours, as mentioned earlier. As we continue to enhance our ex vivo screening platform, our goal is to refine multi-channel imaging techniques to identify compounds or treatments that exhibit specific efficacy against GSC populations while minimizing the impact on other cell types. Concurrently, we are collaborating with computer scientists and artificial intelligence experts to develop machine learning technologies that can automate and enhance the speed and efficiency of ex vivo operations. Furthermore, we are actively engaged with the larger ex vivo determined cancer therapy (EVIDENT; NCT05231655) team at Sheffield University and Hospital sites to share our ex vivo experiences and contribute to the development of additional animal-friendly ex vivo screening platforms for various solid tumours, such as bladder, kidney, head and neck cancers, among others.

Chapter 7 – References

Aarts, M. *et al.* (2012) 'Forced mitotic entry of S-phase cells as a therapeutic strategy induced by inhibition of WEE1', *Cancer Discovery*, 2(6), pp. 524–539. Available at: https://doi.org/10.1158/2159-8290.CD-11-0320/42145/AM/FORCED-MITOTIC-ENTRY-OF-S-PHASE-CELLS-AS-A.

Agnihotri, S. *et al.* (2012) 'Alkylpurine–DNA–N-glycosylase confers resistance to temozolomide in xenograft models of glioblastoma multiforme and is associated with poor survival in patients', *The Journal of Clinical Investigation*, 122(1), pp. 253–266. Available at: https://doi.org/10.1172/JCI59334.

Aguilera, P. and López-Contreras, A.J. (2023) 'ATRX, a guardian of chromatin', *Trends in genetics : TIG*, 39(6), pp. 505–519. Available at: https://doi.org/10.1016/J.TIG.2023.02.009.

Ahmed, S.U. *et al.* (2015) 'Selective Inhibition of Parallel DNA Damage Response Pathways Optimizes Radiosensitization of Glioblastoma Stem-like Cells', *Cancer research*, 75(20), pp. 4416–4428. Available at: https://doi.org/10.1158/0008-5472.CAN-14-3790.

Aisenbrey, E.A. and Murphy, W.L. (2020) 'Synthetic alternatives to Matrigel', *Nature reviews. Materials*, 5(7), p. 539. Available at: https://doi.org/10.1038/S41578-020-0199-8.

Akbani, R. *et al.* (2015) 'Genomic Classification of Cutaneous Melanoma', *Cell*, 161(7), p. 1681. Available at: https://doi.org/10.1016/J.CELL.2015.05.044.

Aldape, K. *et al.* (2019) 'Challenges to curing primary brain tumours', *Nature Reviews Clinical Oncology 2019 16:8*, 16(8), pp. 509–520. Available at: https://doi.org/10.1038/s41571-019-0177-5.

Aldea, M. *et al.* (2023) 'Placing the patient at the heart of discovery science', *European journal of cancer (Oxford, England : 1990)*, 193. Available at: https://doi.org/10.1016/J.EJCA.2023.113306.

Van Allen, E.M. *et al.* (2014) 'The genetic landscape of clinical resistance to RAF inhibition in metastatic melanoma', *Cancer Discovery*, 4(1), pp. 94–109. Available at: https://doi.org/10.1158/2159-8290.CD-13-0617/43140/P/THE-GENETIC-LANDSCAPE-OF-CLINICAL-RESISTANCE-TO.

Arjonen, A. *et al.* (2020) 'Image-based ex vivo drug screen to assess targeted therapies in recurrent thymoma', *Lung cancer (Amsterdam, Netherlands)*, 145, pp. 27–32. Available at: https://doi.org/10.1016/J.LUNGCAN.2020.04.036.

Ausman, J.I., Shapiro, W.R. and Rail, D.P. (1970) 'Studies on the Chemotherapy of Experimental Brain Tumors: Development of an Experimental Model', *CANCER RESEARCH*, 30. Available at: http://aacrjournals.org/cancerres/article-pdf/30/9/2394/2387172/cr0300092394.pdf (Accessed: 31 October 2023).

Bachoo, R.M. *et al.* (2002) 'Epidermal growth factor receptor and Ink4a/Arf: Convergent mechanisms governing terminal differentiation and transformation along the neural stem cell to astrocyte axis', *Cancer Cell*, 1(3), pp. 269–277. Available at: https://doi.org/10.1016/S1535-6108(02)00046-6.

Bai, P. *et al.* (2023) 'The dual role of DNA repair protein MGMT in cancer prevention and

treatment', *DNA Repair*, 123, p. 103449. Available at: https://doi.org/10.1016/J.DNAREP.2023.103449.

Bao, S. *et al.* (2006) 'Glioma stem cells promote radioresistance by preferential activation of the DNA damage response', *Nature 2006 444:7120*, 444(7120), pp. 756–760. Available at: https://doi.org/10.1038/nature05236.

Bao, Z. *et al.* (2016) 'Oleandrin induces DNA damage responses in cancer cells by suppressing the expression of Rad51', *Oncotarget*, 7(37), p. 59572. Available at: https://doi.org/10.18632/ONCOTARGET.10726.

Barrantes-Freer, A. *et al.* (2015) 'CD133 Expression Is Not Synonymous to Immunoreactivity for AC133 and Fluctuates throughout the Cell Cycle in Glioma Stem-Like Cells', *PLoS ONE*, 10(6). Available at: https://doi.org/10.1371/JOURNAL.PONE.0130519.

Barthel, F.P. *et al.* (2019) 'Longitudinal molecular trajectories of diffuse glioma in adults', *Nature 2019 576:7785*, 576(7785), pp. 112–120. Available at: https://doi.org/10.1038/s41586-019-1775-1.

Bauer, N. *et al.* (2011) 'Haematopoietic stem cell differentiation promotes the release of prominin-1/CD133-containing membrane vesicles--a role of the endocytic-exocytic pathway', *EMBO molecular medicine*, 3(7), pp. 398–409. Available at: https://doi.org/10.1002/EMMM.201100147.

Beale, P. *et al.* (1999) 'Effect of gastric pH on the relative oral bioavailability and pharmacokinetics of temozolomide', *Cancer Chemotherapy and Pharmacology*, 44(5), pp. 389–394. Available at: https://doi.org/10.1007/S002800050994/METRICS.

Bernal, A. and Arranz, L. (2018) 'Nestin-expressing progenitor cells: function, identity and therapeutic implications', *Cellular and Molecular Life Sciences*, 75(12), p. 2177. Available at: https://doi.org/10.1007/S00018-018-2794-Z.

Bertier, G., Hétu, M. and Joly, Y. (2016) 'Unsolved challenges of clinical whole-exome sequencing: A systematic literature review of end-users' views ', *BMC Medical Genomics*, 9(1), pp. 1–12. Available at: https://doi.org/10.1186/S12920-016-0213-6/FIGURES/5.

Bessette, H. *et al.* (1992) 'CANCER-p53, guardian of the genome', *DeutSCh, D. Proc. R. Soc*, 5, pp. 661–663.

Bicker, J. *et al.* (2014) 'Blood-brain barrier models and their relevance for a successful development of CNS drug delivery systems: A review'. Available at: https://doi.org/10.1016/j.ejpb.2014.03.012.

Bigner, S.H., Mark, J. and Bigner, D.D. (1990) 'Cytogenetics of Human Brain Tumors'.

Birey, F. *et al.* (2017) 'Assembly of functionally integrated human forebrain spheroids', *Nature 2017 545:7652*, 545(7652), pp. 54–59. Available at: https://doi.org/10.1038/nature22330.

Bleeker, F.E., Molenaar, R.J. and Leenstra, S. (2012) 'Recent advances in the molecular understanding of glioblastoma', *Journal of Neuro-Oncology*, 108(1), p. 11. Available at: https://doi.org/10.1007/S11060-011-0793-0.

Boehnke, K. *et al.* (2016) 'Assay establishment and validation of a high-throughput screening platform for three-dimensional patient-derived colon cancer organoid cultures', *Journal of*

Biomolecular Screening, 21(9), pp. 931–941. Available at: https://doi.org/10.1177/1087057116650965.

De Bont, R. and van Larebeke, N. (2004) 'Endogenous DNA damage in humans: a review of quantitative data', *Mutagenesis*, 19(3), pp. 169–185. Available at: https://doi.org/10.1093/MUTAGE/GEH025.

Braidy, N. *et al.* (2019) 'Role of Nicotinamide Adenine Dinucleotide and Related Precursors as Therapeutic Targets for Age-Related Degenerative Diseases: Rationale, Biochemistry, Pharmacokinetics, and Outcomes', *Antioxidants & Redox Signaling*, 30(2), p. 251. Available at: https://doi.org/10.1089/ARS.2017.7269.

Branzei, D. and Foiani, M. (2008) 'Regulation of DNA repair throughout the cell cycle', *Nature reviews. Molecular cell biology*, 9(4), pp. 297–308. Available at: https://doi.org/10.1038/NRM2351.

Bray, M.-A., Carpenter, A. and Imaging Platform, B.I. of M. and H. (2017) 'Advanced Assay Development Guidelines for Image-Based High Content Screening and Analysis', *Assay Guidance Manual* [Preprint]. Available at: https://www.ncbi.nlm.nih.gov/books/NBK126174/ (Accessed: 3 August 2023).

Brennan, C.W. *et al.* (2013) 'The Somatic Genomic Landscape of Glioblastoma', *Cell*, 155(2), pp. 462–477. Available at: https://doi.org/10.1016/J.CELL.2013.09.034.

Brescia, P. *et al.* (2013) 'CD133 Is Essential for Glioblastoma Stem Cell Maintenance', *Stem Cells*, 31(5), pp. 857–869. Available at: https://doi.org/10.1002/STEM.1317.

Bria, E. *et al.* (2011) 'Outcome of advanced NSCLC patients harboring sensitizing EGFR mutations randomized to EGFR tyrosine kinase inhibitors or chemotherapy as first-line treatment: a meta-analysis', *Annals of Oncology*, 22(10), pp. 2277–2285. Available at: https://doi.org/10.1093/ANNONC/MDQ742.

Brochier, C. and Langley, B. (2013) 'Chromatin modifications associated with DNA double-strand breaks repair as potential targets for neurological diseases', *Neurotherapeutics : the journal of the American Society for Experimental NeuroTherapeutics*, 10(4), pp. 817–830. Available at: https://doi.org/10.1007/S13311-013-0210-9.

Brooks, E.A. *et al.* (2019) 'Applicability of drug response metrics for cancer studies using biomaterials', *Philosophical Transactions of the Royal Society B*, 374(1779). Available at: https://doi.org/10.1098/RSTB.2018.0226.

Bryant, H.E. *et al.* (2005) 'Specific killing of BRCA2-deficient tumours with inhibitors of poly(ADP-ribose) polymerase', *Nature 2005 434:7035*, 434(7035), pp. 913–917. Available at: https://doi.org/10.1038/nature03443.

Von Bueren, A.O. *et al.* (2012) 'Mismatch repair deficiency: a temozolomide resistance factor in medulloblastoma cell lines that is uncommon in primary medulloblastoma tumours', *British Journal of Cancer*, 107(8), p. 1399. Available at: https://doi.org/10.1038/BJC.2012.403.

Bushong, E.A. *et al.* (2001) 'Protoplasmic Astrocytes in CA1 Stratum Radiatum Occupy Separate Anatomical Domains'.

Caccese, M. *et al.* (2020) 'Mismatch-Repair Protein Expression in High-Grade Gliomas: A Large Retrospective Multicenter Study', *International Journal of Molecular Sciences*, 21(18),

pp. 1–12. Available at: https://doi.org/10.3390/IJMS21186716.

Cahoy, J.D. *et al.* (2008) 'A Transcriptome Database for Astrocytes, Neurons, and Oligodendrocytes: A New Resource for Understanding Brain Development and Function'. Available at: https://doi.org/10.1523/JNEUROSCI.4178-07.2008.

Calabrese, C. *et al.* (2007) 'A Perivascular Niche for Brain Tumor Stem Cells', *Cancer Cell*, 11(1), pp. 69–82. Available at: https://doi.org/10.1016/j.ccr.2006.11.020.

Carruthers, R. *et al.* (2015) 'Abrogation of radioresistance in glioblastoma stem-like cells by inhibition of ATM kinase', *Molecular Oncology*, 9(1), pp. 192–203. Available at: https://doi.org/10.1016/j.molonc.2014.08.003.

Chakraborty, U. and Alani, E. (2016) 'Understanding how mismatch repair proteins participate in the repair/anti-recombination decision', *FEMS Yeast Research*, 16(6), p. 71. Available at: https://doi.org/10.1093/FEMSYR/FOW071.

Chamberlain, M.C. (2011) 'Bevacizumab for the treatment of recurrent glioblastoma', *Clinical Medicine Insights: Oncology*. Libertas Academica Ltd., pp. 117–129. Available at: https://doi.org/10.4137/CMO.S7232.

Chang, H.H.Y. *et al.* (2017) 'Non-homologous DNA end joining and alternative pathways to double-strand break repair', *Nature Reviews Molecular Cell Biology 2017 18:8*, 18(8), pp. 495–506. Available at: https://doi.org/10.1038/nrm.2017.48.

Chapman, J.R., Taylor, M.R.G. and Boulton, S.J. (2012) 'Molecular Cell Review Playing the End Game: DNA Double-Strand Break Repair Pathway Choice'. Available at: https://doi.org/10.1016/j.molcel.2012.07.029.

Chen, B.P.C. *et al.* (2005) 'Cell Cycle Dependence of DNA-dependent Protein Kinase Phosphorylation in Response to DNA Double Strand Breaks', *Journal of Biological Chemistry*, 280(15), pp. 14709–14715. Available at: https://doi.org/10.1074/JBC.M408827200.

Chen, B.P.C. *et al.* (2007) 'Ataxia telangiectasia mutated (ATM) is essential for DNA-PKcs phosphorylations at the Thr-2609 cluster upon DNA double strand break', *The Journal of biological chemistry*, 282(9), pp. 6582–6587. Available at: https://doi.org/10.1074/JBC.M611605200.

Chen, J. *et al.* (2012) 'A restricted cell population propagates glioblastoma growth after chemotherapy', *Nature 2012 488:7412*, 488(7412), pp. 522–526. Available at: https://doi.org/10.1038/nature11287.

Chinot, O.L. *et al.* (2014) 'Bevacizumab plus Radiotherapy–Temozolomide for Newly Diagnosed Glioblastoma', *New England Journal of Medicine*, 370(8), pp. 709–722. Available at: https://doi.org/10.1056/nejmoa1308345.

Chou, W.H. *et al.* (2018) 'Ouabain Induces Apoptotic Cell Death Through Caspase- and Mitochondria-dependent Pathways in Human Osteosarcoma U-2 OS Cells', *Anticancer research*, 38(1), pp. 169–178. Available at: https://doi.org/10.21873/ANTICANRES.12205.

Ciccia, A. and Elledge, S.J. (2010) 'The DNA Damage Response: Making It Safe to Play with Knives', *Molecular Cell*, 40(2), pp. 179–204. Available at: https://doi.org/10.1016/J.MOLCEL.2010.09.019.

Clark, A.S. *et al.* (1995) *Antitumor Imidazotetrazines. 32.1 Synthesis of Novel*

Imidazotetrazinones and Related Bicyclic Heterocycles To Probe the Mode of Action of the Antitumor Drug Temozolomide, *J. Med. Chem*. Available at: https://pubs.acs.org/sharingguidelines (Accessed: 9 November 2020).

Clark, P.A. *et al.* (2012) 'Activation of Multiple ERBB Family Receptors Mediates Glioblastoma Cancer Stem-like Cell Resistance to EGFR-Targeted Inhibition', *Neoplasia*, 14(5), pp. 420-IN13. Available at: https://doi.org/10.1596/NEO.12432.

Clynes, D. *et al.* (2014) 'ATRX Dysfunction Induces Replication Defects in Primary Mouse Cells', *PLOS ONE*, 9(3), p. e92915. Available at: https://doi.org/10.1371/JOURNAL.PONE.0092915.

Cohen, A.L., Holmen, S.L. and Colman, H. (2013) 'IDH1 and IDH2 mutations in gliomas', *Current Neurology and Neuroscience Reports*, 13(5), pp. 1–7. Available at: https://doi.org/10.1007/S11910-013-0345-4/FIGURES/1.

Cohen, M.H. *et al.* (2009) 'FDA Drug Approval Summary: Bevacizumab (Avastin®) as Treatment of Recurrent Glioblastoma Multiforme', *The Oncologist*, 14(11), pp. 1131–1138. Available at: https://doi.org/10.1634/theoncologist.2009-0121.

Colman, H. *et al.* (2010) 'A multigene predictor of outcome in glioblastoma', *Neuro-Oncology*, 12(1), pp. 49–57. Available at: https://doi.org/10.1093/neuonc/nop007.

Corbeil, D. *et al.* (2010) 'The intriguing links between prominin-1 (CD133), cholesterol-based membrane microdomains, remodeling of apical plasma membrane protrusions, extracellular membrane particles, and (neuro)epithelial cell differentiation', *FEBS Letters*, 584(9), pp. 1659–1664. Available at: https://doi.org/10.1016/J.FEBSLET.2010.01.050.

Cunanan, K.M. *et al.* (2017) 'Basket Trials in Oncology: A Trade-Off Between Complexity and Efficiency', *Journal of Clinical Oncology*, 35(3), p. 271. Available at: https://doi.org/10.1200/JCO.2016.69.9751.

Curtin, N.J. (2023) 'Targeting the DNA damage response for cancer therapy', *Biochemical Society Transactions*, 51(1), pp. 207–221. Available at: https://doi.org/10.1042/BST20220681.

Daher, A. and de Groot, J. (2018) 'Rapid identification and validation of novel targeted approaches for Glioblastoma: A combined ex vivo-in vivo pharmaco-omic model', *Experimental Neurology*. Academic Press Inc., pp. 281–288. Available at: https://doi.org/10.1016/j.expneurol.2017.09.006.

Dang, L. *et al.* (2009) 'Cancer-associated IDH1 mutations produce 2-hydroxyglutarate', *Nature*, 462. Available at: https://doi.org/10.1038/nature08617.

Dang, L., Yen, K. and Attar, E.C. (2016) 'IDH mutations in cancer and progress toward development of targeted therapeutics', *Annals of Oncology*, 27(4), pp. 599–608. Available at: https://doi.org/10.1093/ANNONC/MDW013.

Dangles-Marie, V. *et al.* (2007) 'Establishment of human colon cancer cell lines from fresh tumors versus xenografts: comparison of success rate and cell line features', *Cancer research*, 67(1), pp. 398–407. Available at: https://doi.org/10.1158/0008-5472.CAN-06-0594.

Daniel, V.C. *et al.* (2009) 'A primary xenograft model of small-cell lung cancer reveals irreversible changes in gene expression imposed by culture in vitro', *Cancer Research*, 69(8),

pp. 3364–3373. Available at: https://doi.org/10.1158/0008-5472.CAN-08-4210/654954/P/A-PRIMARY-XENOGRAFT-MODEL-OF-SMALL-CELL-LUNG.

DJ, B. *et al.* (2015) 'Comprehensive, Integrative Genomic Analysis of Diffuse Lower-Grade Gliomas', *The New England journal of medicine*, 372(26), pp. 2481–2498. Available at: https://doi.org/10.1056/NEJMOA1402121.

Drabløs, F. *et al.* (2004) 'Alkylation damage in DNA and RNA—repair mechanisms and medical significance', *DNA Repair*, 3(11), pp. 1389–1407. Available at: https://doi.org/10.1016/J.DNAREP.2004.05.004.

Du, J. *et al.* (2018) 'A CRISPR/Cas9-based screening for non-homologous end joining inhibitors reveals ouabain and penfluridol as radiosensitizers', *Molecular Cancer Therapeutics*, 17(2), pp. 419–431. Available at: https://doi.org/10.1158/1535-7163.MCT-17-0090/87198/AM/A-CRISPR-CAS9-BASED-SCREENING-FOR-NON-HOMOLOGOUS.

Duffner, F. *et al.* (2005) 'Specific intensity imaging for glioblastoma and neural cell cultures with 5-aminolevulinic acid-derived protoporphyrin IX', *Journal of Neuro-Oncology*, 71(2), pp. 107–111. Available at: https://doi.org/10.1007/S11060-004-9603-2/METRICS.

Duffy, P.E., Huang, Y.-Y. and Rapport, M.M. (1982) 'The relationship of glial fibrillary acidic protein to the shape, motility, and differentiation of human astrocytoma cells', *Experimental Cell Research*, 139, pp. 145–157.

Ennis S Lamon, D.J. *et al.* (2001) 'Use of Chemotherapy plus a Monoclonal Antibody against HER2 for Metastatic Breast Cancer That Overexpresses HER2', *https://doi.org/10.1056/NEJM200103153441101*, 344(11), pp. 783–792. Available at: https://doi.org/10.1056/NEJM200103153441101.

Esposito, F. *et al.* (2021) 'Wee1 Kinase: A Potential Target to Overcome Tumor Resistance to Therapy', *International journal of molecular sciences*, 22(19). Available at: https://doi.org/10.3390/IJMS221910689.

Evans, S.M. *et al.* (2004) 'Hypoxia Is Important in the Biology and Aggression of Human Glial Brain Tumors', *Clinical Cancer Research*, 10(24), pp. 8177–8184. Available at: https://doi.org/10.1158/1078-0432.CCR-04-1081.

Evans, S.M. *et al.* (2008) 'Imaging and Analytical Methods as Applied to the Evaluation of Vasculature and Hypoxia in Human Brain Tumors', *Radiation Research*, 170(6), pp. 677–690. Available at: https://doi.org/10.1667/RR1207.1.

Fael Al-Mayhani, T.M. *et al.* (2009) 'An efficient method for derivation and propagation of glioblastoma cell lines that conserves the molecular profile of their original tumours', *Journal of Neuroscience Methods*, 176(2), pp. 192–199. Available at: https://doi.org/10.1016/J.JNEUMETH.2008.07.022.

Fallahi-Sichani, M. *et al.* (2013) 'Metrics other than potency reveal systematic variation in responses to cancer drugs', *Nature chemical biology*, 9(11), p. 708. Available at: https://doi.org/10.1038/NCHEMBIO.1337.

Farmer, H. *et al.* (2005) 'Targeting the DNA repair defect in BRCA mutant cells as a therapeutic strategy', *Nature*, 434(7035), pp. 917–921. Available at: https://doi.org/10.1038/NATURE03445.

Fathers, C. *et al.* (2012) 'Cell Cycle Inhibition of poly(ADP-ribose) glycohydrolase (PARG)

specifically kills BRCA2-deficient tumor cells', *Cell Cycle*, 11(5), pp. 990–997. Available at: https://doi.org/10.4161/cc.11.5.19482.

Fernandez-Marcos, P.J. and Nóbrega-Pereira, S. (2016) 'NADPH: new oxygen for the ROS theory of aging', *Oncotarget*, 7(32), p. 50814. Available at: https://doi.org/10.18632/ONCOTARGET.10744.

Figueroa, M.E. *et al.* (2010) 'Leukemic IDH1 and IDH2 mutations result in a hypermethylation phenotype, disrupt TET2 function, and impair hematopoietic differentiation', *Cancer cell*, 18(6), pp. 553–567. Available at: https://doi.org/10.1016/J.CCR.2010.11.015.

Flaherty, K.T. *et al.* (2020) 'The Molecular Analysis for Therapy Choice (NCI-MATCH) Trial: Lessons for Genomic Trial Design', *JNCI Journal of the National Cancer Institute*, 112(10), p. 1021. Available at: https://doi.org/10.1093/JNCI/DJZ245.

Gagg, H. *et al.* (2023) 'Ex-vivo drug screening of surgically resected glioma stem cells to replace murine avatars and provide personalise cancer therapy for glioblastoma patients', *F1000Research*, 12, p. 954. Available at: https://doi.org/10.12688/F1000RESEARCH.135809.1/DOI.

Galli, R. *et al.* (2004) 'Isolation and characterization of tumorigenic, stem-like neural precursors from human glioblastoma', *Cancer Research*, 64(19), pp. 7011–7021. Available at: https://doi.org/10.1158/0008-5472.CAN-04-1364.

Garbarino, J. *et al.* (2021) 'Loss of ATRX confers DNA repair defects and PARP inhibitor sensitivity', *Translational Oncology*, 14(9), p. 101147. Available at: https://doi.org/10.1016/J.TRANON.2021.101147.

Genoud, V. *et al.* (2018) 'Responsiveness to anti-PD-1 and anti-CTLA-4 immune checkpoint blockade in SB28 and GL261 mouse glioma models', *OncoImmunology*, 7(12). Available at: https://doi.org/10.1080/2162402X.2018.1501137.

Giffard, R.G. and Swanson, R.A. (2005) 'Ischemia-induced programmed cell death in astrocytes', *Glia*, 50(4), pp. 299–306. Available at: https://doi.org/10.1002/GLIA.20167.

Gilbert, M.R. *et al.* (2013) 'Dose-dense temozolomide for newly diagnosed glioblastoma: A randomized phase III clinical trial', *Journal of Clinical Oncology*, 31(32), pp. 4085–4091. Available at: https://doi.org/10.1200/JCO.2013.49.6968.

Gillet, L.C.J. and Schärer, O.D. (2006) 'Molecular mechanisms of mammalian global genome nucleotide excision repair', *Chemical Reviews*, 106(2), pp. 253–276. Available at: https://doi.org/10.1021/CR040483F/ASSET/IMAGES/LARGE/CR-2004-00483F_0013.JPEG.

Gimple, R.C. *et al.* (2019) 'Glioblastoma stem cells: lessons from the tumor hierarchy in a lethal cancer', *Genes & Development*, 33(11–12), p. 591. Available at: https://doi.org/10.1101/GAD.324301.119.

Gogola, E. *et al.* (2018) 'Selective Loss of PARG Restores PARylation and Counteracts PARP Inhibitor-Mediated Synthetic Lethality', *Cancer Cell*, 33(6), pp. 1078-1093.e12. Available at: https://doi.org/10.1016/J.CCELL.2018.05.008.

Goldberg, A.D. *et al.* (2010) 'Distinct Factors Control Histone Variant H3.3 Localization at Specific Genomic Regions', *Cell*, 140(5), pp. 678–691. Available at: https://doi.org/10.1016/j.cell.2010.01.003.

Gomez-Roman, N. *et al.* (2017) 'A novel 3D human glioblastoma cell culture system for modeling drug and radiation responses', *Neuro-Oncology*, 19(2), pp. 229–241. Available at: https://doi.org/10.1093/NEUONC/NOW164.

Grasso, C.S. *et al.* (2015) 'Functionally defined therapeutic targets in diffuse intrinsic pontine glioma', *Nature Medicine 2015 21:6*, 21(6), pp. 555–559. Available at: https://doi.org/10.1038/nm.3855.

Gravells, P. *et al.* (2017) 'Specific killing of DNA damage-response deficient cells with inhibitors of poly(ADP-ribose) glycohydrolase', *DNA Repair*, 52, pp. 81–91. Available at: https://doi.org/10.1016/J.DNAREP.2017.02.010.

Grube, S. *et al.* (2021) 'Characterization of adherent primary cell lines from fresh human glioblastoma tissue, defining glial fibrillary acidic protein as a reliable marker in establishment of glioblastoma cell culture', *Cancer Reports*, 4(2). Available at: https://doi.org/10.1002/CNR2.1324.

Gupta, A. *et al.* (2020) 'A normalized drug response metric improves accuracy and consistency of anticancer drug sensitivity quantification in cell-based screening', *Communications Biology*, 3(1). Available at: https://doi.org/10.1038/S42003-020-0765-Z.

Gupta, R. *et al.* (2013) 'Expanding the spectrum of IDH1 mutations in gliomas', *Modern Pathology*, 26, pp. 619–625. Available at: https://doi.org/10.1038/modpathol.2012.210.

Hanawalt, P.C. and Spivak, G. (2008) 'Transcription-coupled DNA repair: two decades of progress and surprises', *Nature Reviews Molecular Cell Biology 2008 9:12*, 9(12), pp. 958–970. Available at: https://doi.org/10.1038/nrm2549.

Hanif, F. *et al.* (2017) 'Glioblastoma Multiforme: A Review of its Epidemiology and Pathogenesis through Clinical Presentation and Treatment', *Asian Pacific Journal of Cancer Prevention : APJCP*, 18(1), p. 3. Available at: https://doi.org/10.22034/APJCP.2017.18.1.3.

Hargrave, D., Bartels, U. and Bouffet, E. (2006) 'Diffuse brainstem glioma in children: critical review of clinical trials', *The Lancet Oncology*, 7(3), pp. 241–248. Available at: https://doi.org/10.1016/S1470-2045(06)70615-5.

Hassn Mesrati, M. *et al.* (2020) 'Understanding Glioblastoma Biomarkers: Knocking a Mountain with a Hammer', *Cells*, 9(5). Available at: https://doi.org/10.3390/CELLS9051236.

Hauschild, A. *et al.* (2012) 'Dabrafenib in BRAF-mutated metastatic melanoma: A multicentre, open-label, phase 3 randomised controlled trial', *The Lancet*, 380(9839), pp. 358–365. Available at: https://doi.org/10.1016/S0140-6736(12)60868-X.

He, G. *et al.* (2005) 'Induction of p21 by p53 following DNA damage inhibits both Cdk4 and Cdk2 activities', *Oncogene 2005 24:18*, 24(18), pp. 2929–2943. Available at: https://doi.org/10.1038/sj.onc.1208474.

Hegi, M.E. *et al.* (2005) ' MGMT Gene Silencing and Benefit from Temozolomide in Glioblastoma ', *New England Journal of Medicine*, 352(10), pp. 997–1003. Available at: https://doi.org/10.1056/NEJMOA043331/SUPPL_FILE/997SA1.PDF.

Helena, J.M. *et al.* (2018) 'Deoxyribonucleic Acid Damage and Repair: Capitalizing on Our Understanding of the Mechanisms of Maintaining Genomic Integrity for Therapeutic Purposes', *International Journal of Molecular Sciences*, 19(4). Available at: https://doi.org/10.3390/IJMS19041148.

Hemmati, H.D. *et al.* (2003) 'Cancerous stem cells can arise from pediatric brain tumors', *Proceedings of the National Academy of Sciences of the United States of America*, 100(25), pp. 15178–15183. Available at: https://doi.org/10.1073/PNAS.2036535100/SUPPL_FILE/6535FIG5.JPG.

Hirai, H. *et al.* (2009) 'Small-molecule inhibition of Wee1 kinase by MK-1775 selectively sensitizes p53-deficient tumor cells to DNA-damaging agents', *Molecular Cancer Therapeutics*, 8(11), pp. 2992–3000. Available at: https://doi.org/10.1158/1535-7163.MCT-09-0463/354722/P/SMALL-MOLECULE-INHIBITION-OF-WEE1-KINASE-BY-MK.

Hirai, H. *et al.* (2010) 'MK-1775, a small molecule Wee1 inhibitor, enhances anti-tumor efficacy of various DNA-damaging agents, including 5-fluorouracil', *http://dx.doi.org/10.4161/cbt.9.7.11115*, 9(7), pp. 514–522. Available at: https://doi.org/10.4161/CBT.9.7.11115.

Hirano, T. *et al.* (2015) 'In vitro modeling to determine mutation specificity of EGFR tyrosine kinase inhibitors against clinically relevant EGFR mutants in non-small-cell lung cancer', *Oncotarget*, 6(36), pp. 38789–38803. Available at: https://doi.org/10.18632/ONCOTARGET.5887.

Hoeijmakers, J.H.J. (2001) 'Genome maintenance mechanisms for preventing cancer', *Nature 2001 411:6835*, 411(6835), pp. 366–374. Available at: https://doi.org/10.1038/35077232.

Hol, E.M. and Capetanaki, Y. (2017) 'Type III Intermediate Filaments Desmin, Glial Fibrillary Acidic Protein (GFAP), Vimentin, and Peripherin', *Cold Spring Harbor Perspectives in Biology*, 9(12), p. a021642. Available at: https://doi.org/10.1101/CSHPERSPECT.A021642.

Hothi, P. *et al.* (2012) 'High-Throughput chemical screens identify disulfiram as an inhibitor of human glioblastoma stem cells', *Oncotarget*, 3(10), pp. 1124–1136. Available at: https://doi.org/10.18632/oncotarget.707.

Houl, J.H. *et al.* (2019) 'Selective small molecule PARG inhibitor causes replication fork stalling and cancer cell death', *Nature Communications 2019 10:1*, 10(1), pp. 1–15. Available at: https://doi.org/10.1038/s41467-019-13508-4.

Howard, C.M. *et al.* (2017) 'Analysis of Chemopredictive Assay for Targeting Cancer Stem Cells in Glioblastoma Patients', *Translational Oncology*, 10(2), pp. 241–254. Available at: https://doi.org/10.1016/J.TRANON.2017.01.008.

Hubert, C.G. *et al.* (2016) 'Tumor and Stem Cell Biology A Three-Dimensional Organoid Culture System Derived from Human Glioblastomas Recapitulates the Hypoxic Gradients and Cancer Stem Cell Heterogeneity of Tumors Found In Vivo'. Available at: https://doi.org/10.1158/0008-5472.CAN-15-2402.

Huh, M.S. *et al.* (2016) 'Stalled replication forks within heterochromatin require ATRX for protection', *Cell Death & Disease 2016 7:5*, 7(5), pp. e2220–e2220. Available at: https://doi.org/10.1038/cddis.2016.121.

Hustedt, N. and Durocher, D. (2016) 'The control of DNA repair by the cell cycle', *Nature Cell Biology 2016 19:1*, 19(1), pp. 1–9. Available at: https://doi.org/10.1038/ncb3452.

Ibrahim, A.M. *et al.* (2022) 'Radiation and chemotherapy variable response induced by tumor cell hypoxia: impact of radiation dose, anticancer drug, and type of cancer', *Radiation*

and Environmental Biophysics, 61(2), p. 263. Available at: https://doi.org/10.1007/S00411-022-00974-6.

Ignatova, T.N. *et al.* (2002) 'Human cortical glial tumors contain neural stem-like cells expressing astroglial and neuronal markers in vitro', *Glia*, 39(3), pp. 193–206. Available at: https://doi.org/10.1002/GLIA.10094.

Jackson, E.L. and Alvarez-Buylla, A. (2008) 'Characterization of Adult Neural Stem Cells and Their Relation to Brain Tumors', *Cells Tissues Organs*, 188(1–2), pp. 212–224. Available at: https://doi.org/10.1159/000114541.

Jackson, M., Gomez-Roman, N. and Chalmers, A. (2019) 'Inhibitors of poly(ADP-ribose) glycohydrolase (PARG) exhibit single agent therapeutic activity and sensitize glioblastoma cells to ionizing radiation', *Neuro-Oncology*, 21(Suppl 4), p. iv12. Available at: https://doi.org/10.1093/NEUONC/NOZ167.049.

Jaeckle, K.A. *et al.* (2011) 'Transformation of low grade glioma and correlation with outcome: An NCCTG database analysis', *Journal of Neuro-Oncology*, 104(1), pp. 253–259. Available at: https://doi.org/10.1007/S11060-010-0476-2/FIGURES/2.

Jardim, D.L. *et al.* (2017) 'Factors associated with failure of oncology drugs in late-stage clinical development: A systematic review', *Cancer Treatment Reviews*, 52, pp. 12–21. Available at: https://doi.org/10.1016/J.CTRV.2016.10.009.

Jennings, G.T., Minard, K.I. and Mcalister-Henn, L. (1997) *Expression and Mutagenesis of Mammalian Cytosolic NADP +-Specific Isocitrate Dehydrogenase †*. Available at: https://pubs.acs.org/sharingguidelines (Accessed: 12 October 2020).

Jeuken, J.W.M., Von Deimling, A. and Wesseling, P. (no date) *Molecular pathogenesis of oligodendroglial tumors*.

Jiao, Y. *et al.* (2012) 'Frequent ATRX, CIC, FUBP1 and IDH1 mutations refine the classification of malignant gliomas', *Oncotarget*, 3(7), pp. 709–722. Available at: https://doi.org/10.18632/ONCOTARGET.588.

Jiao, Y., Feng, Y. and Wang, X. (2018) 'Regulation of Tumor Suppressor Gene CDKN2A and Encoded p16-INK4a Protein by Covalent Modifications', *Biochemistry (Moscow)*, 83(11), pp. 1289–1298. Available at: https://doi.org/10.1134/S0006297918110019/METRICS.

Jin, G. *et al.* (2013) 'Disruption of wild-type IDH1 suppresses D-2-hydroxyglutarate production in IDH1-mutated gliomas', *Cancer Research*, 73(2), pp. 496–501. Available at: https://doi.org/10.1158/0008-5472.CAN-12-2852/650682/AM/DISRUPTION-OF-WILD-TYPE-IDH1-SUPPRESSES-D-2.

Johanns, T.M. *et al.* (2016) 'Endogenous neoantigen-specific CD8 T cells identified in two glioblastoma models using a cancer immunogenomics approach', *Cancer Immunology Research*, 4(12), pp. 1007–1015. Available at: https://doi.org/10.1158/2326-6066.CIR-16-0156/470536/AM/ENDOGENOUS-NEOANTIGEN-SPECIFIC-CD8-T-CELLS.

Johansson, B. (1992) 'A review of the pharmacokinetics and pharmacodynamics of disulfiram and its metabolites', *Acta Psychiatrica Scandinavica*, 86(369 S), pp. 15–26. Available at: https://doi.org/10.1111/j.1600-0447.1992.tb03310.x.

Joo, K.M. *et al.* (2008) 'Clinical and biological implications of CD133-positive and CD133-negative cells in glioblastomas', *Laboratory Investigation 2008 88:8*, 88(8), pp. 808–815.

Available at: https://doi.org/10.1038/labinvest.2008.57.

Juhá Sz, S. *et al.* (2018) 'ATRX Promotes DNA Repair Synthesis and Sister Chromatid Exchange during Homologous Recombination', *Molecular Cell*, 71, pp. 11-24.e7. Available at: https://doi.org/10.1016/j.molcel.2018.05.014.

Kamachi, Y., Uchikawa, M. and Kondoh, H. (2000) 'Pairing SOX off: with partners in the regulation of embryonic development', *Trends in Genetics*, 16(4), pp. 182–187. Available at: https://doi.org/10.1016/S0168-9525(99)01955-1.

Kaur, B. *et al.* (2005) 'Hypoxia and the hypoxia-inducible-factor pathway in glioma growth and angiogenesis', *Neuro-Oncology*, 7(2), p. 134. Available at: https://doi.org/10.1215/S1152851704001115.

Khatua, S. *et al.* (2011) 'Diffuse intrinsic pontine glioma—current status and future strategies', *Child's Nervous System 2011 27:9*, 27(9), pp. 1391–1397. Available at: https://doi.org/10.1007/S00381-011-1468-Z.

Kijima, N. and Kanemura, Y. (2017) 'Mouse Models of Glioblastoma', *Glioblastoma*, pp. 131–139. Available at: https://doi.org/10.15586/CODON.GLIOBLASTOMA.2017.CH7.

Kim, H. *et al.* (2020) 'Extrachromosomal DNA is associated with oncogene amplification and poor outcome across multiple cancers', *Nature Genetics 2020 52:9*, 52(9), pp. 891–897. Available at: https://doi.org/10.1038/s41588-020-0678-2.

Kim, S.S. *et al.* (2015) 'A tumor-targeting p53 nanodelivery system limits chemoresistance to temozolomide prolonging survival in a mouse model of glioblastoma multiforme', *Nanomedicine: Nanotechnology, Biology and Medicine*, 11(2), pp. 301–311. Available at: https://doi.org/10.1016/J.NANO.2014.09.005.

Kolenda, J. *et al.* (2011) 'Effects of hypoxia on expression of a panel of stem cell and chemoresistance markers in glioblastoma-derived spheroids', *Journal of Neuro-Oncology*, 103(1), pp. 43–58. Available at: https://doi.org/10.1007/S11060-010-0357-8/FIGURES/9.

Komori, T. (2017) 'The 2016 WHO Classification of Tumours of the Central Nervous System: The Major Points of Revision', *Neurol Med Chir (Tokyo)*, 57, pp. 301–311. Available at: https://doi.org/10.2176/nmc.ra.2017-0010.

Koschmann, C. *et al.* (2016) 'ATRX Loss Promotes Tumor Growth and Impairs Non-Homologous End Joining DNA Repair in Glioma', *Science translational medicine*, 8(328), p. 328ra28. Available at: https://doi.org/10.1126/SCITRANSLMED.AAC8228.

Koschmann, C. *et al.* (2017) 'Mutated Chromatin Regulatory Factors as Tumor Drivers in Cancer', *Cancer Res*, 77(2). Available at: https://doi.org/10.1158/0008-5472.CAN-16-2301.

Koschmann, C., Lowenstein, P.R. and Castro, M.G. (2016) 'ATRX mutations and glioblastoma: Impaired DNA damage repair, alternative lengthening of telomeres, and genetic instability', *https://doi.org/10.1080/23723556.2016.1167158*, 3(3). Available at: https://doi.org/10.1080/23723556.2016.1167158.

Koutsopoulos, S. and Zhang, S. (2013) 'Long-term three-dimensional neural tissue cultures in functionalized self-assembling peptide hydrogels, Matrigel and Collagen I', *Acta Biomaterialia*, 9(2), pp. 5162–5169. Available at: https://doi.org/10.1016/J.ACTBIO.2012.09.010.

Krause, K. *et al.* (2000) 'The tumour suppressor protein p53 can repress transcription of cyclin B', *Nucleic Acids Research*, 28(22), pp. 4410–4418. Available at: https://doi.org/10.1093/NAR/28.22.4410.

Krokan, H.E. and Bjørås, M. (2013) 'Base Excision Repair', *Cold Spring Harbor Perspectives in Biology*, 5(4), p. a012583. Available at: https://doi.org/10.1101/CSHPERSPECT.A012583.

Kuhnt, D. *et al.* (2011) 'Correlation of the extent of tumor volume resection and patient survival in surgery of glioblastoma multiforme with high-field intraoperative MRI guidance NEURO-ONCO LO GY', *Neuro-Oncology*, 13(12), pp. 1339–1348. Available at: https://doi.org/10.1093/neuonc/nor133.

Kupp, R. *et al.* (2016) 'Lineage-Restricted OLIG2-RTK Signaling Governs the Molecular Subtype of Glioma Stem-like Cells', *CellReports*, 16, pp. 2838–2845. Available at: https://doi.org/10.1016/j.celrep.2016.08.040.

Kuznetsov, N.A., Kanazhevskaya, L.Y. and Fedorova, O.S. (2021) 'DNA Demethylation in the Processes of Repair and Epigenetic Regulation Performed by 2-Ketoglutarate-Dependent DNA Dioxygenases', *International Journal of Molecular Sciences*, 22(19). Available at: https://doi.org/10.3390/IJMS221910540.

Lawrence, T.S. and Davis, M.A. (1990) 'The influence of Na+, K+-pump blockade on doxorubicin-mediated cytotoxicity and DNA strand breakage in human tumor cells', *Cancer Chemotherapy and Pharmacology*, 26(3), pp. 163–167. Available at: https://doi.org/10.1007/BF02897193/METRICS.

Ledur, P.F. *et al.* (2016) 'Culture conditions tailored to the cell of origin are critical for maintaining native properties and tumorigenicity of glioma cells', *Neuro-Oncology*, 18(10), pp. 1413–1424. Available at: https://doi.org/10.1093/NEUONC/NOW062.

Ledur, P.F. *et al.* (2017) 'Culture conditions defining glioblastoma cells behavior: what is the impact for novel discoveries?', *Oncotarget*, 8(40), p. 69185. Available at: https://doi.org/10.18632/ONCOTARGET.20193.

Lee, A. *et al.* (2020) 'Anti-epidermal growth factor receptor therapy for glioblastoma in adults', *Cochrane Database of Systematic Reviews*, 2020(5). Available at: https://doi.org/10.1002/14651858.CD013238.PUB2/MEDIA/CDSR/CD013238/IMAGE_N/NCD013238-CMP-003.03.SVG.

Lee, D.H. *et al.* (2017) 'Cardiac glycosides suppress the maintenance of stemness and malignancy via inhibiting HIF-1α in human glioma stem cells', *Oncotarget*, 8(25), p. 40233. Available at: https://doi.org/10.18632/ONCOTARGET.16714.

Lee, J. *et al.* (2006) 'Tumor stem cells derived from glioblastomas cultured in bFGF and EGF more closely mirror the phenotype and genotype of primary tumors than do serum-cultured cell lines', *Cancer Cell*, 9(5), pp. 391–403. Available at: https://doi.org/10.1016/J.CCR.2006.03.030.

Lee, J.Y. *et al.* (2017) 'Digoxin enhances radiation response in radioresistant A549 cells by reducing protein phosphatase 2A', *Bioscience Reports*, 37(6). Available at: https://doi.org/10.1042/BSR20171257/58173.

Lee, Joo Ho *et al.* (2018) 'Human glioblastoma arises from subventricular zone cells with low-level driver mutations', *Nature 2018 560:7717*, 560(7717), pp. 243–247. Available at:

https://doi.org/10.1038/s41586-018-0389-3.

Lee, S.Y. (2016) 'Temozolomide resistance in glioblastoma multiforme', *Genes and Diseases*. Chongqing yi ke da xue, di 2 lin chuang xue yuan Bing du xing gan yan yan jiu suo, pp. 198–210. Available at: https://doi.org/10.1016/j.gendis.2016.04.007.

Lee, T.H. and Kang, T.H. (2019) 'DNA Oxidation and Excision Repair Pathways', *International Journal of Molecular Sciences 2019, Vol. 20, Page 6092*, 20(23), p. 6092. Available at: https://doi.org/10.3390/IJMS20236092.

Letai, A. (2017) 'Functional precision cancer medicine—moving beyond pure genomics', *Nature Medicine 2017 23:9*, 23(9), pp. 1028–1035. Available at: https://doi.org/10.1038/nm.4389.

Leung, J.W.C. *et al.* (2013) 'Alpha thalassemia/mental retardation syndrome X-linked gene product ATRX is required for proper replication restart and cellular resistance to replication stress', *Journal of Biological Chemistry*, 288(9), pp. 6342–6350. Available at: https://doi.org/10.1074/jbc.M112.411603.

Levine, A.J., Hu, W. and Feng, Z. (2006) 'The P53 pathway: what questions remain to be explored?', *Cell Death & Differentiation 2006 13:6*, 13(6), pp. 1027–1036. Available at: https://doi.org/10.1038/sj.cdd.4401910.

Li, H. *et al.* (2015) 'Transcription factor glioma-associated oncogene homolog 1 is required for transforming growth factor-β1-induced epithelial-mesenchymal transition of non-small cell lung cancer cells', *Molecular medicine reports*, 11(5), pp. 3259–3268. Available at: https://doi.org/10.3892/MMR.2015.3150.

Li, J. *et al.* (2002) 'Wild-Type TP53 Inhibits G2-Phase Checkpoint Abrogation and Radiosensitization Induced by PD0166285, a WEE1 Kinase Inhibitor', *https://doi.org/10.1667/0033-7587(2002)157[0322:WTTIGP]2.0.CO;2*, 157(3), pp. 322–330. Available at: https://doi.org/10.1667/0033-7587(2002)157.

Li, J. *et al.* (2021) 'NAD+ bioavailability mediates PARG inhibition-induced replication arrest, intra S-phase checkpoint and apoptosis in glioma stem cells', *NAR Cancer*, 3(4). Available at: https://doi.org/10.1093/NARCAN/ZCAB044.

Li, J. *et al.* (2022) 'Overcoming Temozolomide Resistance in Glioblastoma via Enhanced NAD+ Bioavailability and Inhibition of Poly-ADP-Ribose Glycohydrolase', *Cancers*, 14(15), p. 3572. Available at: https://doi.org/10.3390/CANCERS14153572/S1.

Lin, G.L. *et al.* (2019) 'Therapeutic strategies for diffuse midline glioma from high-throughput combination drug screening', *Science Translational Medicine*, 11(519). Available at: https://doi.org/10.1126/SCITRANSLMED.AAW0064.

Lindahl, T. (1993) 'Instability and decay of the primary structure of DNA'.

Lindahl, T. and Barnes, D.E. (2000) 'Repair of Endogenous DNA Damage', *Cold Spring Harbor Symposia on Quantitative Biology*, 65, pp. 127–134. Available at: https://doi.org/10.1101/SQB.2000.65.127.

van Linde, M.E. *et al.* (2017) 'Treatment outcome of patients with recurrent glioblastoma multiforme: a retrospective multicenter analysis', *Journal of Neuro-Oncology*, 135(1), pp. 183–192. Available at: https://doi.org/10.1007/S11060-017-2564-Z/TABLES/3.

Van Linden, A.A. *et al.* (2013) 'Inhibition of wee1 sensitizes cancer cells to antimetabolite chemotherapeutics in vitro and in vivo, independent of p53 functionality', *Molecular Cancer Therapeutics*, 12(12), pp. 2675–2684. Available at: https://doi.org/10.1158/1535-7163.MCT-13-0424/86012/AM/INHIBITION-OF-WEE1-SENSITIZES-CANCER-CELLS-TO-ANTI.

Liu, C.P. *et al.* (2012) 'Structure of the variant histone H3.3–H4 heterodimer in complex with its chaperone DAXX', *Nature Structural & Molecular Biology 2012 19:12*, 19(12), pp. 1287–1292. Available at: https://doi.org/10.1038/nsmb.2439.

Liu, D., Keijzers, G. and Rasmussen, L.J. (2017) 'DNA mismatch repair and its many roles in eukaryotic cells', *Mutation Research/Reviews in Mutation Research*, 773, pp. 174–187. Available at: https://doi.org/10.1016/J.MRREV.2017.07.001.

Liu, L. and Gerson2, S. (1996) 'Mismatch Repair Mutations Override Alkyltransferase in Conferring Resistance to Temozolomide but not to 1,3-Bis(2-chloroethyl)nitrosourea''. Available at: http://aacrjournals.org/cancerres/article-pdf/56/23/5375/2462072/cr0560235375.pdf?casa_token=svQK-nrGZvEAAAAA:sdBaJZ4sblGym7c1wbDay3T6es1II_lfOyURkqQGMCSTp8tRy2EyDyGx9PHWmlY0909Y5fbX (Accessed: 28 October 2023).

Lodovichi, S. *et al.* (2020) 'Inhibition of DNA Repair in Cancer Therapy: Toward a Multi-Target Approach', *International Journal of Molecular Sciences 2020, Vol. 21, Page 6684*, 21(18), p. 6684. Available at: https://doi.org/10.3390/IJMS21186684.

Lord, C.J. and Ashworth, A. (2016) 'BRCAness revisited', *Nature Reviews Cancer 2016 16:2*, 16(2), pp. 110–120. Available at: https://doi.org/10.1038/nrc.2015.21.

Louis, D.N. *et al.* (2016) 'The 2016 World Health Organization Classification of Tumors of the Central Nervous System: a summary', *Acta Neuropathologica*. Springer Verlag, pp. 803–820. Available at: https://doi.org/10.1007/s00401-016-1545-1.

Lu, C. *et al.* (2012) 'IDH mutation impairs histone demethylation and results in a block to cell differentiation', *Nature 2012 483:7390*, 483(7390), pp. 474–478. Available at: https://doi.org/10.1038/nature10860.

Lu, W.J. *et al.* (2011) 'Inducible expression of stem cell associated intermediate filament nestin reveals an important role in glioblastoma carcinogenesis', *International Journal of Cancer*, 128(2), pp. 343–351. Available at: https://doi.org/10.1002/IJC.25586.

Ludwig, K. and Kornblum, H.I. (2017) 'Molecular markers in glioma', *Journal of Neuro-Oncology*, 134(3), pp. 505–512. Available at: https://doi.org/10.1007/S11060-017-2379-Y/TABLES/2.

Luger, K. *et al.* (1997) 'Crystal structure of the nucleosome core particle at 2.8 Å resolution', *Nature 1997 389:6648*, 389(6648), pp. 251–260. Available at: https://doi.org/10.1038/38444.

Maemondo, M. *et al.* (2010) 'Gefitinib or Chemotherapy for Non–Small-Cell Lung Cancer with Mutated EGFR', *New England Journal of Medicine*, 362(25), pp. 2380–2388. Available at: https://doi.org/10.1056/NEJMOA0909530/SUPPL_FILE/NEJMOA0909530_DISCLOSURES.PDF.

Mäkelä, R. *et al.* (2020) 'Ex vivo assessment of targeted therapies in a rare metastatic

epithelial-myoepithelial carcinoma', *Neoplasia (New York, N.Y.)*, 22(9), pp. 390–398. Available at: https://doi.org/10.1016/J.NEO.2020.06.007.

Malo, N. *et al.* (2006) 'Statistical practice in high-throughput screening data analysis', *Nature Biotechnology 2006 24:2*, 24(2), pp. 167–175. Available at: https://doi.org/10.1038/nbt1186.

Mao, H. *et al.* (2012) 'Deregulated Signaling Pathways in Glioblastoma Multiforme: Molecular Mechanisms and Therapeutic Targets', *http://dx.doi.org/10.3109/07357907.2011.630050*, 30(1), pp. 48–56. Available at: https://doi.org/10.3109/07357907.2011.630050.

Maria, R. *et al.* (2009) 'SOX2 Silencing in Glioblastoma Tumor-Initiating Cells Causes Stop of Proliferation and Loss of Tumorigenicity', *Stem Cells*, 27(1), pp. 40–48. Available at: https://doi.org/10.1634/STEMCELLS.2008-0493.

Marteijn, J.A. *et al.* (2014) 'Understanding nucleotide excision repair and its roles in cancer and ageing', *Nature Reviews Molecular Cell Biology 2014 15:7*, 15(7), pp. 465–481. Available at: https://doi.org/10.1038/nrm3822.

Massard, C. *et al.* (2017) 'High-Throughput Genomics and Clinical Outcome in Hard-to-Treat Advanced Cancers: Results of the MOSCATO 01 Trial', *Cancer discovery*, 7(6), pp. 586–595. Available at: https://doi.org/10.1158/2159-8290.CD-16-1396.

Matallanas, D. *et al.* (2011) 'Raf Family Kinases: Old Dogs Have Learned New Tricks', *Genes & Cancer*, 2(3), p. 232. Available at: https://doi.org/10.1177/1947601911407323.

Mathieu, J. *et al.* (2011) 'HIF induces human embryonic stem cell markers in cancer cells', *Cancer Research*, 71(13), pp. 4640–4652. Available at: https://doi.org/10.1158/0008-5472.CAN-10-3320/656776/P/HIF-INDUCES-HUMAN-EMBRYONIC-STEM-CELL-MARKERS-IN.

McFaline-Figueroa, J.L. *et al.* (2015) 'Minor changes in expression of the mismatch repair protein MSH2 exert a major impact on glioblastoma response to temozolomide', *Cancer Research*, 75(15), pp. 3127–3138. Available at: https://doi.org/10.1158/0008-5472.CAN-14-3616/651835/AM/MINOR-CHANGES-IN-EXPRESSION-OF-THE-MISMATCH-REPAIR.

McLendon, R. *et al.* (2008) 'Comprehensive genomic characterization defines human glioblastoma genes and core pathways', *Nature*, 455(7216), pp. 1061–1068. Available at: https://doi.org/10.1038/nature07385.

Mebratu, Y. and Tesfaigzi, Y. (2009) 'How ERK1/2 activation controls cell proliferation and cell death: Is subcellular localization the answer?', *Cell Cycle*, 8(8), pp. 1168–1175. Available at: https://doi.org/10.4161/CC.8.8.8147.

Mellinghoff, I.K. *et al.* (2005) 'Molecular Determinants of the Response of Glioblastomas to EGFR Kinase Inhibitors', *New England Journal of Medicine*, 353(19), pp. 2012–2024. Available at: https://doi.org/10.1056/NEJMOA051918/SUPPL_FILE/NEJM_MELLINGHOF_2012SA1.PDF.

Meric-Bernstam, F. *et al.* (2015) 'Feasibility of Large-Scale Genomic Testing to Facilitate Enrollment Onto Genomically Matched Clinical Trials', *Journal of Clinical Oncology*, 33(25), p. 2753. Available at: https://doi.org/10.1200/JCO.2014.60.4165.

Michaud, K. *et al.* (2010) 'Pharmacologic inhibition of cyclin-dependent kinases 4 and 6 arrests the growth of glioblastoma multiforme intracranial xenografts', *Cancer Research*,

70(8), pp. 3228–3238. Available at: https://doi.org/10.1158/0008-5472.CAN-09-4559/656118/P/PHARMACOLOGIC-INHIBITION-OF-CYCLIN-DEPENDENT.

Middleton, G. *et al.* (2020) 'The National Lung Matrix Trial of personalized therapy in lung cancer', *Nature 2020 583:7818*, 583(7818), pp. 807–812. Available at: https://doi.org/10.1038/s41586-020-2481-8.

Migliavacca, E., Gorlia, T. and Regli, L. (2008) 'Stem Cell-Related "Self-Renewal" Signature and High Epidermal Growth Factor Receptor Expression Associated With Resistance to Concomitant Chemoradiotherapy in Glioblastoma', *Article in Journal of Clinical Oncology* [Preprint]. Available at: https://doi.org/10.1200/JCO.2007.15.7164.

Mir, S.E. *et al.* (2010) 'In Silico Analysis of Kinase Expression Identifies WEE1 as a Gatekeeper against Mitotic Catastrophe in Glioblastoma', *Cancer Cell*, 18(3), pp. 244–257. Available at: https://doi.org/10.1016/J.CCR.2010.08.011.

Miraglia, S. *et al.* (1997) 'A Novel Five-Transmembrane Hematopoietic Stem Cell Antigen: Isolation, Characterization, and Molecular Cloning', *Blood*, 90(12), pp. 5013–5021. Available at: https://doi.org/10.1182/BLOOD.V90.12.5013.

Mishima, T. and Hirase, H. (2010) 'In Vivo Intracellular Recording Suggests That Gray Matter Astrocytes in Mature Cerebral Cortex and Hippocampus Are Electrophysiologically Homogeneous', *Journal of Neuroscience*, 30(8), pp. 3093–3100. Available at: https://doi.org/10.1523/JNEUROSCI.5065-09.2010.

Miura, Y. *et al.* (2020) 'Generation of human striatal organoids and cortico-striatal assembloids from human pluripotent stem cells', *Nature biotechnology*, 38(12), pp. 1421–1430. Available at: https://doi.org/10.1038/S41587-020-00763-W.

Mohyeldin, A., Garzó N-Muvdi, T.S. and Quiñ Ones-Hinojosa, A. (2010) 'Cell Stem Cell Review Oxygen in Stem Cell Biology: A Critical Component of the Stem Cell Niche', *Stem Cell*, 7, pp. 150–161. Available at: https://doi.org/10.1016/j.stem.2010.07.007.

Møller, M.B. *et al.* (1999) 'Aberrations of the p53 pathway components p53, MDM2 and CDKN2A appear independent in diffuse large B cell lymphoma', *Leukemia*, 13(3), pp. 453–459. Available at: https://doi.org/10.1038/SJ.LEU.2401315.

Mpindi, J.P. *et al.* (2015) 'Impact of normalization methods on high-throughput screening data with high hit rates and drug testing with dose-response data', *Bioinformatics*, 31(23), pp. 3815–3821. Available at: https://doi.org/10.1093/bioinformatics/btv455.

Murai, J. *et al.* (2014) 'Rationale for Poly(ADP-ribose) Polymerase (PARP) Inhibitors in Combination Therapy with Camptothecins or Temozolomide Based on PARP Trapping versus Catalytic Inhibition', *Journal of Pharmacology and Experimental Therapeutics*, 349(3), pp. 408–416. Available at: https://doi.org/10.1124/JPET.113.210146.

Music, D. *et al.* (2016) 'Expression and prognostic value of the WEE1 kinase in gliomas', *Journal of Neuro-Oncology*, 127(2), pp. 381–389. Available at: https://doi.org/10.1007/S11060-015-2050-4/TABLES/2.

Nandakumar, P., Mansouri, A. and Das, S. (2017) 'The Role of ATRX in Glioma Biology', *Frontiers in Oncology*, 7(SEP), p. 236. Available at: https://doi.org/10.3389/FONC.2017.00236.

Nathanson, D.A. *et al.* (2013) 'Targeted therapy resistance mediated by dynamic regulation

of extrachromosomal mutant EGFR DNA', *Science*, 343(6166), pp. 72–76. Available at: https://doi.org/10.1126/SCIENCE.1241328/SUPPL_FILE/PAPV2.PDF.

Navas, L.E. and Carnero, A. (2021) 'NAD+ metabolism, stemness, the immune response, and cancer', *Signal Transduction and Targeted Therapy*, 6(1). Available at: https://doi.org/10.1038/S41392-020-00354-W.

Neftel, C. *et al.* (2019) 'An Integrative Model of Cellular States, Plasticity, and Genetics for Glioblastoma', *Cell*, 178(4), pp. 835-849.e21. Available at: https://doi.org/10.1016/J.CELL.2019.06.024.

Negrini, S., Gorgoulis, V.G. and Halazonetis, T.D. (2010) 'Genomic instability — an evolving hallmark of cancer', *Nature Reviews Molecular Cell Biology 2010 11:3*, 11(3), pp. 220–228. Available at: https://doi.org/10.1038/nrm2858.

Nelson-Rees, W.A., Daniels, D.W. and Flandermeyer, R.R. (1981) 'Cross-contamination of cells in culture', *Science*, 212(4493), pp. 446–451. Available at: https://doi.org/10.1126/science.6451928.

Neuwelt, E. *et al.* (2008) 'Strategies to advance translational research into brain barriers', *The Lancet Neurology*, 7(1), pp. 84–96. Available at: https://doi.org/10.1016/S1474-4422(07)70326-5.

Nevins, J.R. (2001) 'The Rb/E2F pathway and cancer', *Human Molecular Genetics*, 10(7), pp. 699–703. Available at: https://doi.org/10.1093/HMG/10.7.699.

Nicolaidis, S. (2015) 'Biomarkers of glioblastoma multiforme', *Metabolism: Clinical and Experimental*, 64(3), pp. S22–S27. Available at: https://doi.org/10.1016/j.metabol.2014.10.031.

Nobusawa, S. *et al.* (2009) 'IDH1 mutations as molecular signature and predictive factor of secondary glioblastomas', *Clinical Cancer Research*, 15(19), pp. 6002–6007. Available at: https://doi.org/10.1158/1078-0432.CCR-09-0715/347374/P/IDH1-MUTATIONS-AS-MOLECULAR-SIGNATURE-AND.

Noll, A. *et al.* (2016) 'PARG deficiency is neither synthetic lethal with BRCA1 nor PTEN deficiency', *Cancer Cell International*, 16(1), pp. 1–13. Available at: https://doi.org/10.1186/S12935-016-0333-2/FIGURES/5.

Noushmehr, H. *et al.* (2010) 'Identification of a CpG Island Methylator Phenotype that Defines a Distinct Subgroup of Glioma', *Cancer Cell*, 17(5), pp. 510–522. Available at: https://doi.org/10.1016/J.CCR.2010.03.017.

Nowicki, M.O. *et al.* (2019) 'Proteomic Analysis Implicates Vimentin in Glioblastoma Cell Migration', *Cancers*, 11(4). Available at: https://doi.org/10.3390/CANCERS11040466.

Ntafoulis, I. *et al.* (2023) 'Ex vivo drug sensitivity screening predicts response to temozolomide in glioblastoma patients and identifies candidate biomarkers', *British Journal of Cancer 2023 129:8*, 129(8), pp. 1327–1338. Available at: https://doi.org/10.1038/s41416-023-02402-y.

Nykänen, N. *et al.* (2021) 'Ex Vivo Drug Screening Informed Targeted Therapy for Metastatic Parotid Squamous Cell Carcinoma', *Frontiers in oncology*, 11. Available at: https://doi.org/10.3389/FONC.2021.735820.

Ochs, K. and Kaina, B. (2000) 'Apoptosis Induced by DNA Damage O 6-Methylguanine Is Bcl-2 and Caspase-9/3 Regulated and Fas/Caspase-8 Independent 1', *CANCER RESEARCH*, 60, pp. 5815–5824. Available at: http://aacrjournals.org/cancerres/article-pdf/60/20/5815/3250128/ch200005815p.pdf?casa_token=brdiraqzKhcAAAAA:T699qCUcYc wfVER-p8u8_oj8muPDDuNU9ecu2Tg_CUpOZUtt4G2zZFCITK9CxAonyrGNYdkg (Accessed: 28 October 2023).

Office for National Statistics (2020) *Deaths registered weekly in England and Wales, provisional - Office for National Statistics*, *Office for National Statistics*. Available at: https://www.ons.gov.uk/peoplepopulationandcommunity/birthsdeathsandmarriages/death s/datasets/weeklyprovisionalfiguresondeathsregisteredinenglandandwales (Accessed: 21 February 2021).

Ogawa, J. *et al.* (2018) 'Glioblastoma Model Using Human Cerebral Organoids', *Cell Reports*, 23(4), pp. 1220–1229. Available at: https://doi.org/10.1016/j.celrep.2018.03.105.

Ohgaki, H. *et al.* (2004) *Genetic Pathways to Glioblastoma: A Population-Based Study*, *CANCER RESEARCH*.

Ohgaki, H. and Kleihues, P. (2009) 'Genetic alterations and signaling pathways in the evolution of gliomas', *Cancer Science*, 100(12), pp. 2235–2241. Available at: https://doi.org/10.1111/J.1349-7006.2009.01308.X.

Oliveira, A.I. *et al.* (2017) 'Crosstalk between glial and glioblastoma cells triggers the "go-or-grow" phenotype of tumor cells', *Cell Communication and Signaling*, 15(1), pp. 1–12. Available at: https://doi.org/10.1186/S12964-017-0194-X/FIGURES/5.

Omuro, A. and DeAngelis, L.M. (2013) 'Glioblastoma and Other Malignant Gliomas: A Clinical Review', *JAMA*, 310(17), pp. 1842–1850. Available at: https://doi.org/10.1001/JAMA.2013.280319.

Ozawa, M. *et al.* (2019) 'The usefulness of symptoms alone or combined for general practitioners in considering the diagnosis of a brain tumour: a case-control study using the clinical practice research database (CPRD) (2000-2014)', *BMJ Open*, 9(8). Available at: https://doi.org/10.1136/BMJOPEN-2019-029686.

Padfield, E., Ellis, H.P. and Kurian, K.M. (2015) 'Current therapeutic advances targeting EGFR and EGFRvIII in glioblastoma', *Frontiers in Oncology*, 5, p. 125648. Available at: https://doi.org/10.3389/FONC.2015.00005/BIBTEX.

Pang, Y. *et al.* (2023) 'The Chromatin Remodeler ATRX: Role and Mechanism in Biology and Cancer'. Available at: https://doi.org/10.3390/cancers15082228.

Pardal, R., Clarke, M.F. and Morrison, S.J. (2003) 'Applying the principles of stem-cell biology to cancer', *Nature Reviews Cancer 2003 3:12*, 3(12), pp. 895–902. Available at: https://doi.org/10.1038/nrc1232.

Pardridge, W.M. (2005) 'The Blood-Brain Barrier: Bottleneck in Brain Drug Development', *NeuroRX*, 2(1), pp. 3–14. Available at: https://doi.org/10.1602/NEURORX.2.1.3.

Pascal, J.M. and Ellenberger, T. (2015) 'The rise and fall of poly(ADP-ribose): An enzymatic perspective', *DNA Repair*, 32, pp. 10–16. Available at: https://doi.org/10.1016/J.DNAREP.2015.04.008.

Patel, M. *et al.* (2016) 'Glioblastoma Mimicking Meningioma: Report of 2 Cases', *World*

Neurosurgery, 95, pp. 624.e9-624.e13. Available at: https://doi.org/10.1016/J.WNEU.2016.08.048.

Pauli, C. *et al.* (2017) 'Personalized in vitro and in vivo cancer models to guide precision medicine', *Cancer Discovery*, 7(5), pp. 462–477. Available at: https://doi.org/10.1158/2159-8290.CD-16-1154/333616/P/PERSONALIZED-IN-VITRO-AND-IN-VIVO-CANCER-MODELS-TO.

Payne, C.M. *et al.* (2011) 'Molecular and cellular pathways associated with chromosome 1p deletions during colon carcinogenesis', *Clinical and Experimental Gastroenterology*, 4(1), p. 75. Available at: https://doi.org/10.2147/CEG.S17114.

Perry, J. *et al.* (2007) 'Gliadel wafers in the treatment of malignant glioma: a systematic review', *Current Oncology*, 14(5), p. 189. Available at: https://doi.org/10.3747/CO.2007.147.

Pham, M.T. *et al.* (2018) 'Generation of human vascularized brain organoids', *Neuroreport*, 29(7), p. 588. Available at: https://doi.org/10.1097/WNR.0000000000001014.

Phillips, H.S. *et al.* (2006) 'Molecular subclasses of high-grade glioma predict prognosis, delineate a pattern of disease progression, and resemble stages in neurogenesis', *Cancer Cell*, 9(3), pp. 157–173. Available at: https://doi.org/10.1016/j.ccr.2006.02.019.

Pillay, N. *et al.* (2019) 'DNA Replication Vulnerabilities Render Ovarian Cancer Cells Sensitive to Poly(ADP-Ribose) Glycohydrolase Inhibitors', *Cancer Cell*, 35(3), p. 519. Available at: https://doi.org/10.1016/J.CCELL.2019.02.004.

Pirozzi, C.J. and Yan, H. (2021) 'The implications of IDH mutations for cancer development and therapy', *Nature Reviews Clinical Oncology 2021 18:10*, 18(10), pp. 645–661. Available at: https://doi.org/10.1038/s41571-021-00521-0.

Pitz, M.W. *et al.* (2011) 'Tissue concentration of systemically administered antineoplastic agents in human brain tumors', *Journal of Neuro-Oncology*, 104(3), pp. 629–638. Available at: https://doi.org/10.1007/S11060-011-0564-Y/FIGURES/3.

Pokorny, J.L. *et al.* (2015) 'The efficacy of the wee1 inhibitor MK-1775 combined with temozolomide is limited by heterogeneous distribution across the blood-brain barrier in glioblastoma', *Clinical Cancer Research*, 21(8), pp. 1916–1924. Available at: https://doi.org/10.1158/1078-0432.CCR-14-2588/175433/AM/THE-EFFICACY-OF-THE-WEE1-INHIBITOR-MK-1775.

Pomerantz, J. *et al.* (1998) 'The Ink4a Tumor Suppressor Gene Product, p19Arf, Interacts with MDM2 and Neutralizes MDM2's Inhibition of p53', *Cell*, 92(6), pp. 713–723. Available at: https://doi.org/10.1016/S0092-8674(00)81400-2.

Pozdeyev, N. *et al.* (2016) 'Integrating heterogeneous drug sensitivity data from cancer pharmacogenomic studies', *Oncotarget*, 7(32), p. 51619. Available at: https://doi.org/10.18632/ONCOTARGET.10010.

Prassas, I. and Diamandis, E.P. (2008) 'Novel therapeutic applications of cardiac glycosides', *Nature Reviews Drug Discovery 2008 7:11*, 7(11), pp. 926–935. Available at: https://doi.org/10.1038/nrd2682.

Qian, X., Song, H. and Ming, G.L. (2019) 'Brain organoids: Advances, applications and challenges', *Development (Cambridge)*. Company of Biologists Ltd. Available at: https://doi.org/10.1242/dev.166074.

Qin, T. *et al.* (2022) 'ATRX loss in glioma results in dysregulation of cell-cycle phase transition and ATM inhibitor radio-sensitization', *Cell Reports*, 38(2), p. 110216. Available at: https://doi.org/10.1016/J.CELREP.2021.110216.

Quartararo, C.E. *et al.* (2015) 'High-Throughput Screening of Patient-Derived Cultures Reveals Potential for Precision Medicine in Glioblastoma', *ACS Medicinal Chemistry Letters*, 6(8), pp. 948–952. Available at: https://doi.org/10.1021/acsmedchemlett.5b00128.

Raghunandan, M. *et al.* (2020) 'Functional cross talk between the Fanconi anemia and ATRX/DAXX histone chaperone pathways promotes replication fork recovery', *Human Molecular Genetics*, 29(7), pp. 1083–1095. Available at: https://doi.org/10.1093/HMG/DDZ250.

Ranjan, T. *et al.* (2023) 'Cancer stem cell assay-guided chemotherapy improves survival of patients with recurrent glioblastoma in a randomized trial', *Cell Reports Medicine*, 4(5). Available at: https://doi.org/10.1016/j.xcrm.2023.101025.

Rantala, J.K. *et al.* (2020) 'Science Repository Ex Vivo Modelling of Therapy Efficacy for Rare Krukenberg Tumors-A Report of Two Cases A R T I C L E I N F O'. Available at: https://doi.org/10.31487/j.COR.2020.07.01.

Reed, M.R. *et al.* (2021) 'A Functional Precision Medicine Pipeline Combines Comparative Transcriptomics and Tumor Organoid Modeling to Identify Bespoke Treatment Strategies for Glioblastoma', *Cells 2021, Vol. 10, Page 3400*, 10(12), p. 3400. Available at: https://doi.org/10.3390/CELLS10123400.

Reiber, H. (2001) 'Dynamics of brain-derived proteins in cerebrospinal fluid', *Clinica Chimica Acta*, 310(2), pp. 173–186. Available at: https://doi.org/10.1016/S0009-8981(01)00573-3.

Reifenberger, G. *et al.* (2017) 'Advances in the molecular genetics of gliomas - implications for classification and therapy', *Nature reviews. Clinical oncology*, 14(7), pp. 434–452. Available at: https://doi.org/10.1038/NRCLINONC.2016.204.

Reya, T. *et al.* (2001) 'Stem cells, cancer, and cancer stem cells', *Nature 2001 414:6859*, 414(6859), pp. 105–111. Available at: https://doi.org/10.1038/35102167.

Rhodes, D. and Lipps, H.J. (2015) 'G-quadruplexes and their regulatory roles in biology', *Nucleic Acids Research*, 43(18), pp. 8627–8637. Available at: https://doi.org/10.1093/NAR/GKV862.

Rian, B. *et al.* (2001) 'Efficacy and Safety of a Specific Inhibitor of the BCR-ABL Tyrosine Kinase in Chronic Myeloid Leukemia', *https://doi.org/10.1056/NEJM200104053441401*, 344(14), pp. 1031–1037. Available at: https://doi.org/10.1056/NEJM200104053441401.

Ritchie, K. *et al.* (2008) 'Loss of ATRX leads to chromosome cohesion and congression defects', *The Journal of Cell Biology*, 180(2), p. 315. Available at: https://doi.org/10.1083/JCB.200706083.

Romagosa, C. *et al.* (2011) 'p16Ink4a overexpression in cancer: a tumor suppressor gene associated with senescence and high-grade tumors', *Oncogene 2011 30:18*, 30(18), pp. 2087–2097. Available at: https://doi.org/10.1038/onc.2010.614.

Rominiyi, O. *et al.* (2020) 'Tumour treating fields therapy for glioblastoma: current advances and future directions', *British Journal of Cancer 2020 124:4*, 124(4), pp. 697–709. Available at: https://doi.org/10.1038/s41416-020-01136-5.

Rominiyi, O., Al-Tamimi, Y. and Collis, S.J. (2019) 'The "Ins and Outs" of Early Preclinical Models for Brain Tumor Research: Are They Valuable and Have We Been Doing It Wrong?', *Cancers 2019, Vol. 11, Page 426*, 11(3), p. 426. Available at: https://doi.org/10.3390/CANCERS11030426.

Rominiyi, O. and Collis, S.J. (2022) 'DDRugging glioblastoma: understanding and targeting the DNA damage response to improve future therapies', *Molecular Oncology*, 16(1), pp. 11–41. Available at: https://doi.org/10.1002/1878-0261.13020.

Roskoski, R. (2012) 'ERK1/2 MAP kinases: structure, function, and regulation', *Pharmacological research*, 66(2), pp. 105–143. Available at: https://doi.org/10.1016/J.PHRS.2012.04.005.

Rosso, L. *et al.* (2009) 'A New Model for Prediction of Drug Distribution in Tumor and Normal Tissues: Pharmacokinetics of Temozolomide in Glioma Patients', *Cancer Research*, 69(1), pp. 120–127. Available at: https://doi.org/10.1158/0008-5472.CAN-08-2356.

Rowley, R., Hudson, J. and Young, P.G. (1992) 'The wee1 protein kinase is required for radiation-induced mitotic delay', *Nature 1992 356:6367*, 356(6367), pp. 353–355. Available at: https://doi.org/10.1038/356353a0.

Rubio-Viqueira, B. *et al.* (2006) 'An in vivo platform for translational drug development in pancreatic cancer', *Clinical cancer research : an official journal of the American Association for Cancer Research*, 12(15), pp. 4652–4661. Available at: https://doi.org/10.1158/1078-0432.CCR-06-0113.

Sanai, N. *et al.* (2018) 'Phase 0 trial of azd1775 in first-recurrence glioblastoma patients', *Clinical Cancer Research*, 24(16), pp. 3820–3828. Available at: https://doi.org/10.1158/1078-0432.CCR-17-3348/352756/P/PHASE-0-TRIAL-OF-AZD1775-IN-FIRST-RECURRENCE.

Sanborn, J.Z. *et al.* (2013) 'Double minute chromosomes in glioblastoma multiforme are revealed by precise reconstruction of oncogenic amplicons', *Cancer Research*, 73(19), pp. 6036–6045. Available at: https://doi.org/10.1158/0008-5472.CAN-13-0186/650990/AM/DOUBLE-MINUTE-CHROMOSOMES-IN-GLIOBLASTOMA.

Sangweni, N.F. *et al.* (2021) 'The Implication of Low Dose Dimethyl Sulfoxide on Mitochondrial Function and Oxidative Damage in Cultured Cardiac and Cancer Cells', *Molecules*, 26(23). Available at: https://doi.org/10.3390/MOLECULES26237305.

Sasmita, A.O., Wong, Y.P. and Ling, A.P.K. (2018) 'Biomarkers and therapeutic advances in glioblastoma multiforme', *Asia-Pacific Journal of Clinical Oncology*, 14(1), pp. 40–51. Available at: https://doi.org/10.1111/ajco.12756.

Schmitz, M. *et al.* (2007) 'Identification of SOX2 as a novel glioma-associated antigen and potential target for T cell-based immunotherapy', *British Journal of Cancer 2007 96:8*, 96(8), pp. 1293–1301. Available at: https://doi.org/10.1038/sj.bjc.6603696.

Schultz, S. *et al.* (2005) 'Fine needle aspiration diagnosis of extracranial glioblastoma multiforme: Case report and review of the literature', *CytoJournal*, 2, p. 19. Available at: https://doi.org/10.1186/1742-6413-2-19.

Schwartzentruber, J., Korshunov, A., Liu, X.-Y., *et al.* (2012) 'Driver mutations in histone H3.3 and chromatin remodelling genes in paediatric glioblastoma'. Available at:

https://doi.org/10.1038/nature10833.

Schwartzentruber, J., Korshunov, A., Liu, X.Y., *et al.* (2012) 'Driver mutations in histone H3.3 and chromatin remodelling genes in paediatric glioblastoma', *Nature 2012 482:7384*, 482(7384), pp. 226–231. Available at: https://doi.org/10.1038/nature10833.

Seifert, H. *et al.* (2016) 'Extrinsic factors can mediate resistance to BRAF inhibition in central nervous system melanoma metastases', *Pigment Cell & Melanoma Research*, 29(1), pp. 92–100. Available at: https://doi.org/10.1111/PCMR.12424.

Seltzer, M.J. *et al.* (2010) 'Inhibition of glutaminase preferentially slows growth of glioma cells with mutant IDH1', *Cancer Research*, 70(22), pp. 8981–8987. Available at: https://doi.org/10.1158/0008-5472.CAN-10-1666/656480/P/INHIBITION-OF-GLUTAMINASE-PREFERENTIALLY-SLOWS.

Shi, H. *et al.* (2014) 'Acquired resistance and clonal evolution in melanoma during BRAF inhibitor therapy', *Cancer Discovery*, 4(1), pp. 80–93. Available at: https://doi.org/10.1158/2159-8290.CD-13-0642/43066/P/ACQUIRED-RESISTANCE-AND-CLONAL-EVOLUTION-IN.

Shuford, S. *et al.* (2021) 'Prospective prediction of clinical drug response in high-grade gliomas using an ex vivo 3D cell culture assay', *Neuro-oncology advances*, 3(1). Available at: https://doi.org/10.1093/NOAJNL/VDAB065.

Sidaway, P. (2017) 'Glioblastoma subtypes revisited', *Nature Reviews Clinical Oncology 2017 14:10*, 14(10), pp. 587–587. Available at: https://doi.org/10.1038/nrclinonc.2017.122.

De Silva, M.I., Stringer, B.W. and Bardy, C. (2023) 'Neuronal and tumourigenic boundaries of glioblastoma plasticity', *Trends in Cancer*, 9(3), pp. 223–236. Available at: https://doi.org/10.1016/j.trecan.2022.10.010.

Singh, S.K. *et al.* (2004) 'Identification of human brain tumour initiating cells', *Nature 2004 432:7015*, 432(7015), pp. 396–401. Available at: https://doi.org/10.1038/nature03128.

Skaga, E. *et al.* (2019) 'Feasibility study of using high-throughput drug sensitivity testing to target recurrent glioblastoma stem cells for individualized treatment', *Clinical and Translational Medicine*, 8(1). Available at: https://doi.org/10.1186/S40169-019-0253-6.

Snider, N.T. and Omary, M.B. (2014) 'Post-translational modifications of intermediate filament proteins: mechanisms and functions', *Nature Reviews Molecular Cell Biology 2014 15:3*, 15(3), pp. 163–177. Available at: https://doi.org/10.1038/nrm3753.

Snijder, B. *et al.* (2017) 'Image-based ex-vivo drug screening for patients with aggressive haematological malignancies: interim results from a single-arm, open-label, pilot study', *The Lancet. Haematology*, 4(12), pp. e595–e606. Available at: https://doi.org/10.1016/S2352-3026(17)30208-9.

Srivenugopal, K.S. *et al.* (1996) 'Ubiquitination-dependent proteolysis of O6-methylguanine-DNA methyltransferase in human and murine tumor cells following inactivation with O6-benzylguanine or 1,3-bis(2-chloroethyl)-1-nitrosourea', *Biochemistry*, 35(4), pp. 1328–1334. Available at: https://doi.org/10.1021/BI9518205/ASSET/IMAGES/LARGE/BI9518205F00006.JPEG.

Stancheva, G. *et al.* (2014) 'IDH1/IDH2 but not TP53 mutations predict prognosis in Bulgarian glioblastoma patients', *BioMed Research International*, 2014. Available at:

https://doi.org/10.1155/2014/654727.

Stenkvist, B. *et al.* (1979) 'CARDIAC GLYCOSIDES AND BREAST CANCER', *The Lancet*, 313(8115), p. 563. Available at: https://doi.org/10.1016/S0140-6736(79)90996-6.

Stieber, D., Abdul Rahim, S.A. and Niclou, S.P. (2011) 'Novel ways to target brain tumour metabolism', *Expert Opinion on Therapeutic Targets*. Taylor & Francis, pp. 1227–1239. Available at: https://doi.org/10.1517/14728222.2011.588211.

Stommel, J.M. *et al.* (2007) 'Coactivation of receptor tyrosine kinases affects the response of tumor cells to targeted therapies', *Science*, 318(5848), pp. 287–290. Available at: https://doi.org/10.1126/SCIENCE.1142946/SUPPL_FILE/STOMMEL.SOM.PDF.

Stoyanov, G.S. *et al.* (2022) 'Reclassification of Glioblastoma Multiforme According to the 2021 World Health Organization Classification of Central Nervous System Tumors: A Single Institution Report and Practical Significance', *Cureus*, 14(2). Available at: https://doi.org/10.7759/CUREUS.21822.

Strobel, H. *et al.* (2019) 'Temozolomide and Other Alkylating Agents in Glioblastoma Therapy', *Biomedicines 2019, Vol. 7, Page 69*, 7(3), p. 69. Available at: https://doi.org/10.3390/BIOMEDICINES7030069.

Stummer, Walter *et al.* (1998) 'In vitro and in vivo porphyrin accumulation by C6 glioma cells after exposure to 5-aminolevulinic acid', *Journal of Photochemistry and Photobiology B: Biology*, 45(2–3), pp. 160–169. Available at: https://doi.org/10.1016/S1011-1344(98)00176-6.

Stummer, W. *et al.* (1998) 'Technical principles for protoporphyrin-IX-fluorescence guided microsurgical resection of malignant glioma tissue', *Acta Neurochirurgica*, 140(10), pp. 995–1000. Available at: https://doi.org/10.1007/s007010050206.

Stupp, R. *et al.* (2005) 'Radiotherapy plus Concomitant and Adjuvant Temozolomide for Glioblastoma', *New England Journal of Medicine*, 352(10), pp. 987–996. Available at: https://doi.org/10.1056/NEJMOA043330/SUPPL_FILE/987SA1.PDF.

Sulkowski, P.L. *et al.* (2017) '2-Hydroxyglutarate produced by neomorphic IDH mutations suppresses homologous recombination and induces PARP inhibitor sensitivity', *Science translational medicine*, 9(375). Available at: https://doi.org/10.1126/SCITRANSLMED.AAL2463.

Sun, X.Y. *et al.* (2022) 'Generation of vascularized brain organoids to study neurovascular interactions', *eLife*, 11. Available at: https://doi.org/10.7554/ELIFE.76707.

Sunabori, T. *et al.* (2008) 'Cell-cycle-specific nestin expression coordinates with morphological changes in embryonic cortical neural progenitors', *Journal of Cell Science*, 121(8), pp. 1204–1212. Available at: https://doi.org/10.1242/JCS.025064.

Tang, J.B. *et al.* (2011) 'N-methylpurine DNA glycosylase and DNA polymerase β modulate BER inhibitor potentiation of glioma cells to temozolomide', *Neuro-Oncology*, 13(5), pp. 471–486. Available at: https://doi.org/10.1093/NEUONC/NOR011.

Tatsumi, K. *et al.* (2018) 'Olig2-Lineage astrocytes: A distinct subtype of astrocytes that differs from GFAP astrocytes', *Frontiers in Neuroanatomy*, 12(8), p. 312356. Available at: https://doi.org/10.3389/FNANA.2018.00008/BIBTEX.

Técher, H. *et al.* (2017) 'The impact of replication stress on replication dynamics and DNA damage in vertebrate cells', *Nature Reviews Genetics 2017 18:9*, 18(9), pp. 535–550. Available at: https://doi.org/10.1038/nrg.2017.46.

Teng, Y.C. *et al.* (2021) 'ATRX promotes heterochromatin formation to protect cells from G-quadruplex DNA-mediated stress', *Nature Communications 2021 12:1*, 12(1), pp. 1–14. Available at: https://doi.org/10.1038/s41467-021-24206-5.

Tubbs, J.L., Pegg, A.E. and Tainer, J.A. (2007) 'DNA binding, nucleotide flipping, and the helix-turn-helix motif in base repair by O6-alkylguanine-DNA alkyltransferase and its implications for cancer chemotherapy', *DNA Repair*, 6(8), pp. 1100–1115. Available at: https://doi.org/10.1016/J.DNAREP.2007.03.011.

Tunçer, S. *et al.* (2018) 'Low dose dimethyl sulfoxide driven gross molecular changes have the potential to interfere with various cellular processes', *Scientific Reports 2018 8:1*, 8(1), pp. 1–15. Available at: https://doi.org/10.1038/s41598-018-33234-z.

Turcan, S. *et al.* (2012) 'IDH1 mutation is sufficient to establish the glioma hypermethylator phenotype', *Nature 2012 483:7390*, 483(7390), pp. 479–483. Available at: https://doi.org/10.1038/nature10866.

Turcan, S. *et al.* (2017) 'Mutant-IDH1-dependent chromatin state reprogramming, reversibility, and persistence', *Nature Genetics 2017 50:1*, 50(1), pp. 62–72. Available at: https://doi.org/10.1038/s41588-017-0001-z.

Tutt, A.N.J. *et al.* (2021) ' Adjuvant Olaparib for Patients with BRCA1 - or BRCA2 -Mutated Breast Cancer ', *New England Journal of Medicine*, 384(25), pp. 2394–2405. Available at: https://doi.org/10.1056/NEJMOA2105215/SUPPL_FILE/NEJMOA2105215_DATA-SHARING.PDF.

Uwanogho, D. *et al.* (1995) 'Embryonic expression of the chicken Sox2, Sox3 and Sox11 genes suggests an interactive role in neuronal development', *Mechanisms of Development*, 49(1–2), pp. 23–36. Available at: https://doi.org/10.1016/0925-4773(94)00299-3.

Verhaak, R.G.W. *et al.* (2010) 'Integrated Genomic Analysis Identifies Clinically Relevant Subtypes of Glioblastoma Characterized by Abnormalities in PDGFRA, IDH1, EGFR, and NF1', *Cancer Cell*, 17(1), pp. 98–110. Available at: https://doi.org/10.1016/j.ccr.2009.12.020.

Verheijen, M. *et al.* (2019) 'DMSO induces drastic changes in human cellular processes and epigenetic landscape in vitro', *Scientific Reports 2019 9:1*, 9(1), pp. 1–12. Available at: https://doi.org/10.1038/s41598-019-40660-0.

Vik-Mo, E.O. *et al.* (2010) 'Brain tumor stem cells maintain overall phenotype and tumorigenicity after in vitro culturing in serum-free conditions', *Neuro-Oncology*, 12(12), pp. 1220–1230. Available at: https://doi.org/10.1093/NEUONC/NOQ102.

Vogt, N. *et al.* (2004) 'Molecular structure of double-minute chromosomes bearing amplified copies of the epidermal growth factor receptor gene in gliomas'. Available at: www.pnas.orgcgidoi10.1073pnas.0402979101 (Accessed: 5 October 2023).

Wadman, M. (2023) 'FDA no longer has to require animal testing for new drugs', *Science*, 379(6628), pp. 127–128. Available at: https://doi.org/10.1126/SCIENCE.ADG6276.

Wang, J. *et al.* (2009) 'A reproducible brain tumour model established from human glioblastoma biopsies', *BMC Cancer*, 9(1), p. 465. Available at:

https://doi.org/10.1186/1471-2407-9-465.

Wang, Q. *et al.* (2017) 'Tumor Evolution of Glioma-Intrinsic Gene Expression Subtypes Associates with Immunological Changes in the Microenvironment', *Cancer Cell*, 32(1), pp. 42-56.e6. Available at: https://doi.org/10.1016/J.CCELL.2017.06.003.

Wang, Y. *et al.* (2001) 'Radiosensitization of p53 mutant cells by PD0166285, a novel G2 checkpoint abrogator', *Cancer Research*, 61(22), pp. 8211–8217.

Wang, Y. *et al.* (2019) 'G-quadruplex DNA drives genomic instability and represents a targetable molecular abnormality in ATRX-deficient malignant glioma', *Nature Communications 2019 10:1*, 10(1), pp. 1–14. Available at: https://doi.org/10.1038/s41467-019-08905-8.

Wei, L.C. *et al.* (2008) 'Nestin small interfering RNA (siRNA) reduces cell growth in cultured astrocytoma cells', *Brain Research*, 1196, pp. 103–112. Available at: https://doi.org/10.1016/J.BRAINRES.2007.11.026.

Weinberg, R.A. (1995) 'The Retinoblastoma Protein and Cell Cycle Control Review', *Cell*, 81, pp. 323–330.

Weller, M. *et al.* (2020) 'EANO guidelines on the diagnosis and treatment of diffuse gliomas of adulthood', *Nature Reviews Clinical Oncology*, 17, p. 30. Available at: https://doi.org/10.1038/s41571-020-00447-z.

Weller, M. and Le Rhun, E. (2020) 'How did lomustine become standard of care in recurrent glioblastoma?', *Cancer Treatment Reviews*. W.B. Saunders Ltd, p. 102029. Available at: https://doi.org/10.1016/j.ctrv.2020.102029.

Wha Jun, D. *et al.* (2013) 'Ouabain, a Cardiac Glycoside, Inhibits the Fanconi Anemia/BRCA Pathway Activated by DNA Interstrand Cross-Linking Agents', *PLOS ONE*, 8(10), p. e75905. Available at: https://doi.org/10.1371/JOURNAL.PONE.0075905.

Wick, W. *et al.* (2017) 'Lomustine and Bevacizumab in Progressive Glioblastoma', *New England Journal of Medicine*, 377(20), pp. 1954–1963. Available at: https://doi.org/10.1056/nejmoa1707358.

Wilk, A. *et al.* (2020) 'Extracellular NAD+ enhances PARP-dependent DNA repair capacity independently of CD73 activity', *Scientific Reports 2020 10:1*, 10(1), pp. 1–21. Available at: https://doi.org/10.1038/s41598-020-57506-9.

Williams, D. *et al.* (2008) *An Integrated Genomic Analysis of Human Glioblastoma Multiforme*, *New Series*.

Williams, S.T. *et al.* (2022) 'Precision oncology using ex vivo technology: a step towards individualised cancer care?', *Expert Reviews in Molecular Medicine*, 24, p. e39. Available at: https://doi.org/10.1017/ERM.2022.32.

Wong, C.H., Siah, K.W. and Lo, A.W. (2019) 'Estimation of clinical trial success rates and related parameters', *Biostatistics*, 20(2), pp. 273–286. Available at: https://doi.org/10.1093/BIOSTATISTICS/KXX069.

Xu, H. *et al.* (2017) 'CX-5461 is a DNA G-quadruplex stabilizer with selective lethality in BRCA1/2 deficient tumours', *Nature Communications 2017 8:1*, 8(1), pp. 1–18. Available at: https://doi.org/10.1038/ncomms14432.

Xu, J. (2018) 'New Insights into GFAP Negative Astrocytes in Calbindin D28k Immunoreactive Astrocytes', *Brain Sciences*, 8(8). Available at: https://doi.org/10.3390/BRAINSCI8080143.

Yadav, B. *et al.* (2014) 'Quantitative scoring of differential drug sensitivity for individually optimized anticancer therapies', *Scientific Reports 2014 4:1*, 4(1), pp. 1–10. Available at: https://doi.org/10.1038/srep05193.

Yan, H. *et al.* (2009) '*IDH1* and *IDH2* Mutations in Gliomas', *New England Journal of Medicine*, 360(8), pp. 765–773. Available at: https://doi.org/10.1056/NEJMoa0808710.

Yang, J.L. *et al.* (2021) 'Ouabain Induces DNA Damage in Human Osteosarcoma U-2 OS Cells and Alters the Expression of DNA Damage and DNA Repair-associated Proteins', *In vivo (Athens, Greece)*, 35(5), pp. 2687–2696. Available at: https://doi.org/10.21873/INVIVO.12552.

Yang, X.S. *et al.* (2018) 'Ouabain suppresses the growth and migration abilities of glioma U-87MG cells through inhibiting the Akt/mTOR signaling pathway and downregulating the expression of HIF-1α', *Molecular medicine reports*, 17(4), pp. 5595–5600. Available at: https://doi.org/10.3892/MMR.2018.8587.

Yip, S. *et al.* (2009) 'MSH6 mutations arise in glioblastomas during temozolomide therapy and mediate temozolomide resistance', *Clinical cancer research : an official journal of the American Association for Cancer Research*, 15(14), p. 4622. Available at: https://doi.org/10.1158/1078-0432.CCR-08-3012.

Zhang, C. *et al.* (2020) 'Gain-of-function mutant p53 in cancer progression and therapy', *Journal of Molecular Cell Biology*, 12(9), pp. 674–687. Available at: https://doi.org/10.1093/JMCB/MJAA040.

Zhang, F. *et al.* (2018) 'Characterization of drug responses of mini patient-derived xenografts in mice for predicting cancer patient clinical therapeutic response', *Cancer Communications*, 38(1), pp. 1–12. Available at: https://doi.org/10.1186/S40880-018-0329-5.

Zhang, Y., Xiong, Y. and Yarbrough, W.G. (1998) 'ARF promotes MDM2 degradation and stabilizes p53: ARF-INK4a locus deletion impairs both the Rb and p53 tumor suppression pathways', *Cell*, 92(6), pp. 725–734. Available at: https://doi.org/10.1016/S0092-8674(00)81401-4.

Zhao, J. *et al.* (2018) 'High Expression of Vimentin is Associated With Progression and a Poor Outcome in Glioblastoma', *Applied immunohistochemistry & molecular morphology : AIMM*, 26(5), pp. 337–344. Available at: https://doi.org/10.1097/PAI.0000000000000420.

Zhao, L. and Vogt, P.K. (2008) 'Class I PI3K in oncogenic cellular transformation', *Oncogene 2008 27:41*, 27(41), pp. 5486–5496. Available at: https://doi.org/10.1038/onc.2008.244.

Chapter 8 – Supplementary Figures

8.1 Extended Dose response curves

Extended drug dose responses were performed for the design of V02 drug plates, where IC_{50} values were not obtained from the initial V01 plates using primary low passage cell lines Ox5 Edge and Core. This was done to ensure drugs were in the correct IC_{50} range for the updated drug plates. The dose responses for Ox5 Edge and Core are shown below within figure 8.1, some drug were also tested in low passage GBM11 and GBM21 primary cells.

K. VE-821

L. LNT1

M. Metformin

N. Palmoic Acid

O. RAD51 Inhbitior

P. Tinostamustine
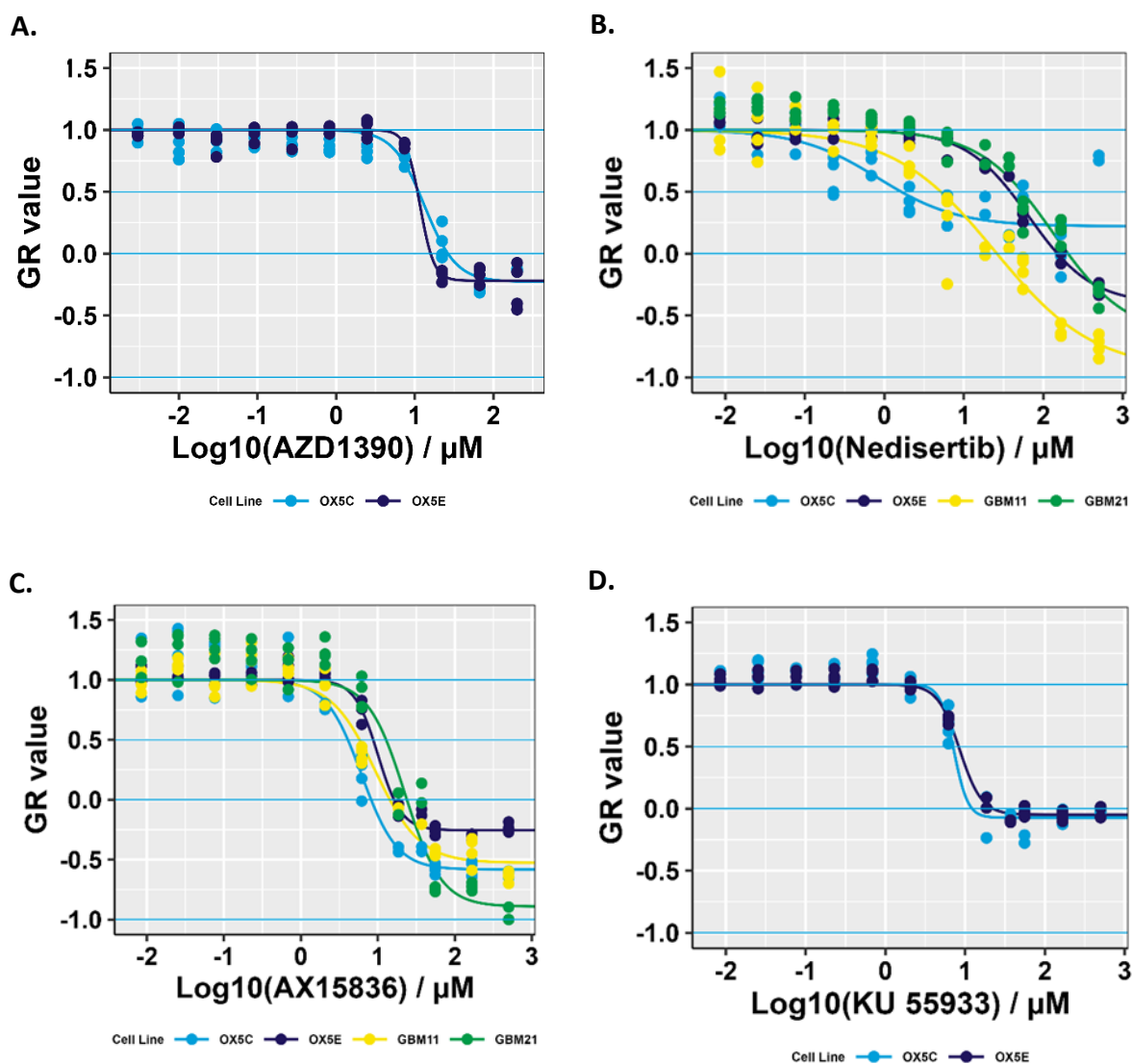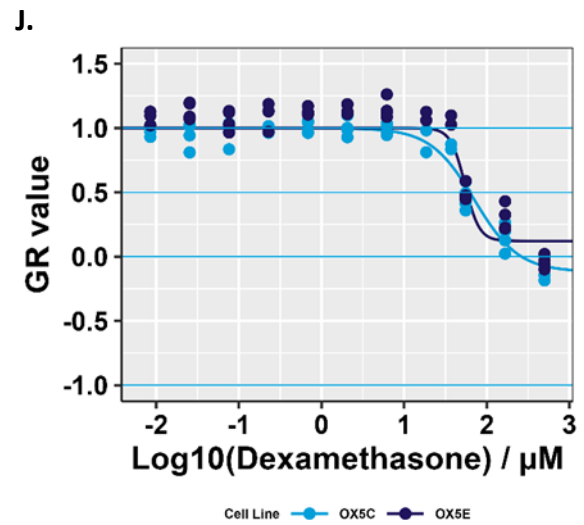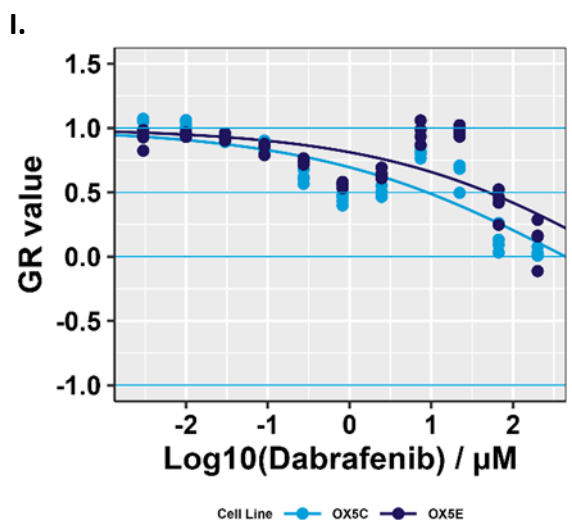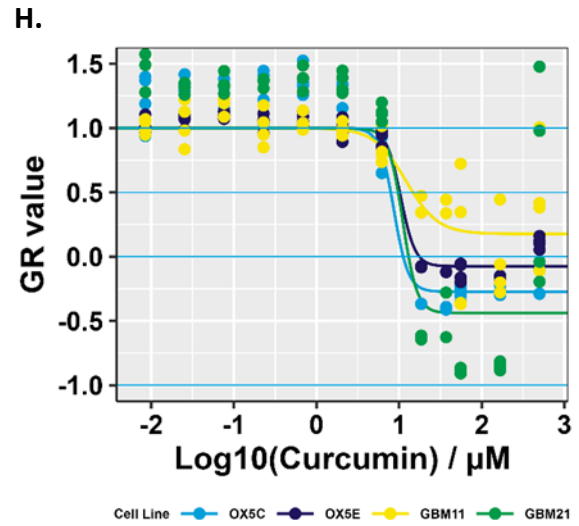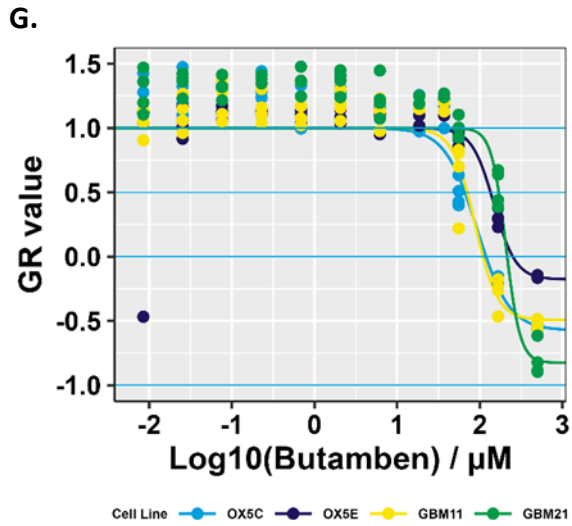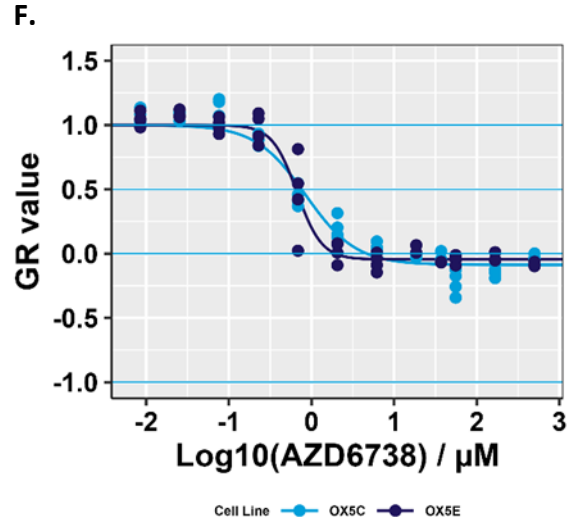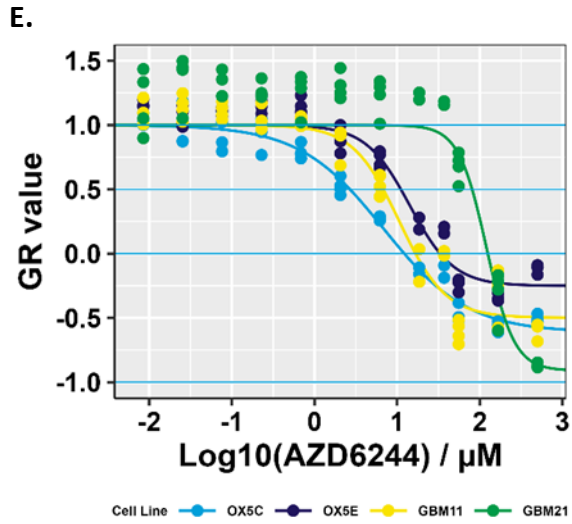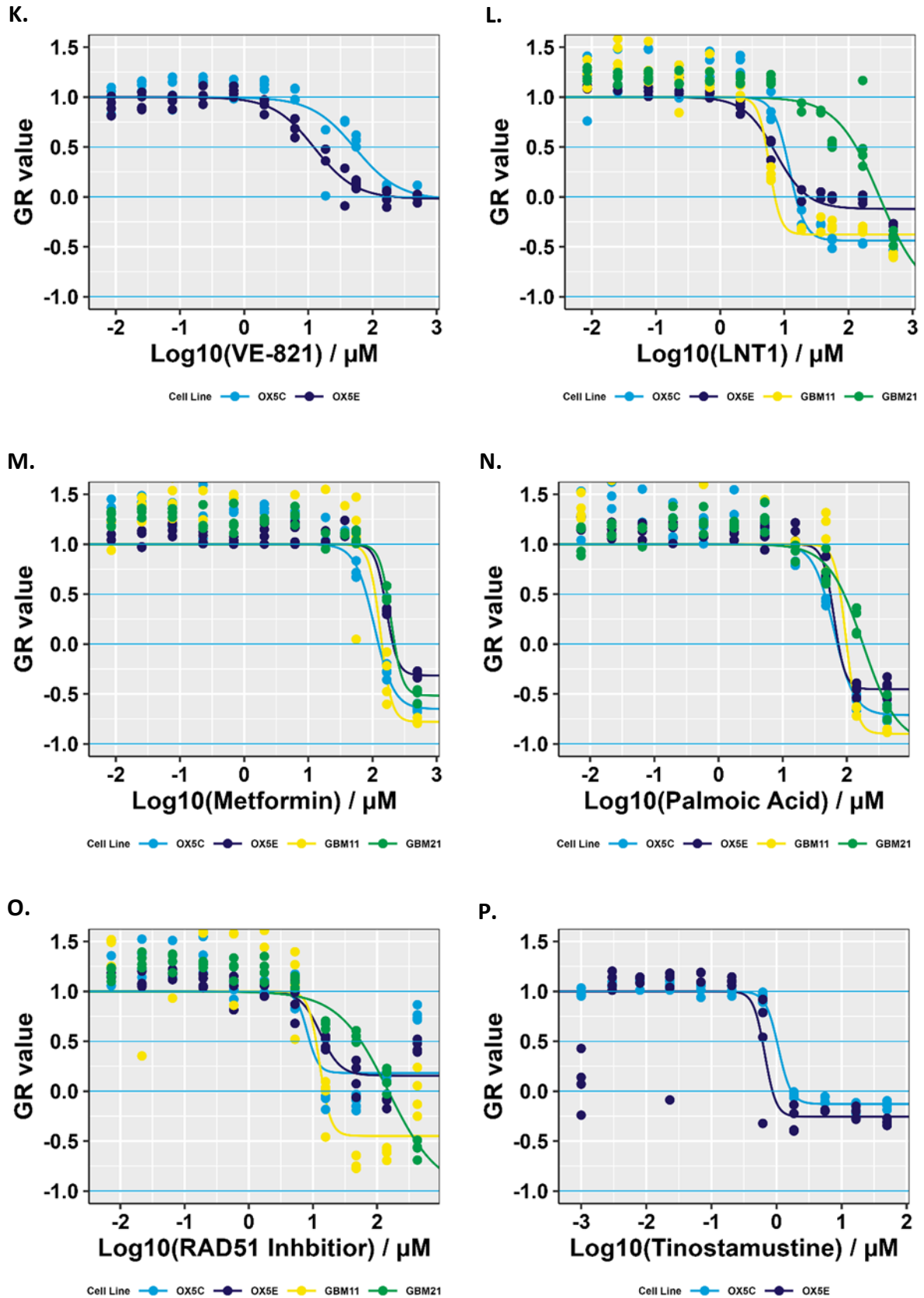
Figure 8.1 - Extended dose response curves for the design of GBM V02 drug plates, where IC50 values were not obtained from V01 plates - **A.** AZD1390. **B.** Nedisertib. **C.** AX15836. **D.** KU55933. **E. AZD6244. F. AZD6738. G. Butamben. H. Curcumin. I. Dabrafenib. J. Dexamethasone. K. VE-821. L. LNT1. M.**

8.2 FACS cell profiles

The cell profiles for the GBM1 and GBM21 are depicted in figure 8.2 following treatment with WEE1 inhibitor.
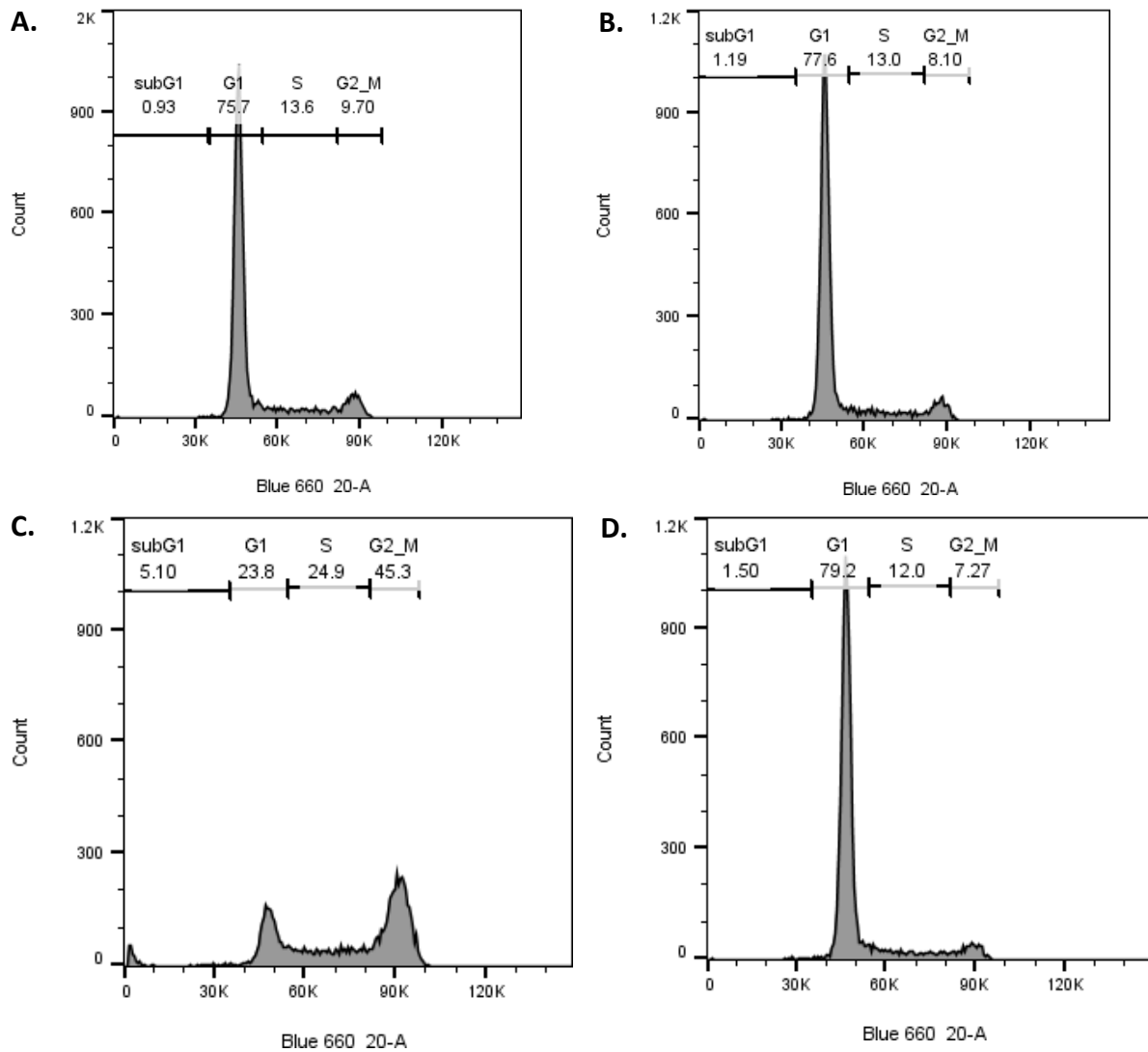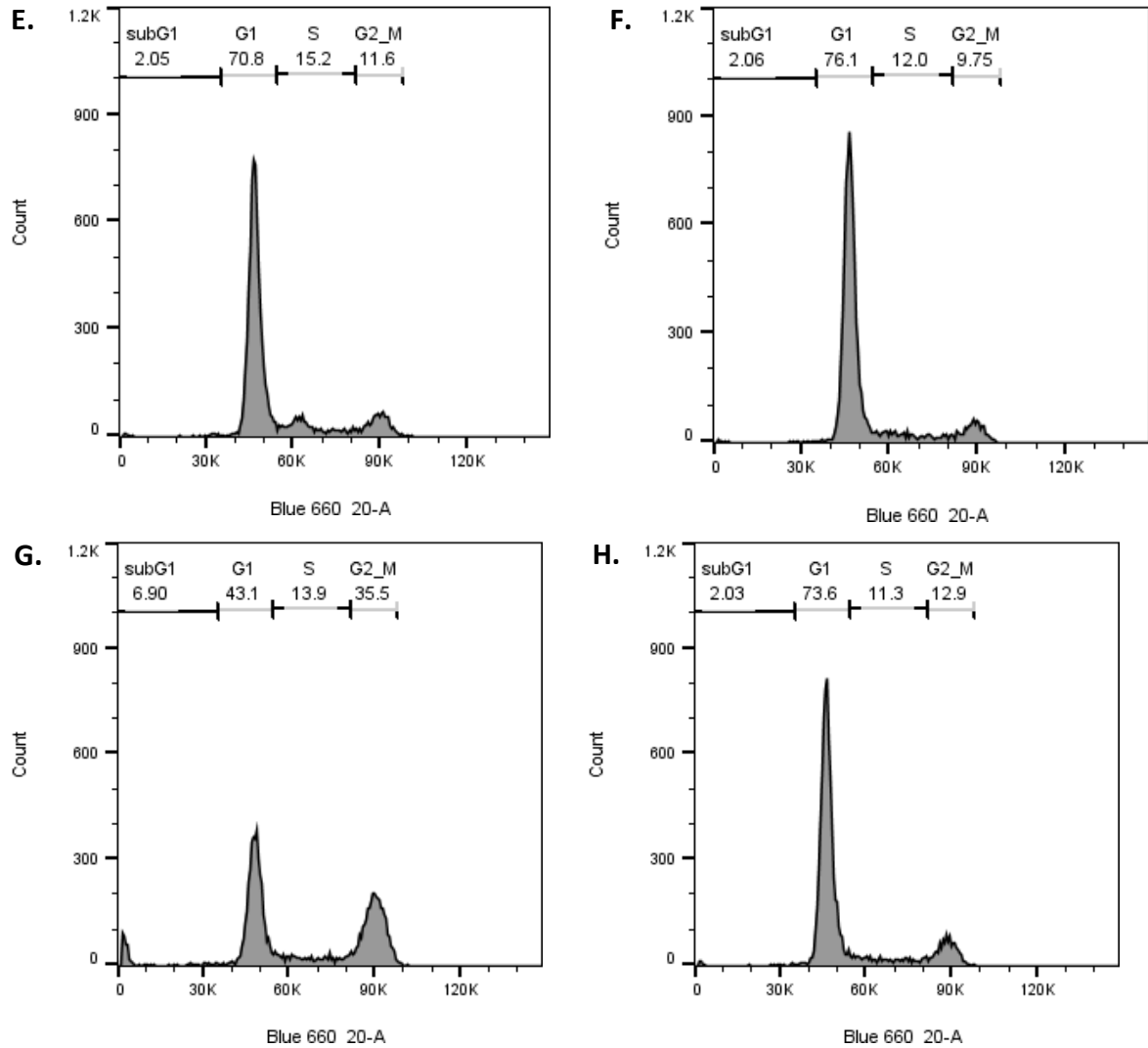
Figure 8.2 - Cell profiles of GBM21 and GBM11 cell cultures following treatment with WEE1 inhibitor AZD1775 - **A.** GBM21 untreated, **B.** GBM21 AZD1775 treatment, **C.** GBM21 nocodazole treatment (16 hour), **D.** GBM21 PI control, **E**. GBM11 untreated, **F.** GBM11 AZD1775 treatment, **G.** GBM11 Nocodazole treatment, **H.** GBM11 PI staining control.

8.3 Patient information sheet and consent form for study

	Department Of Oncology and Metabolism
The University Of Sheffield.	**Academic Unit of Clinical Oncology** Head: Professor Sarah Danson Cancer Clinical Trials Centre Weston Park Hospital Whitham Road, Sheffield S10 2SJ
Sheffield Teaching Hospitals NHS NHS Foundation Trust	Tel: 0114 226 5211 Fax: 0114 226 5678

INFORMATION SHEET FOR PATIENTS

Utilising ex-vivo drug screening to predict patient response to prior treatment

Thank you for taking the time to read this information sheet and for your enthusiasm towards research. We greatly appreciate your time and feedback.

This information sheet describes a research study that you are being invited to take part in. Before you decide whether this is something you would like to do, it is important for you to understand why the research is being done and what it will involve.

Please take your time in reading through this information sheet and discuss it with friends, relatives, your GP and others if you wish. Please talk to us if you have any questions, or if you would want more information. Contact details at the end of this information sheet.

1. What is ex vivo screening?
Ex vivo screening is an experimental method of testing if an anti-cancer treatment will work, or not work on your cancer before you undergo treatment. We take a small part of your cancer from a biopsy, or from your planned surgery. We then break the small part of your cancer down into individual cells. Cancer is made up of individual cells which grow out of control and become a tumour. We then test up to 150 anti-cancer treatments directly on the cells and count how many cells survive. We are testing this method to see if it can predict a patient's response to treatment. It will not change your treatment but, if ex vivo screening is found to predict response to treatment then it could be used in the future to direct patients' treatments.

2. What is the purpose of the study?
Cancer treatments do not work well on some patients and there is no way of predicting this prior to treating the patient. The aim of this study is to test if we can predict which

treatment will work best on different cancers before being given any treatment. We know that there are many reasons why and how a cancer responds to treatment. We also know that even people who have the same type of cancer do not always respond to treatment in the same way, and some patients can have severe side effects. If we show this test works, it will provide information which could show the best treatment for that individual's cancer, but also which treatments would not work. This will save the patient from undergoing pointless treatment, losing time to see if the treatment actually works, or experiencing any side effects of a treatment which will not work

Our plan is to take a piece of your tissue (biopsy or surgical) and a blood sample and test it in the laboratory with a new ex vivo drug screen. In the drug screen test we will include all possible treatments you could undergo as part of your treatment. We will then follow up how your regular treatment directed by your clinical team works and look to see if the ex vivo drug screen could have predicted this in advance.

We will do this by collecting a biopsy or a small part of a surgical sample of the cancer and a blood sample, from people diagnosed with cancer.

3. Why have I been chosen?
We are inviting individuals, who have a suspected diagnosis or diagnosis of cancer, to take part in the study.

4. Do I have to take part?
Your involvement in the study is voluntary, meaning that you can stop taking part at any point in the study and withdraw without having to provide a reason. If you do decide to take part you will be given this information sheet to keep and a member of our designated research team will talk to you about the project. If you want to take part you will be asked you to sign a consent form. If you take part in the study, you are free to withdraw at any time without giving a reason. It is important to know that even if you do or do not participate in the study, your care will not be different to the standard of care you should receive.

5. What will happen to me if I take part in the study?
If you would like to take part, one of our researchers will talk to you about the study, what it involves for you and answer any questions you have. We will then ask you to sign a consent form.

We will take one set of blood samples and ask for a biopsy or part of a surgical sample.

You will have a diagnostic biopsy appointment for your treatment plan. We will ask for a 2nd research specific biopsy to be taken at the same time, so no extra visits will be required. Where possible we will ask for a section of the diagnostic biopsy, as long as this would have no impact on your diagnostic results. The specially trained individual

undertaking the procedure, for example a radiologist or surgeon will make the decision on whether extra biopsies are required. If additional study specific biopsies are required, the participant will be informed prior to the biopsy being taken.

If you are having surgery to remove the cancer, we will take part of the cancer once it has been removed; again, no extra visits will be required.

You will be asked to give a single 18 ml blood sample during this appointment. This should take about 5 minutes. Neither you nor your doctors will receive a result from this blood sample or from the drug screen.

We will look at your medical records for information about your cancer and the treatment you have received.

All this information will be stored anonymously (i.e. labelled with a code number and not your name) on a secure computer database.

6. What are the possible disadvantages and risks of taking part?
The study will involve taking a blood test for research purposes, you may experience some discomfort when the blood is been taken.

If you are undergoing surgery to remove your cancer, we will just take part of the cancer once it has been removed. There is no extra risk to the patient in addition to the surgery itself. This will be the end of your involvement in the study.

If you are having a biopsy or a transurethral resection and there is enough cancer for us to take a small section of it, there will be no extra procedures required. This will be the end of your involvement in the study.

If you are having a biopsy and there is not enough cancer for us to take a section of, we will ask for an extra biopsy to be taken at the same time as the diagnostic biopsy. There will be an increase in risk associated with taking an extra biopsy, as the procedure is being repeated. The risk will differ depending on the biopsy site and accessibility, therefore the risks will be clearly explained on a case by case basis, prior to the biopsy been taken.

This will be the end of your involvement in the study.

You would be able to continue with any other treatments you require (such as surgery, chemotherapy or radiotherapy) whilst on this study and it will not impact any of your standard care.

7. What are the possible benefits of taking part?

There is no immediate clinical benefit to you in taking part. This research may lead to the development of a new predictive test, which would inform doctors of the best treatment for an individual's cancer in the future. Until we find out if the test works, we will not be able to use any results from the drug screen.

8. What if new information becomes available?
If any important new information becomes available that may affect your health during the period of the study, the investigators will contact you to tell you about it.

9. What happens when the research study stops?
Any remaining tissue from the biopsy or surgery and blood samples will be destroyed at the end of the study. DNA and RNA the genetic code extracted from your blood and tumour tissue will be stored for 5 years after the study ends. The samples will only be used for research purposes and not for any financial gain. The samples will be treated as a gift from you to us. Additional studies maybe planned in the future and may use DNA and RNA. Any such studies would have to be reviewed and gain approval from a research ethics committee.

10. Will my taking part in the study be confidential?

How will we use information about you?
We will need to use information from you and from your medical records for this research project.
This information will include your [initials/ NHS number/ name/ contact details/ date of birth/ previous cancer treatment history, if applicable/ future cancer treatments, if applicable/ response to treatment]. People will use this information to do the research or to check your records to make sure that the research is being done properly.
People who do not need to know who you are will not be able to see your name or contact details. Your data will have a code number instead.
We will keep all information about you safe and secure.

Once we have finished the study, we will keep some of the data so we can check the results. We will write our reports in a way that no-one can work out that you took part in the study.

What are your choices about how your information is used?
- You can stop being part of the study at any time, without giving a reason, but we will keep information about you that we already have.
- We need to manage your records in specific ways for the research to be reliable. This means that we won't be able to let you see or change the data we hold about you.
- If you agree to take part in this study, you will have the option to take part in future research using your data saved from this study.

Where can you find out more about how your information is used?
You can find out more about how we use your information
- at www.hra.nhs.uk/information-about-patients/
- our leaflet available from **www.hra.nhs.uk/patientdataandresearch**
- by asking one of the research team
- at https://www.sheffieldclinicalresearch.org/for-patients-public/how-is-your-information-handled-in-research/

by sending an email to sth.InfoGov@nhs.net

11. What will happen to the results of the study?
The results will be presented at scientific conferences and published in scientific journals. You will not be identified in any reports or publications. If you would like a summary of the study results, please contact a member of the study team (see contact details below).

12. Who is organising and funding this study?
The study is being organised by Professor Sarah Danson and Professor Thomas Helleday at Weston Park Hospital, Sheffield. The University of Sheffield is currently funding the study.

13. Who has reviewed the study?
This research protocol will be reviewed in the hospital where patients are seen and by the University of Sheffield. It will also be scientifically reviewed by external reviewers, by the South West -   Frenchay Research Ethics Committee, and by patient and public involvement groups.

14. What if something goes wrong?
If you are harmed by your participation in this study, there are no *special* compensation arrangements. We will be taking a blood sample, which carries negligible risk. If we take part of the tumour as part of routine diagnostic procedures this risk will be negligible. If we ask for a fresh biopsy the risk will be discussed prior to consent, this will be dependent on the type of biopsy taken. If you are harmed due to someone's negligence, then you may have grounds for a legal action. If you have *any* cause to complain about *any* aspect of the way in which you have been approached or treated during the course of this study, the normal National Health Service complaints mechanisms and Patient Advice and Liaison Service (0114 271 2400) are available to you and are not compromised in any way because you have taken part in a research study.

If you have any complaints or concerns in regards to the research project in the first instance the project organiser, Professor Sarah Danson at Weston Park Hospital, Whitham Road, Sheffield, S10 2SJ can be contacted at. Tel: 0114 226 5221.

Or contact Dr David Hughes, Medical Director, Sheffield Teaching Hospitals NHS Foundation Trust, 8 Beech Hill Road, Sheffield, S10 2SB. Tel: 0114 271 2178.

15. Contact for further information.

If you need more information or have any questions concerning this study, please contact:

Professor Sarah Danson, Weston Park Hospital, Sheffield, S10 2SJ.

Tel: 0114 226 5221

Email: s.danson@sheffield.ac.uk

Or:

Dr Greg Wells, the University of Sheffield Medical School, SheffieldS10 2RX.

Tel: 0114 215 9098

Email: G.Wells@sheffield.ac.uk

Thank you for reading this and for taking an interest in this research study.

This study is funded by the University of Sheffield and The Urology Foundation

The
University
Of
Sheffield.

Sheffield Teaching Hospitals **NHS**
NHS Foundation Trust

Department
Of
Oncology and
Metabolism

Academic Unit of Clinical Oncology
Head: Professor Sarah Danson
Cancer Clinical Trials Centre
Weston Park Hospital
Whitham Road, Sheffield S10 2SJ

Tel: 0114 226 5221
Fax: 0114 226 5678

PATIENT CONSENT FORM
Ex-vivo determined cancer therapy (EVIDENT)

Name of Researcher: _____

Identification Number for this study: _____

Please
initial the box if
you agree

1. I confirm that I have read and understand the patient information sheet dated Version 2.0, 12th Nov 2021, STH20854 for the above study and have had the opportunity to ask questions.	
2. I understand that my participation is voluntary and that I am free to withdraw at any time, without giving any reason, without my medical care or legal rights being affected.	
3. I give permission for one set of blood samples to be obtained from me. I understand that DNA and RNA will be extracted from the blood sample and analysed to identify genes which may influence the development of cancer.	
4. I give permission for part of my cancer tissue to be used in this study. Any tissue taken will be surplus to what is needed for diagnostic analysis.	
5. I understand that DNA and RNA may be extracted from the tissue sample and analysed to identify genes which may influence the development of cancer.	

6. I give consent for the storage of clinical information about me on a computer database. I understand that the laboratory and clinical information will be labelled with a code number and that no other personal information will be held with the samples or clinical information (i.e. it will not have my name and address on it).	
7. I understand that sections of any of my medical notes may be looked at by responsible individuals from Sheffield Teaching Hospitals or the University of Sheffield or from regulatory authorities where it is relevant to my taking part in research. I give permission for such individuals directly involved in this study to have access to my records.	
8. I understand that all data (personal and clinical) collected will be treated in accordance with European and national laws for the protection of data.	
9. I agree to the use of my samples and data for future research. Provided this meets appropriate scientific and ethical standards	
10. I understand that I will not benefit financially if this research leads to the development of a new treatment or medical test, but that a proportion of any profits may go towards further research in this field.	
11. I understand that the ex vivo drug screen test is currently experimental and any results obtained cannot be shared with the participant.	
12. If you would like to receive summaries of the research please initial this box and provide contact details below.	
13. I agree to take part in the above study.	

Name of Patient: _____   Email: _____

Signature: _____   Tel: _____

Date: _____

Thank you for agreeing to participate in this research study.

Researcher: _____

Signature: _____

1 copy for medical notes, 1 copy for the participant, original copy for researcher site file.

Date: _____